Robust Model-based Control in Motion Control Systems

August 2021

OHHIRA, Takashi

A Thesis for the Degree of Ph.D. in Engineering

Robust Model-based Control in Motion Control Systems

August 2021

Graduate School of Science and Technology
Keio University

OHHIRA, Takashi

Contents

List of Figures v

List of Tables ix

1 Introduction 1
- 1.1 Background . . . 1
  - 1.1.1 Related studies . . . 4
- 1.2 Main objective of this thesis . . . 7
- 1.3 Thesis structure . . . 7

2 Robust Model-based Motion Control 9
- 2.1 Introduction . . . 9
- 2.2 Disturbance observer . . . 10
  - 2.2.1 Estimation problem . . . 10
  - 2.2.2 Minimal order disturbance observer (MDOB) . . . 11
  - 2.2.3 Identity disturbance observer (IDOB) . . . 13
    - 2.2.3.1 Design of discrete-time IDOB . . . 14
- 2.3 Robust constrained motion control against disturbance . . . 16
  - 2.3.1 Mathematical modeling . . . 17
  - 2.3.2 Output disturbance estimation . . . 19
  - 2.3.3 Linear model predictive control . . . 20
    - 2.3.3.1 Outline of model predictive control scheme . . . 20
    - 2.3.3.2 Outline of optimization control problem . . . 21
  - 2.3.4 Preliminary experiment . . . 24
  - 2.3.5 Model predictive control with disturbance suppression[62] . . . 27
  - 2.3.6 Numerical verification: offset-free control under disturbance influence . . . 28
    - 2.3.6.1 Controller setup . . . 30
    - 2.3.6.2 Results . . . 31
  - 2.3.7 Numerical verification: control input and velocity constraints . . . 33
    - 2.3.7.1 Controller setup . . . 35
    - 2.3.7.2 Results . . . 37
  - 2.3.8 Summary . . . 38
- 2.4 Constrained acceleration control[67] . . . 48
  - 2.4.1 Preliminaries . . . 49
    - 2.4.1.1 Modeling . . . 49
  - 2.4.2 Proposed control system . . . 50
    - 2.4.2.1 IDOB-based acceleration control . . . 50

2.4.2.2 Implicit force control . . . 51
2.4.2.3 Inverse kinematics . . . 52
2.4.2.4 Joint space position control . . . 53
2.4.2.5 Internal model of PFC . . . 54
2.4.2.6 Outline of PFC scheme . . . 54
2.4.2.7 Acceleration constraints . . . 56
2.4.2.8 Stability analysis . . . 57
2.4.3 Experiments . . . 59
2.4.3.1 Controller setup . . . 60
2.4.3.2 Results on HPFC . . . 62
2.4.3.3 Motion generation against external forces . . . 66
2.4.3.4 Modification of T_{ref} . . . 68
2.4.4 Summary . . . 69
2.5 Chapter summary . . . 70

3 Robust Motion Control Considering Observation Noise 71
3.1 Introduction . . . 71
3.2 Kalman filter with disturbance estimation . . . 72
3.2.1 Design of Kalman filter with disturbance estimation . . . 72
3.3 Noise-free constrained motion control . . . 74
3.3.1 Proposed control system . . . 74
3.3.2 Controller setup . . . 75
3.3.3 Numerical verification: disturbance and noise suppressions . . . 75
3.3.3.1 Results . . . 76
3.3.4 Numerical verification: control input and velocity constraints . . . 80
3.3.4.1 Results . . . 80
3.3.5 Summary . . . 81
3.4 Nonlinear Kalman filter with disturbance estimation . . . 95
3.4.1 Modeling . . . 96
3.4.1.1 Quadrotor . . . 96
3.4.1.2 Underwater wave effect . . . 98
3.4.2 Proposed control system design . . . 99
3.4.2.1 Backstepping controller . . . 99
3.4.2.2 UKF with disturbance estimation . . . 100
3.4.3 Numerical verification . . . 102
3.4.3.1 Parameter design . . . 103
3.4.3.2 Simulation verification . . . 104
3.4.4 Summary . . . 105
3.5 Chapter summary . . . 108

4 Robust Disturbance Observer with Variable Gain for Observation Noise Reduction 109
4.1 Introduction . . . 109
4.1.1 Background and related works . . . 110
4.2 Forgetting-factor based adaptive Kalman filter with disturbance estimation[115] 112
4.2.1 Proposed method . . . 113
4.2.1.1 Disturbance estimation performance of KFDs . . . 113
4.2.2 Augmentation of disturbance model . . . 113

4.2.3 Design of adaptive Kalman filter . . . 114
4.2.3.1 Adaptive Kalman filter with disturbance estimation . . . 114
4.2.4 Numerical verification . . . 116
4.2.4.1 Verification of augmented disturbance model . . . 118
4.2.4.2 Forgetting factor design . . . 121
4.2.4.3 AKFD with augmented disturbance models . . . 122
4.2.5 Experiments . . . 125
4.2.6 Results . . . 126
4.2.7 Summary . . . 126
4.3 Variable forgetting factor-based adaptive Kalman filter with disturbance estimation 132
4.3.1 Proposed method . . . 132
4.3.1.1 Adaptive Kalman filter with disturbance estimation . . . 132
4.3.1.2 Design of variable forgetting factor . . . 133
4.3.2 Numerical Verification: Quantization noise reduction . . . 134
4.3.2.1 VFF design of quantization noise reduction . . . 135
4.3.2.2 Results . . . 137
4.3.3 Numerical Verification: observation noise reductions . . . 142
4.3.3.1 Results . . . 142
4.3.4 Discussion . . . 145
4.3.5 Summary . . . 145
4.4 Chapter summary . . . 150

5 Conclusion **151**
Bibliography . . . 153
Acknowledgments . . . 165

List of Figures

1.1 Robust model-based control . . . 3
1.2 Chapter organization . . . 8

2.1 Block diagram of MDOB . . . 11
2.2 Block diagram of acceleration control . . . 12
2.3 Block diagram of IDOB . . . 14
2.4 Block diagram of discrete-time IDOB . . . 15
2.5 Experimental system . . . 17
2.6 Outline control law of MPC systems . . . 20
2.7 Experimental results: Position control with velocity and control input constraints using long prediction horizon. . . . 25
2.8 Experimental results: Position control with position, velocity, and control input constraints. . . . 26
2.9 Simulation results: position (proposed:(a)) . . . 29
2.10 Simulation results: state estimates by IDOB (proposed:(a)) . . . 29
2.11 Simulation results: disturbance estimates by IDOB (proposed:(a)) . . . 29
2.12 Comparison result (b) : position . . . 30
2.13 Comparison result (b) : State estimates by OB . . . 30
2.14 Comparison result (c) : position . . . 30
2.15 Comparison result (c) : state estimates by IDOB . . . 30
2.16 Comparison result (c) : disturbance estimates by IDOB . . . 30
2.17 Simulation results(A): LQR . . . 33
2.18 Simulation results(A): LQR + IDOB . . . 33
2.19 Simulation results(A): constrained TPW-based MPC with IDOB . . . 34
2.20 Simulation results(A): constrained MPC with IDOB . . . 35
2.21 Simulation results(A): proposed TPW-based MPC with IDOB . . . 36
2.22 Simulation results(B): LQR . . . 36
2.23 Simulation results(B): LQR + IDOB . . . 37
2.24 Simulation results(B): constrained TPW-based MPC with IDOB . . . 38
2.25 Simulation results(B): constrained MPC with IDOB . . . 39
2.26 Simulation results(B): proposed TPW-based MPC with IDOB . . . 39
2.27 Simulation results(C): LQR . . . 40
2.28 Simulation results(C): LQR + IDOB . . . 40
2.29 Simulation results(C): constrained TPW-based MPC with IDOB . . . 41
2.30 Simulation results(C): constrained MPC with IDOB . . . 41
2.31 Simulation results(C): proposed TPW-based MPC with IDOB . . . 42
2.32 Simulation results(D): LQR . . . 42
2.33 Simulation results(D): LQR + IDOB . . . 43

2.34 Simulation results(D): constrained TPW-based MPC with IDOB 43
2.35 Simulation results(D): constrained MPC with IDOB 44
2.36 Simulation results(D): proposed TPW-based MPC with IDOB 44
2.37 Simulation results(E): LQR 45
2.38 Simulation results(E): LQR + IDOB 45
2.39 Simulation results(E): constrained TPW-based MPC with IDOB 46
2.40 Simulation results(E): constrained MPC with IDOB 46
2.41 Simulation results(E): proposed TPW-based MPC with IDOB 47
2.42 Modeling of three-link manipulator. 49
2.43 System diagram of the proposed control system. FK and IK denote forward and inverse kinematics. 50
2.44 Acceleration control by IDOB for MIMO systems. 51
2.45 Experiment setup 59
2.46 An example snapshot of experiment 2.4.3.2. 60
2.47 Experiments setup and configuration for 2.4.3.3. The blue arrows show the direction of the external forced disturbance. 60
2.48 Experimental results on F_x^{ref} = 2N in Sec. 2.4.3.2 . The filled area shows the position/force control. The dashed lines in the torque results are the torque limitations ($\tau_{\mathrm{limit},q_1,q_2,q_3}$). 62
2.49 Experimental results on F_x^{ref} = 5N in Sec. 2.4.3.2 . The filled area shows the position/force control. The dashed lines in the torque results are the torque limitations ($\tau_{\mathrm{limit},q_1,q_2,q_3}$) 63
2.50 Experimental validation results on l_1 in 2.4.3.3. In the red and blue filled areas, the first link was disturbed to the left side ($q < y$) by force and to the right side ($y < q$) by forced disturbance. 66
2.51 Experimental validation results on l_2 in 2.4.3.3. In the red and blue filled areas, the second link was disturbed to the left side ($q < y$) by force and to the right side ($y < q$) by forced disturbance. 66
2.52 Experimental validation results on l_3 in 2.4.3.3. In the red and blue filled areas, the third link was disturbed to the left side ($q < y$) by force and to the right side ($y < q$) by forced disturbance. 67
2.53 Experimental results on 2.4.3.4. 68

3.1 Simulation results 77
3.2 Simulation results: disturbance estimates by KFD and IDOB 78
3.3 Simulation results: validation for constraint 78
3.4 Simulation result: position by standard MPC 79
3.5 Comparison results on state estimation with initial state error by IDOB and KFD 80
3.6 Simulation results(A): LQR 82
3.7 Simulation results(A): LQR + KFD 82
3.8 Simulation results(A): constrained TPW-based MPC with KFD 83
3.9 Simulation results(A): constrained MPC with KFD 83
3.10 Simulation results(A): proposed TPW-based MPC with KFD 84
3.11 Simulation results(B): LQR 84
3.12 Simulation results(B): LQR + KFD 85
3.13 Simulation results(B): constrained TPW-based MPC with KFD 85
3.14 Simulation results(B): constrained MPC with KFD 86
3.15 Simulation results(B): proposed TPW-based MPC with KFD 86

3.16 Simulation results(C): LQR . . . 87
3.17 Simulation results(C): LQR + KFD . . . 87
3.18 Simulation results(C): constrained TPW-based MPC with KFD . . . 88
3.19 Simulation results(C): constrained MPC with KFD . . . 88
3.20 Simulation results(C): proposed TPW-based MPC with KFD . . . 89
3.21 Simulation results(D): LQR . . . 89
3.22 Simulation results(D): LQR + KFD . . . 90
3.23 Simulation results(D): constrained TPW-based MPC with KFD . . . 90
3.24 Simulation results(D): constrained MPC with KFD . . . 91
3.25 Simulation results(D): proposed TPW-based MPC with KFD . . . 91
3.26 Simulation results(E): LQR . . . 92
3.27 Simulation results(E): LQR + KFD . . . 92
3.28 Simulation results(E): constrained TPW-based MPC with KFD . . . 93
3.29 Simulation results(E): constrained MPC with KFD . . . 93
3.30 Simulation results(E): proposed TPW-based MPC with KFD . . . 94
3.31 Definition of coordinate frame: relationship between invariant world coordinate frame(Σ_W) and robot coordinate frame (Σ_b) . . . 96
3.32 Configuration of the whole control system using the backstepping control and the UKF with disturbance estimation . . . 96
3.33 Simulation: wave disturbance . . . 98
3.34 Simulation results(a, c, e): position estimates on UKF-based systems . . . 102
3.35 Simulation results(a, c, e): posture estimates on UKF-based systems . . . 103
3.36 Simulation results(b,d,f): EKF-based systems . . . 104
3.37 Simulation results(a,b,c,d) : disturbance estimates . . . 106
3.38 Simulation results : velocity estimation $\dot{\phi}$ . . . 107

4.1 Simulation result: disturbance estimates by IDOB and KFD . . . 113
4.2 System diagram of control system . . . 116
4.3 Simulation results(a): position response . . . 118
4.4 Simulation results(a): disturbance estimates . . . 118
4.5 Simulation results(b): position response . . . 118
4.6 Simulation results(b): disturbance estimates . . . 118
4.7 Simulation results(c): position . . . 119
4.8 Simulation results(c): disturbance . . . 119
4.9 Simulation results(d): position . . . 119
4.10 Simulation results(d): disturbance . . . 119
4.11 Simulation results: position response . . . 120
4.12 Simulation results: disturbance estimates . . . 120
4.13 Simulation results (γ_d): position response . . . 120
4.14 Simulation results(γ_d): disturbance estimates . . . 120
4.15 Comparative results: position response with respect to step-type disturbance . . . 122
4.16 Comparative results: step-type disturbance . . . 122
4.17 Comparative results: position response with respect to ramp-type disturbance . . . 123
4.18 Comparative results: ramp-type disturbance . . . 123
4.19 Comparative results: position response with respect to sine-wave disturbance . . . 123
4.20 Comparative results: sine-wave disturbance . . . 123
4.21 Experimental result: MDOB. . . . 127

4.22 Experimental result: IDOB. 127
4.23 Experimental result: KFD. 128
4.24 Experimental result: KFD w/ $\gamma = 1.05$. 128
4.25 Experimental result: KFD w/ $\gamma = 1.10$. 129
4.26 Experimental result: KFD w/ $\gamma = 1.20$. 129
4.27 Experimental result: KFD based on first-order disturbance model. 130
4.28 Experimental result: KFD based on first-order disturbance model w/ $\gamma = 1.05$. 130
4.29 Experimental result: KFD based on second-order disturbance model. 131
4.30 Experimental result: KFD based on second-order disturbance model w/ $\gamma = 1.05$. 131
4.31 Encoder model 135
4.32 Simulation results: $n = 4$, 16 PPR. 138
4.33 Simulation results: $n = 8$, 256 PPR. 139
4.34 Simulation results: $n = 12$, 65536 PPR. 140
4.35 Simulation results: $n = 48$, 2.8147×10^{14} PPR. 141
4.36 Simulation results: $n = 48$, $T_s = 10^{-3}$[s], white noise (variance 10^{-1}). 143
4.37 Simulation results: $n = 48$, $T_s = 10^{-3}$[s], white noise (variance 10^{-4}). 144
4.38 Verification results: forgetting factor, white noise (variance 10^{-1}) 146
4.39 Verification results: forgetting factor, white noise (variance 10^{-4}) 147
4.40 Discrete-time pole assignment of the observers, white noise (variance 10^{-1}) . . 148
4.41 Continuous-time pole assignment of the observers, white noise (variance 10^{-1}) 148
4.42 Discrete-time pole assignment of the observers, white noise (variance 10^{-4}) . . 149
4.43 Continuous-time pole assignment of the observers, white noise (variance 10^{-4}) 149

List of Tables

2.1 Parameter definition of the cart 19
2.2 Simulation conditions 29
2.3 Parameters of DOB 29
2.4 Parameters of MPC 29
2.5 Simulation results 31

3.1 Parameters on KFD 76
3.2 Parameters on MPC 76
3.3 Verification conditions 76
3.4 Specifications of quadrotor system 97
3.5 Simulated systems 102

4.1 Verification conditions 116
4.2 Parameter of KFD 116
4.3 Parameter of input disturbances 116
4.4 Simulation results 120
4.5 Estimation performance of the proposed γ_d in steady-state 121
4.6 Simulated conditions 122
4.7 List of results of disturbance estimation by KF-D 124
4.8 Simulation results 4.3.2: RMSE of $\dot{q}$. 138
4.9 Simulation results 2.4.4: RMSE in unmeasured variable $\dot{q}$. 142

Chapter 1

Introduction

1.1 Background

Aging populations with fewer births than in previous generations characterize modern societies. According to the background, many studies on robots working with humans have been conducted, and personal and industrial robots performing various tasks have begun to be put into practical use. In particular, flexible human assist robots (FHARs), which are welfare and nursing care robots specializing in human support, are attractive in modern societies.

One of the challenges to introducing FHAR in societies is that a control system simultaneously considering human safety and stable robot motion generation is a must. Ensuring the safety of the daily living environment is an essential issue faced by FHARs. In particular, as long as it operates in the same living environment as humans, it is necessary to avoid physical damage to environments. Additionally, a guaranteed stable motion generation ensuring safety is also required. Moreover, FHARs, which interact with various environments, must consider uncertainty; therefore, their control systems must consider robustness against uncertainty. In order to simultaneously ensure safe and stable motion generation, a control system must satisfy the mechanical and electrical constraints (e.g., maximum speed, torque, moveable range, etc.) imposed on robots. Therefore, while controlling FHAR robots, an advanced motion control method, which can provide robust constrained control, is a must in order to guarantee stable motion generation.

Motion control[1, 2] is one of the key techniques for controlling such robots. Motion control systems vary from a single motor to multiple degrees of freedom humanoid robots. Therefore, control systems in motion control systems include various control systems such as classic control for single-input/single-output systems using transfer function, modern control for multi-input/multi-output (MIMO) systems using state-space model, robust control using characteristics

on systems, etc. Classic control is used in main industrial applications. Moreover, using the behavior validation of the frequency domain of plant systems, robust control is developed. By contrast, modern control is developed for controlling MIMO systems, and it is mainly used for optimal control and observers. In many motion control systems, since simple design and easy implementation are considered, model-free control techniques such as Proportional-Integral-Differential (PID) controller are utilized. Additionally, anti-windup control[3, 4] is one of constrained controls in mode-free control. The method has the ability to consider control input saturation in the control system; however, it does not cope with state constraints (i.e., dynamics constraints).

Model-based control (MBC)[16, 17] systems, which are designed by using a mathematical model of plants, have been used in motion control systems frequently. MBC techniques in motion control represent disturbance observer (DOB), Kalman filter (KF)[18], and linear quadratic regulator(LQR), etc. In MBC systems, an invariant set[5, 6], which provides motion conditions considering constraints on robots and desired motion set, is used for constrained control design. In contrast to model-free constrained control, the MBC-based constrained control provides motion constraints allocated by preliminary conditions. In constrained control systems, an invariant set is occasionally used. The invariant set-based control systems provide motion response within the preliminary conditions (invariant set), in the case of the initial values within the conditions. In particular, the implementations of the invariant set are used by the switching controller and reference governor[6, 7]. These methods have the advantage that is to divide control performance on constraints and tracking; therefore, the stability analysis and tracking error are compensated. However, handling excessive disturbance and controlling high-order plant models are challenging in consideration of constraints satisfaction over the invariant set. The main drawback of MBCs is that accurate system models and state information are required.

Among the constrained control systems in the MBC, model predictive control (MPC)[17, 20–30] is a key technology for realizing advanced motion control. MPC is a control system design method that can directly impose constraints on robots and realize high profitability, high accuracy, and high-performance controls; therefore, the MPC-based systems can design advanced control systems in various systems. However, control performances of MBC systems are decided by modeling and observation accuracies. In FHAR control systems that interact with uncertain environments with unknown parameters, robustness compensation against uncertainty is must be ensured to bring out the control performance of MBC systems. Therefore, applying MPC to FHAR in uncertain environments is challenging owing to robustness issues.

To explicitly consider unknown disturbance and parameter and modeling errors in control system design, robust control theory had been established and is represented by H_∞ and sliding mode control[1]. These robust control systems are based on the model and its uncertainty. Therefore, robust control on MBCs is classified as robust model-based control (RMC).

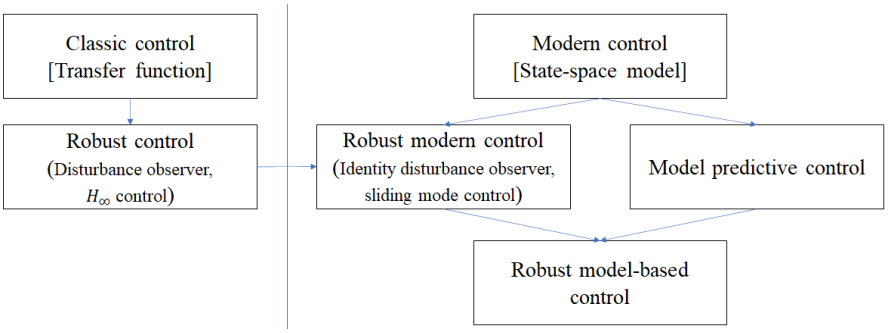

FIGURE 1.1: Robust model-based control

Among the RMC, DOBs [8–15], which are used for estimating and canceling external disturbances, are an essential method in motion control and have been highly evaluated as a method for robust control. Moreover, DOB-based robust motion control is simple and useful for improvements of various motion control systems. Additionally, identity disturbance observers (IDOBs)[1], which are expressed by state-space models, have been developed. Therefore, FHAR control systems are expected that the disturbance observer-based control will be utilized. Additionally, FHAR systems contact the environments; therefore, the safety compensation by the force is a must. In this dissertation, the safe and stable motion generate by utilizing the force information, which can estimate as a disturbance.

Therefore, this thesis focuses on addressing the robust design problem to ensure constrained motion control systems in uncertain environments. Fig. 1.1 shows the definition of RMCs and the relationship of existing typical control system design methods[19]. Additionally, FHAR systems contact the environments; therefore, the safety compensation by the force is a must. In this dissertation, the safe and stable motion generate by utilizing the force information, which can estimate as a disturbance. In other words, how to effectively integrate MPC systems and DOB systems is clarified.

1.1.1 Related studies

The main problem with MBC including MPC is that the control performance is greatly affected by the modeling and parameter errors between the internal model used for design and the actual plant. The control performance of MPC significantly depends more on the accuracy of the internal model for predictions. Feedback control theory reduces the effects of modeling errors. However, in the case of MPC performing online sequential state feedback control, it is challenging to reduce the error within a finite time. Therefore, when applied to an actual robot with parameter variations, the control performance deteriorates significantly. In order to reduce the modeling error, white-box modeling, which completely describes all motion and parameters, is ideal. However, the utilization of white-box modeling in motion control is nearly always limited; therefore, gray-box modeling with uncertainty should be used practically. This thesis focuses on how to solve the modeling error problem. An essential solution to this problem is the nominalization of the plant model by estimating and canceling various disturbances including modeling errors, external forces, parameter errors, etc.

In order to compensate for the disturbance influences, robust MPC (RMPC)[31–36] has been developed. Generally, RMPCs consider bounded disturbance; therefore, robustness is compensated within the bounded set. Additionally, the constraints are strictly modified to compensate for robustness. FHAR control systems occasionally are affected by disturbance above the torque limit. In FHAR systems, the undesired disturbance is easily generated by the contact/interaction of environments; therefore, RMPC, which is conservative, is insufficient to compensate for the robustness.

In order to solve the problem, some studies that integrate disturbance estimations and MPCs (Offset-free MPCs)[37–40] have been conducted. One of the offset-free MPCs is the output disturbance estimation-based MPC method. In this method, an output disturbance observer estimates the estimation error between measured output and estimated output as disturbance estimates. Then, the estimated output disturbance uses for modification of reference or prediction. Hence, the offset-free characteristics depend on the control performance of MPC, and the internal model is not compensated.

Alternatively, input disturbance estimation can be utilized to design the offset-free MPC [41–58]. DOB is a control technique that estimates modeling errors in the internal model, and it is used for nominalization for the plant model. The conventional methods estimate input disturbance, output disturbance, and modeling error, etc. Then, disturbance estimates are used in modifications of reference trajectory generations, optimization problems, etc. However, in the case of independent design of DOB and MPC, MPCs lose optimality; therefore, the integration design frequently provides conservative control performance. Additionally, one of the problems when integrating DOBs and MPCs is the behavior of constraints in cascade control. MPC

systems imposing the constraints are nearly always used as outer loop controllers. According to some studies, since actual control input is affected by the disturbance estimates of DOB as inner loop controller, the control input and output influenced by added disturbance estimate may cause constraint violation. Furthermore, the control input constraint considering the disturbance estimate is always time-varying [36].

Conventional DOB-based MPC systems utilize minimal-order DOB (MDOB) that only estimates input disturbance. MDOB provides nominalization by nominal inertia or mass system; however, it does not provide internal model robustness against multi-input/multi-output (MIMO) systems of multi-degree-of-freedom (MDof) systems. Therefore, in MDof systems, stable motion generation cannot be guaranteed; therefore, an effective MPC structure considering the disturbance estimation and internal model robustness is a must (Chapter 2).

Additionally, since constrained motion control behaves at constraint boundary, RMPC and offset-free MPC systems have a problem against noise influences. In other words, the effectiveness of constrained motion control is frequently lost by noise influences (Chapter 3). Moreover, the limitation of the performance of DOB, which is a trade-off between high-frequency disturbances rejection and low-frequency disturbance rejection, is well known. The disturbance estimation performance of DOBs is decided by the cutoff frequency of the lowpass filter, and the responsiveness and noise sensitivity of DOBs is a trade-off relationship. Therefore, high-frequency disturbance components (noise) remain in the estimates in the low-pass filter-based observer owing to focus on disturbance compensation. The noisy estimates also affect the control performance of MBC systems and constraints guarantee. To cancel the effects of noise, the estimation time constant of the DOB needs to delay; however, this operation makes inadequate performance on the disturbance compensation.

In other words, there are problems with the stability and robustness of DOB-based control in a noisy environment, making it difficult to nominalize the plant model. Moreover, conventional DOB-based control systems are implemented in motor system with optical encoder; however, DOBs do not clearly cope with quantization noise generated by encoder sensor. It is indicated that conventional DOB-based control systems using optical encoders with low-resolution in joint space have the same problems in stability and robustness. Moreover, for making prediction trajectories, the MPC requires information on state variables. Accurate state information supports high precision control; however, the accurate state estimation must consider robustness against noise and disturbances. A robust state estimation method considering disturbance and noise is a must for compensating for the control performance of MPC systems. Therefore, an improved DOB for simultaneously estimating state and disturbance considering various noise reduction is a must (Chapter 4). Finally, as a well-known fact, it is difficult to guarantee closed-loop stability in MPCs in uncertain environments[17, 20] and saturated systems. Generally, stability analysis for MPCs only considers the nominal model. Additionally, in RMPC design, bounded disturbances

only are assumed. Effective methods to guarantee stability are approaches to terminal state constraints and terminal cost function and provide stability under nominal environments. In theory, terminal state constraints can be used for ensuring nominal stability, and the terminal penalty can also ensure the nominal stability conditions. However, to compose the theorem, compensation of internal model robustness is a must. Additionally, the stability conditions require a large computational load for compensating the stable behavior. Therefore, this dissertation focuses on the nominalization of the actual system and attempts to assist the compensation of stable motion generation under the influence of noise and disturbance by using the internal-loop controller and fast MPC. As a result, the influences of unpredictable or unmeasured disturbances, system uncertainty, non-linearity, and instability are reduced in MPC systems, and the stable motion generation by the MPC system is guaranteed.

1.2 Main objective of this thesis

This thesis aims to realize safe FHAR systems against interaction with various environments. In order to achieve the aim, the main objective is to establish a constrained motion control method with robustness against noise and disturbance. In particular, the elemental technologies required to achieve this objective are described.

The main components of this thesis describe a robust MPC method and a noise-free robust simultaneous estimation method of state and disturbance to compensate for the internal model robustness.

1.3 Thesis structure

Figure 1.2 shows the chapter organization of this thesis.

Chapter 1 explained the introduction, background, problem, and objective of this thesis.

In Chapter 2, conventional disturbance estimation methods and the standard MPC are explained. Then, the design method and the verification result of a robust MPC, which integrates DOB and MPC, are shown. The verification results show that MPC with DOB is effective against disturbance and can improve robustness. Moreover, the problem of constrained motion control to stem from observation noise is shown.

In Chapter 3, a noise-free constrained motion control method is described. In this chapter, a Kalman filter with disturbance estimation is used as a DOB for a robust MPC to enhance noise influence reduction. In the method, the constrained motion control system filtered by Kalman filter methods-based DOB is designed. With respect to rejecting noise influences, the verification shows the effectiveness of the proposed design method; however, it is confirmed that the DOB prioritizing the noise rejection makes sluggish disturbance estimation. Therefore, the Kalman filter-based DOB cannot solve the usual problem of existing disturbance estimation methods, which is the trade-off between disturbance estimation speed and noise sensitivity.

In Chapter 4, in order to solve the problem of disturbance estimation, a noise-free robust simultaneous estimation method of state and disturbance is explained. Using variable gains, the estimation method simultaneously provides both robustness against noise and disturbance for MBC systems. Additionally, unlike existing disturbance estimation methods, the proposed method can explicitly and adaptively handle white and quantization noises.

This thesis is concluded in Chapter 5.

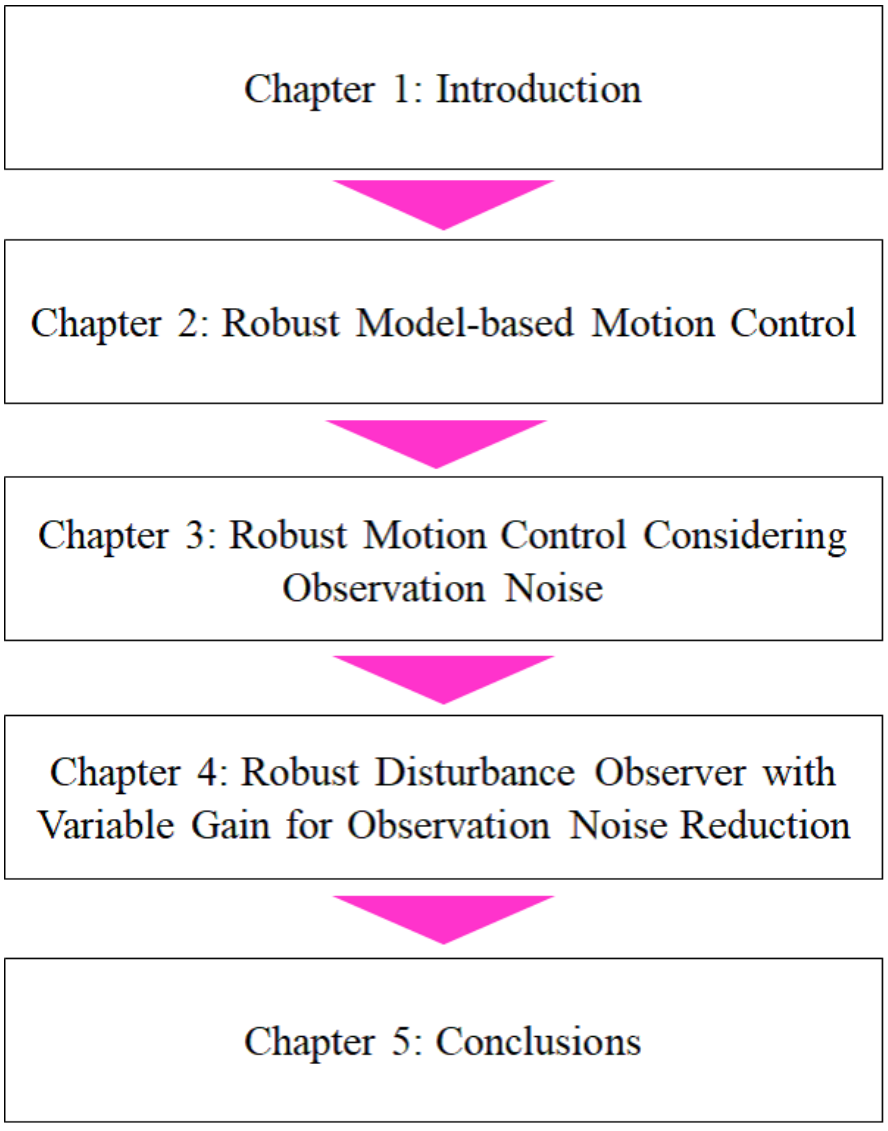

FIGURE 1.2: Chapter organization

Chapter 2

Robust Model-based Motion Control

2.1 Introduction

This chapter describes the robust constrained motion control. In order to design the robust constrained motion control, the integration design methods for robust MPCs by using DOBs are shown in this chapter.

In Sec. 2.2, the design method of DOBs is illustrated. In this section, in contrast to the conventional DOB, a DOB for simultaneously estimating state and disturbance is described. The DOBs have two abilities for canceling the disturbance and for realizing acceleration control.

Secs. 2.3 and 2.4 focus on those two abilities and describes the two integration design methods against each ability. Sec. 2.3 focus on MPC integrated with DOB for canceling the disturbance in constrained systems. Sec. 2.4 focus on MPC integrated with DOB, for realizing constrained acceleration control. In these sections, controller integration design methods that take advantage of the DOBs are proposed. In this chapter, two application examples by each method are shown.

2.2 Disturbance observer

DOBs[8, 12–14, 117] can estimate and cancel unknown disturbances and modeling errors. Furthermore, DOB is known as a robust control technique in motion control systems. Additionally, DOB systems are easily considered to apply to various systems using plant models. Moreover, some design methods for DOBs have been considered: (1) identity disturbance observer (IDOB)[99] simultaneously estimate system state and disturbance, (2) extended state observer (ESO)[118–120] supports to use nonlinear models, (3) model error compensator (MEC)[121] does not require inverse models, and (4) sliding-mode observer-based DOB[122, 123] compensates nonlinear disturbance, etc.

A minimal order disturbance observer (MDOB)[8, 12–14, 117], which focuses on estimating disturbance, is the most familiar method in DOBs. Moreover, the MDOB can estimate the disturbances with external force and model error by using the nominal model. Then, the disturbance estimates are used to cancel the disturbance and to make robust control systems.

Therefore, in this dissertation, the IDOB, which can simultaneously estimate state and disturbance is only focused. Additionally, IDOBs have the ability to robust estimation by simultaneous estimation for state and disturbance; therefore, IDOB can use to improve the control performance of MBCs including MPCs.

2.2.1 Estimation problem

This section describes the simultaneous estimation of state and disturbance. The plant is assumed as a 1-degree of freedom such as an inertial system and a motor system and is defined by a linear time-invariant system. Then, the parameters of the system state are defined as a torque τ [Nm] and an angle y [rad]. The measured variable is assumed as the true angle q.

This equation of motion is given by

$$\ddot{q} = \frac{1}{J}\{\tau - c\dot{q}\}, \tag{2.1}$$

where $\ddot{q}$, J, τ, and c denote a angular acceleration, an inertia, a input torque, and a viscous friction coefficient, respectively.

Additionally, the state vector of the system is described as $\boldsymbol{x} = [q \quad \dot{q}]^{\mathrm{T}}$. Then, the state-space model of the system can be described as

$$\dot{\boldsymbol{x}} = \boldsymbol{A}\boldsymbol{x} + \boldsymbol{B}u, \tag{2.2}$$

$$y = \boldsymbol{C}\boldsymbol{x}, \tag{2.3}$$

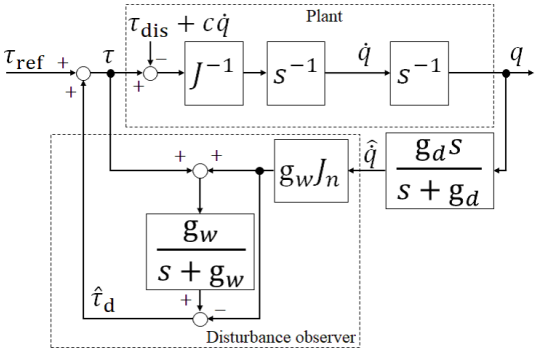

FIGURE 2.1: Block diagram of MDOB

where $u = \tau$, $\boldsymbol{A} = \begin{bmatrix} 0 & 1 \\ 0 & -c/J \end{bmatrix}$, $\boldsymbol{B} = \begin{bmatrix} 0 & 1/J \end{bmatrix}^{\text{T}}$, and $\boldsymbol{C} = \begin{bmatrix} 1 & 0 \end{bmatrix}$.

The estimation problems for the systems are defined to estimate the true angle q, velocity $\dot{q}$, and the disturbance.

2.2.2 Minimal order disturbance observer (MDOB)

Firstly, a design method for MDOB is explained. The disturbance model is described as all disturbances τ_{d} (i.e., external τ_{dis} and internal τ_{p} disturbances) into input disturbances. The disturbance torque model can be described as

$$\dot{\tau}_{\text{dis}} = 0. \tag{2.4}$$

This disturbance model denotes the step-type disturbance; therefore, the DOB based on the disturbance model aims to estimate the step-type disturbance.

The system of Eq. (2.1) extended by the disturbance τ_{dis} can describe as

$$\ddot{q} = \frac{1}{J}\{\tau - c\dot{q} - \tau_{\text{dis}}\}, \tag{2.5}$$

where, τ_{dis} denotes the external disturbances.

Moreover, the nominal inertia J_n for designing the MDOB is used. In practice, the MDOB is used in joint space; therefore, an encoder angle information has to convert into velocity by using pseudo-differential. Therefore, considering the pseudo derivative $G_d(s) = g_d s/(s + g_d)$, the disturbance estimates (τ_{d}) of the MDOB can be described as

$$\begin{aligned} \tau_{\text{d}} &= -\tau_{\text{p}} - c\dot{q} - \tau_{\text{dis}} \\ &= \frac{g_w}{s + g_w}\{\tau + g_w J_n G_d(s) q\} - g_w J_n G_d(s) q, \end{aligned} \tag{2.6}$$

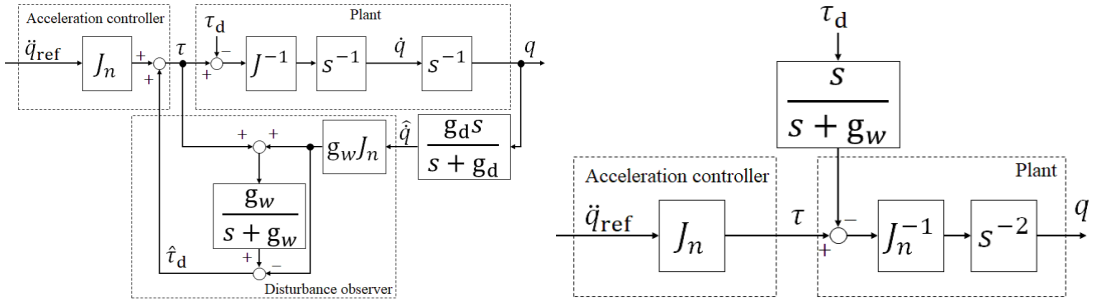

(a) acceleration controller (b) equivalent system

FIGURE 2.2: Block diagram of acceleration control

where τ_{p} denotes the disturbance torque by model errors as internal disturbance, and g_d and g_w denote cutoff frequencies used in the pseudo-derivative and a lowpass filter in the MDOB. If the disturbances are canceled, the system model is nominalized by the MDOB using the nominal inertial system of J_n. On the other hand, the disturbance estimates involve external and internal disturbances. Thus, to estimate external force disturbances, the utilization of a reaction force observer[103] is a must. Fig. 2.1 shows the block diagram of the MDOB.

In the DOB, the disturbance estimation attempts using the step-type disturbance model. Therefore, in theory, the DOB cannot handle time-varying disturbance influences. However, the DOB has the dynamics for disturbance estimation. Therefore, in the case of the DOB design with the fast updating of the disturbance estimates (i.e., using high cutoff frequency), the disturbance estimates by the DOB can track the actual disturbance with a small-time delay.

On the other hand, using the nominalization performance of MDOBs, the MDOBs can handle acceleration control based on nominal inertia. Acceleration control is one of the key techniques in motion control because acceleration can simultaneously treat force control and position control in the same dimensions. Fig. 2.2 shows the MDOB-based acceleration control and its equivalent system. The MDOB handles noise effects by sensors using the cutoff frequencies. In Eq. (2.6), it is confirmed that the second term propagates noise effects to the state and disturbance estimates by $G_d(s)$. Therefore, because the general MDOB utilizes the measured variables to feedback controllers, noise effects sometimes affect the control loop.

2.2.3 Identity disturbance observer (IDOB)

Secondly, the IDOB, which aims to simultaneous estimation of state and disturbance using a state-space model, is described. The configuration of the IDOB is similar to the steady-state Kalman filter. The block diagram of the IDOB is illustrated in Fig. 2.3. Adding Eq. (2.5) in Eq. (2.2), then, a state space model is given by

$$\dot{\boldsymbol{x}} = \boldsymbol{A}\boldsymbol{x} + \boldsymbol{B}u - \boldsymbol{B}\tau_{\mathrm{dis}}, \tag{2.7}$$

$$y = \boldsymbol{C}\boldsymbol{x}, \tag{2.8}$$

where, $\boldsymbol{A}$, $\boldsymbol{B}$, and $\boldsymbol{C}$ denote the system state, input, and output matrices. A new state vector $\boldsymbol{x}$ extended by the disturbance estimates τ_{d} is defined using the augmented state vector $\bar{\boldsymbol{x}} = [q \quad \dot{q} \quad \tau_{\mathrm{d}}]^{\mathrm{T}}$. Moreover, the state-space model dealing with the augmented state vector can be described as

$$\dot{\bar{\boldsymbol{x}}} = \bar{\boldsymbol{A}}\bar{\boldsymbol{x}} + \bar{\boldsymbol{B}}u, \tag{2.9}$$

$$y = \bar{\boldsymbol{C}}\bar{\boldsymbol{x}}, \tag{2.10}$$

where $\bar{\boldsymbol{A}} = \begin{bmatrix} \boldsymbol{A} & -\boldsymbol{B} \\ \boldsymbol{0} & 0 \end{bmatrix}$, $\bar{\boldsymbol{B}} = \begin{bmatrix} \boldsymbol{B} & 0 \end{bmatrix}^{\mathrm{T}}$, and $\bar{\boldsymbol{C}} = \begin{bmatrix} \boldsymbol{C} & 0 \end{bmatrix}$.

The IDOB based on the state space observer can be described as

$$\dot{\bar{\boldsymbol{x}}} = (\bar{\boldsymbol{A}} - \boldsymbol{L}\bar{\boldsymbol{C}})\bar{\boldsymbol{x}} + \bar{\boldsymbol{B}}u + \boldsymbol{L}\boldsymbol{y}, \tag{2.11}$$

$$= (\bar{\boldsymbol{A}} - \begin{bmatrix} \boldsymbol{L}_{\mathrm{state}} \\ \boldsymbol{L}_{\mathrm{dis}} \end{bmatrix}\bar{\boldsymbol{C}})\bar{\boldsymbol{x}} + \bar{\boldsymbol{B}}\tau + \begin{bmatrix} \boldsymbol{L}_{\mathrm{state}} \\ \boldsymbol{L}_{\mathrm{dis}} \end{bmatrix}\boldsymbol{y}. \tag{2.12}$$

$\boldsymbol{L}$ is the observer gain matrix which are structured by state $\boldsymbol{L}_{\mathrm{state}}$ and disturbance $\boldsymbol{L}_{\mathrm{dis}}$. The nominal stability of the IDOB is compensated by the eigenvalues (pole) design. The IDOB is capable to reduce the influences of noise than the MDOB via $(\bar{\boldsymbol{A}} - \boldsymbol{H}\bar{\boldsymbol{C}})$. The IDOB is designed by using pole placement methods; therefore, the observable of the extended system is a must.

The observability matrix, which guarantees for the observable on the extended systems, is given by

$$\mathrm{rank}\boldsymbol{U}_o = n_x, \tag{2.13}$$

where $\boldsymbol{U}_o = [\bar{\boldsymbol{C}} \quad \bar{\boldsymbol{C}}\bar{\boldsymbol{A}} \quad \bar{\boldsymbol{C}}\bar{\boldsymbol{A}}^2]^{\mathrm{T}}$ and n_x denotes the number of state variables. The observable of the extended model is given by

$$\mathrm{rank}\boldsymbol{U}_o = \mathrm{rank}\begin{bmatrix} 1 & 0 & 0 \\ 0 & 1 & 0 \\ 0 & -c/J & -1/J \end{bmatrix} = n_x. \tag{2.14}$$

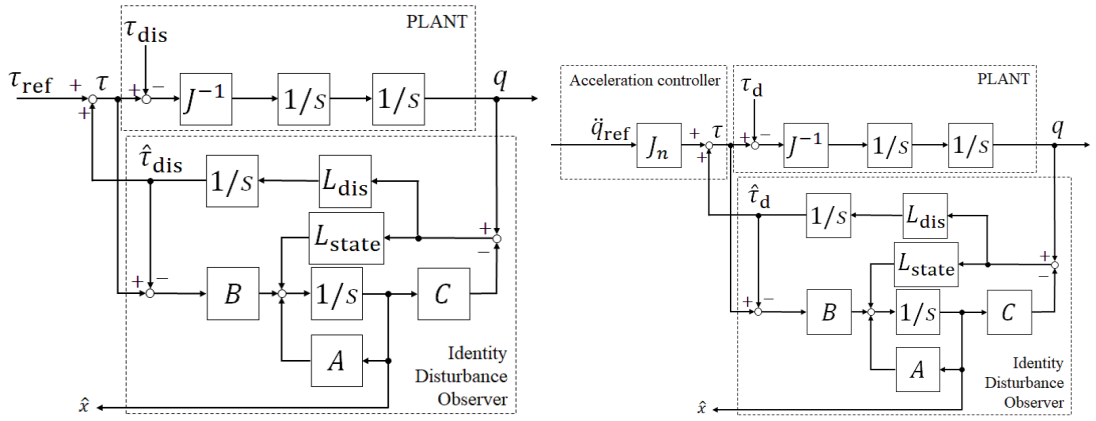

(a) disturbance suppression (b) acceleration controller

FIGURE 2.3: Block diagram of IDOB

Therefore, the extended model is observable, and the IDOB can be designed using pole placement methods. On the other hand, the observability of the IDOB can also be compensated by $\det(\boldsymbol{U}_o) \neq 0$. Additionally, the observability of the extended model follows the observability of the original state-space model.

As with the MDOBs, the IDOB can handle the acceleration control. Fig. 2.3 shows the IDOB-based acceleration control. IDOB can handle multi variables and its acceleration control in a single system. In order to design acceleration control by the IDOB, the disturbance estimation is defined as

$$\tau_{\mathrm{d}} = -\tau_{\mathrm{dis}} - c\dot{q}. \tag{2.15}$$

Additionally, the system matrix of the IDOB is defined as $\boldsymbol{A} = \begin{bmatrix} 0 & 1 \\ 0 & 0 \end{bmatrix}$.

2.2.3.1 Design of discrete-time IDOB

Standard MPCs are defined by discrete-time systems. Therefore, to integrate IDOB into discrete-time control systems, the design of discrete-time IDOB is described in this section.

The sampling time is defined as T_s [s]. Using the sampling time and zero-order hold, the continuous-time state-space model (Eqs. (2.2) and (2.3)) can be transformed to the discrete-time state-space model, which can be defined as

$$\boldsymbol{x}(k+1) = \boldsymbol{A}_d\boldsymbol{x}(k) + \boldsymbol{B}_d u(k), \tag{2.16}$$

$$y(k) = \boldsymbol{C}_k\boldsymbol{x}(k). \tag{2.17}$$

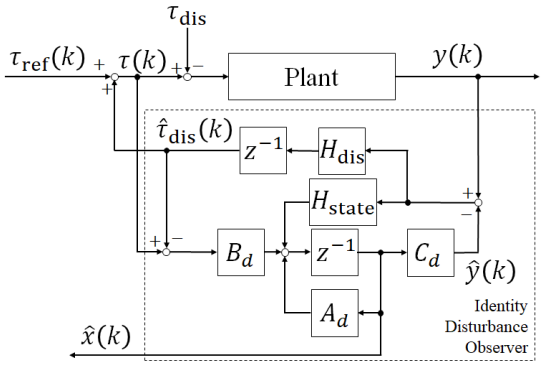

FIGURE 2.4: Block diagram of discrete-time IDOB

where $\boldsymbol{A}_d$, $\boldsymbol{B}_d$, and $\boldsymbol{C}$ denote coefficient matrices in the discrete-time state-space model, respectively.

In discrete-time systems, the step-type disturbance model is given by

$$\tau_{\text{d}}(k+1) = \tau_{\text{d}}(k). \tag{2.18}$$

Using the discrete-time models, the extended state-space model in discrete-time can be described as

$$\bar{\boldsymbol{x}}(k+1) = \bar{\boldsymbol{A}}_d\bar{\boldsymbol{x}}(k) + \bar{\boldsymbol{B}}_d u(k), \tag{2.19}$$

$$y(k) = \bar{\boldsymbol{C}}_d\bar{\boldsymbol{x}}(k), \tag{2.20}$$

where $\bar{\boldsymbol{A}}_d = \begin{bmatrix} \boldsymbol{A}_d & -\boldsymbol{B}_d \\ \boldsymbol{0} & 1 \end{bmatrix}$, $\bar{\boldsymbol{B}}_d = \begin{bmatrix} \boldsymbol{B}_d & 0 \end{bmatrix}^{\text{T}}$, and $\bar{\boldsymbol{C}}_d = \begin{bmatrix} \boldsymbol{C}_d & 0 \end{bmatrix}$, respectively.

If the extended model has observability, the discrete-time IDOB can design.

The discrete-time IDOB can be described as

$$\bar{\boldsymbol{x}}(k+1) = (\bar{\boldsymbol{A}}_d - \boldsymbol{H}\bar{\boldsymbol{C}}_d)\bar{\boldsymbol{x}}(k) + \bar{\boldsymbol{B}}_d u(k) + \boldsymbol{H}\boldsymbol{y}(k), \tag{2.21}$$

$$= (\bar{\boldsymbol{A}}_d - \begin{bmatrix} \boldsymbol{H}_{\text{state}} \\ \boldsymbol{H}_{\text{dis}} \end{bmatrix}\bar{\boldsymbol{C}}_d)\bar{\boldsymbol{x}}(k) + \bar{\boldsymbol{B}}_d\tau(k) + \begin{bmatrix} \boldsymbol{H}_{\text{state}} \\ \boldsymbol{H}_{\text{dis}} \end{bmatrix}\boldsymbol{y}(k), \tag{2.22}$$

where $\boldsymbol{H}$ denotes the observer gain matrix in the discrete-time IDOB. In the design of discrete-time IDOB, the observability of the extended model is a must. The guarantee the observability follows Eqs. (2.13) and (2.14). Fig. 2.4 shows the block diagram of the discrete-time IDOB. In the rest of this dissertation, the discrete-time IDOB are handled as the IDOB.

2.3 Robust constrained motion control against disturbance

In this section, a constrained motion control method based on the integration of IDOB and MPC is described. MPC can be expected to make high control performance near the limit of mechanical and mathematical performances, considering these constraints. However, the control close to the limit value of the constraint always has the problem that constraint violation due to the influence of disturbance. In the constraint violation situation, MPC falls into an unstable state with no optimal control input, and the advantage of being able to consider constraints is lost. In a general MPC system, the disturbance is canceled because it contains an integrator for calculating the control input. However, the cancel speed is sluggish and tracking errors remain due to the influence of disturbance. This problem is an obstacle to achieving high control performance by MPC.

Additionally, many studies of guarantee of nominal stability of MPC use a nominal plant model. For assisting the stability of MPC, the nominalization method is a must. Some studies suggest that offset-free MPC (robust MPC) can be implemented by output disturbance observers. In order to design offset-free MPCs, it is required as many disturbance estimation variables as there are state variables. Additionally, observation of the state variables is also needed. Also, the estimated disturbance in offset-free MPC is used to compensate for prediction trajectory or reference trajectory. Therefore, it does not use to directly nominal the plant model. Furthermore, implementing acceleration control, which is important for motion control systems, is challenging. Therefore, in this section, controller integration design methods that take advantage of the disturbance observer are proposed.

Therefore, by using IDOB, this section describes an MPC with offset-free characteristics and disturbance suppression. The DOBs can definitely assist to realizes the nominal control performance of MPCs. Generally, offset-free MPC is described as output disturbance estimation rejection in reference trajectory. In this chapter, nominalization of MPC systems is focused and DOBs for input disturbance estimation are used. High-bandwidth MDOB, which has been widely used for disturbance estimation, has the advantage of being able to perform fast disturbance estimation, and a robust control system can be constructed by directly canceling the disturbance. Some studies in MPC with DOB are being conducted to eliminate and suppress disturbance. The conventional DOB control directly removes the disturbance estimate for the real disturbance. The direct disturbance cancellation occasionally makes unexpected motion such as vibration, noise, etc. In that case, the control performance deteriorates. When used in combination with an MPC that operates near the limit value, conventional DOB control may cause constraint violation due to the influence of vibration and noise.

In this method, in contrast to many conventional DOB controls, the disturbance estimate is not directly canceled against the actual disturbance. For canceling and suppressing the input and

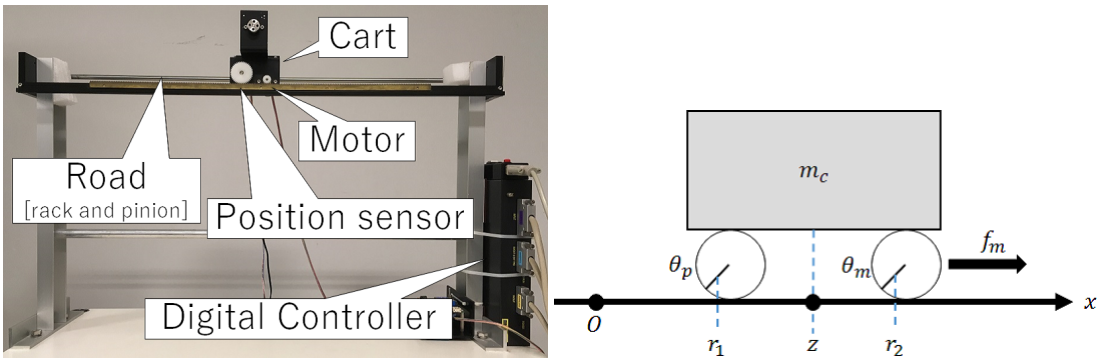

(a) cart robot (b) model description

FIGURE 2.5: Experimental system

output disturbance, the extended state-space system including the disturbance is regarded as the internal model, the optimization control problem of MPC is formulated. By the extended system as the internal model, the disturbance is suppressed via the optimization of the control input even for the system with oscillation or vibration. The coefficient matrices of the extended system used in the IDOB design are used for the design of the prediction model. However, the output matrix ($\boldsymbol{C}_{\mathrm{MPC}}$) for designing MPCs is redefined as full state observation based on the estimates of IDOB, and the disturbance is also included in the control variables. The MPC includes pseudo-feedback control on the disturbance and derives the optimal control input that indirectly suppresses and eliminates the influence of the disturbance. In this method, except for using the extended system for the internal model, it basically follows the design method found in many studies and does not perform optional special design.

2.3.1 Mathematical modeling

This section introduces the mathematical model of the plant.

MPC prediction and IDOB estimation are governed by the mathematical model. The plant is a simple one degree of freedom mass-damper system as a cart, and the physical parameters of the mathematical model are defined in Fig. 2.5 and Table 2.1. The position of the cart (z) is given by

$$z = r_1\theta_p \tag{2.23}$$

$$z = r_2\theta_m \tag{2.24}$$

The driving force is given by

$$f_m = \frac{\tau}{r_2}. \tag{2.25}$$

The motion equations of the motor and the cart can be described as

$$J\ddot{\theta}_m + C_m\dot{\theta}_m = \tau - \tau_{ex} \tag{2.26}$$

$$m_c\ddot{z} + C_c\dot{z} = \frac{\tau_{ex}}{r_2} \tag{2.27}$$

From Eq. (2.24), we obtain

$$\theta_m = \frac{z}{r_2}. \tag{2.28}$$

Substituting Eq. (2.28) into Eq. (2.25), we have

$$\frac{J}{r_2}\ddot{z} + \frac{C_m}{r_2}\dot{z} = \tau - \tau_{ex}. \tag{2.29}$$

Dividing both sides of Eq. (2.29) by r_2, it is given by

$$\frac{J}{r_2^2}\ddot{z} + \frac{C_m}{r_2^2}\dot{z} = \frac{\tau}{r_2} - \frac{\tau_{ex}}{r_2}. \tag{2.30}$$

Adding Eqs. (2.27) and (2.30),

$$(m_c + \frac{J}{r_2^2})\ddot{z} + (C_c + \frac{C_m}{r_2^2})\dot{z} = \frac{\tau}{r_2} = f_m. \tag{2.31}$$

Defining $m_c + \frac{J}{r_2^2} = M$ and $C_c + \frac{C_m}{r_2^2} = C$, the motion equation can be described as

$$M\ddot{z} + C\dot{z} = f_m. \tag{2.32}$$

Moreover, the state space model of the cart is derived. From Eq. (2.32), we obtain

$$\frac{dv}{dt} = \dot{v} = -\frac{C_c}{M}v + \frac{1}{M}f_m, \tag{2.33}$$

where each variable denotes mass (= M), viscous friction (= C_c), position (= z), velocity (= v) and the state variable ($x = [z \quad v]^{\mathrm{T}}$). The state space model can be described as

$$\dot{x} = \begin{bmatrix} \dot{z} \\ \dot{v} \end{bmatrix} = \begin{bmatrix} 0 & 1 \\ 0 & -\frac{C_c}{M} \end{bmatrix}\begin{bmatrix} z \\ v \end{bmatrix} + \begin{bmatrix} 0 \\ \frac{1}{M} \end{bmatrix} f_m \tag{2.34}$$

$$y = \begin{bmatrix} 1 & 0 \end{bmatrix}\begin{bmatrix} z \\ v \end{bmatrix}. \tag{2.35}$$

TABLE 2.1: Parameter definition of the cart

m_c	Mass
z	Position
v	Velocity
r_1	Radius of the front wheel
r_2	Radius of the rear wheel
θ_p	Angle of the front wheel
θ_m	Angle of the rear wheel
C_c	Viscous friction of the system
C_m	Viscous friction of the motor
τ_{ex}	External forces
τ	Torque
J	Motor inertia
f_m	Driving force

2.3.2 Output disturbance estimation

The disturbance estimated by IDOBs is explained. The extended system assuming only the input disturbance was shown. In the extended system, the influences of the output disturbance are explained.

A state-space model with input and output disturbances (d_i and d_o) can be described as

$$\dot{\boldsymbol{x}} = \boldsymbol{A}\boldsymbol{x} + \boldsymbol{B}u - \boldsymbol{B}d_i \tag{2.36}$$

$$y(k) = \boldsymbol{C}\boldsymbol{x} + d_o \tag{2.37}$$

Applying the KFD to this system, the disturbance estimates ($\hat{d}$) are given by

$$\hat{d} = d_i + P(s)^{-1}d_o, \tag{2.38}$$

where, $P(s) = \{s(Ms + C_c)\}^{-1}$.

From (2.38), the IDOBs including the KFDs can handle the influences of all disturbance as the input disturbance estimates in theory. In particular, if the output disturbance can be defined as time-invariant, the disturbance estimates can be described as

$$\hat{d} = d_i + s(Ms + C_c)d_o = d_i + (Ms + C_c)\dot{d}_o = d_i \tag{2.39}$$

The influences of the time-invariant output disturbance do not appear in the disturbance estimates.

2.3.3 Linear model predictive control

2.3.3.1 Outline of model predictive control scheme

Preliminaries on problems to apply MPCs in motion control systems are explained. In the case of single-input/single-output (SISO) systems, its control variables, and manipulated variables can theoretically be perfectly tracked by using the inverse model. By contrast, in the case of multi-input/multi-output(MIMO) systems, tracking system design is challenging unless a high-precision servo system or perfect tracking control[59] can be constructed. In order to control MIMO systems, the method of solving the infinite time-optimal control problem by the Riccati equation, which is a linear quadratic regulator (LQR), had been developed in the 1960s. Then, the concept of MPC[60, 61], which is the optimal control theory in finite-time optimization, was developed in the 1970s. In this thesis, an MPC, which optimizes control input variation, as standard MPC. The MPC can directly handle to suppression of sudden change of control inputs by external disturbances based on weighted design, in contrast to MPC that optimizes control input. Fig. 2.6 shows the basis graphical concept of the standard MPC. MPC is a control method to optimize control inputs from the current time k to the finite-time $k+N_u$. N_u is a control horizon that denotes the number of steps that allow the change of the control inputs. In order to optimize

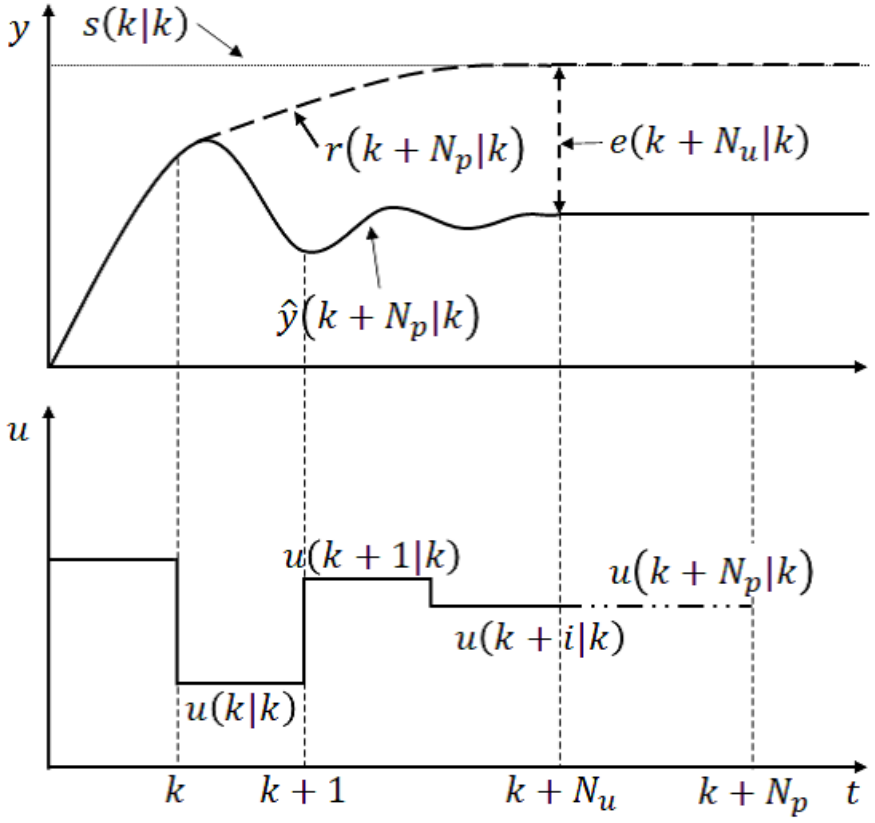

FIGURE 2.6: Outline control law of MPC systems

the control inputs, minimization of tracking-error predictions is used based on a model of plants. The predicted trajectories is for finite-time horizon (k to $k + N_p$, where N_p denotes prediction steps). In the control law, the optimum amount of change in the control input is constant from $k + N_u$ to $k + N_p$. In order for the control variables to track set values $s_{(k+N_p|k)}$, which denotes global reference values, a reference trajectory $r_{(k+N_p|k)}$in the prediction horizon is tracked. Using a predicted control output that minimizes the total prediction tracking error, the control inputs are determined by the optimization problem. Then, the first element of the optimal control input trajectory is applied to plants. MPC sequentially calculates this scheme for each sampling time.

General MPCs [17, 23] have characteristics as follows:

- Multivariable control system can be controlled
- Input and output constraints of plants explicitly can be handled
- Future behavior is predicted
- The computational load is heavy and a long sampling time is require
- Control performance is depended on internal models.
- In theory, various mathematical models can be applied

Additionally, a feature of MPC is that the optimization control problem can express quadratic programming (QP) problems. QP problems can easily formulate constrained optimization problems. In MPC systems, this constraint can directly impose on the input and output variables of plants depending on modeling. Utilization to the advantages, many studies on MPC have been carried out on mechatronic and robotics systems in motion control. The basic LMPC is described. In this study, the model of the plant is described as linear models; therefore, the linear MPC is used in the actuator control system. Note that, LMPC is a simple control method; therefore, the LMPC-based proposed system can easily expand to other systems.

2.3.3.2 Outline of optimization control problem

In this chapter, the control problem for MPCs is defined for a servo problem for $\boldsymbol{x}$. Additionally, the decision variables as the optimize parameters are defined as the future trajectory of the difference of the control input Δu. The optimization control problem for tracking control of linear systems is used and is given by

$$J = \sum_{i=1}^{N_p} \|r(k+i|k) - y(k+i|k)\|_Q^2 + \sum_{i=0}^{N_u-1} \|\Delta u(k+i|k)\|_R^2 \tag{2.40}$$

where k denotes the current sampling instant, and $\|\boldsymbol{\alpha}\|_X^2 = \boldsymbol{\alpha}^T X \boldsymbol{\alpha}$. $r(k+i|k)$ and $y(k+i|k)$ denote the desired and predicted control variables in $k+i$. Q and R are the weight matrices for tracking error and control input, N_p and N_u denote prediction and control horizons. Note that, in this chapter, the DOB for guaranteeing robustness is introduced to the control system as an inner-loop controller. Therefore, the control input obtained from the MPC (u) is not available as the current input torque $\tau(k)$. Moreover, the u is integral of optimized control input variation; therefore, the MPC has an integrator in the output of the controller. This integrator performs the control input generation. However, it cannot provide the disturbance rejection performance because the integrator is not handled tracking-error information.

Additionally, the bounded constraints can be imposed for $\boldsymbol{x}$ and u. The constraints are given by

$$\begin{aligned} \boldsymbol{x}_{\text{low}} &\leq \boldsymbol{x}(k+i|k) \leq \boldsymbol{x}_{upp}, \quad i = 1, 2, ..., N_p \\ u_{\text{low}} &\leq u_{\text{MPC}}(k+i|k) \leq u_{upp}, \quad i = 0, 1, ..., N_u - 1 \\ \Delta u_{\text{low}} &\leq \Delta u(k+i|k) \leq \Delta u_{upp}, \quad i = 0, 1, ..., N_u - 1 \end{aligned} \tag{2.41}$$

where $*_{\text{low}}$ and $*_{\text{upp}}$ denote the lower and upper bounds on each variable. The MPC minimizes Eq. (3.12) and optimizes the difference of the control input $\Delta u(k)$. Moreover, the control input obtained from the MPC can be described as

$$u(k) = u(k-1) + \Delta u(k). \tag{2.42}$$

By using IDOB, the state estimates can be used in LMPC systems; therefore, the state estimates($\hat{x}$) by IDOB are used as control variables ($\hat{y}$).

The predicted state trajectory $\boldsymbol{Z}(k)$ from the current time k to the prediction horizon N_p is given by

$$\boldsymbol{Z}(k) = \begin{bmatrix} \hat{\boldsymbol{x}}(k+1|k) \\ \vdots \\ \hat{\boldsymbol{x}}(k+N_p|k) \end{bmatrix} = \boldsymbol{\Psi}\boldsymbol{x}(k) + \boldsymbol{\Gamma}u(k-1) + \boldsymbol{\Theta}\Delta\boldsymbol{U}(k), \tag{2.43}$$

where, $\boldsymbol{\Psi}$, $\boldsymbol{\Gamma}$, and $\boldsymbol{\Theta}$ denote the matrices for prediction.

Then, the predicted tracking error trajectory $\boldsymbol{\varepsilon}(k)$ is given by

$$\boldsymbol{\varepsilon}(k) = \boldsymbol{T}_{ref}(k) - \boldsymbol{\Psi}\hat{x}(k) - \boldsymbol{\Gamma}u(k-1) \tag{2.44}$$

where $\boldsymbol{T}_{ref}$ is a reference trajectory.

Using each trajectory, the optimization problem can be transformed as

$$\begin{aligned} &\underset{\Delta U}{\text{minimize.}} \quad \boldsymbol{V}(k) = -\Delta \boldsymbol{U}^{\mathrm{T}}(k)\boldsymbol{G} + \Delta \boldsymbol{U}^{\mathrm{T}}(k)\boldsymbol{H}\Delta \boldsymbol{U}(k) \\ &\text{subject to.} \quad \boldsymbol{\Omega}\Delta \boldsymbol{U}(k) \leq \boldsymbol{\omega} \end{aligned}$$

$$\Delta \boldsymbol{U}(k) = \begin{bmatrix} \Delta u(k|k) \\ \vdots \\ \Delta u(k+N_u-1|k) \end{bmatrix}$$

$$\boldsymbol{G} = 2 \cdot \boldsymbol{\Theta}^{\mathrm{T}} \cdot \boldsymbol{Q} \cdot \boldsymbol{\varepsilon}(k)$$

$$\boldsymbol{H} = \boldsymbol{\Theta}^{\mathrm{T}} \cdot \boldsymbol{Q} \cdot \boldsymbol{\Theta} + \boldsymbol{R}$$

where, the optimal control input is obtained by accumulating the first element ($\hat{\Delta u}(k|k) = \Delta u$) of ΔU. Based on [17], each variable is defined as $\Psi = \begin{bmatrix} \boldsymbol{A}_d \\ \vdots \\ \boldsymbol{A}_d^{N_u} \\ \vdots \\ \boldsymbol{A}_d^{N_p} \end{bmatrix}$, $\Gamma = \begin{bmatrix} \boldsymbol{B}_d \\ \vdots \\ \sum_{i=0}^{N_u} \boldsymbol{A}_d^i \boldsymbol{B}_d \\ \vdots \\ \sum_{i=0}^{N_p-1} \boldsymbol{A}_d^i \boldsymbol{B}_d \end{bmatrix}$, $\Theta = \begin{bmatrix} \boldsymbol{B}_d & \dots & 0 \\ \boldsymbol{A}_d\boldsymbol{B}_d + \boldsymbol{B}_d & \dots & 0 \\ \vdots & \ddots & \vdots \\ \sum_{i=0}^{N_u-1} \boldsymbol{A}_d^i \boldsymbol{B}_d & \dots & \boldsymbol{B}_d \\ \sum_{i=0}^{N_u} \boldsymbol{A}_d^i \boldsymbol{B}_d & \dots & \boldsymbol{A}_d\boldsymbol{B}_d + \boldsymbol{B}_d \\ \vdots & \vdots & \vdots \\ \sum_{i=0}^{N_p-1} \boldsymbol{A}_d^i \boldsymbol{B}_d & \dots & \sum_{i=0}^{N_p-N_u} \boldsymbol{A}_d^i \boldsymbol{B}_d \end{bmatrix}$, where $\boldsymbol{A}_d$ and $\boldsymbol{B}_d$ denote discretized system and input matrices. Ω and ω denote the matrix and vector reflecting the constraints.

2.3.4 Preliminary experiment

In this section, the effectiveness of the simple integrated system of the LMPC and the IDOB are shown. Additionally, a fast implementation method is provided. In order to confirm the feasibility of the integration methods, some experiments of position control of the cart system were carried out. The experimental conditions of the experiments are as follows;

1. Position control with velocity and control input constraints, ($N_p = 100$, and $N_u = 3$),
2. Position control with position, velocity, and control input constraints, ($N_p = 30$, and $N_u = 3$).

In all experiments, the position reference was set to 0.1 [m]. The velocity and control input constraints were set to 1.0 [m/s] and 2 [N]. The control input constraint was defined by covering the actuator limit value 2.074 [N]. In the second experiment, the position constraint is imposed with $z_{ref}/2$ [m]. Additionally, the weight matrices on MPC were set to $\boldsymbol{Q} = \mathrm{diag}(10^2, 1)$ and the weight $R = 1$.

In the experiment, the sampling time of the control system is 1 [ms]. Each system was implemented by a digital signal processor (sBOXII by MIS Corporation) via MATLAB coder by Mathworks Inc. Moreover, Hildreth's QP algorithm was used to solve the MPC problem.

However, the MPC has a computational load problem. In order to implement the control system with 1 [ms], the constraints and iteration number were reduced. In contrast to conventional design, the state constraints (position or velocity constraints) are reduced to 8 steps on prediction. Additionally, the number of iterations of the QP solver is limited by 60 steps, and the maximum permissible error is set to 10^{-8}.

The experimental results are shown in Figs. 2.7 and 2.8. The results show the effectiveness of the MPC with respect to the constraints. Moreover, it is confirmed that the MPC systems can consider the control input and output constraints.

On the other hand, the simple integrated system has the problem of control input constraints. In this system, the actual control input ($\tilde{u}$) can be described as

$$\tilde{u}(k) = u(k) + \hat{d}(k) = u(k-1) + \Delta u(k) + \hat{d}(k). \tag{2.45}$$

The control input constraints on the MPC are imposed on the MPC output (Δu); however, the actual control input consists of the sum of the MPC output and disturbance estimates. To address the problem, the two solutions are proved in this chapter. One is a modification of the optimal control problem by using the disturbance estimates and models, and another one is a utilization of a time-varying constraint modified by current disturbance estimates.

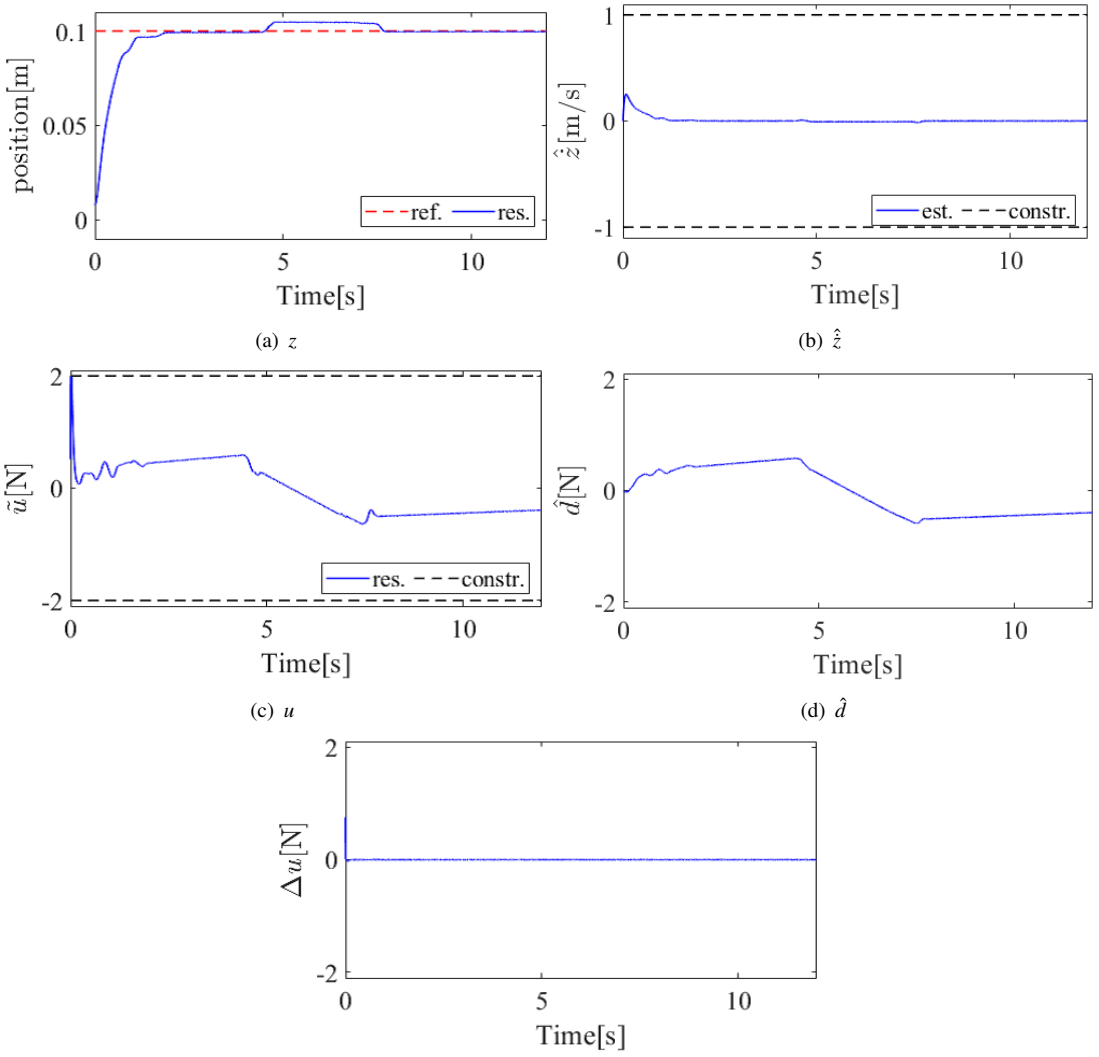

(a) z (b) $\hat{z}$

(c) u (d) $\hat{d}$

(e) Δu

FIGURE 2.7: Experimental results: Position control with velocity and control input constraints using long prediction horizon.

In particular, the second result is indicated that the constraints are preferred to the references in MPC control systems. Additionally, the robot has gear on the actuator. On the motion with constraint boundary, the gear ratio and resolution generate vibration and numerical instability in the control system. Therefore, it is evident that the bounded motion control systems must consider the noise influences and sensor resolution. Chapter 4 presented the solution to address the noise problem.

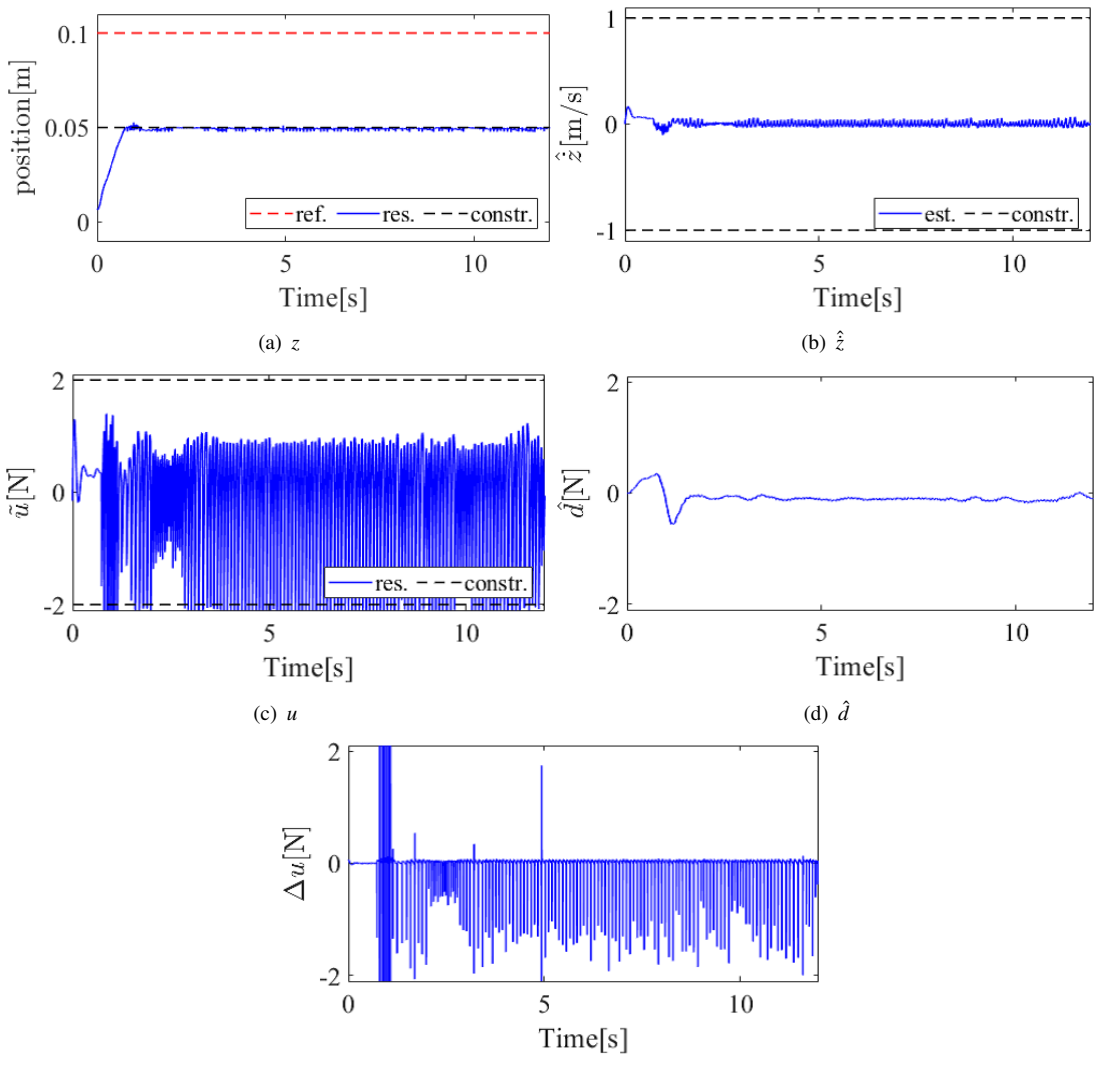

(a) z (b) $\hat{\dot{z}}$

(c) u (d) $\hat{d}$

(e) Δu

FIGURE 2.8: Experimental results: Position control with position, velocity, and control input constraints.

2.3.5 Model predictive control with disturbance suppression[62]

In contrast to the conventional method, the MPC explained in this section uses the extended model including disturbance as the internal model. The state vector of the extended model is defined by $\bar{\boldsymbol{x}} = [z \quad v \quad \hat{d}]^{\mathrm{T}}$, and the extended model is given by

$$\bar{\boldsymbol{x}}(k+1) = \begin{bmatrix} \boldsymbol{A}_d & -\boldsymbol{B}_d \\ \boldsymbol{0} & 1 \end{bmatrix} \bar{\boldsymbol{x}}(k) + \begin{bmatrix} \boldsymbol{B} \\ 0 \end{bmatrix} f_m(k) \tag{2.46}$$

$$y = \begin{bmatrix} \boldsymbol{C}_d & 0 \end{bmatrix} \bar{\boldsymbol{x}}(k) \tag{2.47}$$

where, $\boldsymbol{A}_d$, $\boldsymbol{B}_d$, and $\boldsymbol{C}_d$ denote the discretized coefficient matrix of the system (Eqs. (2.34) and (2.35)).

The MPC treats all extended state variables as control variables. Moreover, the control law is given by

$$J = \sum_{i=1}^{N_p} \|\boldsymbol{r}(k+i|k) - \bar{\boldsymbol{x}}(k+i|k)\|_Q^2 + \sum_{i=0}^{N_u-1} \|\Delta u(k+i|k)\|_R^2. \tag{2.48}$$

where $\boldsymbol{r}$ denotes the reference for the extended state vector.

Therefore, the control variables can include the disturbance estimates. The tracking error between the disturbance set-point value (= 0) and the estimated value (= $\hat{d}$) should be minimized while optimizing the control input. Therefore, the control input considered the tracking error is derived. Note that is the well-known fact that the error is never minimized because the disturbance is not controllable. However, the proposed method can indirectly suppress the influence of the disturbance by constructing a pseudo-feedback loop using the optimization problem minimizing the error of the disturbance.

The constraint violation creates a solution, ”no solution". The available solution is a must for online MPC systems. To avoid the problem, this chapter uses a countermeasure using iterative methods among several available methods. The iterative method solves the optimization method by using the iterative step of searching for the optimal solution, and the interactive solution approaches an actual solution. Therefore, the interactive solution has the ability to approximately behave as the optimal solution. Note that the approximate solution frequently violated the constraints. The MPC system using the approach can handle the constraint violations. Moreover, in the proposed method, the constraint violations by external and internal disturbances are considerably reduced by the disturbance estimates. Thus, the infeasible or unsatisfactory solutions as control inputs are reduced.

Additionally, the optimization control problem calculates the control input rate Δu. Δu is then used by the accumulator to derive the control input. Thus, u is not clearly obtained from the

MPC. However, to solve the optimization control problem, the predicted state trajectory is used. Moreover, the predicted trajectory is used for optimizing the control input rate. Therefore, the control input is always considered in the solved control problem. Through this scheme, the MPC can handle control input constraints directly. In the light of this information, the optimization control problem with disturbance estimates can explicitly cancel the disturbance by using the control inputs with disturbance estimates. However, in the case of implementation of the hard constraints, the imposed constraints have to be set tighter than the original.

2.3.6 Numerical verification: offset-free control under disturbance influence

The effectiveness of disturbance suppression by the proposed method is shown. Moreover, position control simulations of a simple mass-damper system with input and output disturbances are used to verify. In the verifications, the set points are set to [position(m), velocity (m/s), disturbance (N)] = [1, 0, 0]. By setting the disturbance reference to 0, the influence of input and output disturbances can be suppressed, and the offset-free characteristic of the proposed method can be shown. Additionally, MPC has the ability to activation of the constraints imposed on the state vector. Therefore, in some simulations, the constraints are imposed on the position (1m). By the constraints, overshoot motion is suppressed under disturbance-free situations.

In order to verify the effectiveness of the proposed method against disturbance by simulation, comparative verification shown in Table. reftable:teiann was carried out. The MPC used for comparison is general LMPC. Each tuning parameter has the same value as the proposed method, shown in Table 2.4.

In Table 2.2, (a) is the proposed method; (b) is the general MPC; (c) is the conventional DOB control and MPC that directly removes the disturbance. The comparison results are shown the effectiveness of the disturbance suppression function. The effectiveness of offset-free control by the proposed method can be quantitatively evaluated by comparing each result. The conditions of disturbance are set to 1) step type and 1N (10s) in plant input; 2) step type and 0.5N(10s) in plant output. The DOB in the verification (a, b, c) can estimate the stationary disturbance (d_i) at the input; however, it cannot estimate the effect of the stationary disturbance (d_o in 10s) at the output.

TABLE 2.2: Simulation conditions

	Estimation	MPC	Disturbance rejection	Output disturbance	Constraint
(a)	DOB	prop.	proposed	Const.	reference position
(b)	OB*	conv.	Non	Const.	reference position
(c)	DOB	conv.	conv.	Const.	reference position

where, *:OB denotes normal state observer.

TABLE 2.3: Parameters of DOB

Pole $\boldsymbol{p}$	[0.80 0.82 0.84]
Sampling time δ_1[s]	0.01

TABLE 2.4: Parameters of MPC

Weight matrix on tracking error $\boldsymbol{Q}_m$	diag(10^2 10^1 10^{-2})
Last of weight matrix on tacking error $\boldsymbol{Q}_{m-last}$	$3 \times \boldsymbol{Q}_m$
Weight on control input rate R_m	10^{-1}
Each horizon $[N_p \quad N_u]$	[20 5]
Sampling time for control δ_2[s]	0.10

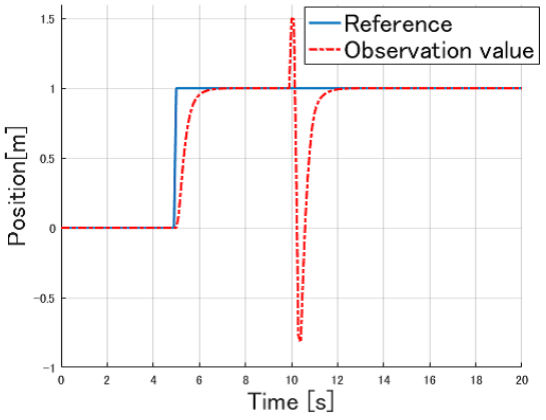

FIGURE 2.9: Simulation results: position (proposed:(a))

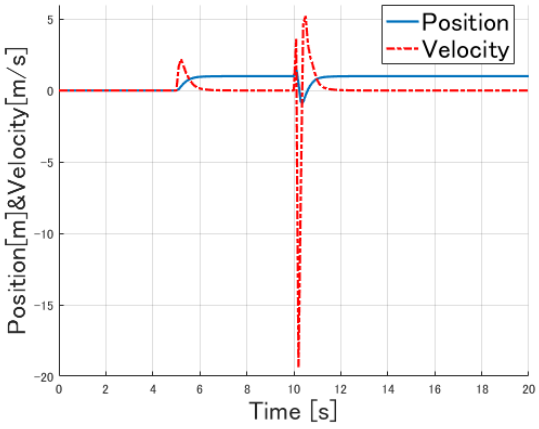

FIGURE 2.10: Simulation results: state estimates by IDOB (proposed:(a))

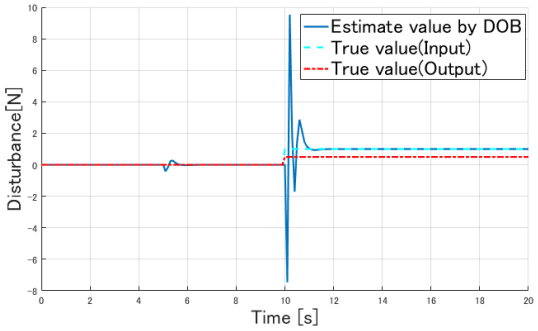

FIGURE 2.11: Simulation results: disturbance estimates by IDOB (proposed:(a))

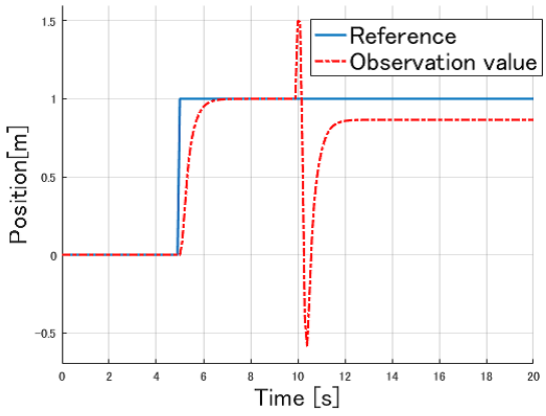

FIGURE 2.12: Comparison result (b) : position

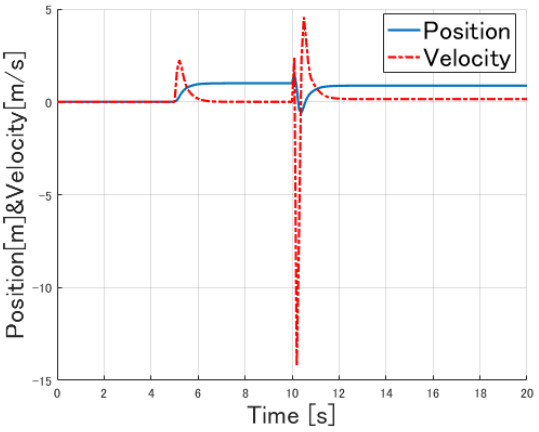

FIGURE 2.13: Comparison result (b) : State estimates by OB

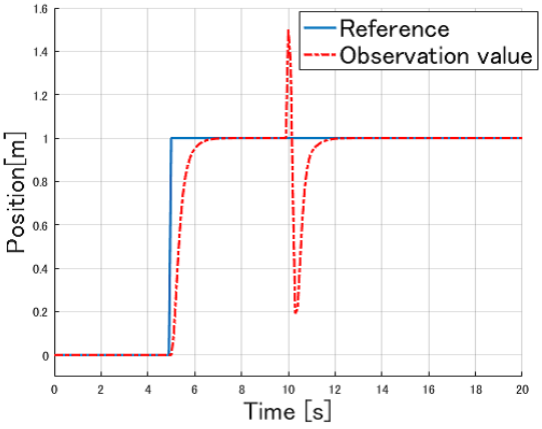

FIGURE 2.14: Comparison result (c) : position

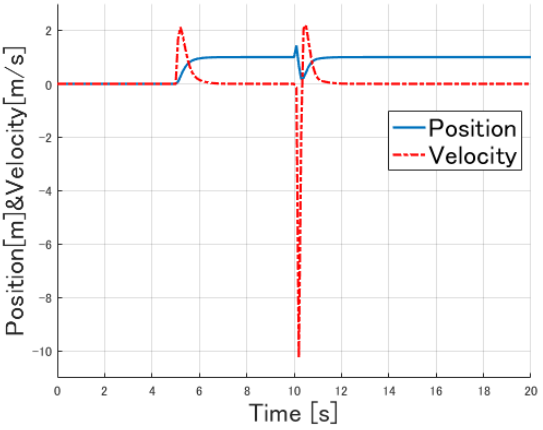

FIGURE 2.15: Comparison result (c) : state estimates by IDOB

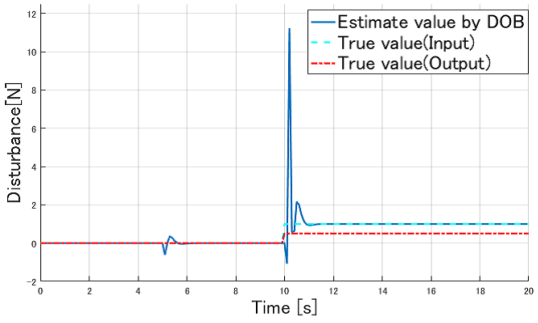

FIGURE 2.16: Comparison result (c) : disturbance estimates by IDOB

2.3.6.1 Controller setup

Tables 2.3 and 2.4 shows the parameters of the control systems. The parameters for DOB and MPC were empirically determined by trial and error. The prediction and control horizons are

designed in consideration of tracking performance and computational load. Furthermore, in order to improve the control performance, only a last weight matrix of $\boldsymbol{Q}$ and $\boldsymbol{R}$ set to tripled from the normal weight. The setup is based on a terminal cost function. $\boldsymbol{Q}_{mpc}$ and $\boldsymbol{R}_{mpc}$ are set to

$$\boldsymbol{Q}_{mpc} = \begin{bmatrix} \boldsymbol{Q}_m & & 0 \\ & \ddots & \\ 0 & & \boldsymbol{Q}_{m-last} \end{bmatrix}, \text{and } \boldsymbol{R}_{mpc} = \begin{bmatrix} \boldsymbol{R}_m & & 0 \\ & \ddots & \\ 0 & & \boldsymbol{R}_m \end{bmatrix} \in \mathbb{R}^{10\times 10}.$$

2.3.6.2 Results

Figs. 2.9-2.11 show the results of the proposed method in (a). Fig. 2.9 shows the reference and response of the position. Fig. 2.10 shows the estimated state by DOB. Fig. 2.11 shows the estimates and real of input and output disturbances. The tracking control by the proposed method can be performed without steady-state error even after being affected by a strong disturbance. Compared to the results of the conventional method, the proposed method is the usefulness of removing the influence of the disturbance.

From Fig. 2.10, sudden vibrations in the state estimates can be seen in 10s. The vibrations are generated by applying a strong disturbance; however, it quickly converges to the set point. Therefore, it is evident that the tracking performance of the proposed method is useful. Additionally, a large velocity can be seen in 10 s. Then, it is trying to rapidly accelerate and follow the set value, the motion can suppress by imposing constraints on the motor output and speed.

From Fig. 2.11, it is confirmed that the disturbance estimates cannot be affected constant output disturbances. Moreover, the disturbance estimates are varied in 5s, owing to the control input for motion control by MPC. In the controller design, the variation of disturbance estimates by control input must be suppressed by tuning parameters for stability. In applications to actual systems, it is worthy of evaluation that the proposed method can obtain the same control performance without directly the disturbance rejection, unlike the conventional method. Moreover, since the proposed method MPC does not include a special design method, it can be expected to be applied to complicated systems and other model-based control methods. z Moreover, since the proposed

TABLE 2.5: Simulation results

	Tracking error	Estimation error
(a)	P	P
(b)	N	*
(c)	P	P

where, P and N denote positive and negative.

method MPC does not include a special design method, it can be expected to be applied to complicated systems and other MBDCs.

Figs. 2.12-2.16 show the comparison results in disturbance suppression ((b), (c)). Figs. 2.12-2.13 shows the results of general MPC system. The results indicate that MPC has the ability to suppress disturbance; however, its performance is not sufficient. The state variables have a steady-state tracking error while affecting the disturbance, and the performance of removing the steady-state deviation is inadequate. Therefore, it is evident that the proposed method can add the ability to remove the steady-state error owing to the influence of disturbance.

Figs. 2.14-2.15 show the results of MPC with DOB. In these results, by contrast to the proposed method, the disturbance estimate is directly canceled. From the results, it has the same performance on disturbance suppression as the proposed method. The direct disturbance rejection occasionally generates undesired motion. The proposed method can eliminate the undesired motion while keeping equivalent control performance. In particular, the proposed method has the ability of improved control performance in noisy environments, where disturbance estimates are significantly influenced by noise.

Overall, the proposed method can cancel and suppress the disturbances while considering control output constraints, and achieve offset-free control.

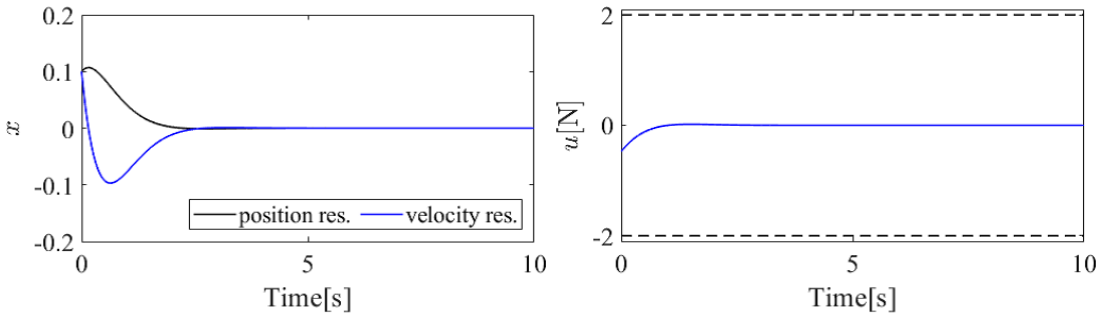

(a) state (b) control inputs

FIGURE 2.17: Simulation results(A): LQR

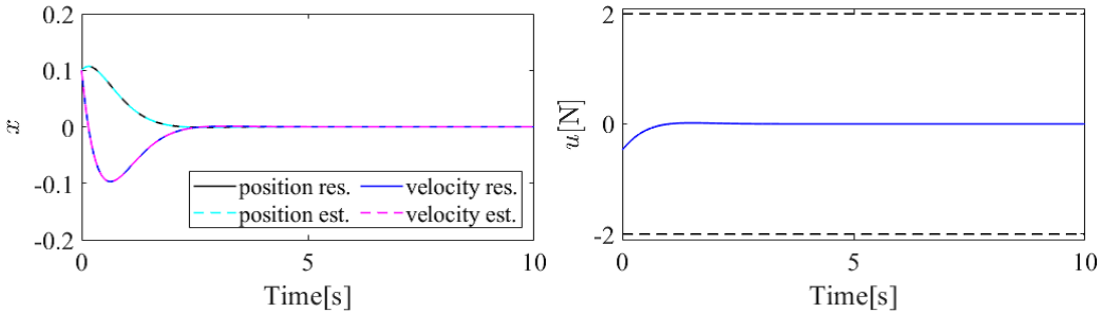

(a) state estimates (b) control inputs

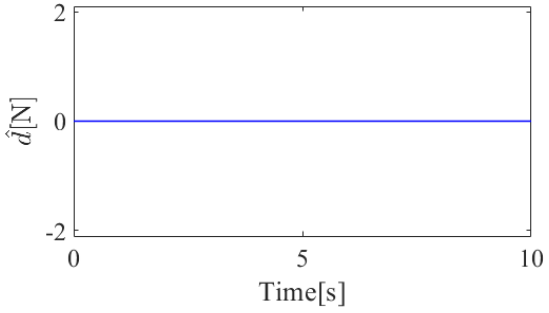

(c) disturbance estimate

FIGURE 2.18: Simulation results(A): LQR + IDOB

2.3.7 Numerical verification: control input and velocity constraints

In the previous section, the disturbance suppression performance of the proposed method under the state constraints is shown. In this section, the constrained control performances under the control input constraints and state constraints are verified.

Constrained state regulation simulations of the mass-damper system are used to verify the effectiveness of the proposed method. In the verifications, the initial state of the plant and IDOBs are set to [position(m), velocity (m/s)] = [0.1, 0.1]. Moreover, the constraints are imposed on velocity (= 1 m/s) and control inputs (= 2N).

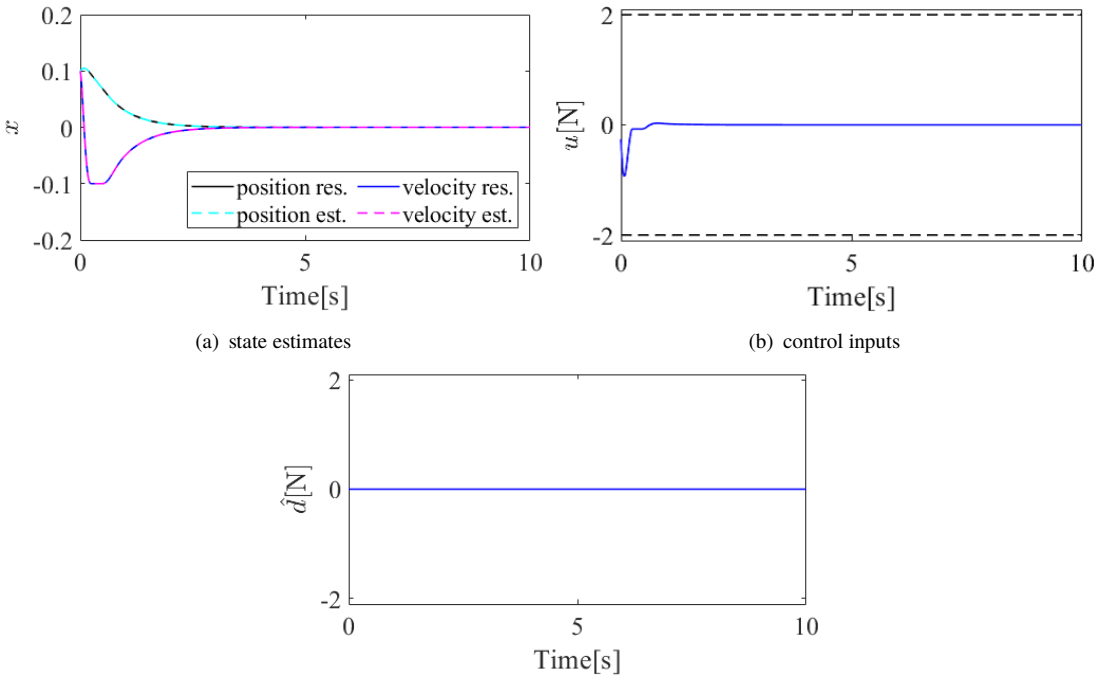

(a) state estimates

(b) control inputs

(c) disturbance estimate

FIGURE 2.19: Simulation results(A): constrained TPW-based MPC with IDOB

In the verification, an MPC with terminal penalty weights (TPW) [65] is used for designing the proposed methods. The TPW-based MPC has closed-loop stability when all constraints are not activated. Additionally, the response characteristic of the MPC can be approximated by LQR systems having the same weight matrices; therefore, tune-up and design are simple.

Considering the terminal penalty weight, the optimization control problem of the MPC can be desired as

$$J = \sum_{i=1}^{N_p-1} \|r(k+i|k) - y(k+i|k)\|_Q^2 + \sum_{i=0}^{N_p-1} \|\Delta u_{\mathrm{MPC}}(k+i|k)\|_R^2 + \|r(k+N_p|k) - y(k+N_p|k)\|_{Q_t}^2, \quad (2.49)$$

where, Q_t denotes the terminal penalty weight, and it is given by the Cholesky decomposition of the Riccati matrix of the approximated LQR[66]. As the drawback of this method, each horizon is set to the same horizon ($N_p = N_u$) for approximating the MPC systems by the LQR systems; therefore, the computational load is heavier than standard MPCs.

The verified disturbance conditions are as follows:

A without disturbance

B Step type disturbance: 1N (within the input constraints)

C Step type disturbance: 2N (Same as the input constraint)

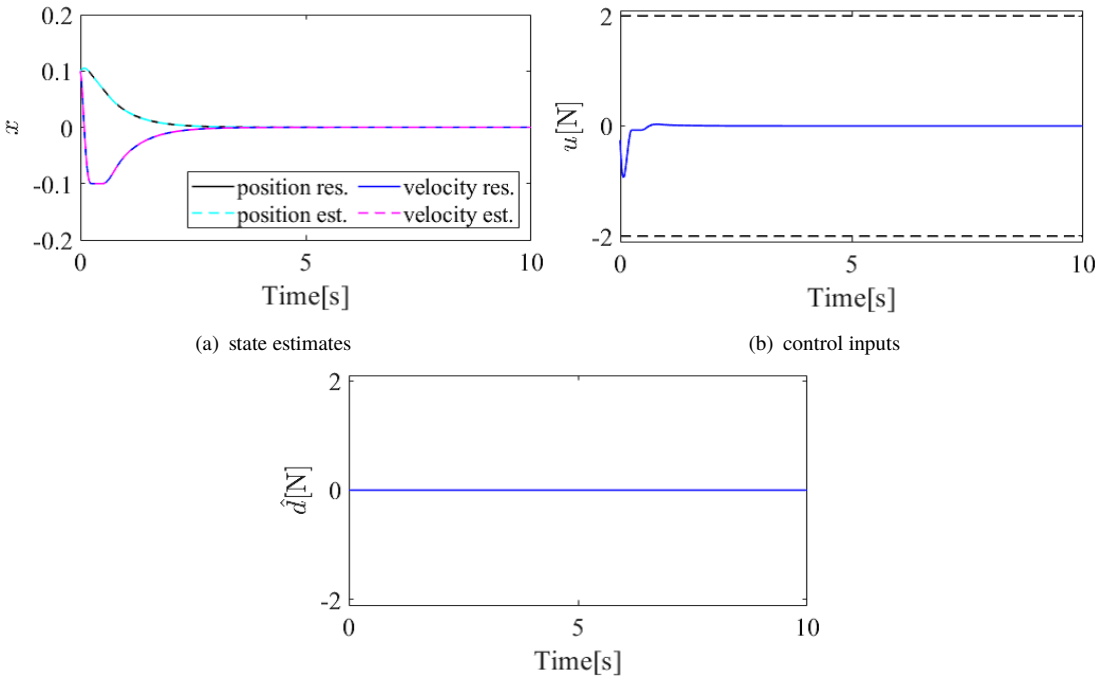

(a) state estimates

(b) control inputs

(c) disturbance estimate

FIGURE 2.20: Simulation results(A): constrained MPC with IDOB

D Parameter error: $j = 0.5J_n$

E Parameter error: $j = 1.5J_n$

Additionally, in order to verify the effectiveness of the proposed method, some control systems are compared:

- LQR
- LQR with IDOB
- TPW-based MPC with IDOB
- MPC with IDOB
- TPW-based proposed MPC using IDOB

Additionally, the first LQR system uses actual state information in the simulation.

2.3.7.1 Controller setup

The sampling time is set to 10 [ms]. The continuous poles of IDOB were set to [-8 -9 -10]. Moreover, the weights of the LQR and MPCs were set to $Q = \mathrm{diag}(1, 1)$ and $R = 1$. Additionally,

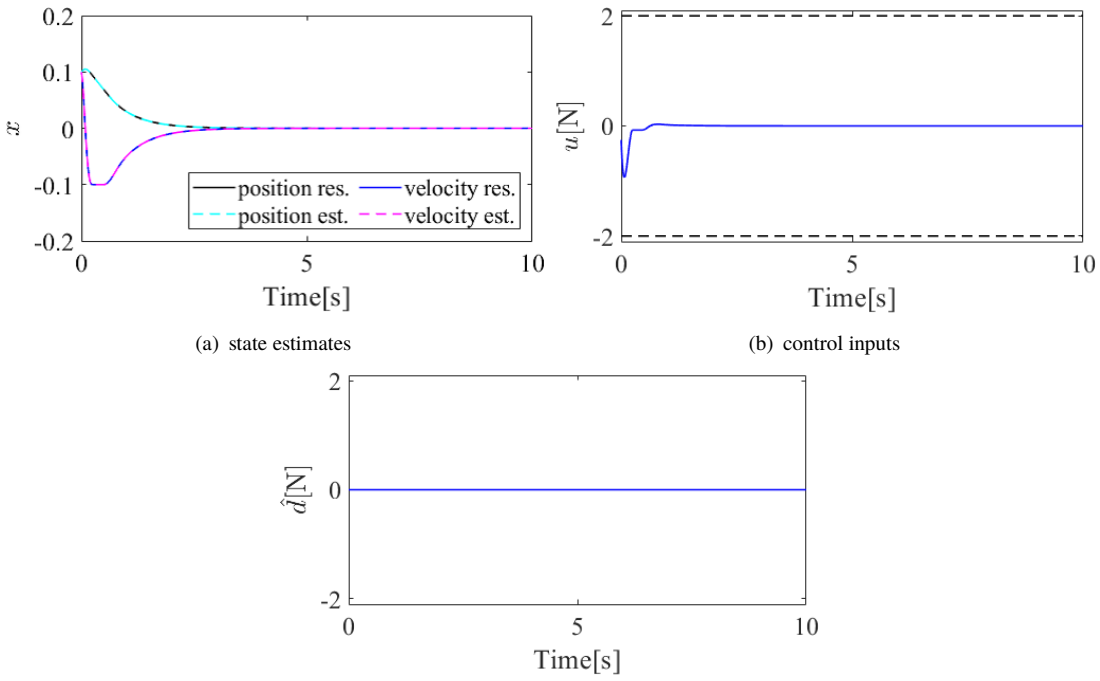

(a) state estimates

(b) control inputs

(c) disturbance estimate

FIGURE 2.21: Simulation results(A): proposed TPW-based MPC with IDOB

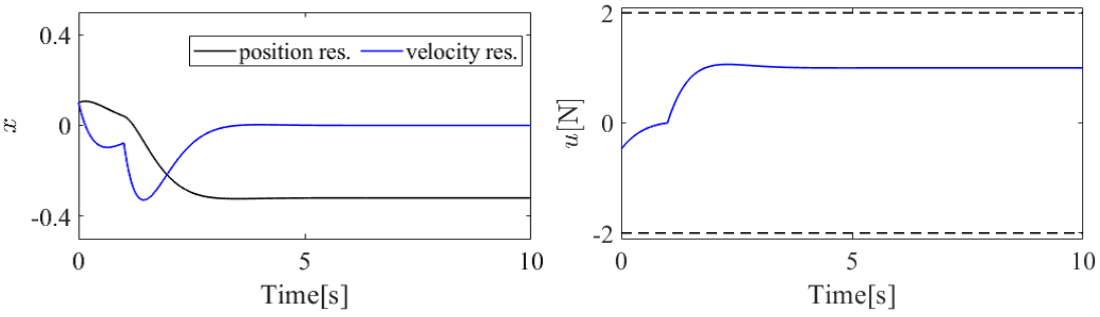

(a) state

(b) control inputs

FIGURE 2.22: Simulation results(B): LQR

considering the closed-loop response time, the prediction horizon was set to 114 by the eigenvalue of the system matrix.

In the proposed MPC design, the weight matrix (Q) is augmented by $Q = \mathrm{diag}(1, 1, 1)$ including disturbance term. In this section, the solver of MPCs was implemented by Hildreth QP[23]. Moreover, considering the computational load, the number of iterations is set to 40 steps and the allowable error is set 10^{-8}. By using the short iteration number, the constraints are flexibly handled under the influences of the disturbances.

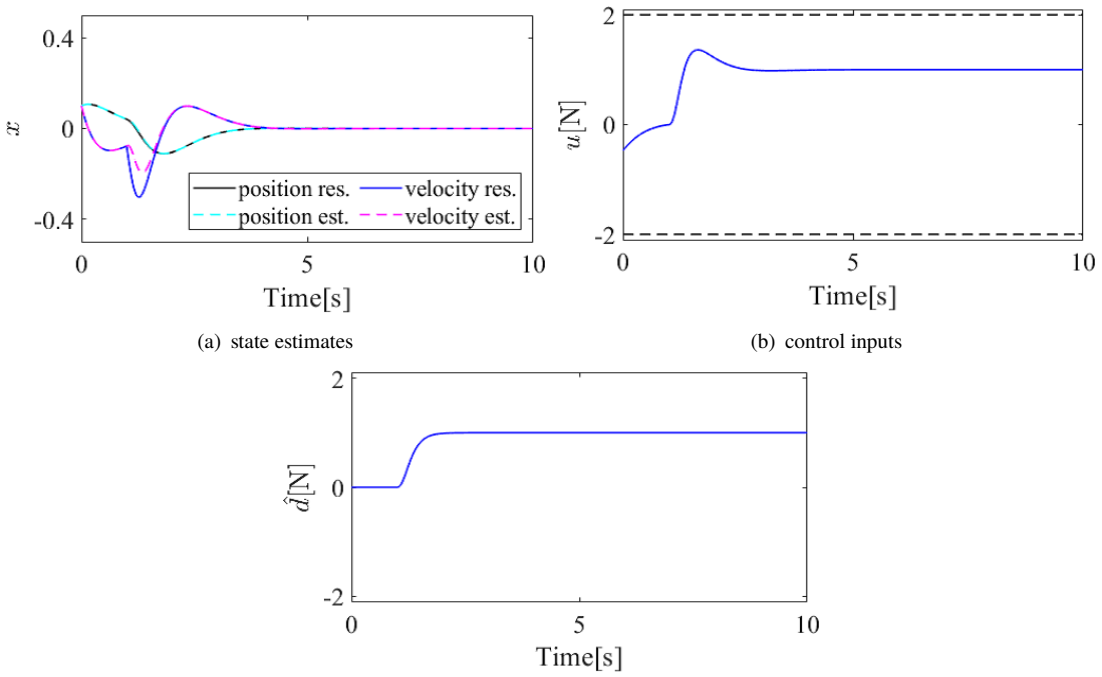

(a) state estimates

(b) control inputs

(c) disturbance estimate

FIGURE 2.23: Simulation results(B): LQR + IDOB

2.3.7.2 Results

The simulation results are shown in Figs. 2.17-2.41.

In the results with respect to A(= without disturbance), it is confirmed that the LQR and MPCs have a similar response, and each MPC can ensure the velocity constraints. Moreover, it is also confirmed that the state estimates of the IDOBs are matched to actual values.

In the results with respect to B(= step-type disturbance 1N), it is confirmed that the LQR and MPCs keep a similar response, and each MPC can ensure the velocity constraints on the estimated velocities. Moreover, it is also confirmed that the state estimates of the IDOBs have errors while estimating the disturbance. Therefore, the actual velocities violate the constraints. In order to solve this, fast disturbance estimation is a must. Furthermore, it is evident that the fast disturbance estimation assists to ensure the constraints.

In the results with respect to C(= step-type disturbance 2N), it is confirmed that the LQR and MPCs are significantly influenced by disturbance because the external disturbance is equivalent to the control input limitation. However, from Fig. 2.31, it is evident that the proposed MPC method can achieve to recover the constraint violation on control input and velocity. The conventional methods cannot recover the constrained motion from disturbance influences. The recovery ability is useful for handling unknown environments and for robust constrained motion control. Therefore, the proposed method is useful compared to the conventional MPCs.

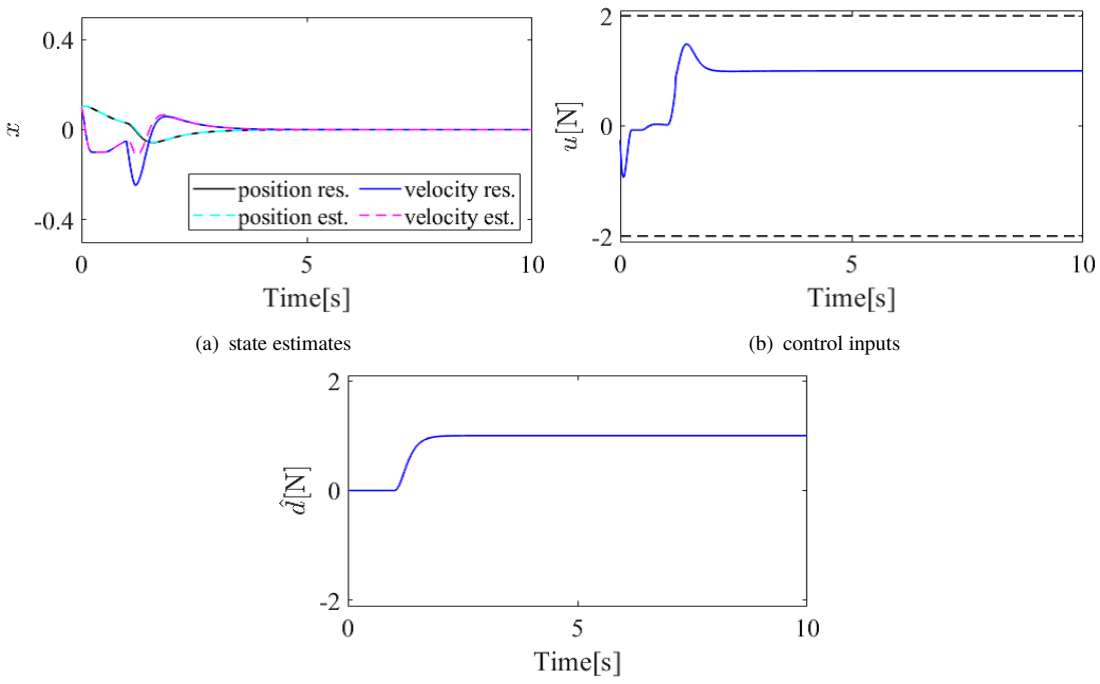

(a) state estimates

(b) control inputs

(c) disturbance estimate

FIGURE 2.24: Simulation results(B): constrained TPW-based MPC with IDOB

In the results with respect to D and E (mass variation), it is confirmed that the LQR and MPCs have a similar response, and each MPC can ensure the velocity constraints. In the case of lighter mass than designed mass, the estimation performance of the IDOBs is reduced by parameter error; therefore, the velocity constraints cannot be secured by the estimation error. Moreover, the estimated state is vibrational; therefore, underestimated mass has to eliminate in designing MPCs. In the case of heavier mass than designed mass, the estimation and control performances of the IDOBs and MPC are less affected by the mass variation; however, small estimation errors have occurred.

Overall, the proposed method is more useful under large disturbances. In particular, it can achieve a robust MPC design and can generate stable constrained motion. Additionally, the constraint recovery ability is effective for working with unknown environments.

2.3.8 Summary

In this section, the practical integration method of IDOB and LMPC was explained. Additionally, the proposed method is an offset-free MPC including disturbance suppression. Moreover, some simulation verifications show the effectiveness of the proposed method.

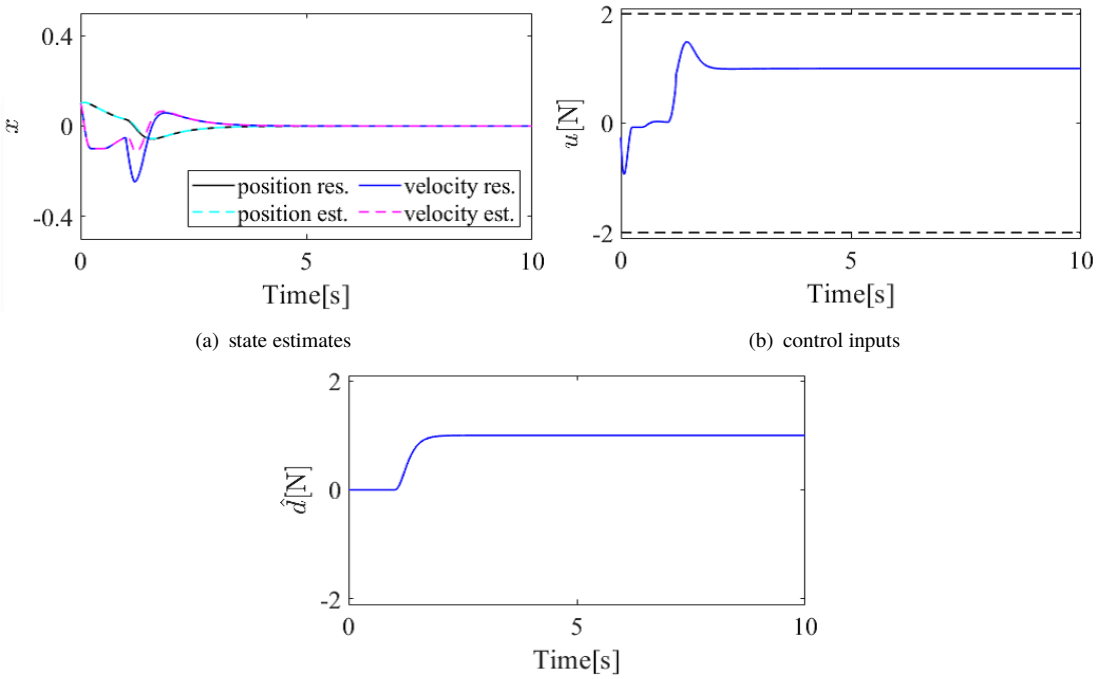

(a) state estimates

(b) control inputs

(c) disturbance estimate

FIGURE 2.25: Simulation results(B): constrained MPC with IDOB

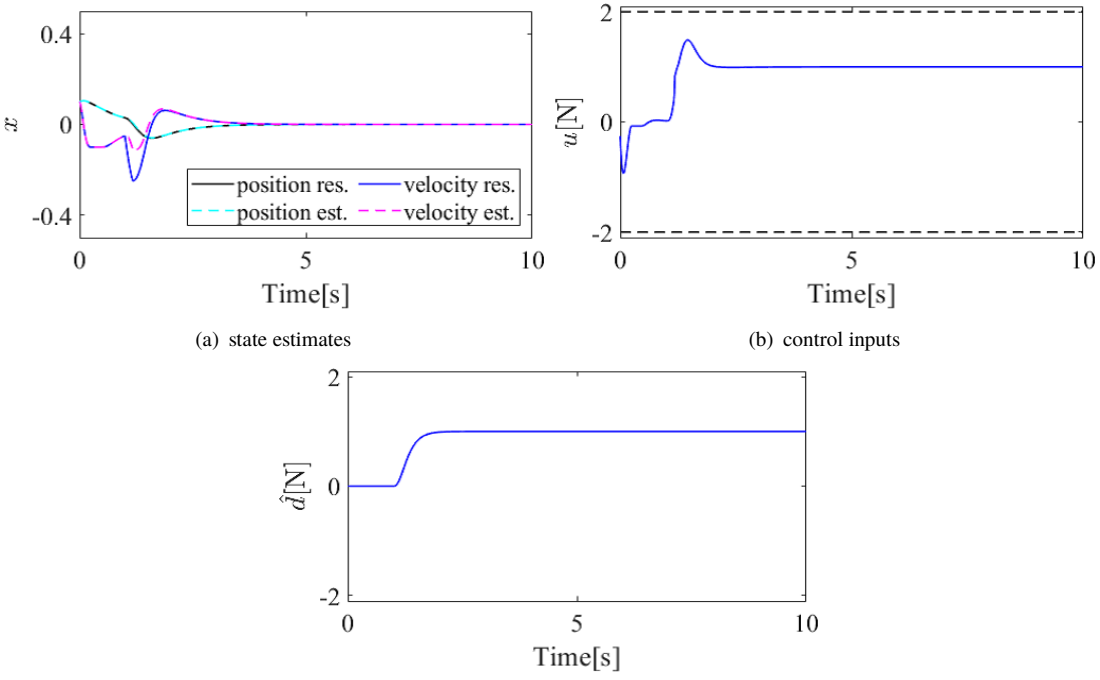

(a) state estimates

(b) control inputs

(c) disturbance estimate

FIGURE 2.26: Simulation results(B): proposed TPW-based MPC with IDOB

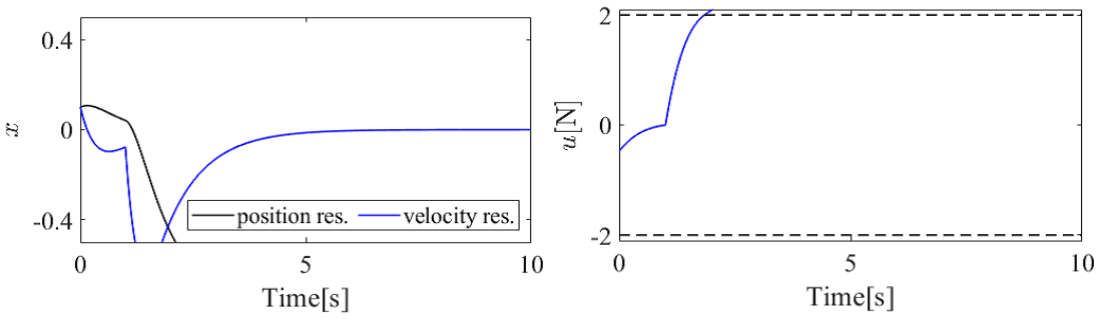

(a) state (b) control inputs

FIGURE 2.27: Simulation results(C): LQR

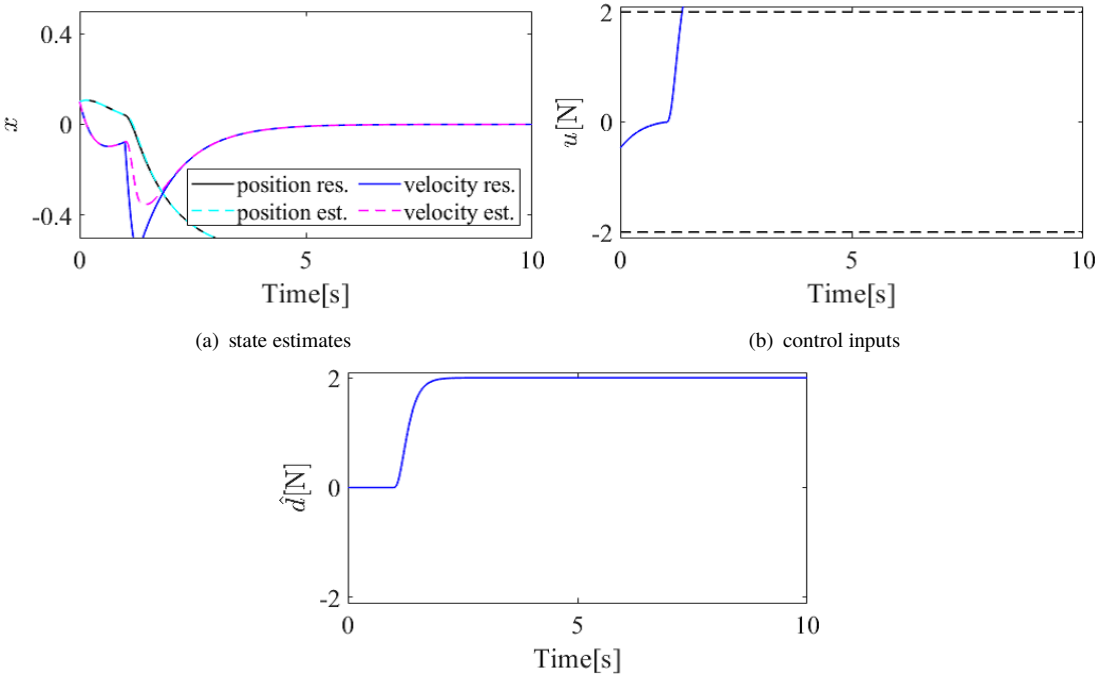

(a) state estimates (b) control inputs

(c) disturbance estimate

FIGURE 2.28: Simulation results(C): LQR + IDOB

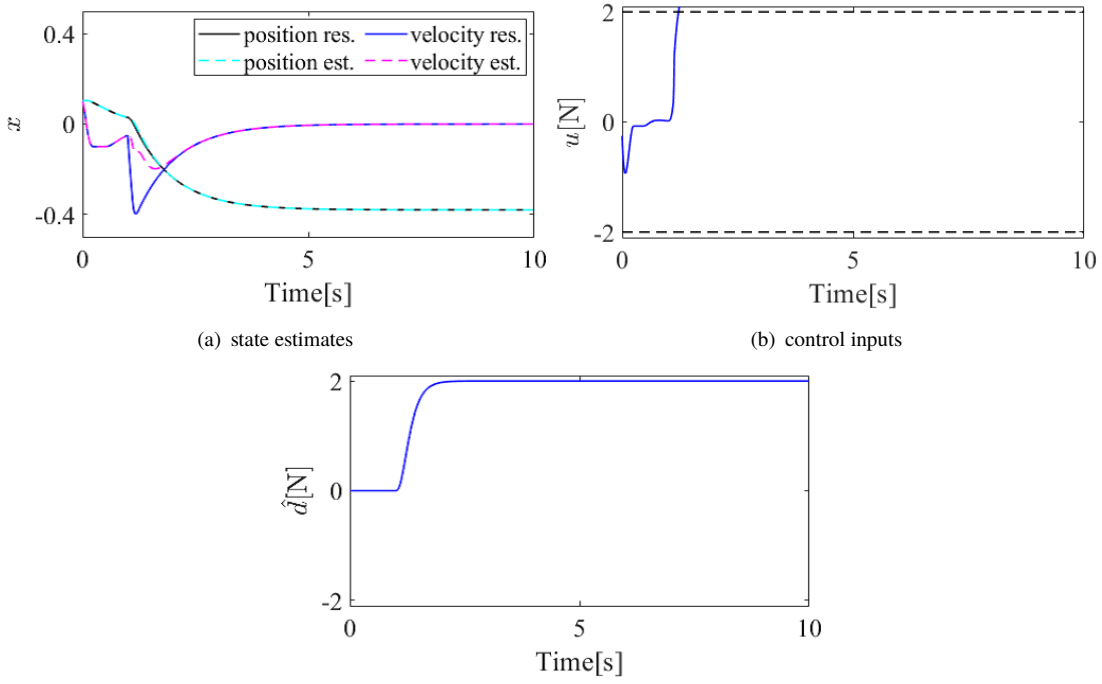

(a) state estimates

(b) control inputs

(c) disturbance estimate

FIGURE 2.29: Simulation results(C): constrained TPW-based MPC with IDOB

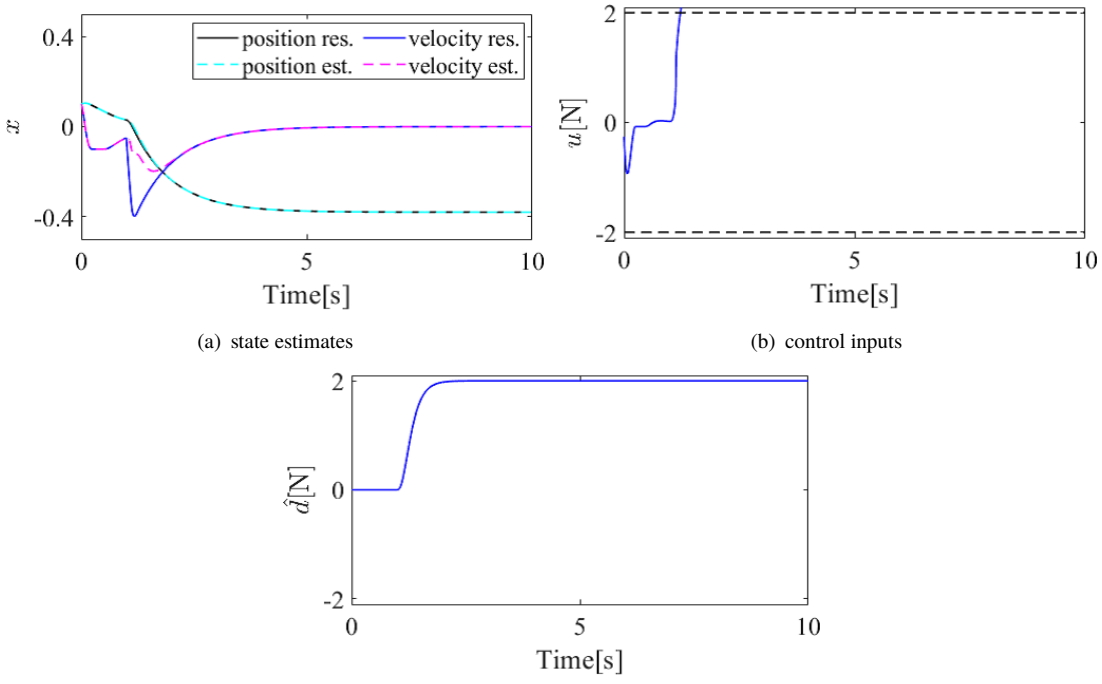

(a) state estimates

(b) control inputs

(c) disturbance estimate

FIGURE 2.30: Simulation results(C): constrained MPC with IDOB

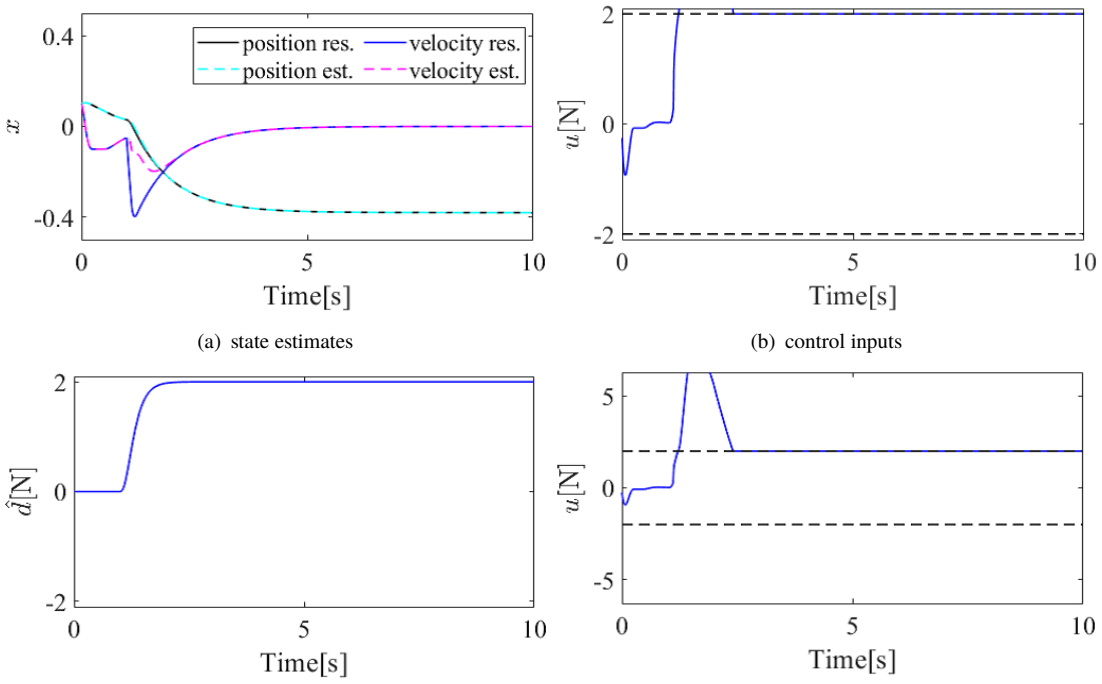

(a) state estimates

(b) control inputs

(c) disturbance estimate

(d) disturbance estimate (large-scale)

FIGURE 2.31: Simulation results(C): proposed TPW-based MPC with IDOB

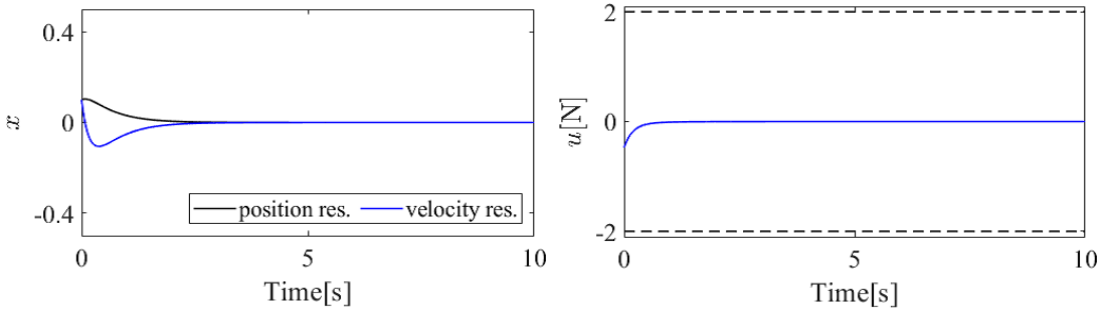

(a) state

(b) control inputs

FIGURE 2.32: Simulation results(D): LQR

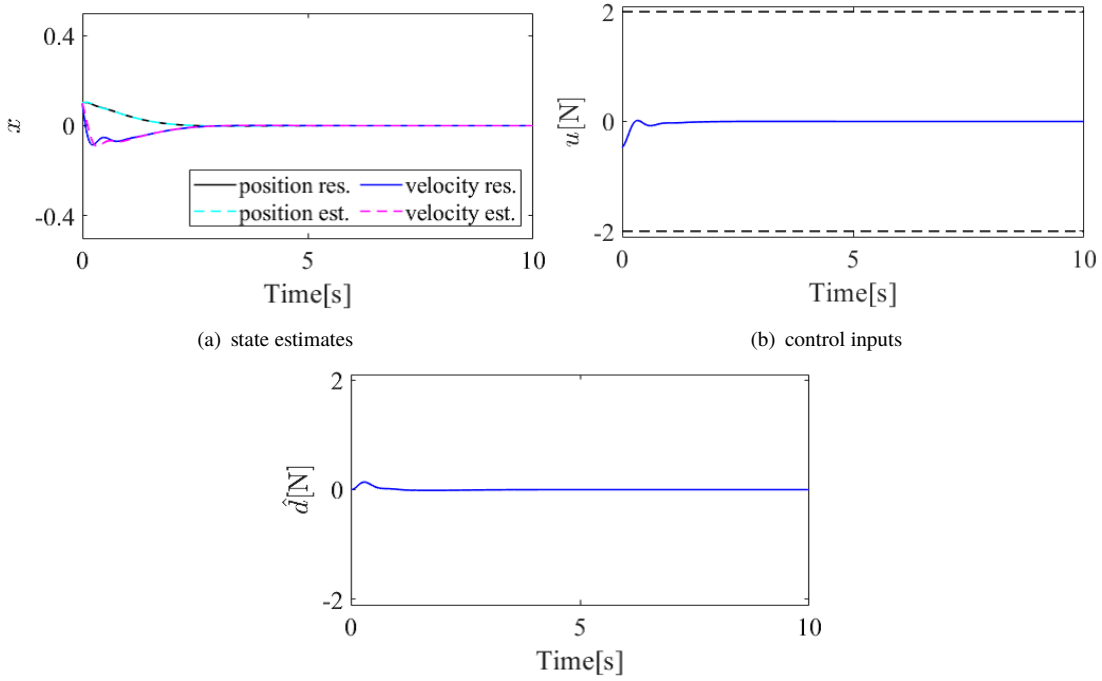

(a) state estimates

(b) control inputs

(c) disturbance estimate

FIGURE 2.33: Simulation results(D): LQR + IDOB

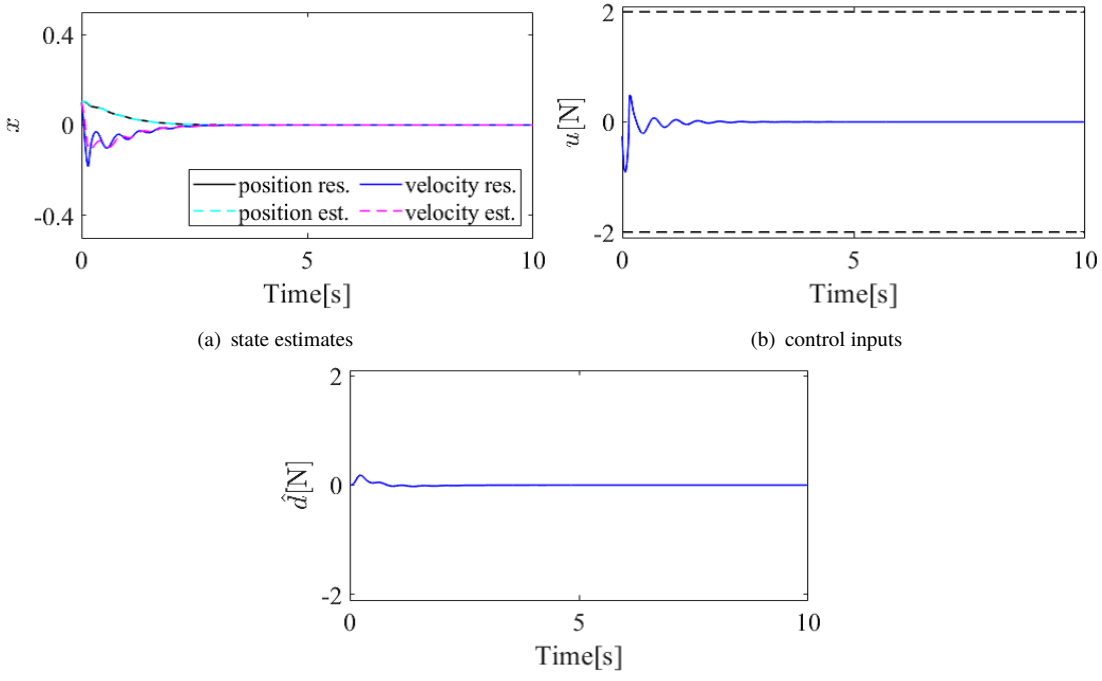

(a) state estimates

(b) control inputs

(c) disturbance estimate

FIGURE 2.34: Simulation results(D): constrained TPW-based MPC with IDOB

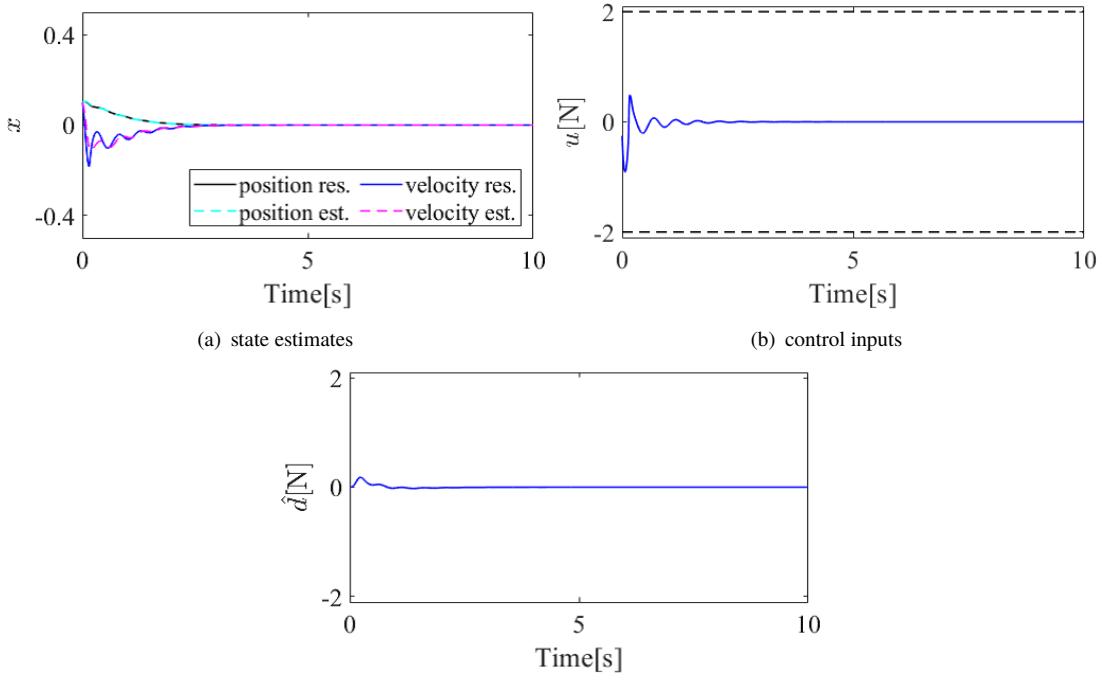

(a) state estimates

(b) control inputs

(c) disturbance estimate

FIGURE 2.35: Simulation results(D): constrained MPC with IDOB

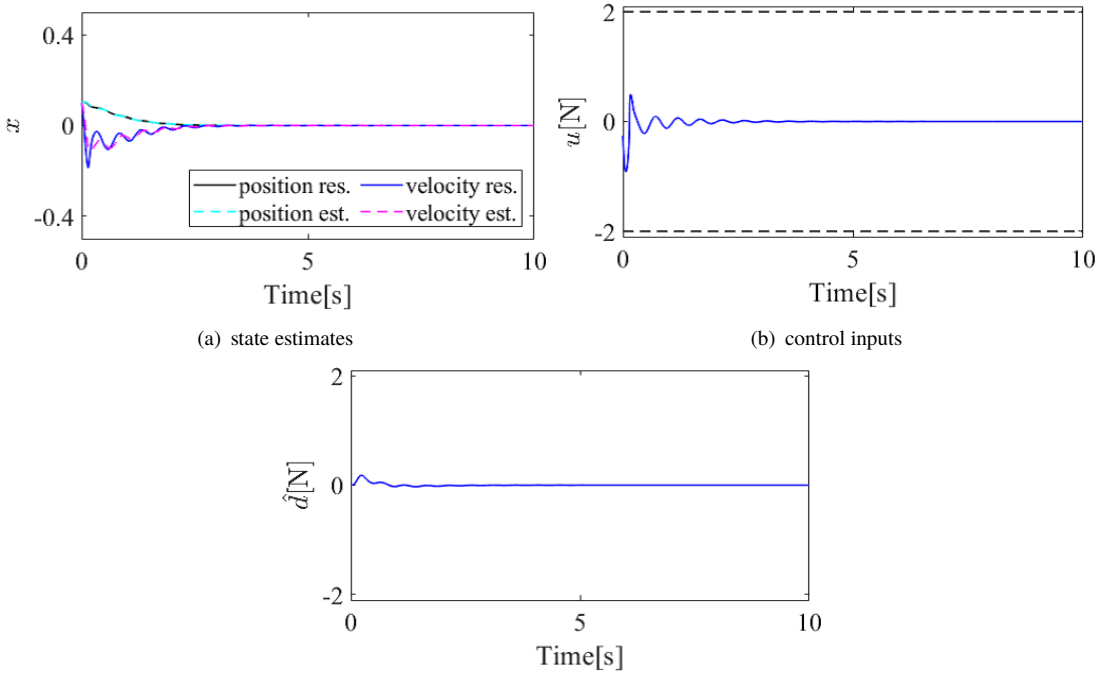

(a) state estimates

(b) control inputs

(c) disturbance estimate

FIGURE 2.36: Simulation results(D): proposed TPW-based MPC with IDOB

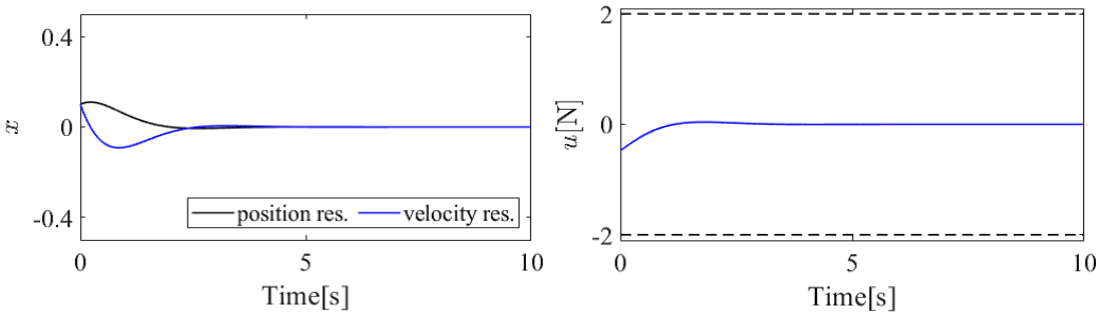

(a) state (b) control inputs

FIGURE 2.37: Simulation results(E): LQR

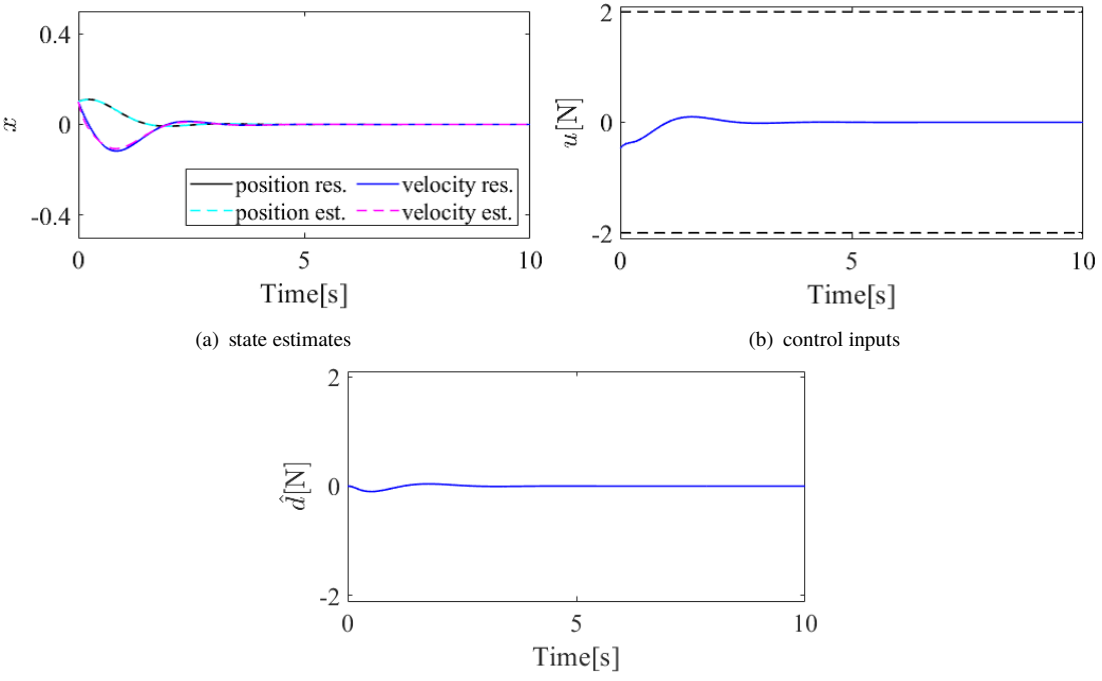

(a) state estimates (b) control inputs

(c) disturbance estimate

FIGURE 2.38: Simulation results(E): LQR + IDOB

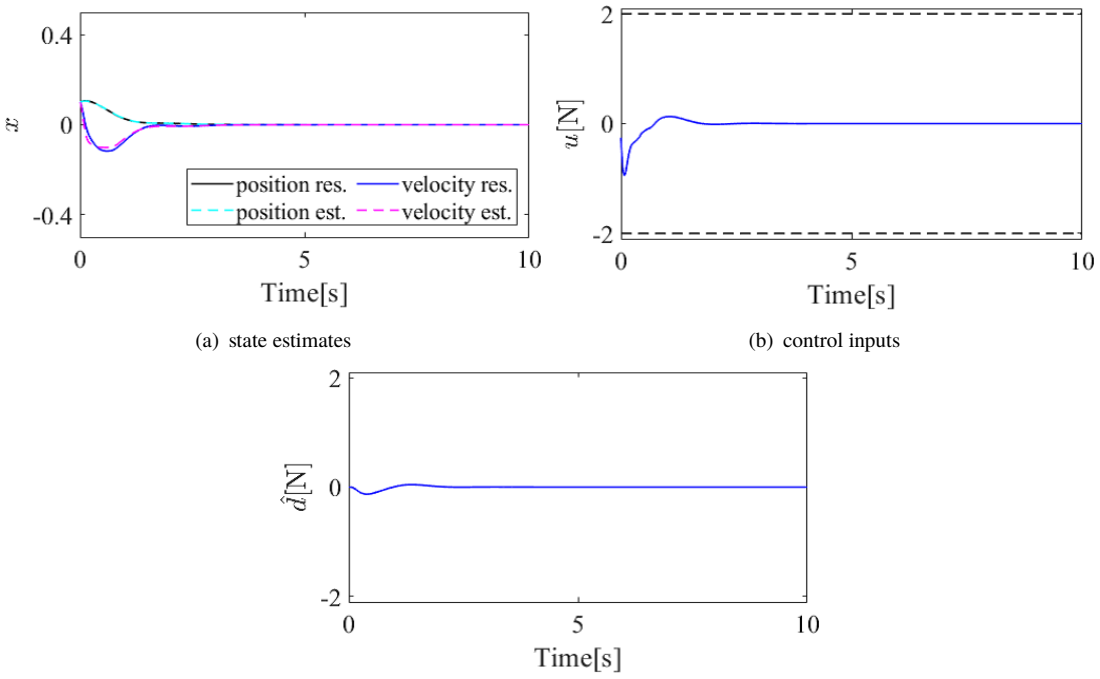

(a) state estimates

(b) control inputs

(c) disturbance estimate

FIGURE 2.39: Simulation results(E): constrained TPW-based MPC with IDOB

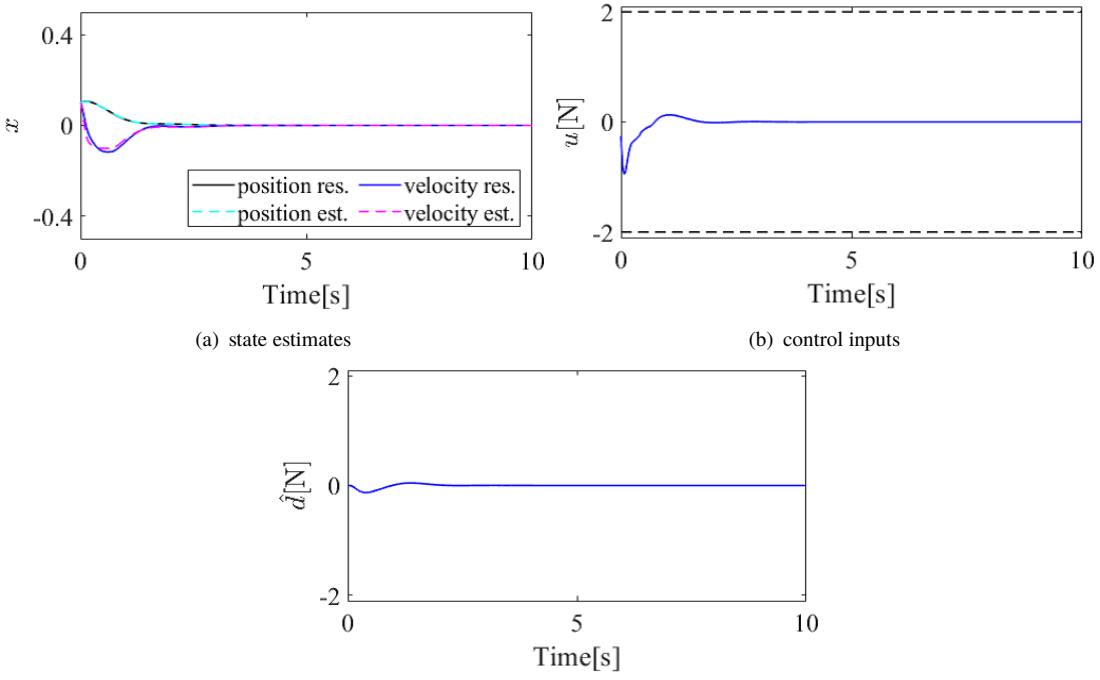

(a) state estimates

(b) control inputs

(c) disturbance estimate

FIGURE 2.40: Simulation results(E): constrained MPC with IDOB

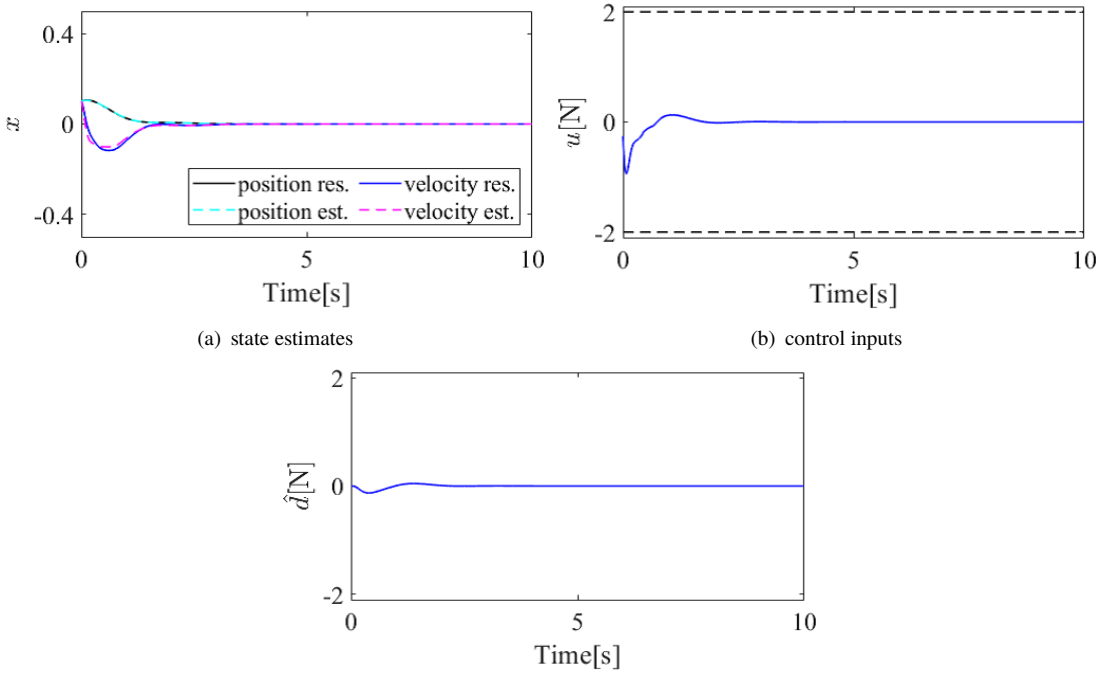

(a) state estimates

(b) control inputs

(c) disturbance estimate

FIGURE 2.41: Simulation results(E): proposed TPW-based MPC with IDOB

2.4 Constrained acceleration control[67]

In the previous section, the integration method of MPC and IDOB is explained. Online iteration method-based MPCs cannot handle high-frequency motion control. In particular, human-interactive robots are required high-speed response against environments. For instance, when the MPC is applied to a manipulator with an unknown environment, the force cannot control without environmental parameters used in the internal model. Therefore, in this section, the practical constrained acceleration control method for a fast motion control system is explained using hybrid position/force control (HPFC) for a multi-degree-of-freedom manipulator(MDoFMs).

This section explains a robust HPFC strategy for MDoFMs considering the input torque saturation in joint space. In particular, the proposed position/force control utilizes the joint space position control with torque constraints for avoiding the undesired behavior on force control with respect to contact motion. In order to consider the torque constraints, the position control system on each joint space is utilized and the reference is calculated by using inverse kinematics[90] by the workspace position reference based on the implicit position control law. In the proposed control system, predictive functional control (PFC)[91–94], which is an MPC, is used as each position control system in each joint space. MPC is well-known as a control system that can treat the constraints on control input and system state. However, the MPC has a heavy computational load and requires the accuracy of the internal models. When MPC attempts to apply to force control, the force cannot be controlled since the design of the internal model cannot use environmental parameters. However, the proposed method can achieve force control via position control; therefore, the MPC is not required environmental parameters. Moreover, a short sampling time is a must for achieving force control. The PFC can design with a short sampling time because of avoiding iterative online optimization. Therefore, the PFC is effective for systematically considering torque saturation in short sampling control systems. In order to apply PFCs to MDoFMs, it is necessary to utilize the DOB method[9–11, 95–99]. The MDoFM control with DOB is possible to make independent position control in each joint by decoupling using the nominal inertia matrix and by constructing acceleration control. Therefore, to use this decoupling controller, the proposed method utilizes the IDOB-based acceleration control system on each joint position control. Fortunately, the decoupling-based joint control can independently design the responses on each joint position; therefore, it is easy to use redundancy. Moreover, the proposed control system can treat disturbance cancellation and fast motion control with torque constraints. In this section, some experiments including HPFC control of a planar three-link manipulator are carried out to show the usefulness and validity of the proposed control systems.

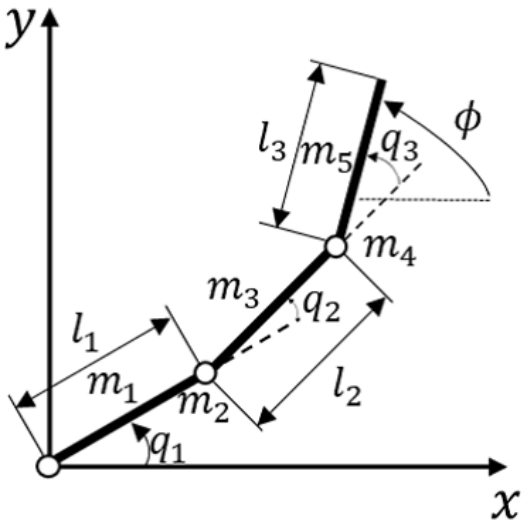

FIGURE 2.42: Modeling of three-link manipulator.

2.4.1 Preliminaries

2.4.1.1 Modeling

To verify the proposed method, a planar three-link manipulator is used in this section. The modeling of the manipulator is shown in Fig. 2.42. In the manipulator system, the position and angle of the end-effector on a plane can be controlled. When the end-effector angle is appropriately controlled, force control can be achieved by a single-axis force sensor. To verify the HPFC system, position control and force control are required in the same system; therefore, this robot is suitable for validating the proposed method.

The state vector ($\boldsymbol{q}$) and the input torque vector ($\boldsymbol{\tau}$) in a joint space are described as $\boldsymbol{q} = [q_1 \ q_2 \ q_3]^{\mathrm{T}}$ and $\boldsymbol{\tau} = [\tau_1 \ \tau_2 \ \tau_3]^{\mathrm{T}}$, respectively. Moreover, the position and posture of the end-effector of the workspace are described as $\boldsymbol{X} = [x \ y \ \phi]^T$. Then, using the Lagrange equation, the equations of motion in the joint space can be described as

$$\ddot{\boldsymbol{q}} = \boldsymbol{J}^{-1}\{\boldsymbol{\tau} - \boldsymbol{D}(\dot{\boldsymbol{q}}) - \boldsymbol{H}(\boldsymbol{q}, \dot{\boldsymbol{q}}) - \boldsymbol{\tau}_{\mathrm{dis}}\}, \tag{2.50}$$

where $\boldsymbol{J}$, $\boldsymbol{D}$, and $\boldsymbol{H}$ are the inertial matrix, the friction function, and the and a Coriolis and centrifugal forces, respectively. Moreover, $\boldsymbol{\tau}_{\mathrm{dis}}$ is the disturbance torque generated by model errors and external force.

Then, the workspace position by the forward kinematics can be described as

$$\boldsymbol{X} = \begin{bmatrix} J_{a1} & J_{a2} & J_{a3} \end{bmatrix}^{\mathrm{T}}, \tag{2.51}$$

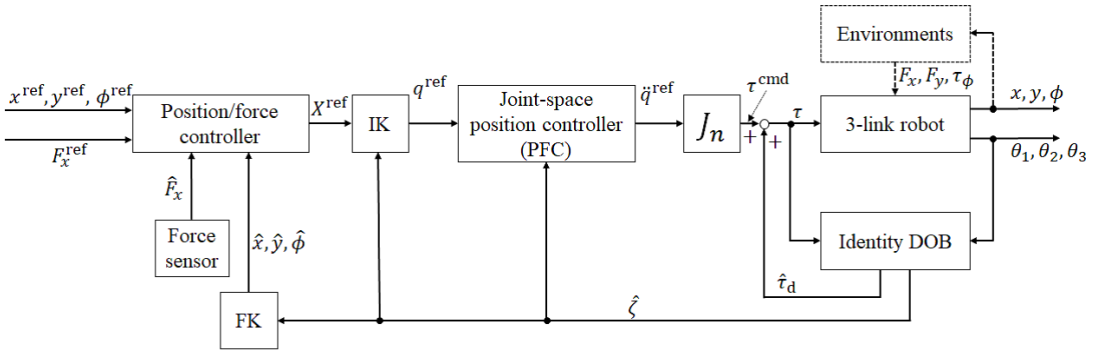

FIGURE 2.43: System diagram of the proposed control system. FK and IK denote forward and inverse kinematics.

where $J_{a1} = L_1 \cos q_1 + L_2 \cos(q_1 + q_2) + L_3 \cos(q_1 + q_2 + q_3)$, $J_{a2} = L_1 \sin q_1 + L_2 \sin(q_1 + q_2) + L_3 \sin(q_1 + q_2 + q_3)$, and $J_{a3} = q_1 + q_2 + q_3$.

Additionally, the differential kinematics for translating the velocities in the joint space and workspace is given by

$$\dot{\boldsymbol{X}} = \boldsymbol{J}_{aco}\dot{\boldsymbol{q}} \tag{2.52}$$

where $\boldsymbol{J}_{aco}$ is a 3×3 Jacobian matrix based on Eq. (2.51). The Jacobian matrix of $\boldsymbol{q}$ is represented by $\boldsymbol{J}_{aco}(\boldsymbol{q})$; however, $(\boldsymbol{q})$ is omitted in this section.

2.4.2 Proposed control system

The control system diagram is shown in Fig. 2.43. The proposed control system can divide into four parts: 1) IDOB for nominalizing the plant model, for improving robustness, and for designing the acceleration control, 2) implicit law of force control used for transforming the workspace position reference to the workspace force reference, 3) inverse kinematics for converting to the joint space position command from the workspace position reference, and 4) PFC for the acceleration control considering torque constraints in joint space. This section describes the case of force control on the x-axis.

2.4.2.1 IDOB-based acceleration control

The IDOB used in the joint space is shown in Fig. 2.44. In the IDOB, the equation of disturbance can be described as

$$\hat{\boldsymbol{\tau}}_{\text{d}} = \boldsymbol{D}(\dot{\boldsymbol{q}}) + \boldsymbol{H}(\boldsymbol{q}, \dot{\boldsymbol{q}}) + \boldsymbol{\tau}_{\text{dis}}. \tag{2.53}$$

This equation is used for designing acceleration control and for normalizing the system model.

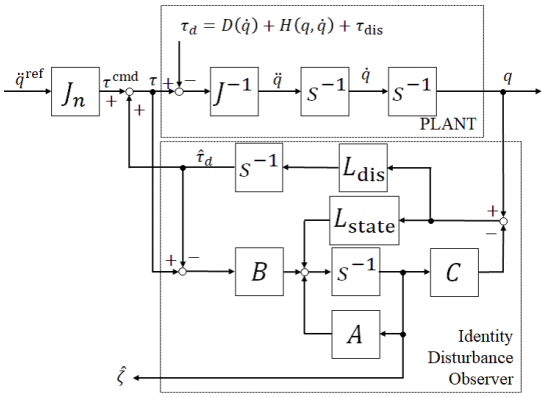

FIGURE 2.44: Acceleration control by IDOB for MIMO systems.

The state vector by position and velocity is defined as $\boldsymbol{\zeta} = [\boldsymbol{q}^{\mathrm{T}} \quad \dot{\boldsymbol{q}}^{\mathrm{T}}]^{\mathrm{T}}$. Moreover, to estimate the state and disturbance simultaneously, new state vector extended by disturbance is defined as $\bar{\boldsymbol{\zeta}} = [\boldsymbol{\zeta}^{\mathrm{T}} \quad \boldsymbol{\tau}_d^{\mathrm{T}}]^{\mathrm{T}}$. Then, the extended state-space model can be described as

$$\begin{aligned} \begin{bmatrix} \dot{\hat{\boldsymbol{\zeta}}} \\ \dot{\hat{\boldsymbol{\tau}}}_d \end{bmatrix} &= \bar{\boldsymbol{A}}\hat{\bar{\boldsymbol{\zeta}}} + \bar{\boldsymbol{B}}\boldsymbol{\tau}, \\ &= \begin{bmatrix} \boldsymbol{A} & -\boldsymbol{B} \\ \boldsymbol{0} & \boldsymbol{0} \end{bmatrix} \begin{bmatrix} \hat{\boldsymbol{\zeta}} \\ \hat{\boldsymbol{\tau}}_d \end{bmatrix} + \begin{bmatrix} \boldsymbol{B} \\ \boldsymbol{0} \end{bmatrix} \boldsymbol{\tau}, \qquad (2.54) \\ \boldsymbol{y} &= \bar{\boldsymbol{C}}\hat{\bar{\boldsymbol{\zeta}}} = \begin{bmatrix} \boldsymbol{C} & \boldsymbol{0} \end{bmatrix} \begin{bmatrix} \hat{\boldsymbol{\zeta}} \\ \hat{\boldsymbol{\tau}}_d \end{bmatrix}, \qquad (2.55) \end{aligned}$$

where $\boldsymbol{A}$, $\boldsymbol{B}$, $\boldsymbol{C}$, and $\boldsymbol{0}$ are the system, input, output, and zero matrices defined by appropriate orders, respectively. Moreover, $\bar{\boldsymbol{A}}$, $\bar{\boldsymbol{B}}$, and $\bar{\boldsymbol{C}}$ are the extended system, input, and output matrices.

Using the disturbance estimation of Eq. (2.53), the matrices are given by

$$\begin{aligned} \boldsymbol{A} &= \begin{bmatrix} \boldsymbol{0} & \boldsymbol{I} \\ \boldsymbol{0} & \boldsymbol{0} \end{bmatrix}, \qquad (2.56) \\ \boldsymbol{B} &= \begin{bmatrix} \boldsymbol{0} \\ \boldsymbol{J}_n^{-1} \end{bmatrix}, \qquad (2.57) \\ \boldsymbol{C} &= \begin{bmatrix} \boldsymbol{I} & \boldsymbol{0} \end{bmatrix}, \qquad (2.58) \end{aligned}$$

where $\boldsymbol{I}$ and $\boldsymbol{0}$ are 3×3 dimension identity and zero matrices.

2.4.2.2 Implicit force control

The converting law of a force command ($\boldsymbol{F}^{\text{ref}}$) into the position command ($\boldsymbol{X}^{\text{ref}}$) is described in the workspace. In the experimental validation, force control of the x-axis was performed, and

other state variables (y, ϕ) were controlled by the position controller. Therefore, this section concerns converting F_x^{ref} to x^{ref}.

By position-based impedance control, the conversion of the nominal position command (x_n^{ref}) can be described as

$$x_n^{\mathrm{ref}} = x_{\mathrm{cp}} + \frac{1}{K_e} F_x^{\mathrm{ref}}, \tag{2.59}$$

where x_{cp} and K_e are the contact position and the environmental stiffness parameter, respectively. To apply the force control with the environmental parameters is challenging under uncertain environments. Furthermore, excessive force is usually possible due to the variation of stiffness and contact points. Such a control system using constant parameters cannot deal with various environments.

To control the force with unknown environments, a modified impedance command is proposed in this section, and it can be described as

$$x^{\mathrm{ref}} = x + \frac{1}{K_f}(F_x^{\mathrm{ref}} - F_x), \tag{2.60}$$

$$\tilde{x} = \frac{1}{K_f}(F_x^{\mathrm{ref}} - F_x), \tag{2.61}$$

$$x^{\mathrm{ref}} = x + \tilde{x}, \tag{2.62}$$

where K_f denotes the convert gain and F_x denotes the observed force. As shown by Eq. (2.60), the force tracking error is integrated into the position command. Eq. (2.62) is capable to consider the force reference and position deviation. Moreover, the proposed reference method can achieve fast force control by position control. This assists to reject impact force, bouncing motion, and hunting motion owing to contact motion. On the other hand, in the case of position control of all variables, the control system inputs the workspace position command.

2.4.2.3 Inverse kinematics

The implicit force control using the workspace position control considers the stable contact motion with torque constraints. In the implicit law, the transformation of the workspace position command ($\boldsymbol{X}^{\mathrm{ref}}$) to the position reference in joint space ($\boldsymbol{q}^{\mathrm{ref}}$) is required. In this section, the inverse kinematics method using the Levenvetg-Marquardt method[90] is utilized with small modifications to consider the singular points in the workspace posture of the manipulator.

Additionally, the equations of inverse kinematics can be described as

$$\begin{aligned}
\boldsymbol{q}^{\mathrm{ref}}(k) &= \boldsymbol{q}(k) + \tilde{\boldsymbol{q}}^{\mathrm{ref}}(k), && (2.63)\\
\tilde{\boldsymbol{q}}^{\mathrm{ref}}(k) &= \boldsymbol{H}(k)\boldsymbol{M}(k), && (2.64)\\
\boldsymbol{H}(k) &= \{\boldsymbol{J}_{aco}^{\mathrm{T}}(k)\boldsymbol{W}_e\boldsymbol{J}_{aco}(k) \\
&\quad +\boldsymbol{W}_n(k)\}^{-1}, && (2.65)\\
\boldsymbol{M}(k) &= \boldsymbol{J}_{aco}^{\mathrm{T}}(k)\boldsymbol{W}_e\boldsymbol{X}_e(k) + \boldsymbol{X}_e(k), && (2.66)\\
\boldsymbol{W}_e &= \mathrm{diag}(w_1, w_2, w_3), && (2.67)\\
\boldsymbol{W}_n(k) &= \mathrm{diag}(\boldsymbol{X}_e(k)) + \lambda\boldsymbol{I}, && (2.68)
\end{aligned}$$

where k is the current sample time. Moreover, in this section, singular states can be avoided using a small bias $\lambda(= 10^{-8})$ and the tracking error vector in Eq. (2.68). Additionally, $\boldsymbol{W}_e$ denotes a diagonal matrix including weights (w_1, w_2, and w_3) in each joint. $\boldsymbol{W}_n$ denotes and a diagonal matrix of the error vector and a damping factor in the workspace. $\boldsymbol{X}_e$ denotes a tracking error vector of the workspace position. Moreover, this method can control the manipulator from the singular state, and it can calculate the joint angle reference using the reference velocity. In this section, velocity constraints by maximum speed (30 rad/s) in actual motor are imposed on $\tilde{\boldsymbol{q}}^{\mathrm{ref}}$, and the constraints can be described as $2\pi \cdot 30/60 = \pi$[rad/s]. Overall, joint angle control for workspace position control is effective, since it can avoid singular states.

2.4.2.4 Joint space position control

In joint space, the position control system uses acceleration control by the IDOB and the PFC. General MPCs control MIMO systems with system state constraints via online optimization. In contrast to this, PFCs control the system state with input constraints. Moreover, online optimization is not required. PFCs do not explicitly handle output constraints; however, it is possible to design using a small sampling time than standard MPCs. Therefore, in acceleration control, PFCs are to easily use like general PD control. Moreover, the control parameters for designing PFC are defined as the target response time and a damping factor on prediction tracking errors. The PFC is easier to implement a joint space controller with the torque constraints and the nominal response in each joint actuator with PFCs than it is with PD systems.

The proposed control system utilizes each independent PFCs as position control in each joint. Furthermore, the independent PFCs are designed based on decoupling by the IDOB. Therefore, it can generate the acceleration reference for each joint angle and perform position control in joint space with torque constraints. Moreover, by using the target response time, the response in joint angles can be controlled explicitly and independently.

The main problem of MBC systems is the error of internal models. The model errors in the internal model create a reduction of the control performance of MBC systems. In the IDOB -based PFC, the internal model system is different from the internal models used in conventional systems. In the proposed method, the system $1/s^2$ is utilized based on the nominalization obtained from the IDOB. Therefore, the internal model does not use the physical parameters of the manipulator, and it is systematically to decide the control performance. In the proposed system, the offset-free tracking performance in joint space position is dependent on the performance of disturbance estimation and cancellation of the IDOB. The design method of PFC follows [94]. The description in this section focuses on the first joint angle (q_1), and the design methods of the internal model and the torque constraints are explained.

2.4.2.5 Internal model of PFC

A state vector $\boldsymbol{x}_q = [q_1 \;\; \dot{q}_1]$ in joint space is defined using the state estimates by the IDOB, and the digital state-space model is given by

$$\boldsymbol{x}_q(k+1) = \boldsymbol{A}_q \boldsymbol{x}_q(k) + \boldsymbol{B}_q u(k), \tag{2.69}$$

$$y(k) = \boldsymbol{C}_q \boldsymbol{x}_q(k), \tag{2.70}$$

where the coefficient matrices can be described as

$$\boldsymbol{A}_q = \begin{bmatrix} 1 & T_s \\ 0 & 1 \end{bmatrix}, \tag{2.71}$$

$$\boldsymbol{B}_q = \begin{bmatrix} 0 \\ T_s \end{bmatrix}, \tag{2.72}$$

$$\boldsymbol{C}_q = \begin{bmatrix} 1 & 0 \end{bmatrix}. \tag{2.73}$$

where T_s denotes the sampling time of the control systems. Moreover, the control input (u) directly can be described as the acceleration reference ($\ddot{q}_1^{\mathrm{ref}}$) and the physical parameters are not used for designing the internal model.

2.4.2.6 Outline of PFC scheme

In this section, the acceleration reference derivation is described. General PFC method as position control is described on [93] and [94]. In design of the PFC, the reference trajectory ($T(k+i)$) in the prediction horizon is defined as

$$T(k+i) = s(k+i) - \alpha^i (s(k) - y(k)), \tag{2.74}$$

where s denotes the setpoint, which is obtained by inverse kinematics as the joint angle reference, and α denotes the damping factor of the reference trajectory[94]. The damping factor is given by

$$\alpha = e^{-3T_s/T_{\text{ref}}}, \tag{2.75}$$

where T_{ref} is the closed-loop target response time of the internal system. Moreover, α is defined by Eq. (2.75); therefore, T_{ref} is the main tuning parameter of the controller. Moreover, the PFC does not optimize all sample points on the prediction horizon in each sampling time. To calculate the control input, the coincidence points, which are the calculation points within the prediction horizon, are decided on the prediction trajectory. The coincidence points (h_j) are given by

$$h_j = T_{\text{ref}}/(T_s(n-j+1)), \tag{2.76}$$

where $h_j (j = 1, 2, ..., n)$ denote the sample step points ($h_j \cdot T_s$ = calculation points) of coincidence points in prediction horizon and n denotes the number of coincidence points. Moreover, n is a control parameter for deciding the shape of control inputs.

The cost function (V) using these coincidence points based on future tracking error minimization between the reference trajectory and the output prediction ($\hat{y}$) can be described as

$$\begin{aligned} V(k) &= \sum_{j=1}^{n} \{\hat{y}(k+h_j) - T(k+h_j)\}^2, & (2.77) \\ &= \sum_{j=1}^{n} \{y_b(h_j)^{\mathrm{T}}\mu(k) + C_q(A_q^{h_j} - I)\boldsymbol{x}_q(k) \\ &\quad +(\alpha^{h_j} - 1)(s(k) - y(k))\}^2. & (2.78) \end{aligned}$$

where μ denote the optimal control input as the decision variable. Moreover, the optimal control inputs for all coincident points are calculated by a combination of basis functions (e.g., step, ramp, and parabola functions[92, 93]). $y_b(h_j)$ is the state response generated by each base function input. In the case of $n = 3$, the state response depending on the first coincidence point can be described as

$$y_b(h_j) = \boldsymbol{\Theta}(h_j)\boldsymbol{u}_{\text{s}} + \boldsymbol{\Theta}(h_j)\boldsymbol{u}_{\text{r}} + \boldsymbol{\Theta}(h_j)\boldsymbol{u}_{\text{p}} \tag{2.79}$$

where $\boldsymbol{\Theta} = [\boldsymbol{C}_q\boldsymbol{A}_q^{h_j}\boldsymbol{B}_q \ ... \ \boldsymbol{C}_q\boldsymbol{A}_q^{0}\boldsymbol{B}_q \in \mathbb{R}^{h_j}]$, $\boldsymbol{u}_{\text{s}} = [1 \ ... \ 1]^{\mathrm{T}} \in \mathbb{R}^{h_j}$, $\boldsymbol{u}_{\text{r}} = [0 \ T_s \ 2T_s \ ... \ h_jT_s]^{\mathrm{T}} \in \mathbb{R}^{h_j}$, and $\boldsymbol{u}_{\text{p}} = [0 \ \ (T_s)^2 \ \ (2T_s)^2 \ \ ... \ \ (h_jT_s)^2]^{\mathrm{T}} \in \mathbb{R}^{h_j}$. The state prediction of PFC is calculated by using the forced response to the base functions and the free responses to the system ($\boldsymbol{C}_q\boldsymbol{A}_q^i\boldsymbol{x}_q(k)$).

Therefore, the control input vector μ and closed-form solution can be given by

$$\begin{aligned}\boldsymbol{\mu}(k) &= -\{\sum_{j=1}^{n}\{y_b(h_j)y_b(h_j)^{\mathrm{T}}\}^{-1} \\ &\quad \times \sum_{j=1}^{n}\{\boldsymbol{C}_q(\boldsymbol{A}_q^{h_j}) - \boldsymbol{I})\boldsymbol{x}_q(k) \\ &\quad +(\alpha^{h_j} - 1)(s(k) - y(k))\}y_b(h_j). \end{aligned} \tag{2.80}$$

The first element in μ based on the receding horizon control is input to the system as the control inputs.

2.4.2.7 Acceleration constraints

PFCs handle the control input constraints on the internal model system. In this section, the PFC of the proposed method derives the control input as the acceleration reference in each joint angle. Therefore, the constraints treated by the PFC are described as the constraints on acceleration reference. Considering stable motion generation with torque saturation, the torque constraint, which is an essential constraint for stable manipulator control, is treated by the PFC. Moreover, the torque constraints are effective for suppressing wind-up problems[3, 4] in disturbance estimation by DOBs. For designing the torque constraints via the acceleration constraints, the torque constraint based on the torque limit (τ_{limit}) determined from the actual system can be described as

$$-\tau_{\mathrm{limit}} \leq \tau_1 \leq \tau_{\mathrm{limit}}. \tag{2.81}$$

Using the acceleration reference and the disturbance estimates at (k), the input torque is given by

$$\tau_1(k) = j_n\ddot{q}_1^{\mathrm{ref}}(k) + \hat{\tau}_d(k), \tag{2.82}$$

where j_n is the nominal inertia parameter of q_1. The control input as acceleration reference with torque limit can be described as

$$-\tau_{\mathrm{limit}} \leq j_n\ddot{q}_1^{\mathrm{ref}}(k) + \hat{\tau}_d(k) \leq \tau_{\mathrm{limit}}, \tag{2.83}$$

$$j_n^{-1}(-\tau_{\mathrm{limit}} - \hat{\tau}_d(k)) \leq \ddot{q}_1^{\mathrm{ref}}(k) \leq j_n^{-1}(\tau_{\mathrm{limit}} - \hat{\tau}_d(k)). \tag{2.84}$$

The PFC system based on this constraint can explicitly impose the torque constraints via the acceleration reference. Additionally, due to the IDOB use of the torque-bounded control input, the acceleration constraints can avoid overestimating disturbance estimates.

2.4.2.8 Stability analysis

The nominal closed-loop stability in the proposed system is explained. The number of coincidence points uses $n = 3$ in this analysis. The PFC system represented by Eq. (2.80) has a closed-form optimal solution; therefore, the controller can be described as a linear time-invariant controller. The actual control input ($\mu_1 = \ddot{q}_1^{\mathrm{ref}}$) can be obtained by

$$\mu_1 = \boldsymbol{f}_{fo}\{\boldsymbol{r}_{fi}(q_1^{\mathrm{ref}} - \hat{q}_1) - \boldsymbol{f}_{fr}\hat{\boldsymbol{x}}_q + \boldsymbol{I}^{3\times1}\hat{q}_1\}, \tag{2.85}$$

where $\boldsymbol{f}_{fo} \in \mathbb{R}^n$, $\boldsymbol{r}_{fi} = [1-\alpha^{h_1}\ \ 1-\alpha^{h_2}\ \ 1-\alpha^{h_3}]^{\mathrm{T}} \in \mathbb{R}^n$, and $\boldsymbol{f}_{fr} = [\boldsymbol{C}_q\boldsymbol{A}_q^{h_1}\ \ \boldsymbol{C}_q\boldsymbol{A}_q^{h_2}\ \ \boldsymbol{C}_q\boldsymbol{A}_q^{h_3}]^{\mathrm{T}} \in \mathbb{R}^{n\times2}$ are the vector regarding μ_1 of the inverse matrix on forced response (y_b), the reference trajectory generation vetor, and the vector of the free response, respectively. Using Eq. (2.70), the elements of position on $\boldsymbol{f}_{fr}$ are given by $\boldsymbol{f}_{fr,1,1}, \boldsymbol{f}_{fr,2,1}, \boldsymbol{f}_{fr,3,1} = 1$, where $\boldsymbol{f}_{fr,v,w}$ are w-th column and the elements of v-th row in $\boldsymbol{f}_{fr}$. Therefore, using each matrix element, the closed-form optimal control input can be described as

$$\begin{aligned}
\mu_1 &= \boldsymbol{f}_{fo,1}\{\boldsymbol{r}_{fi,1}(q_1^{\mathrm{ref}} - \hat{q}_1) - \boldsymbol{f}_{fr,1,2}\hat{\dot{q}}_1\} \\
&\quad + \boldsymbol{f}_{fo,2}\{\boldsymbol{r}_{fi,2}(q_1^{\mathrm{ref}} - \hat{q}_1) - \boldsymbol{f}_{fr,2,2}\hat{\dot{q}}_1\} \\
&\quad + \boldsymbol{f}_{fo,3}\{\boldsymbol{r}_{fi,3}(q_1^{\mathrm{ref}} - \hat{q}_1) - \boldsymbol{f}_{fr,3,2}\hat{\dot{q}}_1\}, \\
&= k_p(q_1^{\mathrm{ref}} - \hat{q}_1) - k_d\hat{\dot{q}}_1,
\end{aligned} \tag{2.86}$$

where $k_p = (\boldsymbol{f}_{fo,1}\boldsymbol{r}_{fi,1} + \boldsymbol{f}_{fo,2}\boldsymbol{r}_{fi,2} + \boldsymbol{f}_{fo,3}\boldsymbol{r}_{fi,3})$ and $k_d = (\boldsymbol{f}_{fo,1}\boldsymbol{f}_{fr,1,2} + \boldsymbol{f}_{fo,2}\boldsymbol{f}_{fr,2,2} + \boldsymbol{f}_{fo,3}\boldsymbol{f}_{fr,3,2})$. In the case of unconstrained, from Eq. (2.87), the PFC system used in the proposed system is approximated as simple PD control. Moreover, the discrete-time transfer function ($G(z)$) using the nominal internal model, can be described as

$$G(z) = \frac{T_s^2 k_p z^2}{(1 + T_s^2 k_p + T_s k_d)z^2 - (T_s k_d + 2)z + 1}. \tag{2.87}$$

The asymptotic and Lyapunov stabilities and on the proposed joint controller can both be ensured using to set the absolute value of the eigenvalues of the denominator to <1. In the actual system, a large sampling time presumably creates unexpected motion; therefore, the sampling time has to be set to the smallest value in allocable. Moreover, the main control parameter of the PFC is T_{ref}, and the condition of the stability can be designed as $T_{\mathrm{ref}} > 0$. Thus, the PFC used in the proposed system is optimal and stable. Furthermore, if the torque or acceleration constraints are active, the stability is improved because stable motion generation is ensured by the constraints. Moreover, the disturbance estimates by the IDOB usually compensates for the robustness of the joint space controller[10]. Additionally, the accuracy of the disturbance estimate is compensated within the torque limit. Moreover, the excessive disturbance estimates are rejected by the torque constraints, because the IDOB uses the constrained control input for the estimation. The

constrained disturbance estimates contribute to the stable estimation of the IDOB, better than the IDOB-based PFC systems make both robust and stable of the proposed controller in the joint space. The implicit force control method is designed as a simple feedback system via position control. Moreover, the inverse kinematics system has numerically stability and convergence performances[90]. Overall, both robust and stability of the proposed method are compensated by constrained motion control and accurate disturbance estimations. Note that the saturated control input cannot stabilize unstable systems; therefore, the motion generation considering to avoid control input saturation is a must in designing the constraints control systems.

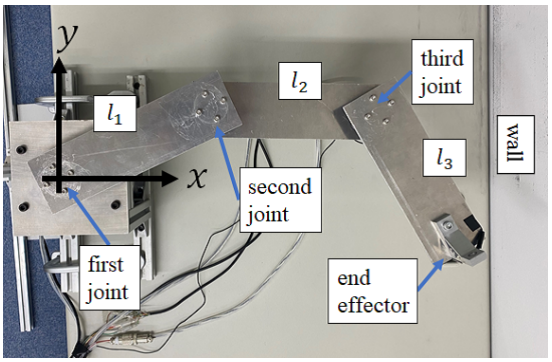

(a) *x*-*y*

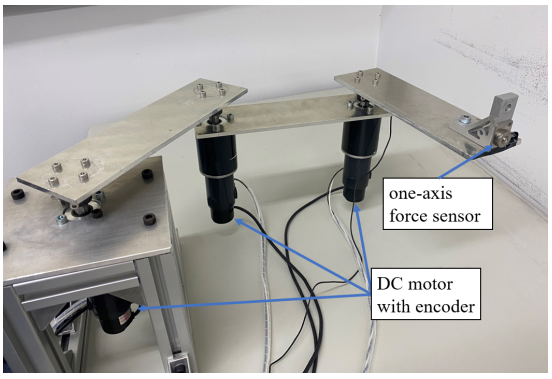

(b) appearance

FIGURE 2.45: Experiment setup

2.4.3 Experiments

The three experiments were conducted to verify the control performance of position/force control and guaranteed robustness to external forces. In the first experiment, the position/force control performance by the implicit force control under both with and without torque saturation is demonstrated. In the second experiment, the stable motion against excessive external forces of the proposed method without the force sensor is validated. The final experiment verified the effectiveness of the redundancy of the manipulator using the target response time. Fig. 2.45 shows the three-link manipulator utilized for the experiments. DC motors with optical encoders (made by harmonic-drive systems) on each joint are used in the manipulator. Moreover, the tip of the end-effector on the manipulator attached a single-axis force sensor (made by A&D Corporation). The proposed control system for the manipulator was implemented using a digital signal processor (sBOXII made by MIS Corporation). In the controller design, the physical parameters are link distance ($\{l_1, l_2, l_3\} = 0.20$ m) and mass ($\{m_1, m_3, m_5\} = 0.22$ kg, $\{m_2, m_4\} = 0.77$ kg). The force sensor requires the lowpass filter for the noise reduction; therefore, the time constant 0.05 s was used for the filter. In all experiments, the proposed control systems were discretized by $T_s = 0.001$ s. By using the motor and motor-driver specifications, the torque limitations of each link torque were defined as τ_{limit,q_1}=τ_{limit,q_2}=20.7360 Nm for the first joint and second joint, respectively, and

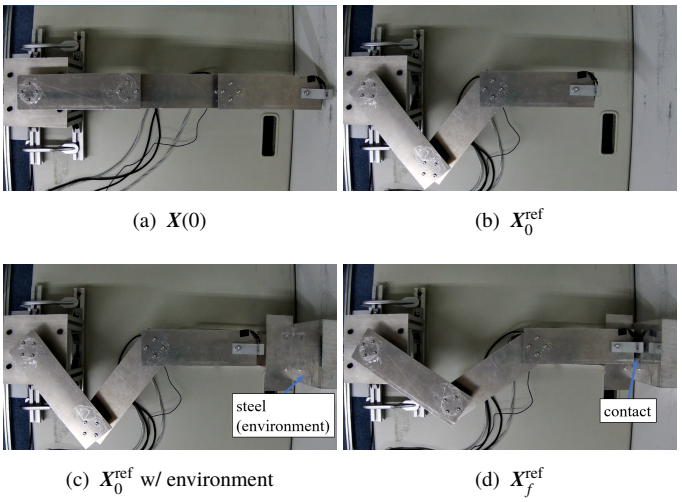

(a) $\boldsymbol{X}(0)$ (b) $\boldsymbol{X}_0^{\text{ref}}$

(c) $\boldsymbol{X}_0^{\text{ref}}$ w/ environment (d) $\boldsymbol{X}_f^{\text{ref}}$

FIGURE 2.46: An example snapshot of experiment 2.4.3.2.

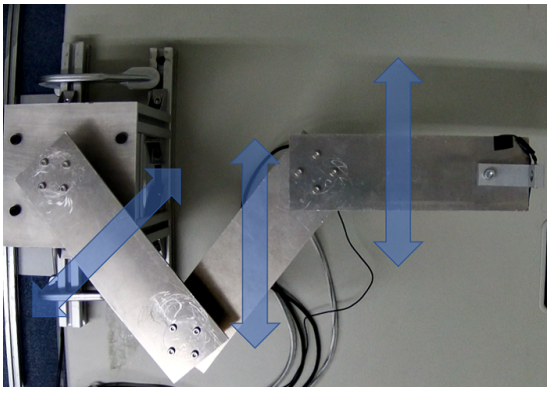

FIGURE 2.47: Experiments setup and configuration for 2.4.3.3. The blue arrows show the direction of the external forced disturbance.

τ_{limit,q_3}=12.6720 Nm for the third joint. Moreover, the saturation function based on the actual limitations was implemented in the plant input in the experimental systems.

2.4.3.1 Controller setup

In the experimental validations, conventional HPFC by acceleration control using IDOB and IDOB-based resolved acceleration control (DRAC)[100] were compared with the proposed method. Through the comparison of HPFC, it is validated that the torque bounded control system using the constrained position control system in each joint space brings equivalent control performance in HPFC with respect to conventional methods. Furthermore, through the comparison of DRAC, the usefulness of HPFC implemented by the constrained joint space control was verified. In the all systems, the IDOB was designed by using the nominal inertia matrix $\boldsymbol{J}_n$ = diag(2.6683, 1.6772, 0.8155) and the pole with [-40, -41, -42, -43, -44, -45, -46, -47, -48]. The $\boldsymbol{J}_n$ parameter was set by actual physical parameters. In order to avoid the singular

points, the initial state conditions of the IDOB used the initial angle reference (q_0^{ref}) with respect to the initial state reference. This is because the initial joint angles of the manipulator were allocated in the singular points. The singular state generates the overestimation of the Jacobian matrix. By using the angle reference as the initial state of the IDOB, the singular points for the Jacobian matrix were easily avoided. Additionally, the workspace position information in all results was derived by using the forward kinematics based on the state estimates by the IDOB.

The convert gain in the proposed implicit law was given by $K_f = 10F_x^{\mathrm{ref}}$ which was determined by considering contact velocity. The number of coincidence points and target response time in the PFC systems were set to $n = 3$ and $T_{\mathrm{ref},q_1} = T_{\mathrm{ref},q_2} = T_{\mathrm{ref},q_3} = 1.0$ s, and used for the experiments 2.4.3.2 and 2.4.3.3. The control performance of the proposed control system could be improved by using redundancy with modification of the target closed-loop response time, the results of which were shown in the final experiment 2.4.3.4. Furthermore, considering the difference of the motor outputs, the weight parameters used in the inverse kinematic were designed as $\{w_1, w_2, w_3\} = 10^2, 10^2, 10^1$.

The compared HPFC and DRAC systems were designed as the controller equations for the control input, which, for HPFC, can be represented as

$$\begin{aligned}
\boldsymbol{\tau} &= \boldsymbol{J}_n\{\boldsymbol{q}^{\mathrm{ref}} + \boldsymbol{\tau}_{\mathrm{d}}\}, && (2.88)\\
&= \boldsymbol{J}_n\{\boldsymbol{q}_{\mathrm{pos}}^{\mathrm{ref}} + \boldsymbol{q}_{\mathrm{force}}^{\mathrm{ref}} + \boldsymbol{\tau}_{\mathrm{d}}\}, && (2.89)\\
\boldsymbol{q}_{\mathrm{pos}}^{\mathrm{ref}} &= \boldsymbol{K}_{phx}\boldsymbol{J}_{aco}^{+}\{\boldsymbol{S}(\boldsymbol{X}_0^{\mathrm{ref}} - \hat{\boldsymbol{X}}) - \boldsymbol{K}_{dhx}\dot{\boldsymbol{q}} && (2.90)\\
\boldsymbol{q}_{\mathrm{force}}^{\mathrm{ref}} &= \boldsymbol{K}_{phf}\boldsymbol{J}_{aco}^{\mathrm{T}}\{(\boldsymbol{I} - \boldsymbol{S})(\boldsymbol{F}^{\mathrm{ref}} - \boldsymbol{F}^{\mathrm{res}}), && (2.91)
\end{aligned}$$

and, for the DRAC, as

$$\begin{aligned}
\boldsymbol{\tau} &= \boldsymbol{J}_n\{\boldsymbol{q}^{\mathrm{ref}} + \boldsymbol{\tau}_{\mathrm{d}}\}, && (2.92)\\
&= \boldsymbol{J}_n\boldsymbol{J}_{aco}^{+}\{\boldsymbol{K}_{px}(\boldsymbol{X}^{\mathrm{ref}} - \hat{\boldsymbol{X}})\\
&\quad -\boldsymbol{K}_{dx}\dot{\boldsymbol{q}} - \dot{\boldsymbol{J}}_{aco}\dot{\boldsymbol{q}}\}, && (2.93)
\end{aligned}$$

where ($\boldsymbol{K}_{phx}$, $\boldsymbol{K}_{px}$) and ($\boldsymbol{K}_{dhx}$, $\boldsymbol{K}_{dx}$) are the proportional and differential gains for the position control, respectively, $\boldsymbol{K}_{phf}$ denotes the proportional gain for the force control, and $\boldsymbol{S}$ is a select matrix (diag(0,1,1)). $\boldsymbol{J}_{aco}^{+}$ is the pseudo-inverse matrix of $\boldsymbol{J}_{aco}$. The Jacobian matrix in this section is a square matrix; therefore, it does not require usually the pseudo-inverse matrix. However, it was used due to the ability to treat the singular point. The velocity feedback-loop was added to the position controller on the force control, which was introduced to reject the impact force. The reference generator and the IDOB for DRAC were set the same as the proposed control system. Furthermore, these parameters were adjusted using trial and error via each experiment.

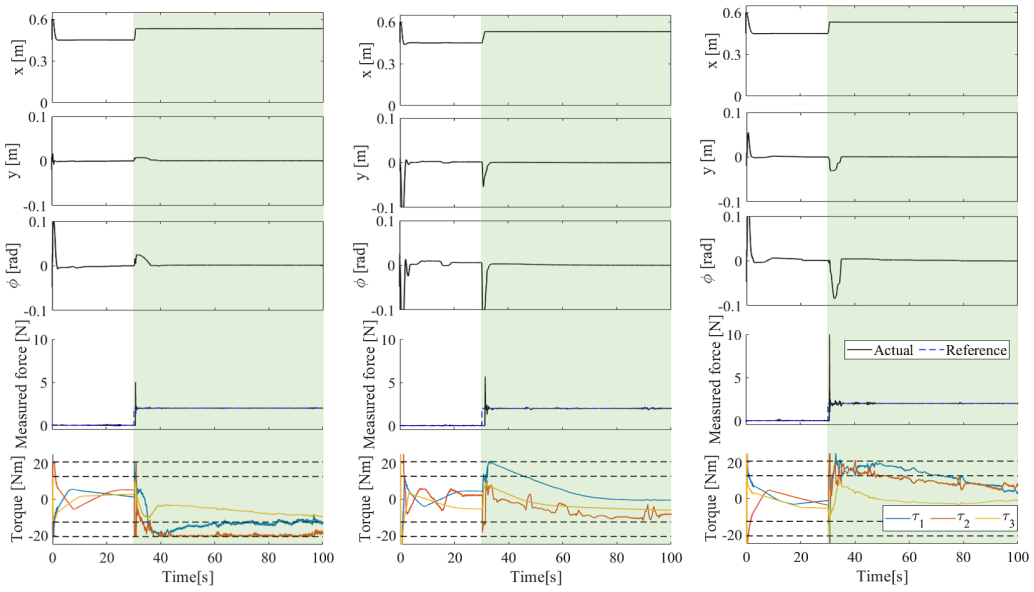

(a) prop. (b) conv. HPFC (c) conv. DRAC

FIGURE 2.48: Experimental results on $F_x^{\text{ref}} = 2\text{N}$ in Sec. 2.4.3.2 . The filled area shows the position/force control. The dashed lines in the torque results are the torque limitations $(\tau_{\text{limit},q_1,q_2,q_3})$.

2.4.3.2 Results on HPFC

The first experiment verified the control performance for tracking control of the position and force by the proposed control system when it comes into contact with the rigid environment. In the case of the rigid environment contact, because of saturation on input torque by the reaction force, conventional force control systems can frequently generate unstable motion, when the manipulator comes into contact with the rigid objects. The proposed control system considering the torque saturation by the designed constraints can avoid unstable behavior. This experiment considered two force references on the x-axis: 2 and 5 N. Moreover, in each control system, the force reference 2 N did not make the saturation on the torque but the force reference 5 N did.

The validated control scheme began from an initial state $\boldsymbol{X}(0) = [x(0) \;\; y(0) \;\; \phi(0)] = [0.6 \;\; 0 \;\; 0]$ and then moved to the initial position $\boldsymbol{X}_0^{\text{ref}} = [x_0^{\text{ref}} \;\; y_0^{\text{ref}} \;\; \phi_0^{\text{ref}}] = [0.45 \;\; 0 \;\; 0]$; the position and force control were handled from around 30 s. The references of the position and force control were set to $\boldsymbol{X}_f^{\text{ref}} = [F_x^{\text{ref}} \;\; y^{\text{ref}} \;\; \phi^{\text{ref}}] = [(2 \text{ or } 5 \text{ N}) \;\; 0 \text{ m} \;\; 0 \text{ rad}]$. The workspace force reference F_x^{ref} was transformed to the workspace position reference by using the proposed implicit force control law described in 2.4.2.2. Fig. 2.46 shows a snapshot in the experiments. In Fig. 2.46(b)-(c), an environment of steel was installed, and the force control performance was verified by contact with the steel. Moreover, the switching of references from position control to hybrid control was performed manually. The workspace position reference of the proposed method is (2.62). It is necessary for the posture angle control of the end effector by the controllers because the uniaxial

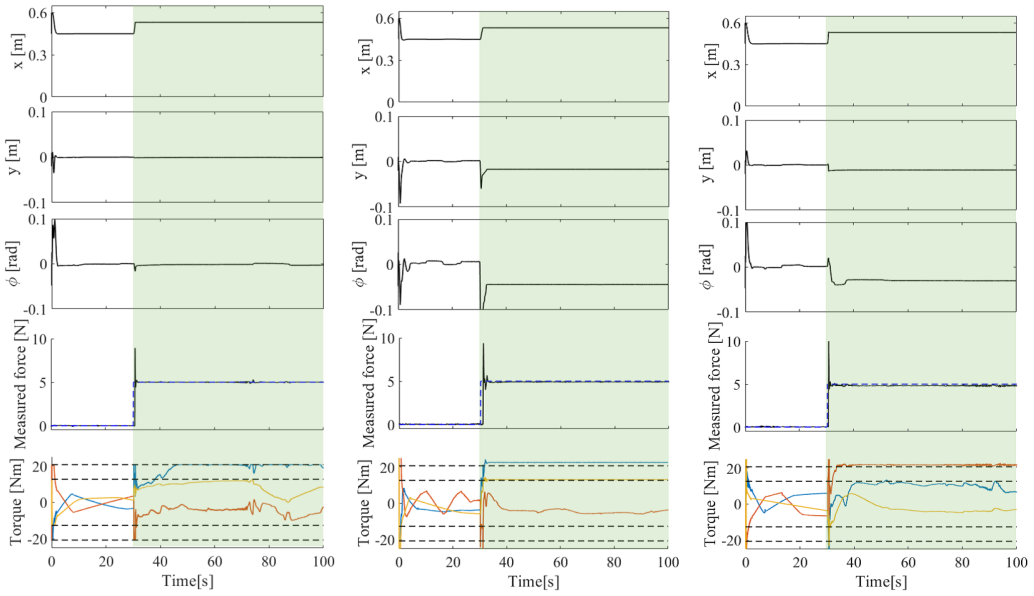

(a) prop. (b) conv. HPFC (c) conv. DRAC

FIGURE 2.49: Experimental results on $F_x^{\text{ref}} = 5$N in Sec. 2.4.3.2 . The filled area shows the position/force control. The dashed lines in the torque results are the torque limitations ($\tau_{\text{limit},q_1,q_2,q_3}$)

force sensor was utilized. Therefore, proper attitude control is required to perform appropriate force control. Moreover, in the proposed method, considering the independent position control of the workspace and joint space, the initial joint position control by the initial angle reference ($\boldsymbol{q}_0^{\text{ref}}$) was used to move from initial state $\boldsymbol{X}(0)$ to $\boldsymbol{X}_0^{\text{ref}}$. Conventional workspace position control systems are difficult to control the initial posture (elbow up or down), but the proposed control system can easily control the initial posture. However, the proposed method can be directly controlled the posture.

In the HPFC system, the control gain matrices were given by (2N): $\boldsymbol{K}_{phx} = \{\text{diag}(30, 30, 30)\}$, $\boldsymbol{K}_{dhx} = 2\sqrt{\boldsymbol{K}_{phx}}$, $\boldsymbol{K}_{phf} = \text{diag}(40, 40, 40)$, and (5N): $\boldsymbol{K}_{phx} = \{\text{diag}(30, 30, 30)\}$, $\boldsymbol{K}_{dhx} = 2\sqrt{\boldsymbol{K}_{phx}}$, $\boldsymbol{K}_{phf} = \text{diag}(20, 20, 20)$. For the DRAC system, the control gain matrices were set as (2N): $\boldsymbol{K}_{px} = \text{diag}(15, 15, 15)$ and $\boldsymbol{K}_{dx} = 2\sqrt{\boldsymbol{K}_{px}}$, and (5N): $\boldsymbol{K}_{px} = \text{diag}(30, 30, 30)$ and $\boldsymbol{K}_{dx} = 2\sqrt{\boldsymbol{K}_{px}}$.

The validated results on F_x^{ref} =2 N by each controller are illustrated by Fig. 2.48. From the results of the proposed method, it is confirmed that; the maximum impact force is 5.0152 N, the free motion time from force control start to contact is 522 ms, and the mean error on force tracking for 50-100 s is 0.0032 N. In the HPFC system, the maximum impact force is 5.6958 N, the free-motion time is 1,070 ms, and the mean error of steady-state force tracking for 50-100 s is 0.0008 N. In the DRAC system, the impact force is 10.2835 N, the free-motion time is 517 ms, and the mean error of force tracking for 50-100 s is -0.0007N. From the results, it is confirmed that the proposed control system has comparable force control performance with respect to conventional control systems. Additionally, in the proposed system, the fluctuations for position

and posture are minimal. Furthermore, it has a smaller impact force than the HPFC system, and the free motion time is shorter (i.e., the motion control is faster). The proposed system also brings a smaller impact force than the DRHC system, and the free-motion time is equivalent. Hence, the proposed control system can simultaneously handle the impact force rejection and fast motion control; however, the mean error on the force is slightly larger than conventional systems, and an undesired torque saturation is made. These are attributed to the design of the target closed-loop response time. Therefore, this force tracking error can be suppressed by improving the tune-up, and Sec. 2.4.3.4 illustrates its result. Additionally, it is confirmed that the proposed control system is effective and useful for ensuring stable motion control when torque inputs are not saturated.

The validated results on F_x^{ref} =5 N are shown in Fig. 2.49. The results are indicated that the torque inputs of each controller are saturated while controlling the force. Therefore, in theory, each controller does not realize complete force control because the control input is not enough for the force control. In the results of the proposed control system, the maximum impact force is 8.9371 N, the free-motion time is 520 ms, and the mean error on force tracking for 50-100 s is 0.0010 N. Moreover, the variation of torque in the initial position control was made by the disturbance estimates affected by nonlinear friction. In the results of the conventional HPFC system, the maximum impact force is 9.3942 N, the free-motion time is 899 ms, and the mean error on force tracking for 50-100 s is 0.0809 N. In the results of the conventional DRAC system, the maximum impact force is 15.2608 N, the free-motion time is 434 ms, and the mean error for 50-100 s is 0.1835 N. Indeed, in force control performance, the proposed control system can better suppress impact force compared with the conventional HPFC system. The validated results are indicated that that the DRAC has a large reaction force and mean tracking error. Moreover, with respect to implicit force control, it was difficult to control the force by using the DRAC system while considering posture control. By contrast, the proposed method by using the implicit control and the torque saturation can suppress the bouncing motion caused by the contact. Moreover, the free-motion time of the proposed method is decided by the adaptive gain without references and environmental paramFeters; therefore, the proposed implicit control law is effective for stable force control with uncertain environments. Considering the position control results, the results of y and ϕ indicates that the proposed control system has a better tracking performance than the conventional systems. By contrast, the conventional control systems cannot accurately control the position and posture due to the input torque saturation by contact because the torque saturation generates these tracking errors. Additionally, the results are indicated that the torque inputs calculated from the conventional controllers are clearly saturated, and vibrational motion and tracking error are caused. However, the torque beyond the mechanical limitation is rejected by the saturation function; therefore, unstable motion by excessive control inputs is avoided.

Overall, the results are indicated that the proposed method can perform the stable position/force control explicitly considering the torque limitation via the acceleration reference. Moreover, the

target response time can be implemented while considering the saturation on each actuator, and it is useful for generating the stable coupled workspace motion. In essence, the proposed control system can avoid unstable motion generation and excessive control inputs and optimize joint motion control. Consequently, the unnecessary variations in position and posture are rejected by constrained robust joint space controller, and the proposed control system can achieve stable motion control in hybrid position/force control.

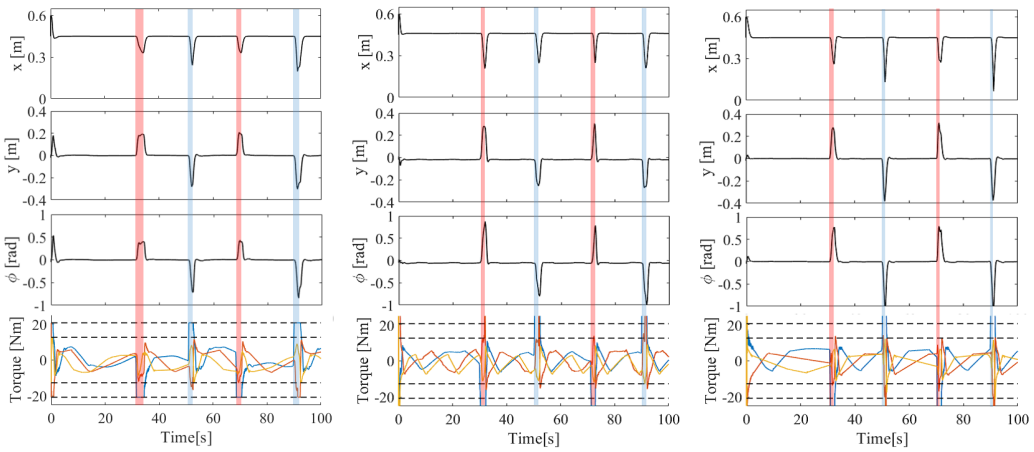

(a) prop. (b) HPFC (c) DRAC

FIGURE 2.50: Experimental validation results on l_1 in 2.4.3.3. In the red and blue filled areas, the first link was disturbed to the left side ($q < y$) by force and to the right side ($y < q$) by forced disturbance.

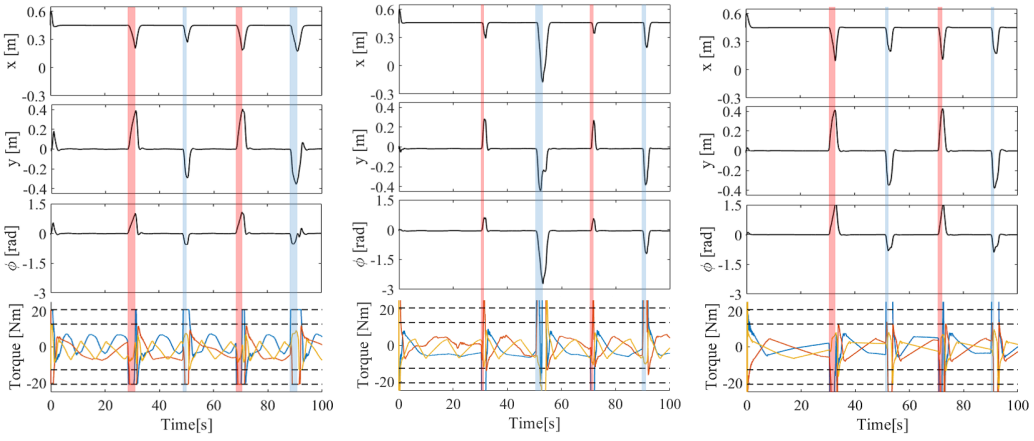

(a) prop. (b) HPFC (c) DRAC

FIGURE 2.51: Experimental validation results on l_2 in 2.4.3.3. In the red and blue filled areas, the second link was disturbed to the left side ($q < y$) by force and to the right side ($y < q$) by forced disturbance.

2.4.3.3 Motion generation against external forces

Torque-bounded control systems are effective to guarantee stable motion against external disturbances with undesired contact. Furthermore, the torque-bounded robot control systems oppose the external disturbance force until the torque is reached to the constraints, then, it moves according to the external force after constraint activation. In particular, this behavior assists safety motion generation for various robot tasks. The proposed control system has the potential to apply in these areas. Fig. 2.47 shows a setup for the experiment. In this experiment, the external

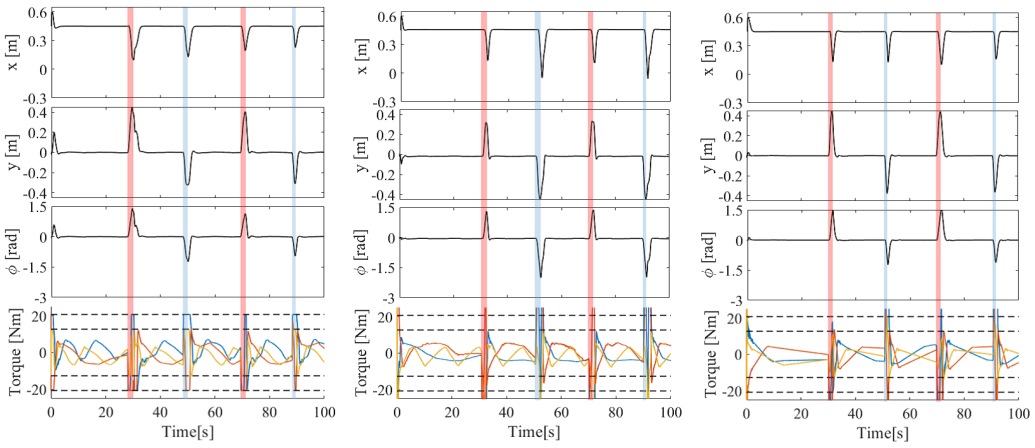

(a) prop. (b) HPFC (c) DRAC

FIGURE 2.52: Experimental validation results on l_3 in 2.4.3.3. In the red and blue filled areas, the third link was disturbed to the left side ($q < y$) by force and to the right side ($y < q$) by forced disturbance.

disturbance forces of roughly $\pi/2$ [rad] to each link are forcibly applied. The controller parameters use the same as Sec. 2.4.3.2. Note that the initial state values in the proposed method are defined by the joint space position. In this experiment, the initial states were set to the workspace position to verify the workspace behavior against external disturbances.

The experimental results on each link are shown in Figs. 2.50-2.52. From the results, it is confirmed that the proposed control system can always perform the stable motion generation for the manipulator under torque saturation regardless of the contact points on the robot arm. Furthermore, after torque saturation, the position and posture increase monotonically. Therefore, it is evident that the proposed method can generate the constrained stable motion adapted to external disturbance torques. Additionally, the proposed system can suppress overshoot and avoid vibration based on the imposed torque constraints. Moreover, the stable recovery motion is generated by the target response time. By contrast, the HPFC system generates large and unwanted motion against excessive disturbance (see the result of l_2). Indeed, the HPFC system is occasionally dangerous owing to create excessive reaction motion with excessive torque. In theory, the excessive torque against the large disturbance is always generated by simple feedback. The same can be indicated for the DRAC system. The excessive reactions by the conventional simple feedback system are problematic, and it is not ensured the safety motion generation. Therefore, the proposed method with target response time and constrained motion control is effective for the safety contact motion generation. Additionally, considering unmeasured disturbances, the disturbance torque estimation method assists to improve the overall control performance of the proposed method. Therefore, the proposed control system is expected to extend with reaction torque observer [101]-[103].

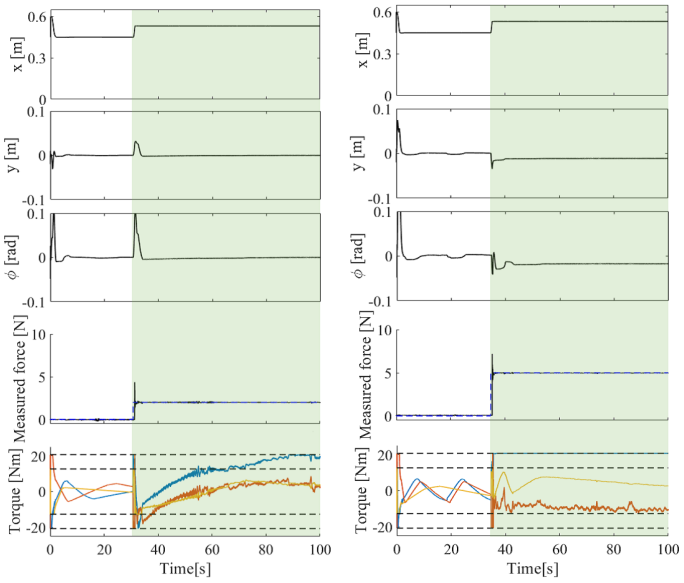

(a) Trackability improvement (b) Impact force improvement

FIGURE 2.53: Experimental results on 2.4.3.4.

2.4.3.4 Modification of T_{ref}

This section attempts to improve the position/force tracking control performance for the experiment in Sec. 2.4.3.2 for a force response of 2 N and to suppress the impact force in the case of the force reference 5 N. It is validated to the effectiveness of independent control response on all links and redundancy. The results on the improved control performance in Sec. 2.4.3.2 for a force of 2 N are shown in Fig. 2.53(a). Moreover, the target response times of each link are modified as $T_{\text{ref},q_1} = 1.0$ s, $T_{\text{ref},q_2} = 1.0$ s, and $T_{\text{ref},q_3} = 0.7$ s. Furthermore, in the results of the experiment of Sec. 2.4.3.2, the force tracking error was observed as 0.0032N. Thus, the target response time of q_3 must decrease to track the posture and force of the end effector effectively. For the results, the maximum impact force is 4.3555 N, the contact-free time is 544 ms, and the mean error on force tracking for 50 -100 s is -0.0004 N. These results indicate the improved performance of force tracking control. It is evident that the control performance can easily be improved by the modified target time.

Fig. 2.53(b) shows the results regarding 5 N and reducing the impact force. The target response times on each PFC system were set to $T_{\text{ref},q_1} = 1.2$ s, $T_{\text{ref},q_2} = 0.5$ s, and $T_{\text{ref},q_3} = 0.7$ s. The maximum impact force is 7.1967 N, and the contact-free motion time from force control start to contact is 482 ms. From the results, it is confirmed that the impact force was reduced, and fast motion control was performed. Thus, it is evident that the proposed system can easily adjust compared to conventional methods. On the other hand, because the focus in this section concerns force control, the tracking errors in posture and position remain. To effectively balance

the position control and force control, the target time design considering the force reference and the contact-free motion is required.

2.4.4 Summary

In this section, an application example of the MPC ingested IDOB was shown. Unlike the previous section, this section described a constrained acceleration control strategy by the fast MPC with the IDOB. In this section, by using the constrained acceleration control, it was shown that the robust constrained motion control can be achieved as a robust HPFC strategy based on PFC-based joint space position control with torque constraints for an MDoFM. The proposed system in this section is useful to consider the control with target response time and torque saturation compared to conventional controllers. Moreover, the experimental results indicate that the proposed system is effective in improving safety motion generation against external disturbance forces and torque-bounded control. In future studies, an optimal method for setting target response time by control target tasks is a must. Additionally, the proposed system can be easily extended to high dimensional manipulator systems by the inverse kinematics and decoupling control by DOB-based control. Considering the stable/safe motion generation, the proposed system is particularly effective for robot systems interacting with unknown environments.

2.5 Chapter summary

In this chapter, the integration methods of MPCs and DOBs were shown.

In Sec. 2.2, the conventional DOBs were explained. In Sec. 2.3, how to integrate the IDOB to MPCs was shown, and its verification results showed the effectiveness and usefulness of the IDOB-based MPC. In Sec. 2.4, considering implementing the acceleration control and fast motion control, a PFC, which is a fast MPC, with the IDOB system was shown. The experimental results show the IDOB-based PFC can achieve robust constrained motion control for stable motion generation.

Chapter 3

Robust Motion Control Considering Observation Noise

3.1 Introduction

In the previous chapter, robust constrained motion control systems by IDOB-MPC are explained.

The main drawback of the DOBs is high noise sensitivity, and the influences of the noise occasionally limit the application of DOB. Therefore, in this chapter, a DOB with observation noise reduction is introduced. The design of the DOB is based on the Kalman filter(KF) which estimates the state vector considering noise influences. In addition to this, the verification results of the KF-based DOB with MPC are shown. The simultaneous state and disturbance estimation with observation noise reduction are useful for improving the control performance of MBC systems. In particular, the influences of noise often cause constraint violations, which is a problem with MPC systems. The constrained MPC operates at the bound of the constraints; therefore, the influences of the noise sometimes make a fatal problem. The main objective of this chapter is to address the problem of MPC made by noise influences. This chapter describes a constrained motion control system based on MPC and Kalman filter with disturbance estimation (KFD).

In Sec. 3.2, the design method of DOB with observation noise reduction is explained. In Sec. 3.3, the novel DOB-based MPC is explained. In Sec.3.4, a design method of nonlinear DOBs based on nonlinear KF-DOB to apply nonlinear systems is described.

Sec. 3.5 concludes this chapter with a clarification of the problem of the KF-based DOB.

3.2 Kalman filter with disturbance estimation

The KFD aims to estimate the state and disturbance and to eliminate noise influences simultaneously, in a motor system affected by noise. In order to design the KFD, the extended state-space model used in the IDOB uses as an internal model of the KF. In theory, by using the extended model as the internal model in the KF, the KF can estimate the disturbance. Moreover, the noise reduction performance by KF is better than by DOBs. Therefore, the KFD can probably perform the accurate state estimation with disturbance estimation without noise influences.

In this section, the mathematical model described in Sec. 2.3.1 is utilized for verification. Moreover, the extended system design is the same as the previous chapter; however, the KFD design is defined with the discrete-time model.

3.2.1 Design of Kalman filter with disturbance estimation

In this section, the design method of the KFD is explained.

The state vector $x(k) = [z \ v]^{\mathrm{T}}$, the control input $u(k)$, measured output $y(k)$, and coefficient matrices of the discrete-time state-space model ($\boldsymbol{A}_d$, $\boldsymbol{B}_d$, and $\boldsymbol{C}_d$) are defined. The sampling time of the KFD is δ_1. The state-space model of the plant with the disturbance is then given by

$$x(k+1) = \boldsymbol{A}_d x(k) + \boldsymbol{B}_d u(k) - \boldsymbol{B}_d d(k), \tag{3.1}$$

$$y(k) = \boldsymbol{C}_d x(k). \tag{3.2}$$

The extended state space model for augmented state vector ($\bar{X} = [x \quad \hat{d}]^{\mathrm{T}}$) is given by

$$\begin{bmatrix} x(k+1) \\ d(k+1) \end{bmatrix} = \begin{bmatrix} \boldsymbol{A}_d & -\boldsymbol{B}_d \\ 0 & \boldsymbol{I} \end{bmatrix} \begin{bmatrix} x(k) \\ d(k) \end{bmatrix} + \begin{bmatrix} \boldsymbol{B}_d \\ 0 \end{bmatrix} u(k), \tag{3.3}$$

$$y(k) = \begin{bmatrix} \boldsymbol{C}_d & 0 \end{bmatrix} \begin{bmatrix} x(k) \\ d(k) \end{bmatrix}. \tag{3.4}$$

This extended system can use to estimate both input and output disturbances. Eqs. (3.3) and (3.4) are used to design the KFD. Adding the system and observation noises based on normal white noise to the extended system, the modified extended system can be described as

$$\bar{X}(k+1) = \bar{A}_d \bar{X}(k) + \bar{B}_d u(k) + \bar{B}_d v(k), \tag{3.5}$$

$$y(k) = \bar{C}_d \bar{X}(k) + w(k), \tag{3.6}$$

where $\bar{A_d} = \begin{bmatrix} \boldsymbol{A}_d & -\boldsymbol{B}_d \\ 0 & \boldsymbol{I} \end{bmatrix}$, $\bar{B_d} = \begin{bmatrix} \boldsymbol{B}_d \\ 0 \end{bmatrix}$ and $\bar{C_d} = \begin{bmatrix} \boldsymbol{C}_d & 0 \end{bmatrix}$. Moreover, the input and output noises are defined as independent white noise and can be described as $v \sim \mathrm{N}(0, \sigma_v^2)$ and $w \sim \mathrm{N}(0, \sigma_w^2)$. σ_v and σ_w denote each variance.

The KFD design method follows the general KF design[16]. Generally, state estimation of the KFs are calculated by the following time-update equations,

$$\hat{X}^-(k) = \bar{A_d}\hat{X}(k-1) + \bar{B_d}u(k-1) \tag{3.7}$$

$$P^-(k) = \bar{A_d}P(k-1)\bar{A_d}^T + \bar{B_d}\sigma_v^2\bar{B_d}^T \tag{3.8}$$

$$G(k) = P^-(k)\bar{C_d}(\bar{C_d}P^-(k)\bar{C_d}^T + \sigma_w^2)^{-1} \tag{3.9}$$

$$\hat{X}(k) = \hat{X}^-(k) + G(k)(y(k) - \bar{C_d}\hat{X}^-(k)) \tag{3.10}$$

$$P(k) = (I - G(k)\bar{C_d})P^-(k) \tag{3.11}$$

where $\hat{X}^-(k)$ and $P^-(k)$ denote a priori state estimation and a priori covariance matrix. Moreover, $\hat{X}(k)$, $P(k)$, and $G(k)$ denote the state estimates, covariance matrix, and Kalman gain, respectively. Furthermore, σ_v^2 and σ_w^2 denote the variances for the system and observation noises.

By using the extended system and Eqs.(3.7)-(3.11), the KFD can be designed.

3.3 Noise-free constrained motion control

An MPC system with the KFD is robust and cancels disturbances using the special method. Moreover, the feasibility of the KFD-based MPC system is verified under the condition of strong external disturbances, observation noise, and friction force. In the verification results, the superior control performance over the conventional MPC system is shown.

Standard MPCs optimize control inputs considering the constraints imposed on system state and control inputs. The constraints of MPC are occasionally violated by the influences of noise and disturbances. Moreover, the problem is called constraint violation of the MPC[17]. With respect to the constraint violation, MPC cannot achieve safe and reliable motion control by constrained control. In the conventional method, the switched MPC has been developed to avoid constraint violation by noise influences. The switched MPC system has constrained MPC system and unconstrained MPC. In this system, the constraints violation is avoided by switching unconstrained MPC. The unconstrained MPC can describe a time-invariant system; therefore, the stability of the control system is compensated. However, the computational load is heavier than standard MPC, and unexpected motion is clearly generated.

As described in the previous chapter, to suppress or remove disturbances, some researchers were incorporated the DOB into MPC[41, 42, 47, 49–51]. The DOB performs disturbance rejection and estimation and robust control. However, DOBs cannot always be compensated for expected performances in noisy environments. In other words, the application of DOBs is limited. By contrast, the KFD has the potential to estimate disturbances and reduce the influences of noise in noisy environments.

This section introduces that the KFD-based MPC system can treat the influences of both noise and disturbances. In order to integrate the KFD to the MPC, the MPC with disturbance suppression is used in this section.

3.3.1 Proposed control system

This section provides the details of the proposed method.

The proposed control system includes an additional KFD, which estimates the state and disturbance. The designs on MPC and KFD uses the cart model (Eqs. (2.46) and (2.47)) including disturbance estimates (= $\hat{d}$). Moreover, each observation matrix of the MPC and KFD are independently set to ($C = [1 \quad 0 \quad 0]$) in KFD and ($C = I^{3\times3}$) in MPC.

Moreover, the control law (Eq. (2.48)) is given by

$$J = \sum_{i=1}^{N_p} ||\boldsymbol{r}(k+i|k) - \bar{\boldsymbol{x}}(k+i|k)||_Q^2 + \sum_{i=0}^{N_u-1} ||\Delta u(k+i|k)||_R^2. \tag{3.12}$$

where $\boldsymbol{r}$ denotes the reference for the extended state vector. The estimates of the extended state vector are obtained from the KFD.

In the proposed control system, disturbances other than low-frequency disturbances are regarded as noise effects. The KFD attenuates the influences of system and observation noises.

3.3.2 Controller setup

Tables 3.1 and 3.2 show the parameters for the MPC and KFD. The design of KFD is as follows; the system noise to 18 times the real input noise, the output noise to 0.09 times the real sensor noise, and small initial values set to the error covariance matrix. All parameters for KFD were tuned up considering the disturbance estimation speed. The overestimated system noise generates fast disturbance estimation; however, the estimates are significantly affected by the noise influences. The entries Q_m and R_m in Q_{mpc} and R_{mpc}, respectively, are appropriately expanded by each prediction horizon. For assisting the stability, the final weighting matrix $[Q_{m-last}]$ of Q_{mpc} was set to triple the normal weight.

The weight matrices can be described as

$$Q_{mpc} = \begin{bmatrix} Q_m & & 0 \\ & \ddots & \\ 0 & & Q_{m-last} \end{bmatrix} \in \mathbb{R}^{60\times 60}$$

$$\text{and, } R_{mpc} = \begin{bmatrix} R_m & & 0 \\ & \ddots & \\ 0 & & R_m \end{bmatrix} \in \mathbb{R}^{5\times 5}.$$

where all tuning parameters (Q_f, R_f, Q_{mpc}, R_{mpc} and H_p, H_u) in the MPC were set with trial and error.

3.3.3 Numerical verification: disturbance and noise suppressions

To show the effectiveness of the proposed method, simple simulations with disturbance, system noise, and observation noise are conducted in the mass-damper system. The references were position 1 m, velocity 0 m/s, disturbance 0 N·m. Moreover, the position constraint was set to 1

TABLE 3.1: Parameters on KFD

Covariance of system noise	$Q_{kl} = Q_n \times 18$
Covariance of observation noise	$R_{kl} = R_n \times 0.09$
Initial value for covariance matrix	$P_0 = \mathrm{diag}(10^{-6}\ 10^{-6}\ 10^{-2})$
Sampling time for estimation	$\delta_1[s] = 0.01$

TABLE 3.2: Parameters on MPC

Weight matrix on tracking error	$Q_m = \mathrm{diag}(2 \cdot 10^3\ 10^2\ 10^{-2})$
End of weight matrix on tracking error	$Q_{m-last} = 3 \times Q_m$
Weight matrix on amount of control input change	$R_m = 10^{-1}$
Horizons	$[N_p\ N_u] = [20\ 5]$
Sampling time for control	$\delta_2[s] = 0.1$

m. Using this constraint, the MPC can effectively suppress overshoot, and the effectiveness of the proposed method for the constraints violation by noise influences can be shown.

The simulation conditions are shown in Table 3.3.

3.3.3.1 Results

Fig. 3.1 shows the simulation results. The observation, reference, and estimation positions are shown in Fig. 3.1(a). The position and velocity estimated by the KF are shown in Fig. 3.1(b), and Fig. 3.1(c) shows the disturbance estimates. The compare results on the disturbance estimates by the KF and DOB are shown in Fig. 3.2. Using the half position constraints, Fig. 3.3 shows the constrained control ability of the proposed method.

Fig. 3.4 shows the verification results by the conventional MPC method. From all results, it is confirmed that the proposed method can perform accurate position control under noise and disturbances. Fig. 3.3 indicates that constraints were definitely imposed by the proposed method.

TABLE 3.3: Verification conditions

Covariance of system noise	$Q_n = 10^{-3}$
Covariance of observation noise	$R_n = 2\ cdot10^{-4}$
Input disturbance	$d = 0.5 \quad (\mathrm{in} \quad 10\ [s])$

where, $eX = 10^X$

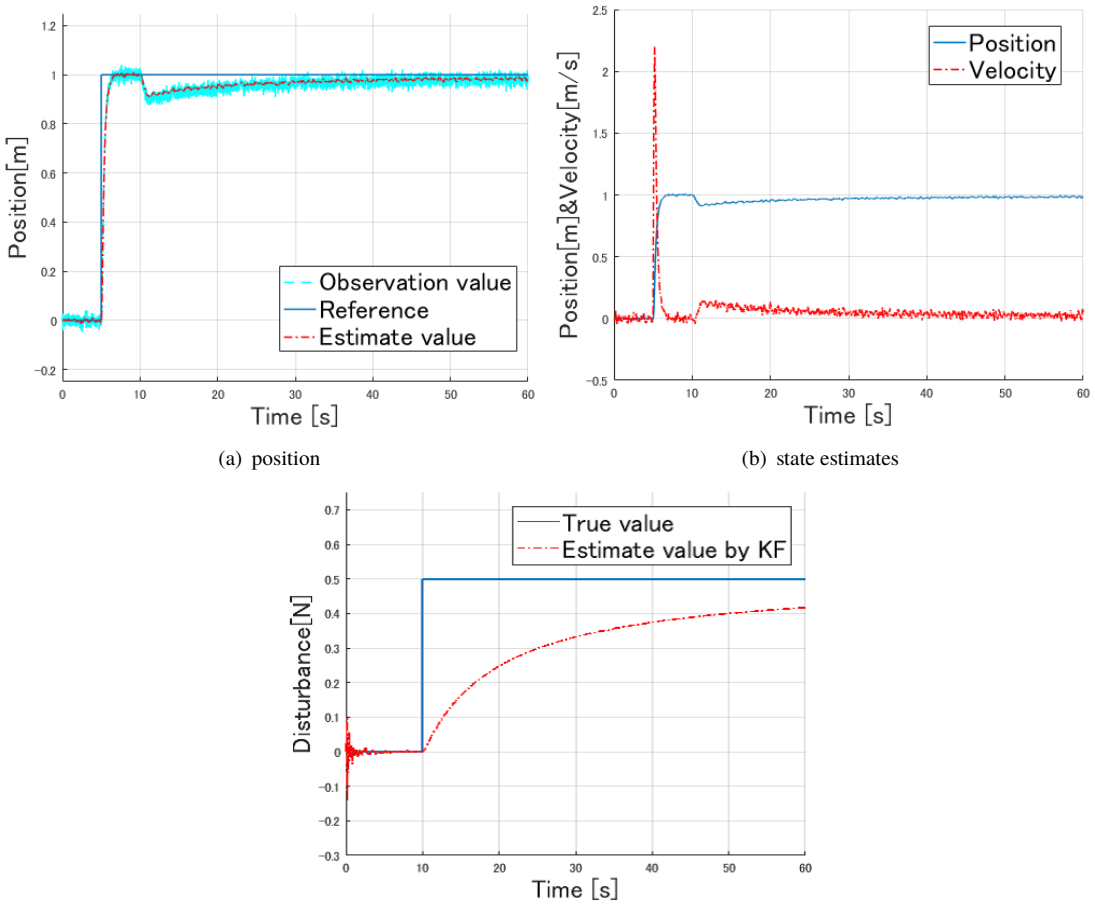

(a) position

(b) state estimates

(c) disturbance estimates

FIGURE 3.1: Simulation results

From the position results, the proposed method can achieve an accurate state estimation under the noise environment. The estimation ability is clearly obtained from general KFs. With respect to the disturbance estimation, the proposed method can better suppress the disturbance influences than the standard MPC. It is indicated that the proposed MPC system can perform accurately constrained control under the influence of noise and disturbances.

However, the estimation speed of the KFD is sluggish, and it generates a tracking error. Fig. 3.1(c) shows that the estimated disturbance does not converge to the actual disturbance. Although disturbance estimation is sluggish in the KFD than in the conventional DOBs, the noise sensitivity of the KFD is better than the DOBs. Additionally, the control performance of the proposed MPC depends on the estimation speed of the KFD. This sluggish estimation cannot be improved by modified some parameters. In the case of the KFD based on steady-state KF, the pole of the KFD is assigned as $10^3\times$[-6.9098 -0.0012+0.004i -0.0012-0.0004i]. Consider the pole information of the KFD, it is evident that the estimation speed on velocity and disturbance is slow. Additionally, if the disturbance estimation of the KFD can be improved, the control performance of the proposed MPC system will also be improved.

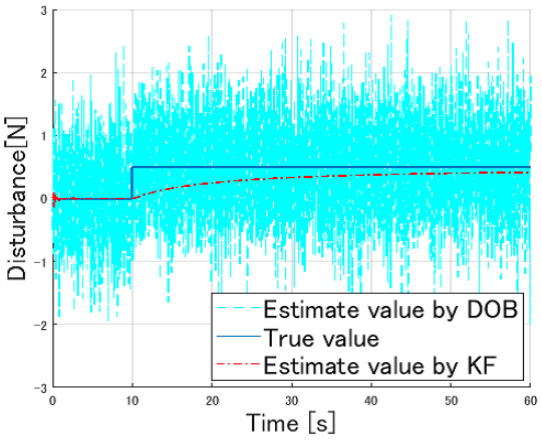

FIGURE 3.2: Simulation results: disturbance estimates by KFD and IDOB

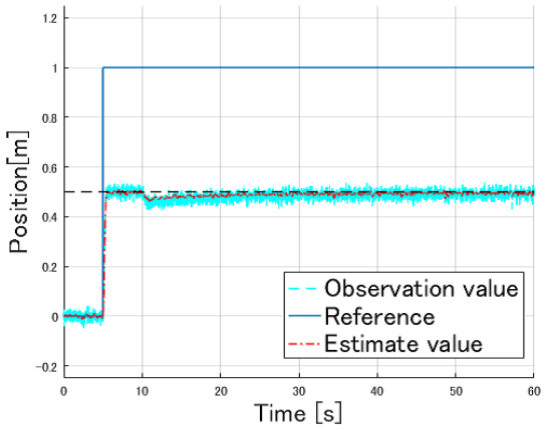

FIGURE 3.3: Simulation results: validation for constraint

The improved KFD is described in the next chapter.

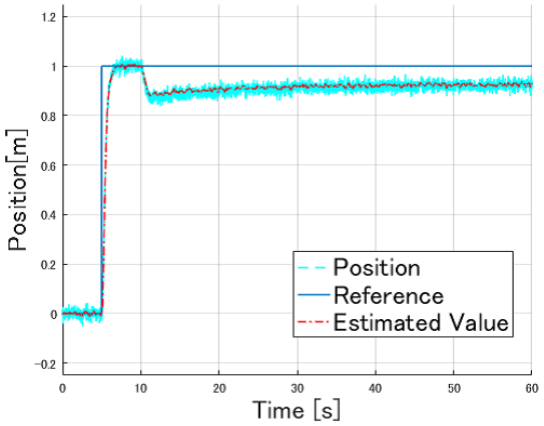

FIGURE 3.4: Simulation result: position by standard MPC

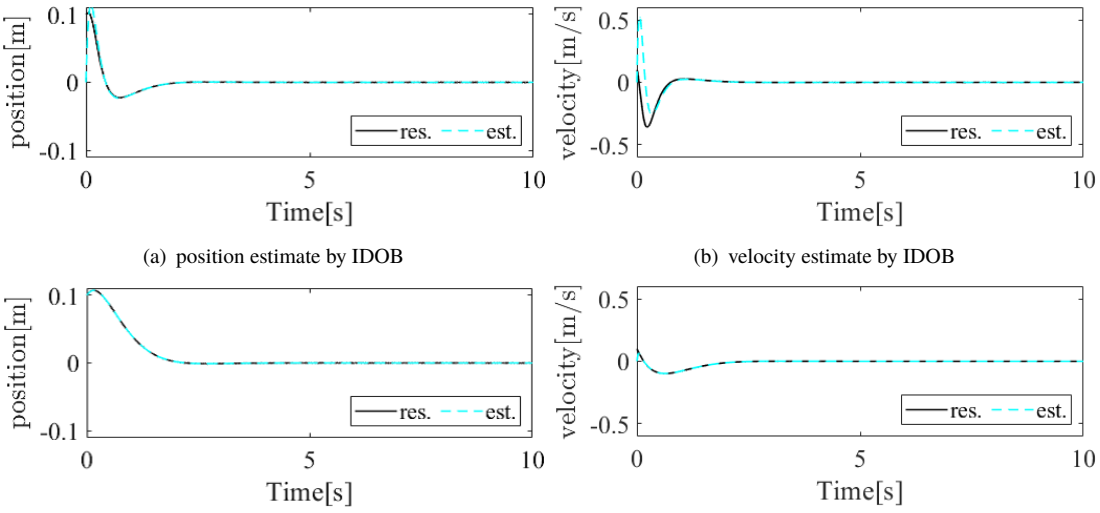

(a) position estimate by IDOB

(b) velocity estimate by IDOB

(c) position estimate by KFD

(d) velocity estimate by KFD

FIGURE 3.5: Comparison results on state estimation with initial state error by IDOB and KFD

3.3.4 Numerical verification: control input and velocity constraints

The previous section explains the disturbance and noise suppression performance of the proposed method under the state constraints. This section describes the constrained control performances under the control input constraints and state constraints. The simulation and compared methods are the same as Sec. 2.3.6. However, the small observation noise (variance; 10^{-8}) is added to the position response. In this section, the TPW-MPC was used in the proposed method.

In contrast to Sec. 2.3.6, the initial values of plant and KFD are different. Fig. 3.5 shows state estimation results by IDOB and KFD. From the results, the KFD has the robustness to initial state error. The IDOB estimation is affected by the errors of the initial state. By contrast, KFD can handle the error by the adaptivity of the KF law. It is an advantage of the KFD method.

Therefore, the initial values were set to [0.1 0.1] for the plant, and [0 0] for the KFD.

3.3.4.1 Results

The simulation results are shown in Figs. 3.6-3.30. Additionally, in order to verify the effectiveness of the proposed method, some control systems are compared:

- LQR w/o state observer
- LQR with IDOB
- TPW-based MPC with IDOB

- MPC with IDOB
- TPW-based proposed MPC using IDOB

The LQR, which is an unconstrained state feedback controller, is compared to the proposed systems. Additionally, the first LQR system uses actual state information in the simulation.

In the results with respect to A(= without disturbance), it is confirmed that the LQR and MPCs have a similar response, and each MPC can ensure the velocity constraints, as is the case with IDOB. Therefore, the MPCs can ensure the constraints, if there is no disturbance.

In the results with respect to B(= step-type disturbance 1N), it is confirmed that state estimation by KFD has large errors and the constraints actives to estimated values. However, the activated constraints are not effective for actual values because large estimation errors occur.

In the results with respect to C(= step-type disturbance 2N), it is confirmed that the results are significantly influenced by disturbance. However, from Fig. 3.20, it is evident that the proposed method can achieve to recover the constraint violation on control input, as is the case with integrated to IDOB. Therefore, even as integrated to KFD, the recovery performance is not lost. From the results, the effectiveness of the proposed design method is shown.

In the results with respect to D and E (mass variation), it is confirmed that the KFD-based MPCs can handle the mass variation. The handling performance is obtained by sluggish estimation, that is, the KFD cannot generate excessive reaction against disturbance and noise.

Overall, the proposed method is only useful under large disturbances. In particular, it has the potential for achieving a robust MPC design and for generating stable constrained motion considering noise. Additionally, the constraint recovery ability is effective for working with unknown environments, as is the case with IDOB.

However, the sluggish disturbance estimation as to the estimation errors affects other variable estimations. Therefore, the improved KFD is a must.

3.3.5 Summary

In this section, KFD-based MPC was explained. The main drawback of the KFD is definitely sluggish and insufficient in disturbance estimation. The verification results showed the potential of the KFD which can improve the control performance of the MPC. However, the solution to the drawback is a must. In this chapter, improved KFD is provided and explained in the next chapter.

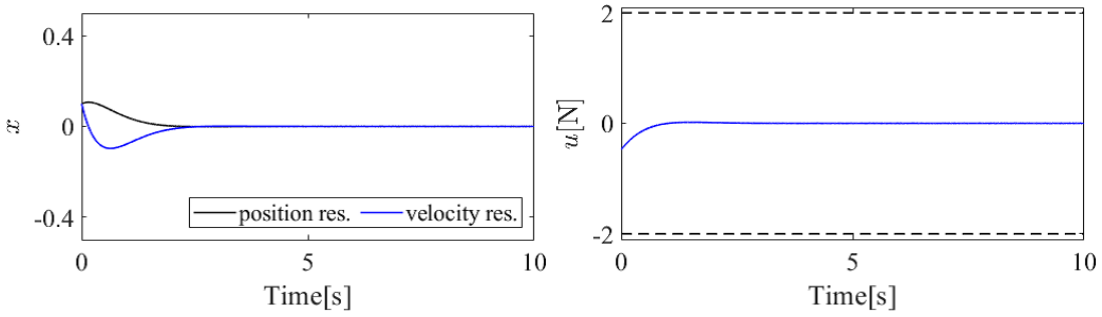

(a) state (b) control inputs

FIGURE 3.6: Simulation results(A): LQR

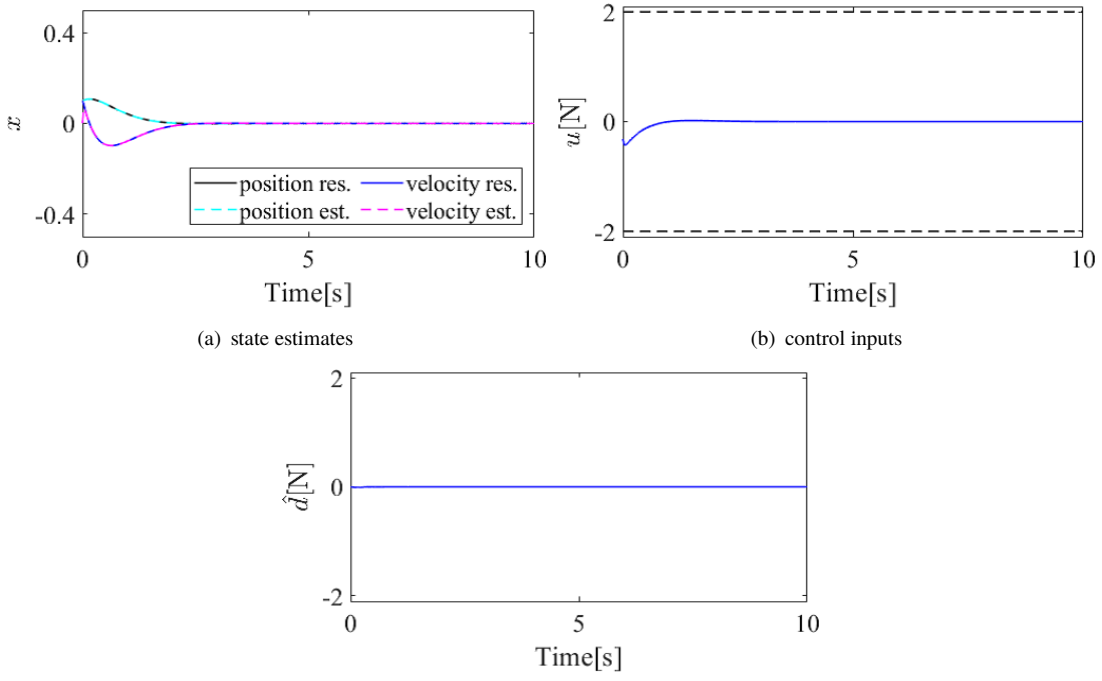

(a) state estimates (b) control inputs

(c) disturbance estimate

FIGURE 3.7: Simulation results(A): LQR + KFD

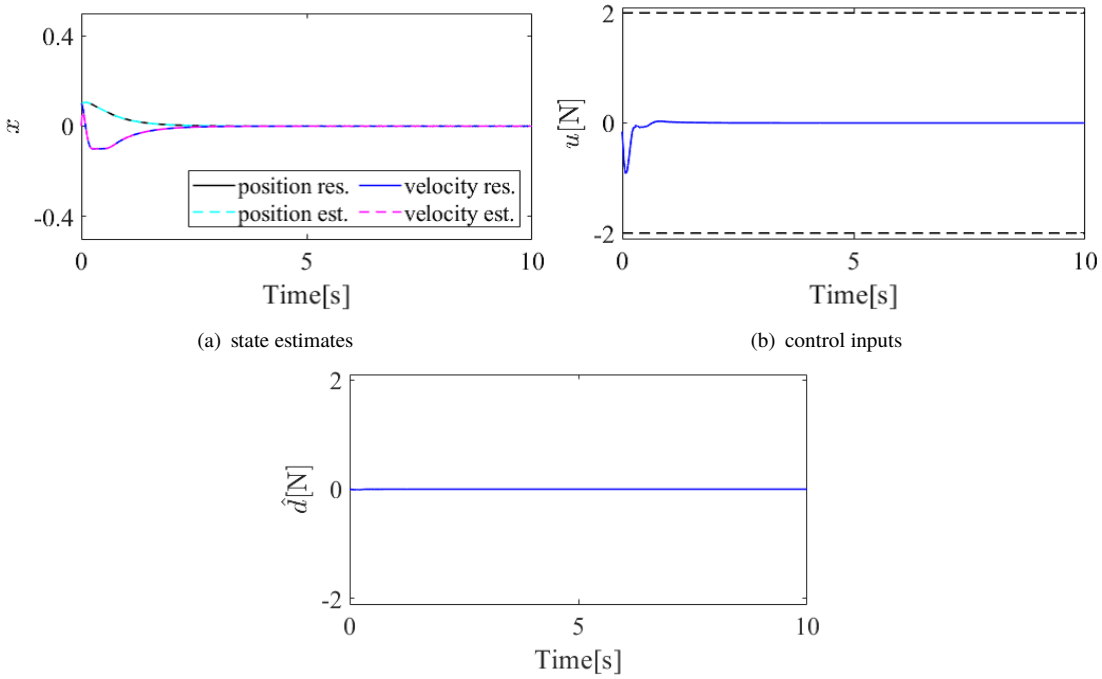

(a) state estimates

(b) control inputs

(c) disturbance estimate

FIGURE 3.8: Simulation results(A): constrained TPW-based MPC with KFD

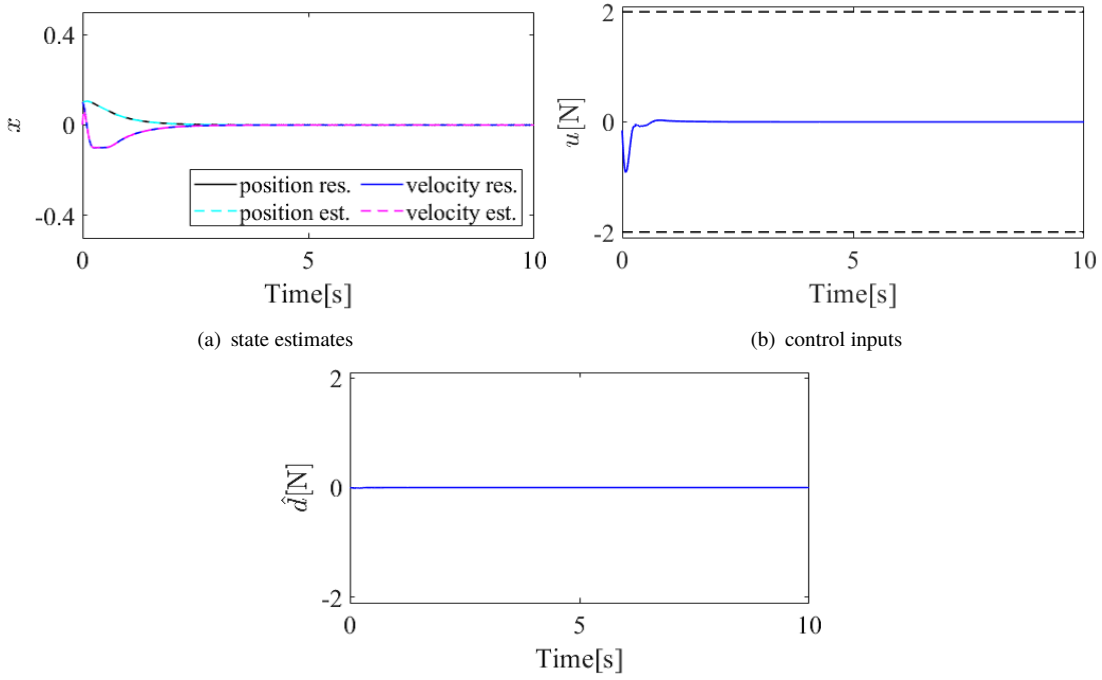

(a) state estimates

(b) control inputs

(c) disturbance estimate

FIGURE 3.9: Simulation results(A): constrained MPC with KFD

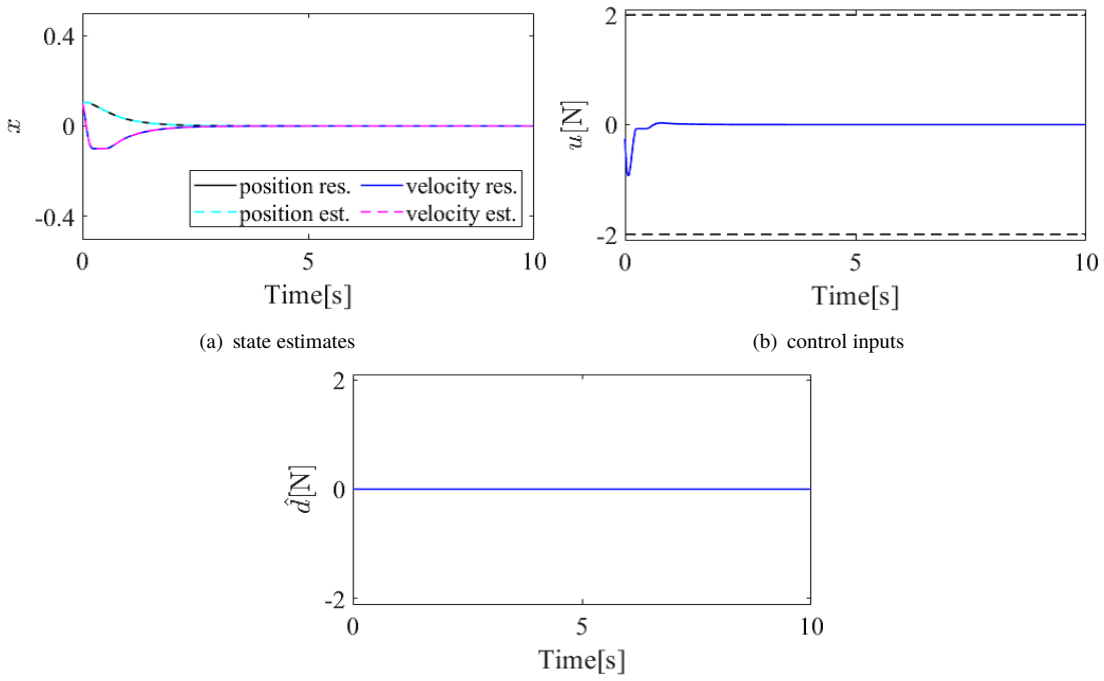

(a) state estimates

(b) control inputs

(c) disturbance estimate

FIGURE 3.10: Simulation results(A): proposed TPW-based MPC with KFD

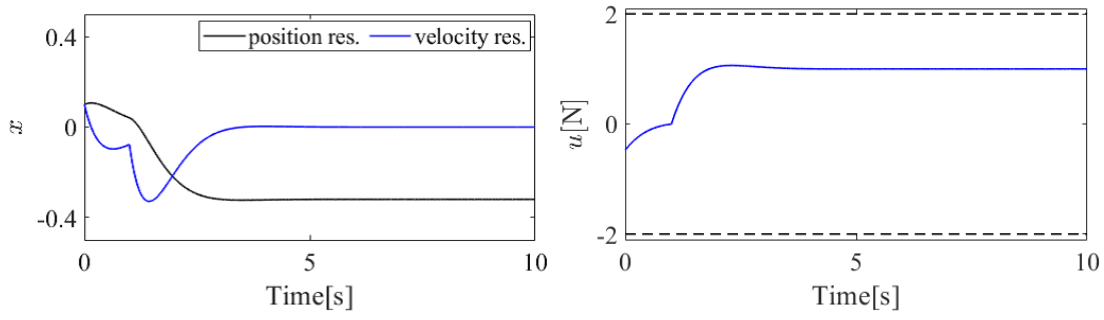

(a) state

(b) control inputs

FIGURE 3.11: Simulation results(B): LQR

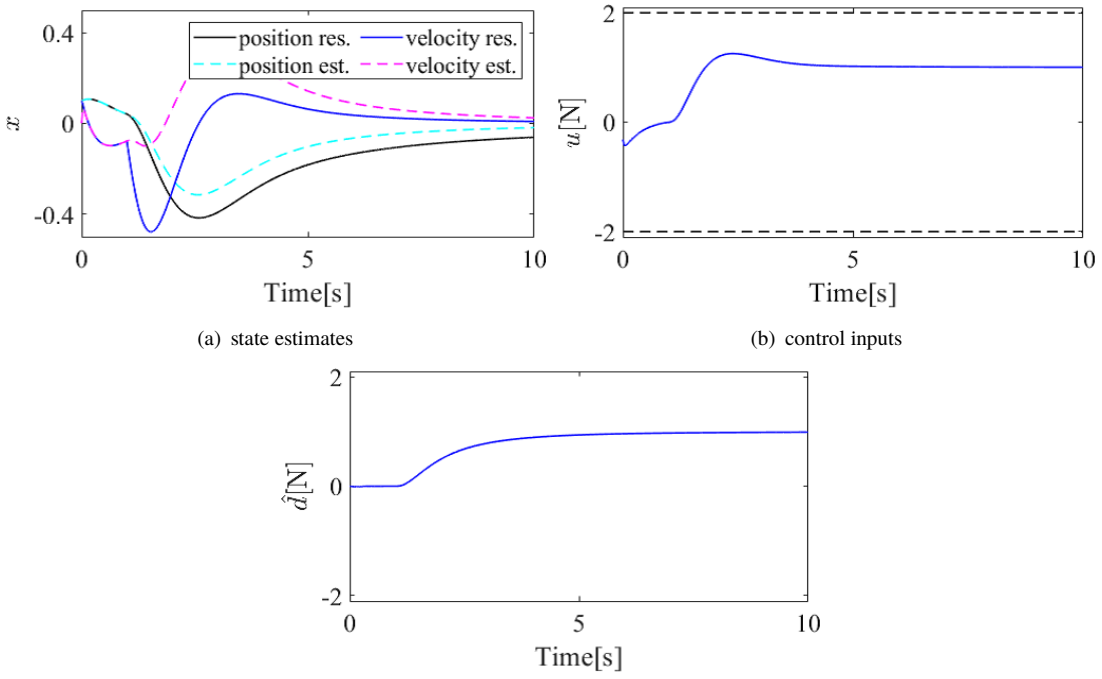

(a) state estimates

(b) control inputs

(c) disturbance estimate

FIGURE 3.12: Simulation results(B): LQR + KFD

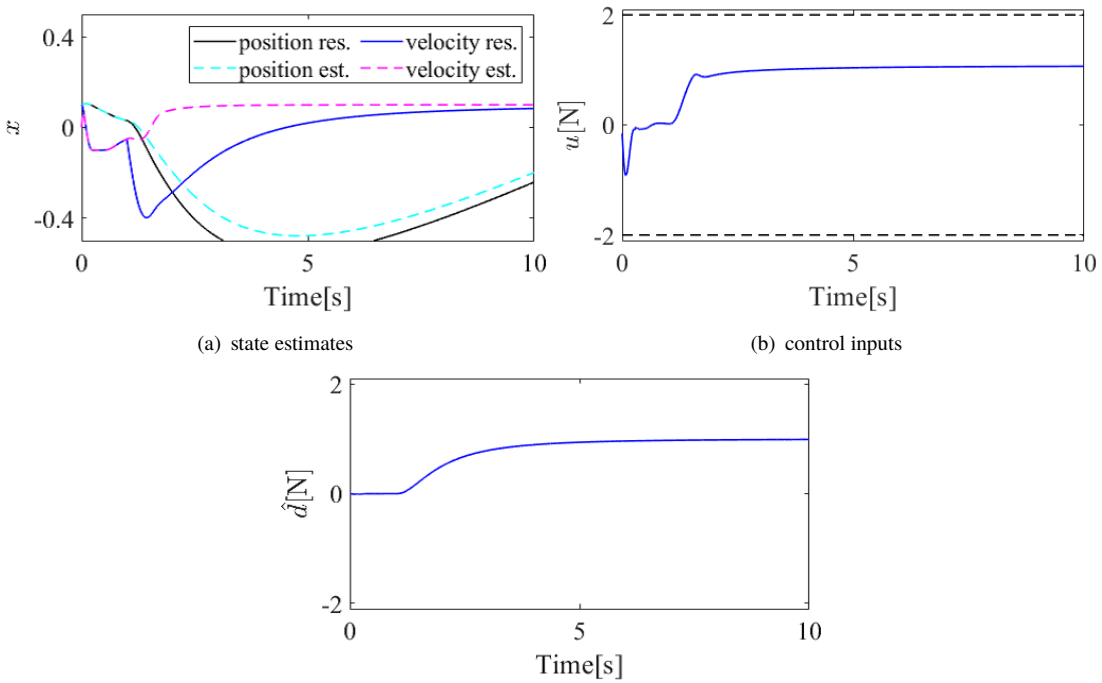

(a) state estimates

(b) control inputs

(c) disturbance estimate

FIGURE 3.13: Simulation results(B): constrained TPW-based MPC with KFD

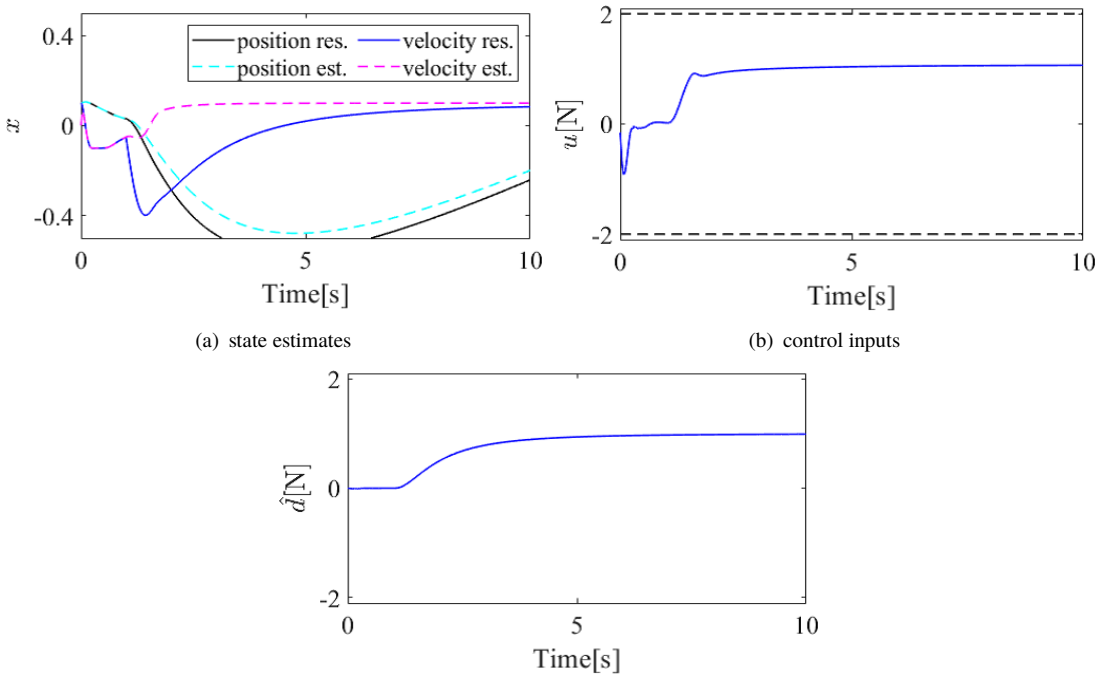

(a) state estimates

(b) control inputs

(c) disturbance estimate

FIGURE 3.14: Simulation results(B): constrained MPC with KFD

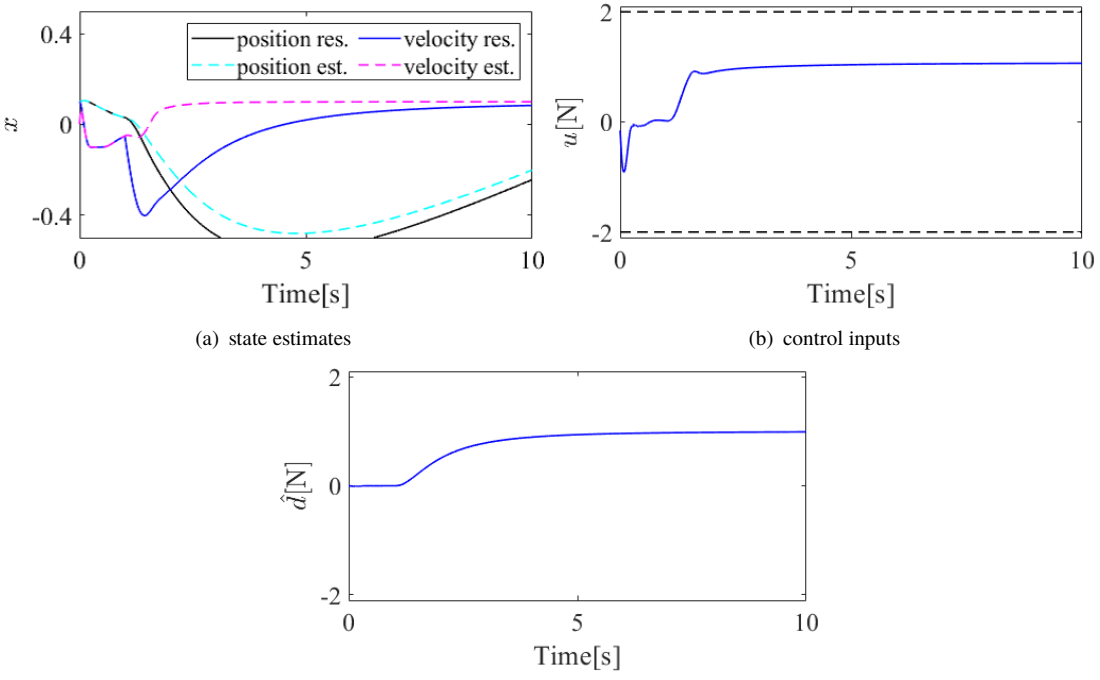

(a) state estimates

(b) control inputs

(c) disturbance estimate

FIGURE 3.15: Simulation results(B): proposed TPW-based MPC with KFD

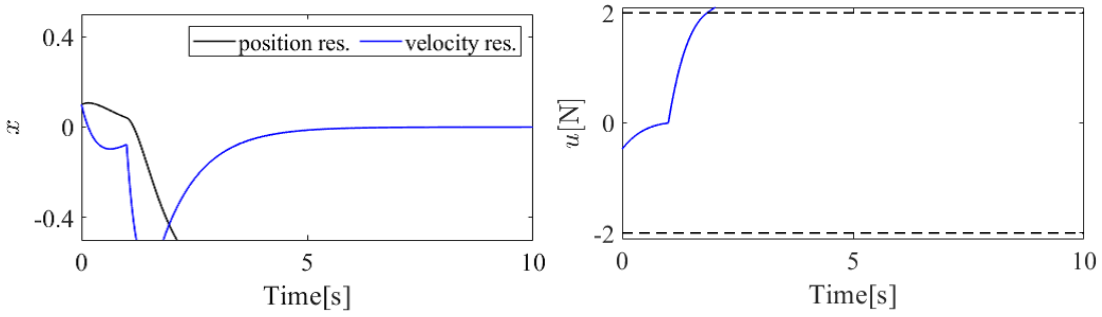

(a) state (b) control inputs

FIGURE 3.16: Simulation results(C): LQR

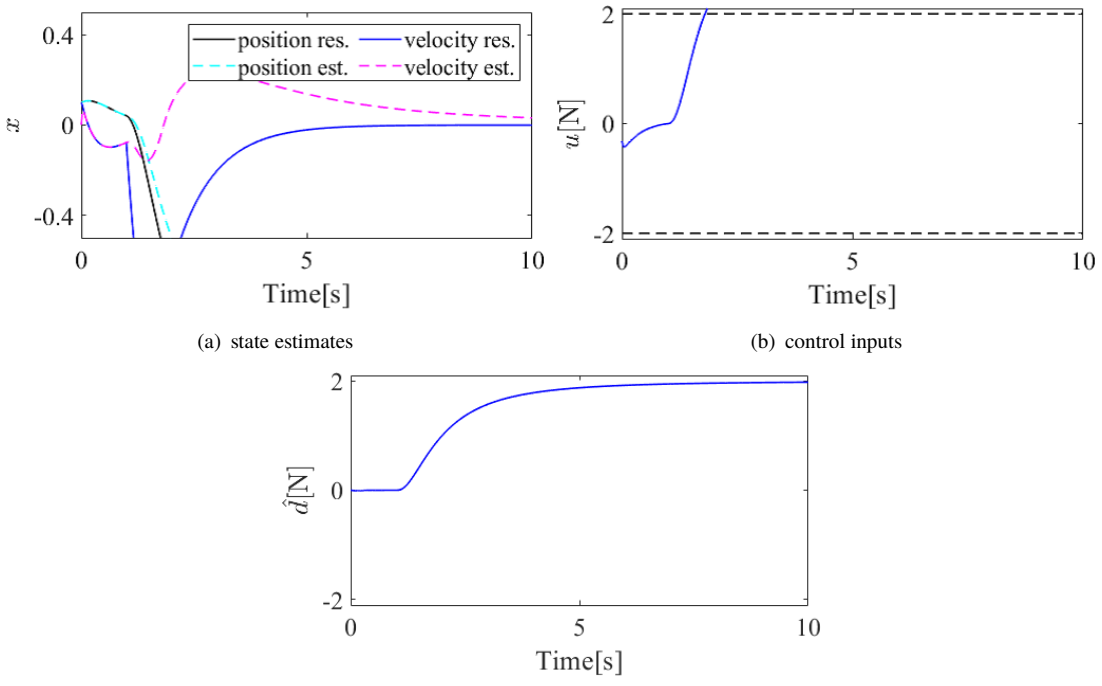

(a) state estimates (b) control inputs

(c) disturbance estimate

FIGURE 3.17: Simulation results(C): LQR + KFD

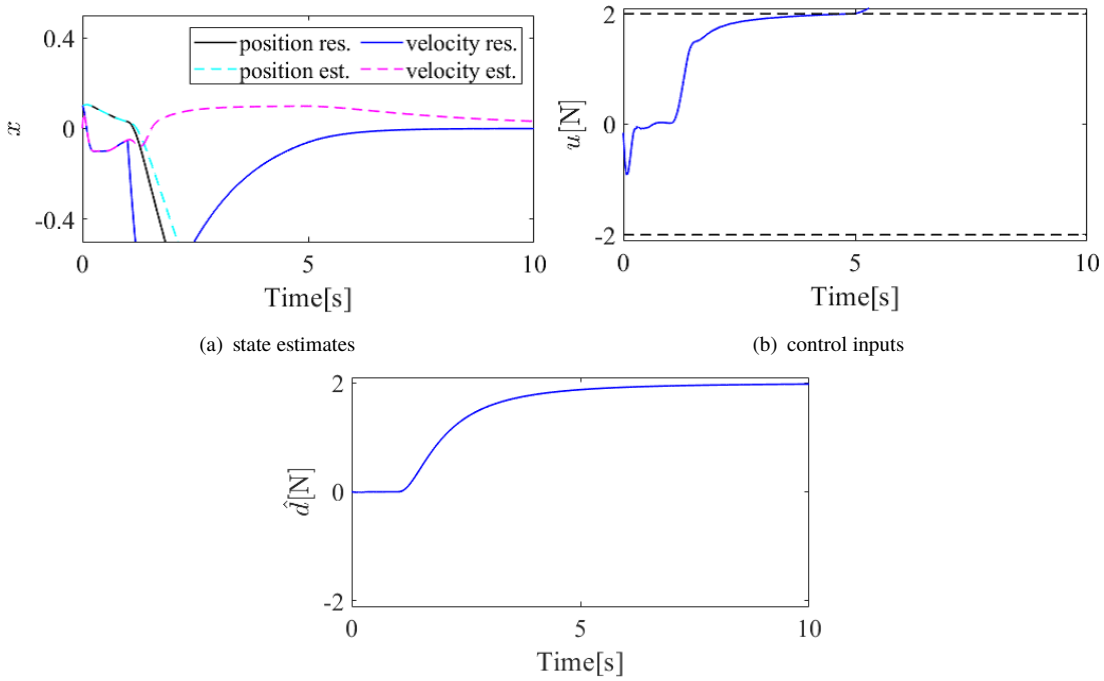

(a) state estimates

(b) control inputs

(c) disturbance estimate

FIGURE 3.18: Simulation results(C): constrained TPW-based MPC with KFD

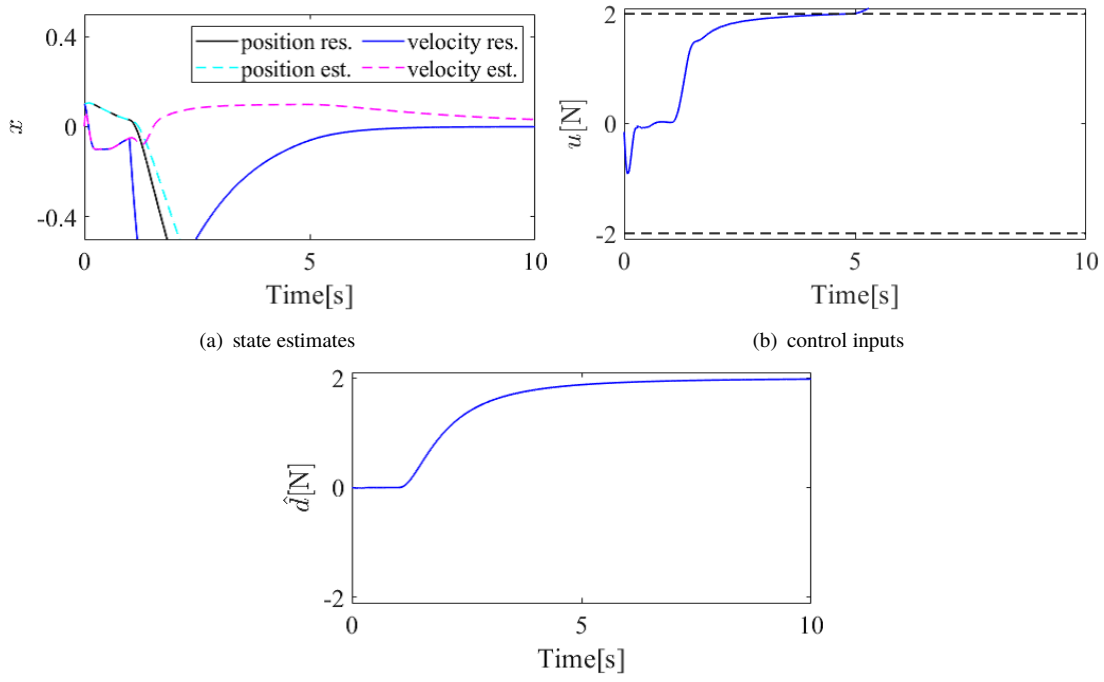

(a) state estimates

(b) control inputs

(c) disturbance estimate

FIGURE 3.19: Simulation results(C): constrained MPC with KFD

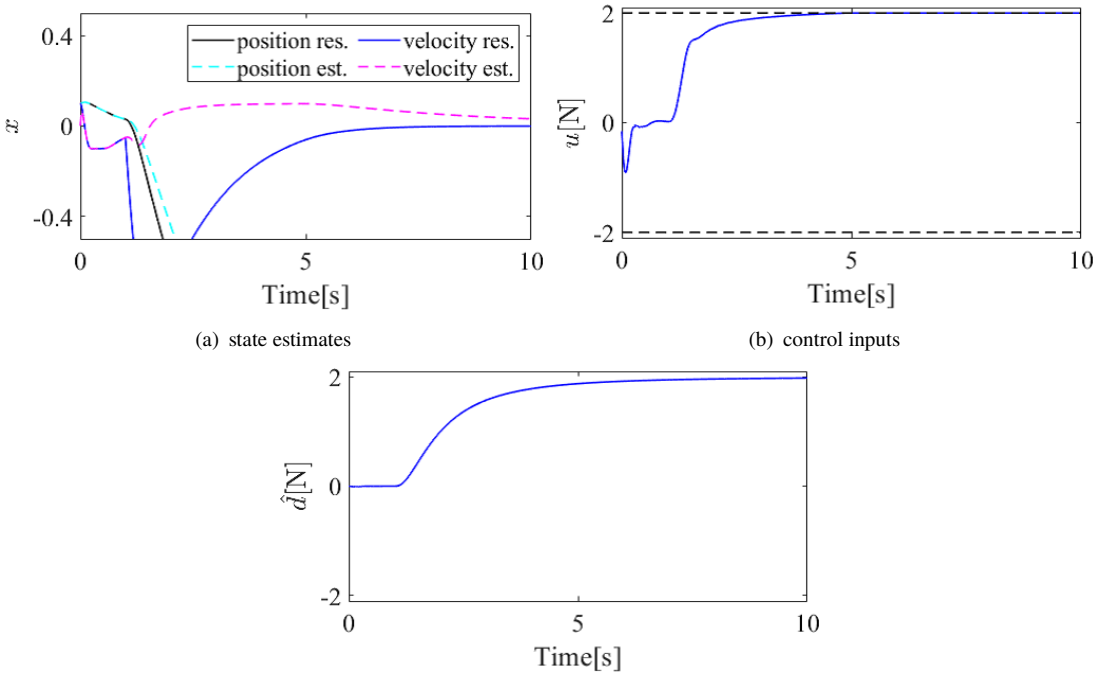

(a) state estimates

(b) control inputs

(c) disturbance estimate

FIGURE 3.20: Simulation results(C): proposed TPW-based MPC with KFD

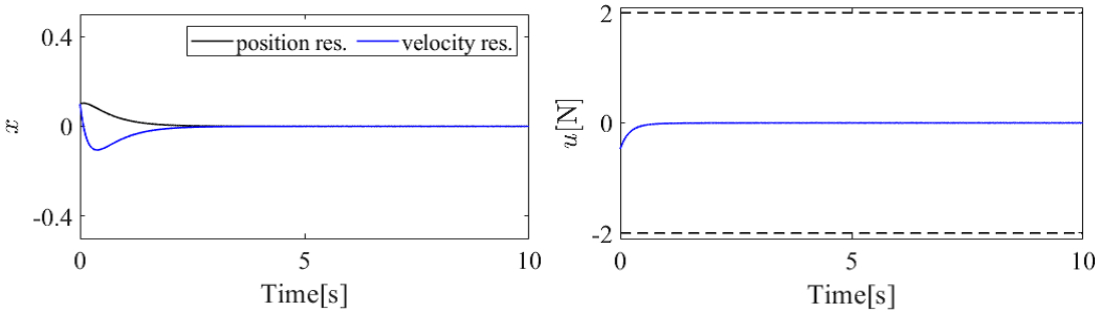

(a) state

(b) control inputs

FIGURE 3.21: Simulation results(D): LQR

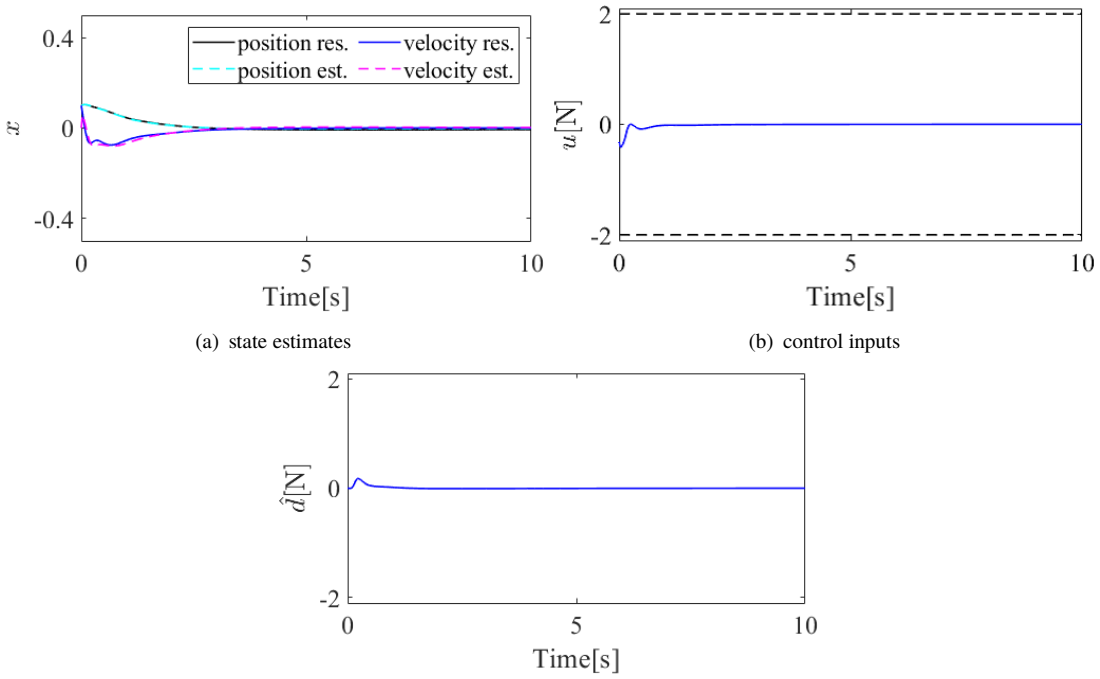

(a) state estimates

(b) control inputs

(c) disturbance estimate

FIGURE 3.22: Simulation results(D): LQR + KFD

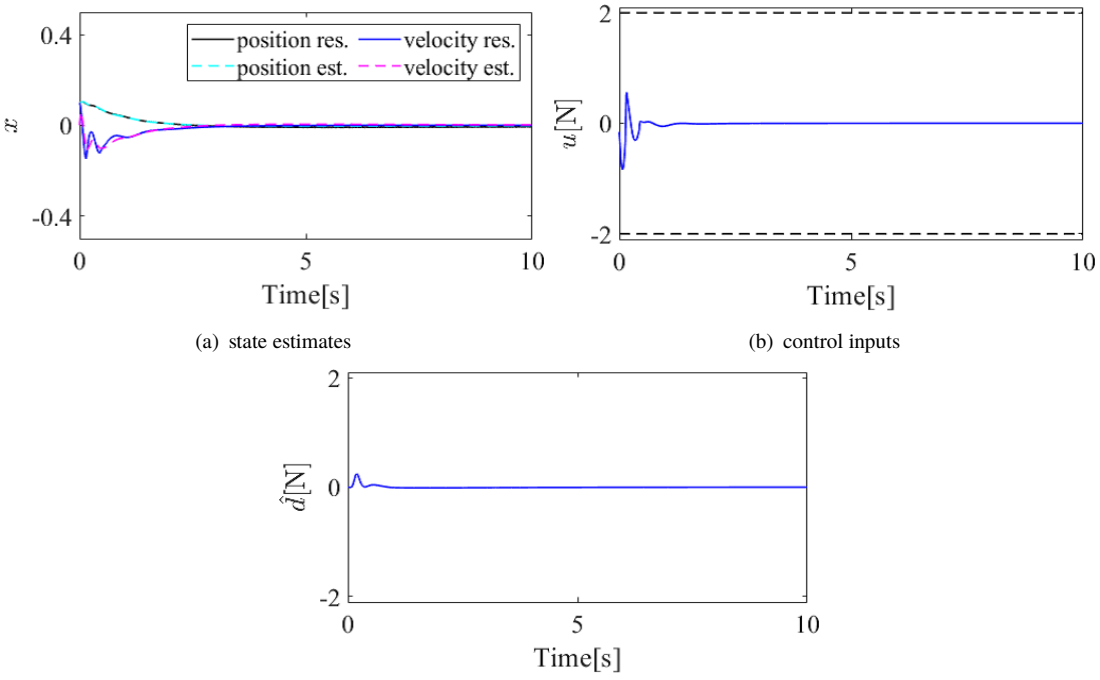

(a) state estimates

(b) control inputs

(c) disturbance estimate

FIGURE 3.23: Simulation results(D): constrained TPW-based MPC with KFD

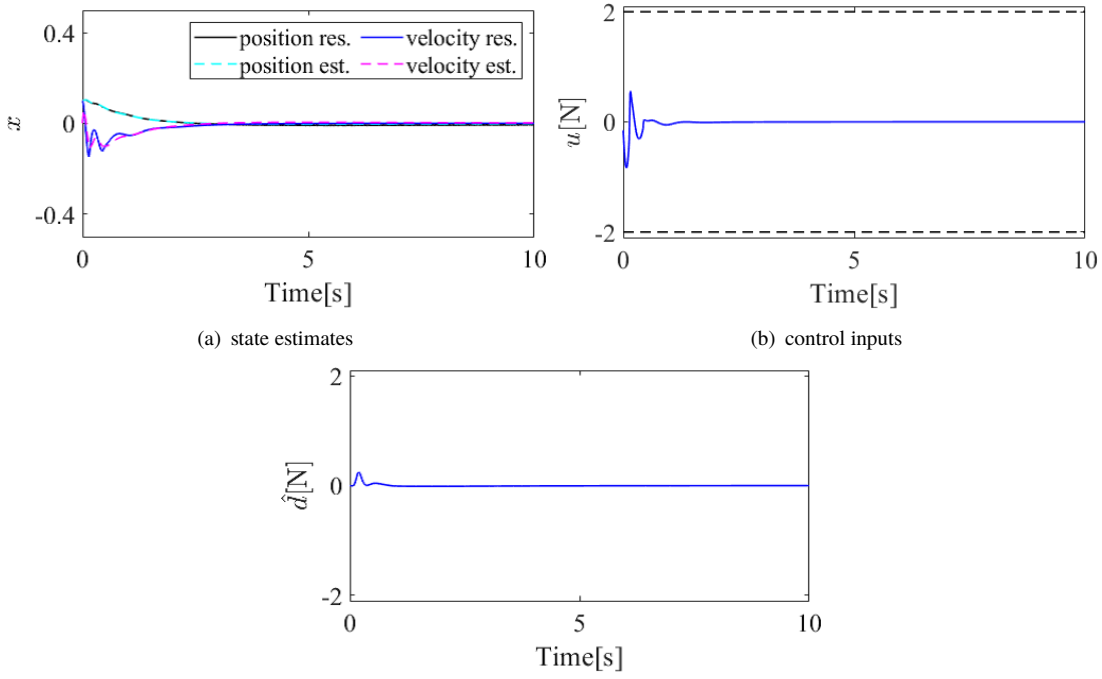

(a) state estimates

(b) control inputs

(c) disturbance estimate

FIGURE 3.24: Simulation results(D): constrained MPC with KFD

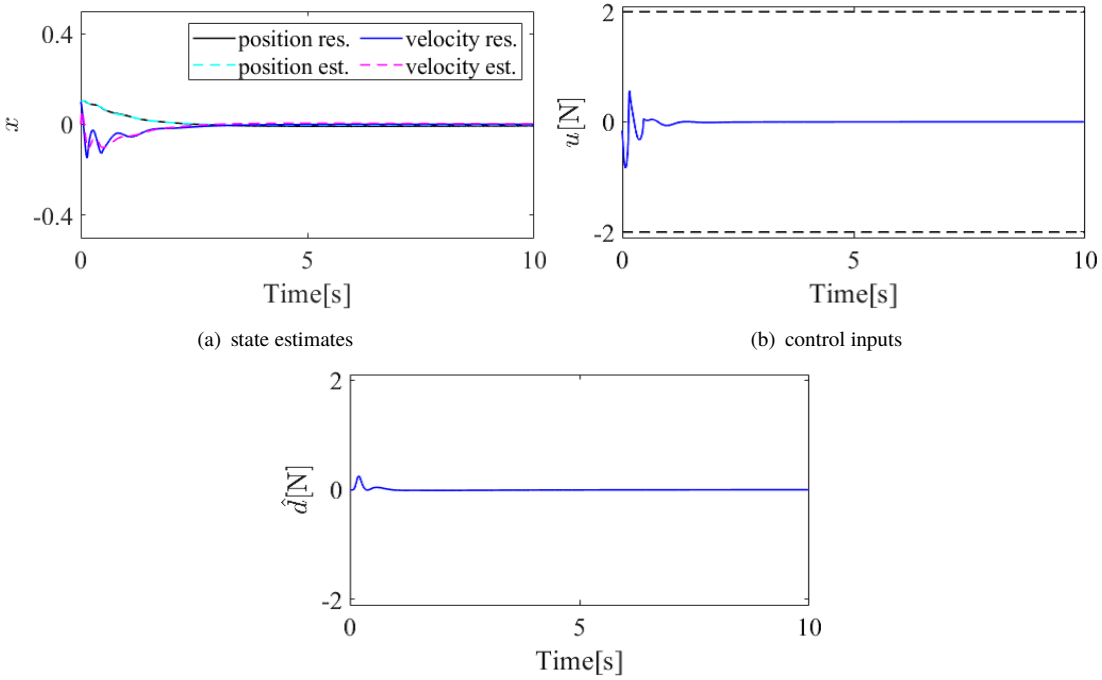

(a) state estimates

(b) control inputs

(c) disturbance estimate

FIGURE 3.25: Simulation results(D): proposed TPW-based MPC with KFD

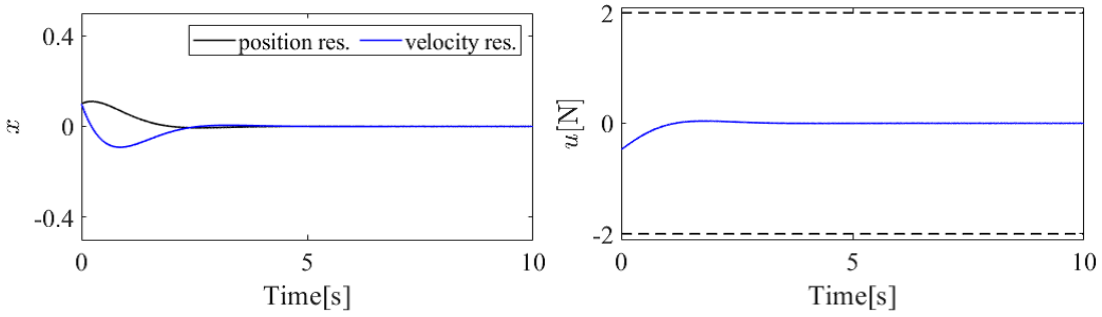

(a) state (b) control inputs

FIGURE 3.26: Simulation results(E): LQR

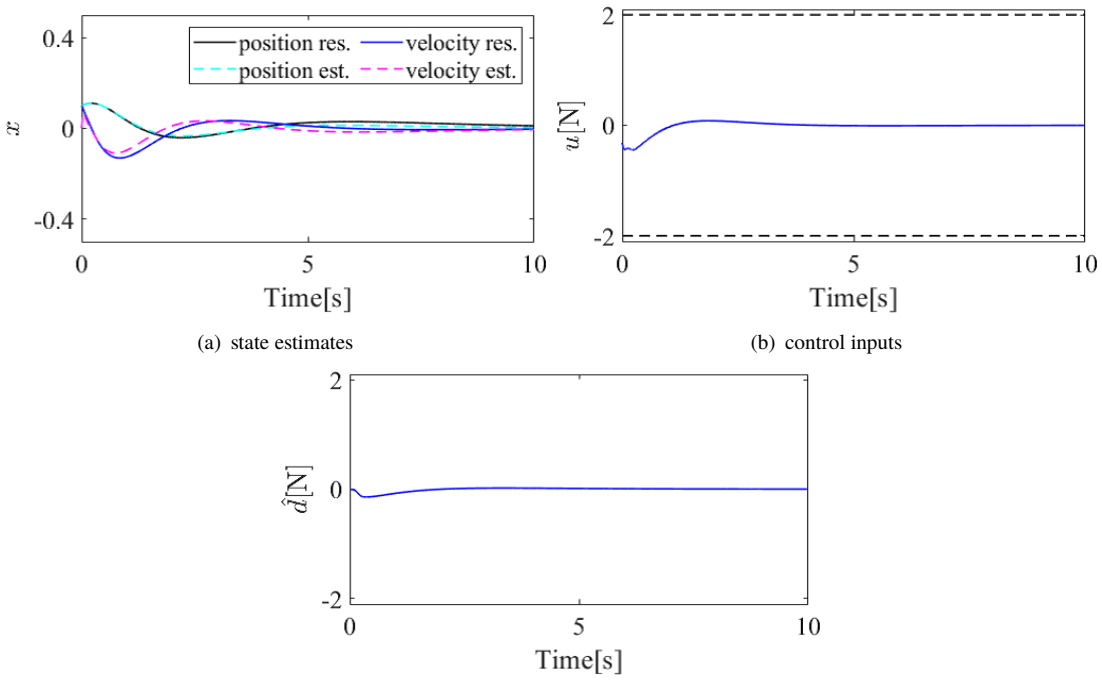

(a) state estimates (b) control inputs

(c) disturbance estimate

FIGURE 3.27: Simulation results(E): LQR + KFD

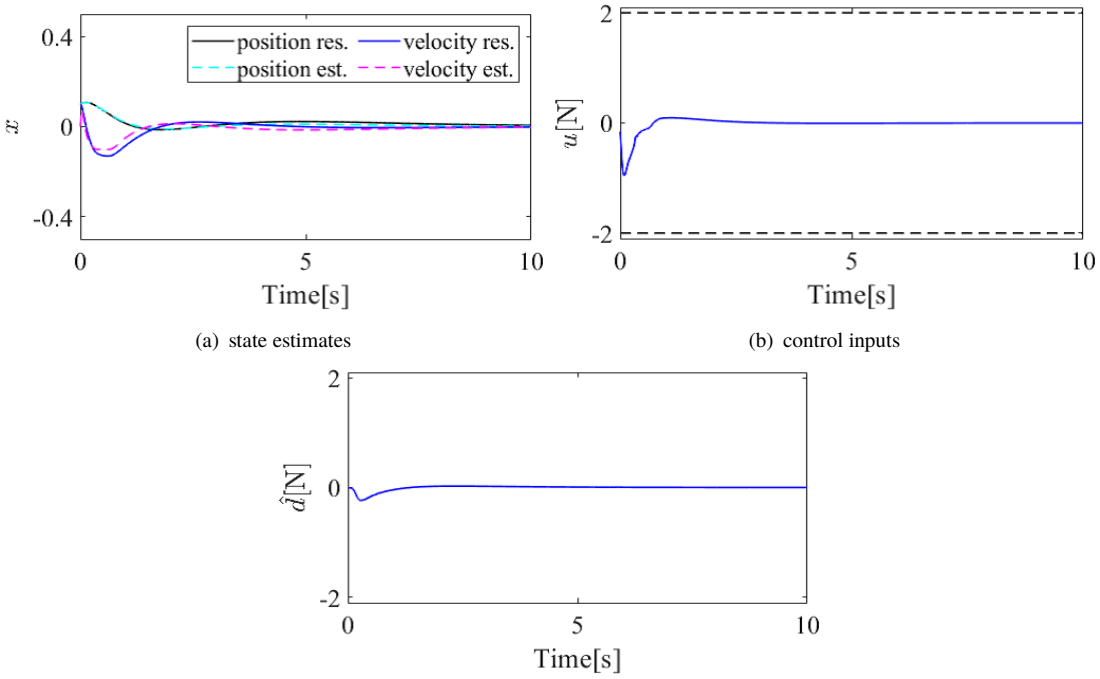

(a) state estimates

(b) control inputs

(c) disturbance estimate

FIGURE 3.28: Simulation results(E): constrained TPW-based MPC with KFD

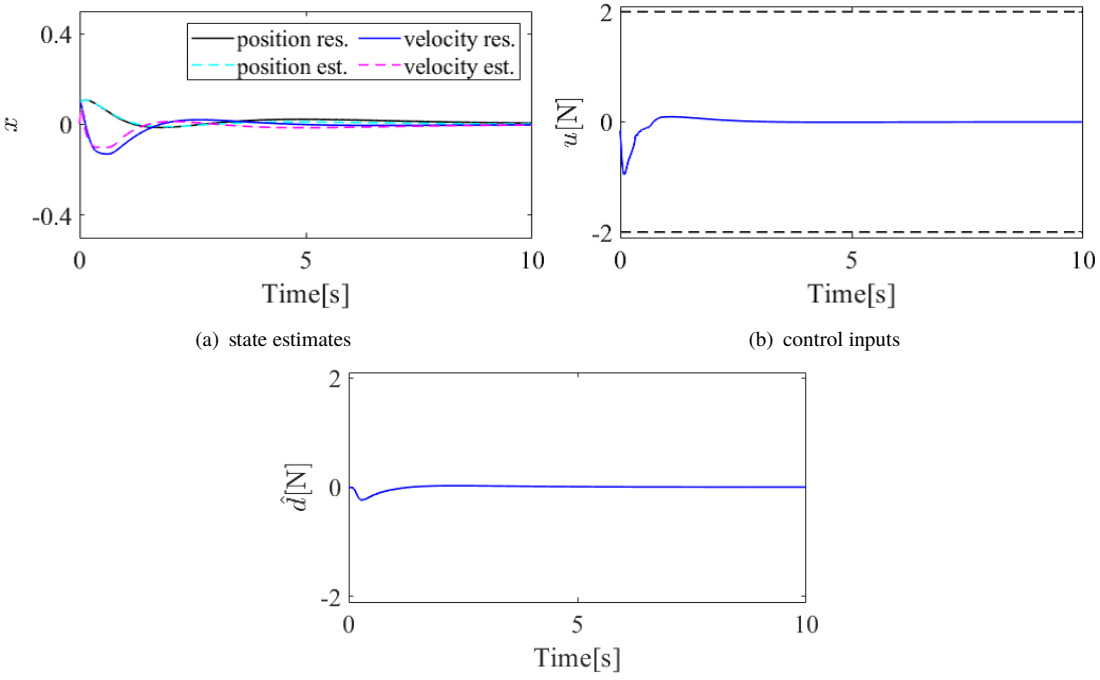

(a) state estimates

(b) control inputs

(c) disturbance estimate

FIGURE 3.29: Simulation results(E): constrained MPC with KFD

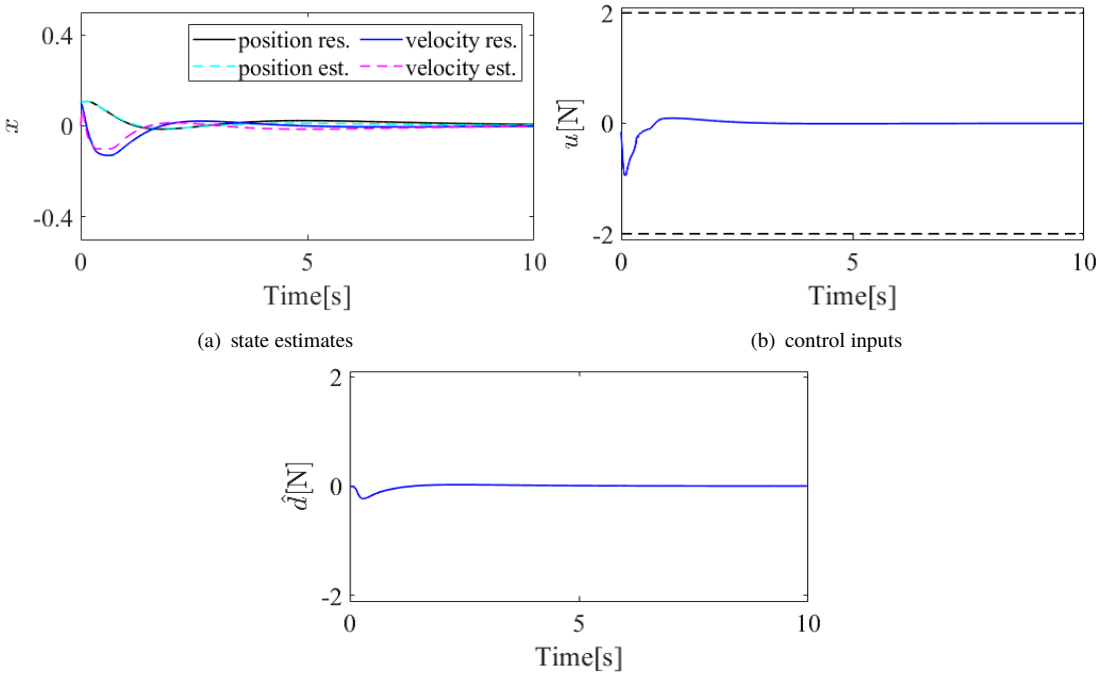

(a) state estimates

(b) control inputs

(c) disturbance estimate

FIGURE 3.30: Simulation results(E): proposed TPW-based MPC with KFD

3.4 Nonlinear Kalman filter with disturbance estimation

In the previous section, the KFD is explained.

General KF can easily expand to nonlinear systems via nonlinear Kalman filters; therefore, the KFD has the potential to apply to nonlinear systems. In this section, an example of the nonlinear Kalman filter with disturbance estimation considering dynamic disturbance is shown. The application example uses the quadrotor type robot that has nonlinearity and coupled motion. The quadrotor application shows the usefulness and effectiveness of the KFD in nonlinear systems.

To show the application ability of KFD to nonlinear systems, this section explains an underwater quadrotor control system using backstepping control and an unscented Kalman filter (UKF) with disturbance estimation.

Autonomous underwater vehicles (AUVs) have been put to practical use and are expected to be used to inspect for revetments and the bottom of a ship in a narrow workspace. Moreover, the tasks have a safety problem since the working space between the others and the work object becomes close. Thus, if such tasks can automate using the AUVs, safety for the tasks is improved. Generally, the AUVs are a large system[111–113]. A quadrotor-type robot can control posture and position using four actuators, and it is widely used as aerial workers[106, 110]. Furthermore, it brings merits for such tasks in narrow places. However, the quadrotor systems are lightweight systems. Thus, it can easily be affected by underwater waves. Additionally, the quadrotor has nonlinearity dynamics and underactuated systems; therefore, its control system handling the effects is a must. A quadrotor control system used backstepping control was developed, and it had some suitable merit for controlling the quadrotor systems[110]. In this section, to show the effectiveness of the nonlinear Kalman filter-based KFD, the backstepping control-based quadrotor control system is used. To design backstepping control, accurate system state estimation is a must. In conventional control systems, nonlinear KF techniques such as extended Kalman filter (EKF) and unscented Kalman filter (UKF)[134], are often used for estimating the system state. Additionally, it was shown that UKF estimation has a high performance for quadrotor systems[136]. When underwater tasks are considered, the systems state estimation by EKF or UKF is affected by unknown wave disturbances.

DOBs, which can estimate unknown input disturbances, are well known in the motion control field. Generally, DOBs are assuming time-invariant disturbances. Therefore, DOBs are strongly affected by time-varying disturbances including wave disturbance. This section provides a method to integrate an internal model of second-order (sine-wave) disturbance into general UKF for making an accurate system state estimation.

The proposed estimation law based on UKF can estimate the effects of the waves as input disturbance estimates. Additionally, the UKF using the estimated disturbances can perform

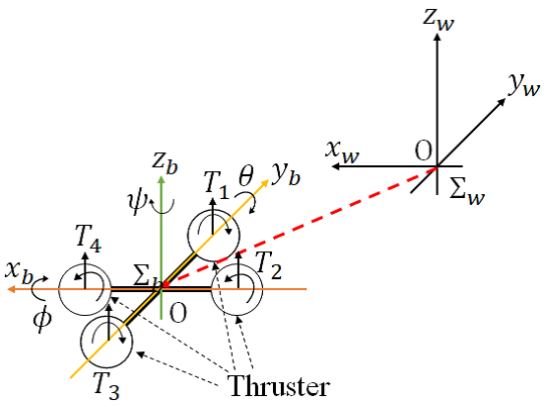

FIGURE 3.31: Definition of coordinate frame: relationship between invariant world coordinate frame(Σ_W) and robot coordinate frame (Σ_b)

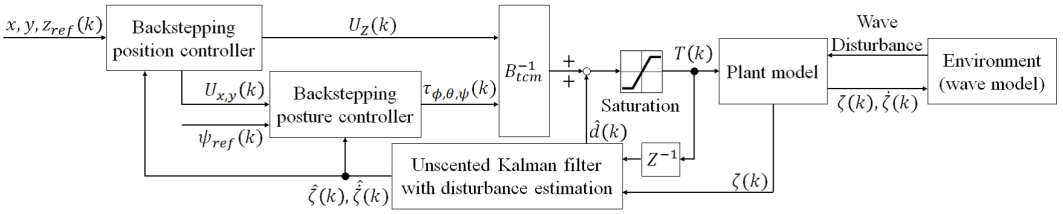

FIGURE 3.32: Configuration of the whole control system using the backstepping control and the UKF with disturbance estimation

accurate system state estimation. As a result, the control performance of the backstepping control-based quadrotor controller can be improved. The proposed method is tested using numerical simulation.

3.4.1 Modeling

This section describes an underwater quadrotor. Table 3.4 shows physical parameters. The world and robot coordinate frames (Σ_W and Σ_b) are defined by Fig. 3.31. The robot position is handled as the differential position from the origin to the current state. The position of the water surface is $z_w = 0$.

3.4.1.1 Quadrotor

The mathematical model is defined based on [106, 110]. The state vector $\boldsymbol{\zeta} = [x\ y\ z\ \phi\ \theta\ \psi]^{\mathrm{T}}$ and the input thrust vector $\boldsymbol{T}[\mathrm{N}] = [T_1\ T_2\ T_3\ T_4]^{\mathrm{T}}$ are defined.

The motion equation can be described as

$$\boldsymbol{M}\ddot{\boldsymbol{\zeta}} + \boldsymbol{D}(\dot{\boldsymbol{\zeta}}) + \boldsymbol{C}(\dot{\boldsymbol{\zeta}}) + \boldsymbol{G}(\boldsymbol{\zeta}) = \boldsymbol{E}(\boldsymbol{\zeta})\boldsymbol{B}_{tcm}\boldsymbol{T}. \tag{3.13}$$

TABLE 3.4: Specifications of quadrotor system

Notation [Unit]	Value	Explanation
m [kg]	1.3800	Mass
I_x [kg m^2]	0.8540	Moment of inertia on x-axis
I_y [kg m^2]	0.8540	Moment of inertia on y-axis
I_z [kg m^2]	0.9361	Moment of inertia on z-axis
D_m [N/ (m/s)]	0.0436	Coefficient of viscous friction for movement system
D_p [N/ (m/s)]	0.0082	Coefficient of viscous friction for posture system
F_m	0.0196	Attenuation coefficient proportional to square value on movement system
F_p	0.1037	Attenuation coefficient proportional to square value on posture system
h [m]	0.1090	Distance from COM to thruster
g [m/s^2]	9.8067	Gravity acceleration
$W(=-mg)$	-13.5323	Gravity constant
w_{rho} [kg m^3]	1000	Water density
V_r [m^2]	0.0011	Volume on x-y coordinates
$B(=V_r w_{rho} g)$	10.7866	Buoyancy constant
$G_z = (W - B)$	- 2.7457	Gravity and buoyancy constants
T_{lim} [N]	±25	Output saturation of actuator

$\boldsymbol{M}$, $\boldsymbol{D}(\dot{\boldsymbol{\zeta}})$, $\boldsymbol{C}(\dot{\boldsymbol{\zeta}})$, $\boldsymbol{G}(\boldsymbol{\zeta})$, $\boldsymbol{E}(\boldsymbol{\zeta})$, and $\boldsymbol{B}_{tcm}$ are a mass matrix, dynamic friction, Coriolis forces, gravity and buoyancy effects, input transform function, and thruster control matrix, respectively.

Moreover, each variable is given by $\boldsymbol{M} = \mathrm{diag}(m, m, m, I_x, I_y, I_z)$, $\boldsymbol{D}(\dot{\boldsymbol{\zeta}}) = \begin{bmatrix} D_m\dot{x} + F_m|\dot{x}|\dot{x} \\ D_m\dot{+}F_m|\dot{y}|\dot{y} \\ D_p\dot{z} + F_p|\dot{z}|\dot{z} \\ D_p\dot{\phi} + F_p|\dot{\phi}|\dot{\phi} \\ D_p\dot{\theta} + F_p|\dot{\theta}|\dot{\theta} \\ D_m\dot{\psi} + F_m|\dot{\psi}|\dot{\psi} \end{bmatrix}$,

$$\boldsymbol{C}(\dot{\boldsymbol{\zeta}}) = \begin{bmatrix} \dot{z}\dot{\theta} - \dot{y}\dot{\psi} \\ \dot{x}\dot{\psi} - \dot{z}\dot{\phi} \\ \dot{y}\dot{\phi} - \dot{x}\dot{\theta} \\ (I_z - I_y)\dot{\theta}\dot{\psi} \\ (I_x - I_z)\dot{\phi}\dot{\psi} \\ (I_y - I_x)\dot{\phi}\dot{\theta} \end{bmatrix}, \boldsymbol{G}(\boldsymbol{\zeta}) = \begin{bmatrix} -\sin\theta G_z \\ \sin\phi\cos\theta G_z \\ \cos\phi\cos\theta G_z \\ 0 \\ 0 \\ 0 \end{bmatrix}, \boldsymbol{B}_{tcm} = \begin{bmatrix} 1 & 1 & 1 & 1 \\ -h & 0 & h & 0 \\ 0 & h & 0 & -h \\ h & -h & h & -h \end{bmatrix},$$

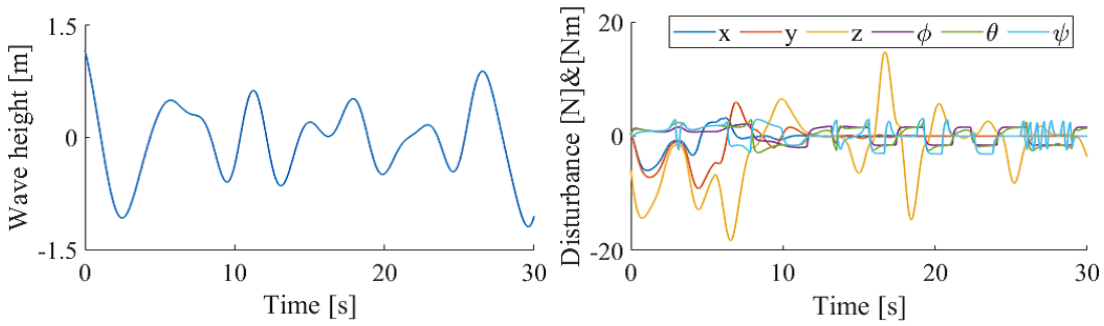

(a) surface wave height

(b) input disturbance in (a)

FIGURE 3.33: Simulation: wave disturbance

$$\boldsymbol{E}(\dot{\zeta}) = \begin{bmatrix} \sin\theta\sin\psi + \cos\phi\sin\theta\cos\psi & 0 & 0 & 0 \\ -\sin\phi\cos\psi + \cos\phi\sin\theta\sin\psi & 0 & 0 & 0 \\ \cos\phi\cos\theta & 0 & 0 & 0 \\ 0 & 1 & 0 & 0 \\ 0 & 0 & 1 & 0 \\ 0 & 0 & 0 & 1 \end{bmatrix}.$$

$\boldsymbol{D}(\dot{\boldsymbol{\zeta}})$ includes the wave effect using the Morison equation (e.g., $F_m|\dot{x}|\dot{x}$ about x). The original Morison equation uses many complex parameters. Therefore, these influences are simply designed by adding and dividing into inertial force $\boldsymbol{M}$ and drag force $\boldsymbol{D}(\dot{\boldsymbol{\zeta}})$ using the parameters $m, I_x, I_y, I_z, F_m, F_p$.

Additionally, since the input thrust can be independently controlled, the force and torque inputs are obtained from the $\boldsymbol{E}(\boldsymbol{\zeta})$ and $\boldsymbol{B}_{tcm}$.

$$\boldsymbol{E}(\boldsymbol{\zeta})\boldsymbol{B}_{tcm}\boldsymbol{T} = \begin{bmatrix} U_x & U_y & U_z & \tau_\phi & \tau_\theta & \tau_\psi \end{bmatrix}^{\mathrm{T}} \tag{3.14}$$

For the system state calculation, the $\boldsymbol{\zeta}$ is calculated by using a double integral of Eq. (3.15).

$$\ddot{\boldsymbol{\zeta}} = \boldsymbol{M}^{-1}\{\boldsymbol{E}(\boldsymbol{\zeta})\boldsymbol{B}_{tcm}\boldsymbol{T} - (\boldsymbol{D}(\dot{\boldsymbol{\zeta}}) + \boldsymbol{C}(\dot{\boldsymbol{\zeta}}) + \boldsymbol{G}(\boldsymbol{\zeta}))\} \tag{3.15}$$

3.4.1.2 Underwater wave effect

The effect model of an underwater wave by using the JONSWAP Spectrum[108], is described. Surface wave behavior can be represented by this spectrum. For the simulations, the z-axis waves are only considered, and the x-axis and y-axis disturbances are designed via $\boldsymbol{E}(\boldsymbol{\zeta})$. The underwater wave is generated by the surface waves and system state. Using the position disturbances, the disturbances on posture torque are calculated by the atan2 function and a low-pass filter. Response of the designed model for the surface wave is shown in Fig. 3.33.

3.4.2 Proposed control system design

Fig. 3.32 shows the system diagram of the proposed system. A backstepping quadrotor control system is used. This controller can control underactuated and nonlinear systems. Moreover, the motions of x and y are coupled to two-state. One is x and pitch-angle (θ), and the other is y and roll-angle (ϕ). Thus, the coupled motion is considered by the reference to the controller (see (3.26)). Additionally, the compensation for the wave effects and the accurate system state estimation is simultaneously made by the UKF with disturbance estimation.

3.4.2.1 Backstepping controller

The backstepping control-based quadrotor control system is introduced. The controller has been designed using the Lyapunov stabilization theorem for state variables $\boldsymbol{\zeta}$. Moreover, to design the backstepping controller, the new control vector $\boldsymbol{q}$ is defined by,

$$\boldsymbol{q} = \begin{bmatrix} q_1 = x & q_2 = \dot{x} & q_3 = y & q_4 = \dot{y} & q_5 = z & q_6 = \dot{z} \\ q_7 = \phi & q_8 = \dot{\phi} & q_9 = \theta & q_{10} = \dot{\theta} & q_{11} = \psi & q_{12} = \dot{\psi} \end{bmatrix}. \tag{3.16}$$

The $x\ (= q_1)$ is describe. An error variable of Z_1 for q_1 is defined by the reference x_{ref}.

$$Z_1 = x_{ref} - q_1 \tag{3.17}$$

A positive-definite Lyapunov function using Eq. (3.17) is defined and can be described as

$$V(Z_1) = \frac{1}{2} Z_1^2. \tag{3.18}$$

Then, a derivative of Eq. (3.18) is given by

$$\frac{d}{dt} V(Z_1) \quad = \quad \frac{1}{2} \cdot \frac{d}{dt} Z_1^2 = Z_1(\dot{x}_{ref} - q_2). \tag{3.19}$$

If Eq. (3.19) is negative-definite, Eq. (3.18) becomes a Lyapunov function. To make stabling for Z_1, a pseudo-control input q_2 is derived as

$$q_2 = \dot{x}_{ref} + \alpha_1 Z_1. \tag{3.20}$$

The α_1 is the control parameter for stabilizing the q_1 and is defined within a stabilizing condition $\alpha_1 > 0$. Then, Eq. (3.20) is substituted in Eq. (3.19) as,

$$\frac{d}{dt} V(Z_1) \quad = \quad Z_1\{\dot{x}_{ref} - (\dot{x}_{ref} + \alpha_1 Z_1)\} = -\alpha_1 Z_1^2. \tag{3.21}$$

Then, new value Z_2 of Eq. (3.21) is defined as

$$Z_2 = q_2 - \dot{x}_{ref} - \alpha_1 Z_1 \tag{3.22}$$

A Lyapunov function to stabilize the system on the q_1 can be described as

$$V(Z_1, Z_2) = \frac{1}{2}Z_1^2 + \frac{1}{2}(q_2 - \dot{x}_{ref} - \alpha_1 Z_1)^2. \tag{3.23}$$

Additionally, the differential function for Eq. (3.23) can be described as

$$\begin{aligned} \frac{d}{dt}V(Z_1, Z_2) &= -\alpha_1 Z_1^2 + Z_2(-G_z/m \sin q_9 + u_x/mU_z) \\ &\quad -Z_2\{\ddot{x}_{ref} - \alpha_1(Z_2 + \alpha_1 Z_1) - Z_1\} \\ &\quad -\alpha_1 Z_1^2, \end{aligned} \tag{3.24}$$

where, $u_x = \sin\theta \sin\psi + \cos\phi \sin\theta \cos\psi$ and $\ddot{x} = -G_z/m \sin q_9 + U_z \cdot u_x/m$ without friction term. The friction term is designed as the modeling error. The control input using Eq. (3.17) satisfies two conditions ($\ddot{x}_{ref} = 0$ and $\dot{V}(Z_1, Z_2) < 0$), and can be described as

$$U_x = \frac{m}{U_z \cdot u_x}(Z_1 - \frac{G_z}{m} \sin q_9 - \alpha_1\{Z_2 + \alpha_1 Z_1\} - \alpha_2 Z_2). \tag{3.25}$$

α_2 is a stabilizing parameter of Z_2.

The quadrotor system is defined as an underactuated system. In particular, the x motion simultaneously occurs with the θ motion. The x is controlled by controlling the θ. Therefore, to control x, U_x is used as the angle reference on θ. The angle reference is defined as

$$\theta_{ref} = \begin{cases} |U_x| & U_x > 0 \cap U_z > 0 \\ -|U_x| & U_x > 0 \cap U_z < 0 \\ -|U_x| & U_x < 0 \cap U_z > 0 \\ |U_x| & U_x < 0 \cap U_z < 0 \\ 0 & \text{(otherwise)} \end{cases} \tag{3.26}$$

Moreover, the reference contains with posture motion ($\theta_{ref} > \pi/2$, and $\theta_{ref} < -\pi/2$). Thus, the absolute value on the U_x is handled as the reference on θ with a saturation function ($-\pi/4 \leq \theta_{ref} \leq \pi/4$).

3.4.2.2 UKF with disturbance estimation

The backstepping control system requires the system state observation ($\boldsymbol{\zeta}$ and $\dot{\boldsymbol{\zeta}}$). Moreover, $\boldsymbol{\eta}(k) = \boldsymbol{\zeta}(k)$ with noise is assumed. Therefore, for estimating the true $\boldsymbol{\zeta}$ and the $\dot{\boldsymbol{\zeta}}$, an observer simultaneously considering the influences of nonlinearity and disturbance is required. Moreover,

the system state observer has to consider the effects of the wave. In the proposed system, the UKF, which simultaneously handles the nonlinearity and underwater wave effects, is used.

A UKF for estimating a higher-order disturbance is proposed, and it can treat sine wave type disturbances and noise influences. This method simultaneously estimates the system state and the disturbance while canceling the noise effects. If such a system state observer can be used, the accurate state estimation for nonlinear systems can be handled under the effects of noise and disturbance. The design of UKF is explained in [16] and is not special. Thus, the internal model for the UKF is only described. This section uses an internal model extended by disturbance. An augmented model for the UKF is designed using a second-order model for input disturbance. Moreover, the second-order model can be described as

$$\boldsymbol{d}(k) = \boldsymbol{d}(k-1) + \delta\dot{\boldsymbol{d}}(k-1), \tag{3.27}$$

$$\dot{\boldsymbol{d}}(k) = \dot{\boldsymbol{d}}(k-1) + \delta\ddot{\boldsymbol{d}}(k-1). \tag{3.28}$$

$\boldsymbol{d}$ is the input disturbance, and $\delta = 0.01$s denotes the sampling time. Furthermore, the state variables including the disturbance can be described as,

$$\begin{aligned}
\bar{\boldsymbol{\zeta}}(k) &= [\boldsymbol{\zeta}(k)\ \dot{\boldsymbol{\zeta}}(k)\ \boldsymbol{d}(k)\ \dot{\boldsymbol{d}}(k)\ \ddot{\boldsymbol{d}}(k)]^{\mathrm{T}} \in \mathbb{R}^{24\times 1} \\
&= [x(k)\ y(k)\ z(k)\ \phi(k)\ \theta(k)\ \psi(k)... \\
&\quad \dot{x}(k)\ \dot{y}(k)\ \dot{z}(k)\ \dot{\phi}(k)\ \dot{\theta}(k)\ \dot{\psi}(k)... \\
&\quad d_{T_1}(k)\ d_{T_2}(k)\ d_{T_3}(k)\ d_{T_4}(k)... \\
&\quad \dot{d}_{T_1}(k)\ \dot{d}_{T_2}(k)\ \dot{d}_{T_3}(k)\ \dot{d}_{T_4}(k)... \\
&\quad \ddot{d}_{T_1}(k)\ \ddot{d}_{T_2}(k)\ \ddot{d}_{T_3}(k)\ \ddot{d}_{T_4}(k)]^{\mathrm{T}}.
\end{aligned} \tag{3.29}$$

The output equation is defined as

$$\boldsymbol{\eta}(k) = \boldsymbol{\zeta}(k) = \boldsymbol{C}\bar{\boldsymbol{\zeta}}(k) = \left[\ \boldsymbol{I}^{\in\mathbb{R}^{6\times 6}} \quad \boldsymbol{0}^{\in\mathbb{R}^{6\times 18}}\ \right]\bar{\boldsymbol{\zeta}}. \tag{3.30}$$

The augmented model for the UKF internal model can be described as

$$\bar{\boldsymbol{\zeta}}(k) = f(\boldsymbol{\zeta}(k-1), \boldsymbol{T}(k-1)) = \bar{\boldsymbol{\zeta}}(k-1) + \delta\begin{bmatrix} \hat{\dot{\boldsymbol{\zeta}}}(k-1) \\ \hat{\ddot{\boldsymbol{\zeta}}}(k-1) \\ \dot{\boldsymbol{d}}(k-1) \\ \ddot{\boldsymbol{d}}(k-1) \\ \boldsymbol{0}^{4\times 1} \end{bmatrix}. \tag{3.31}$$

The control inputs from $\boldsymbol{T}(k-1)$ to $\boldsymbol{T}(k-1) + \hat{\boldsymbol{d}}(k-1)$, and $\hat{\dot{\boldsymbol{\zeta}}}(k-1)$ are obtained using discretized Eq. (3.15). In theory, the UKF using the augmented system can handle a sine wave disturbance.

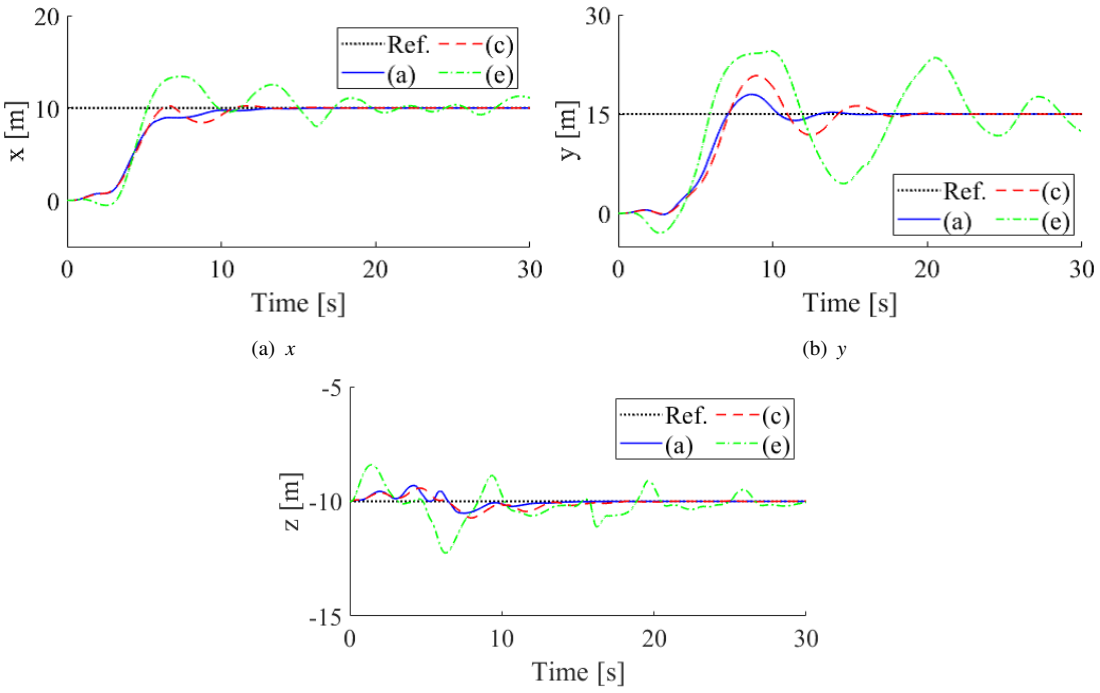

(a) x (b) y

(c) z

FIGURE 3.34: Simulation results(a, c, e): position estimates on UKF-based systems

TABLE 3.5: Simulated systems

Symbol	KF	Disturbance model
(a)	UKF	second-order (prop.)
(b)	EKF	second-order
(c)	UKF	zero-order
(d)	EKF	zero-order
(e)	UKF	none (conv.)
(f)	EKF	none (conv.)

3.4.3 Numerical verification

The effectiveness of the proposed control system was validated by simulations of motion control of the underwater quadrotor. Moreover, the initial state is set to $\boldsymbol{\zeta}(0)$ =[0 0 -10 0 0 0], and the reference vector are set to $\boldsymbol{\zeta}_{ref}$ =[10 15 -10 0 0 0]. Furthermore, the proposed control system and multiple control systems using conventional KFs were compared. Table 3.5 shows the compared methods. All control systems can handle the underwater quadrotor control in theory because the backstepping controller treats the disturbances by waves as the modeling error.

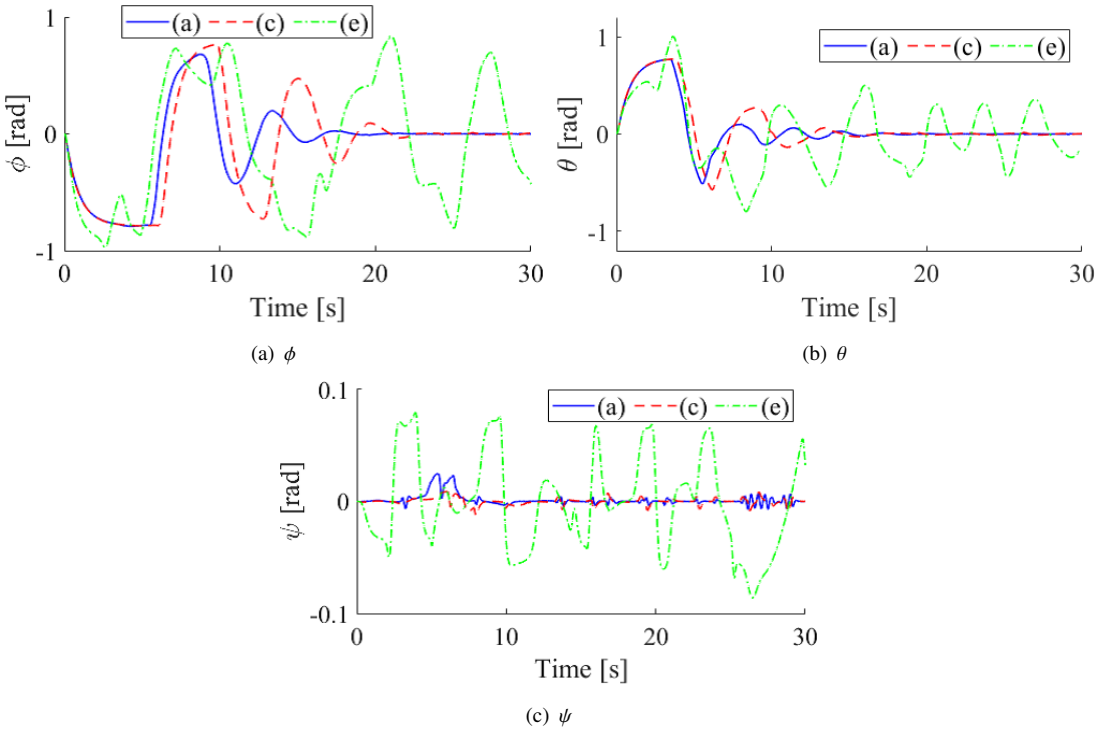

(a) ϕ (b) θ (c) ψ

FIGURE 3.35: Simulation results(a, c, e): posture estimates on UKF-based systems

3.4.3.1 Parameter design

In an adjustment of the backstepping control system, a discrete-time linear quadratic regulator (DLQR) was used for designing the controller parameters $(\alpha_1, ..., \alpha_{12})$. The weight matrices of the tracking error $\boldsymbol{Q}_{LQR}$ and input $\boldsymbol{R}_{LQR}$ for DLQR were designed by trial and error in a simulation as ($\boldsymbol{Q}_{LQR} = \text{diag}\{10^2, 10^2, 10^3, 4\times10^3, 4\times10^3, 5\times10^4, 1, 1, 10^2, 10^3, 10^3, 5\times10^2\}$) and ($\boldsymbol{R}_{LQR} = 10^3 \times \boldsymbol{I}^{6\times6}$). The controller parameters obtained from the DLQR are given by {α_1, ..., α_{12}} = { 0.3152, 0.3152, 3.1285, 1.9756, 1.9756, 6.9341, 0.8908, 0.8908, 2.9469, 2.0775, 2.0775, 3.6262 }. The variances of the system W_s and observation V_m, V_p are set to ($W_s = 0.1$) and ($[V_m, V_p] = [0.1, \quad 0.01]$). Moreover, the parameters on W_s, V_m, and V_p denote a wave disturbance, position sensor resolution, and angle sensor resolution. In the initial parameters of the UKF, the covariance matrices for estimation error $\boldsymbol{P}_0$, state vector $\boldsymbol{Q}_{ukf}$, and observation vector $\boldsymbol{R}_{ukf}$ were set to $\boldsymbol{P}_0 = \text{diag}(10^{-1}\cdot\boldsymbol{I}^{3\times3}, 10^{-2}\cdot\boldsymbol{I}^{3\times3}, 10\cdot\boldsymbol{I}^{3\times3}, \boldsymbol{I}^{3\times3}, 1\cdot\boldsymbol{I}^{4\times4}, 10\cdot\boldsymbol{I}^{4\times4}, 10^2\cdot\boldsymbol{I}^{4\times4})$, $\boldsymbol{Q}_{ukf} = \text{diag}(10^{-2}\cdot\boldsymbol{I}^{3\times3}, 10^{-3}\cdot\boldsymbol{I}^{3\times3}, \boldsymbol{I}^{3\times3}, 10^{-1}\cdot\boldsymbol{I}^{3\times3}, 5\cdot10^5\cdot\boldsymbol{I}^{4\times4}, 1/\delta\cdot10^6\cdot\boldsymbol{I}^{4\times4}, 1/\delta^2\cdot10^6\cdot\boldsymbol{I}^{4\times4})$, $\boldsymbol{R}_{ukf} = \text{diag}(V_m, V_m, V_m, V_p, V_p, V_p)$. All parameters were decided by a simulation that considers the estimation speed.

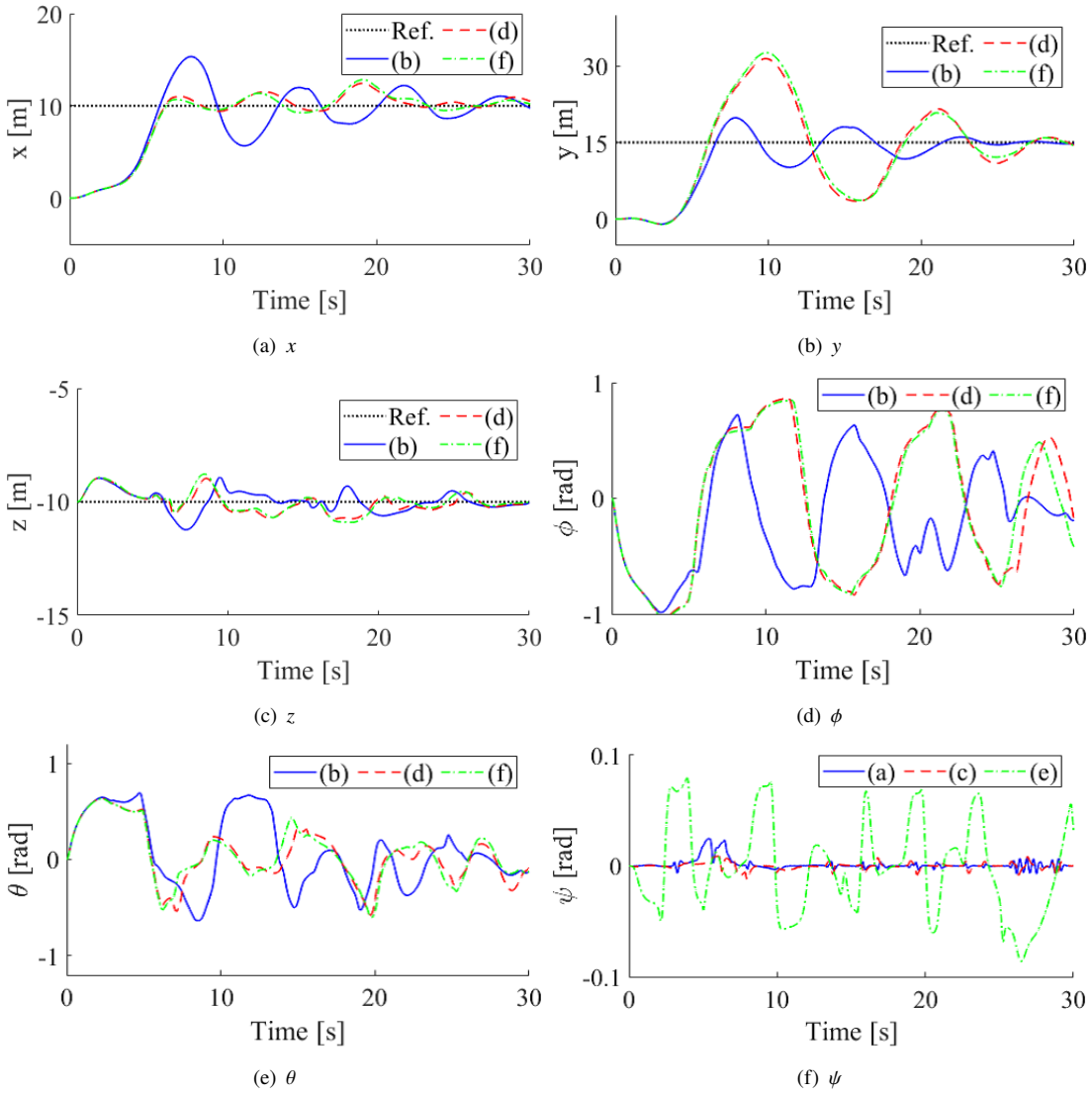

(a) x (b) y (c) z (d) ϕ (e) θ (f) ψ

FIGURE 3.36: Simulation results(b,d,f): EKF-based systems

3.4.3.2 Simulation verification

Fig. 3.34 and 3.35 show the results of the response on position and posture by UKF-based control systems and Fig. 3.36 shows the results of EKF-based systems. Moreover, the surface wave used in the simulations is shown in Fig. 3.33(i). Additionally, the disturbances in (a) for state vector by the wave are shown in Fig. 3.33(ii). Moreover, Fig. 3.37 shows the results of the disturbance estimation using zero and second-order models for the disturbance. Fig. 3.38 shows the results of the velocity estimates on the ϕ with the highest reference.

In the UKF systems (a,c), the simulation results show that the control variables converge into the reference values considering the unknown disturbance from the wave effects (see Figs. 3.34 – 3.36) Moreover, it is shown that (a) and (c) can cancel disturbance compared to other systems. By contrast, in the EKF-based control systems (b,d,f) and the general UKF-based control system (e),

the control variables cannot converge into the reference and cannot make the tracking control with oscillation rejection. Moreover, it is confirmed that EKF-based backstepping control systems have oscillation on x, y, and z. The results indicate that the UKF-based control systems have advantages for underwater quadrotor control over EKF systems.

Additionally, Fig. 3.37 shows the results on the disturbance estimate, and it indicates that the estimation performance of the disturbance using the UKF-based systems is more than the EKF-based systems. Furthermore, it is confirmed that the system (a) using the second-order disturbance model can cancel the high-frequency disturbance by the effects of the underwater waves than the system (c) using the zero-order model. By contrast, it is confirmed that the estimation performance of disturbance using the EKF systems is insufficient. From Fig. 3.37 (ii, iv), the EKF using the zero-order model (d) cannot treat the disturbance estimation, and the EKF using the second-order model cannot estimate the disturbance by the wave effects. This difference between the UKFs and EKFs was obtained from how to treat the system noise. Moreover, the UKF-based systems treat the system noise as the estimation error covariance of the state vector. Thus, the UKF-based systems can treat the uncertainty by the disturbance using the disturbance estimates as state variables. By contrast, the EKF-based systems handle the system noise against the input thrust. Thus, the EKF-based systems do not handle the uncertainty of the disturbance as the state variable. It is indicated that the UKF with disturbance estimation can effectively suppress unknown disturbances. Moreover, it is also indicated that the UKF-based systems have adaptive performances against wave disturbances. Furthermore, Figs. 3.34(i, ii) and 3.35(i, ii) show that the proposed control system suppresses the underwater wave effects than other systems. In Fig. 3.38, it is evident that the velocity estimation by the UKF is more than the other systems. The verification results show the usefulness and validity of the proposed control system.

3.4.4 Summary

This section showed the effectiveness of the UKF with disturbance estimation for the underwater quadrotor control method considering the unknown waves. Moreover, this section showed the usefulness of the UKF with the second-order disturbance model for wave disturbance estimation. Furthermore, the proposed control system can improve the control performances of MBC systems for nonlinear systems using the disturbance model and estimate.

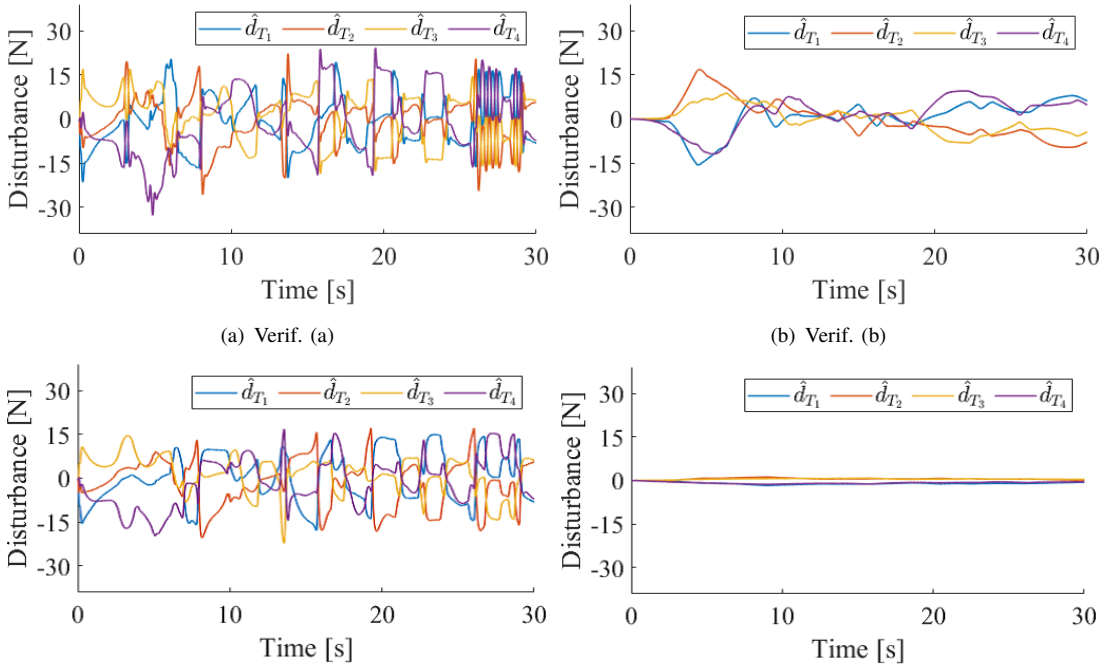

(a) Verif. (a)

(b) Verif. (b)

(c) Verif. (c)

(d) Verif. (d)

FIGURE 3.37: Simulation results(a,b,c,d) : disturbance estimates

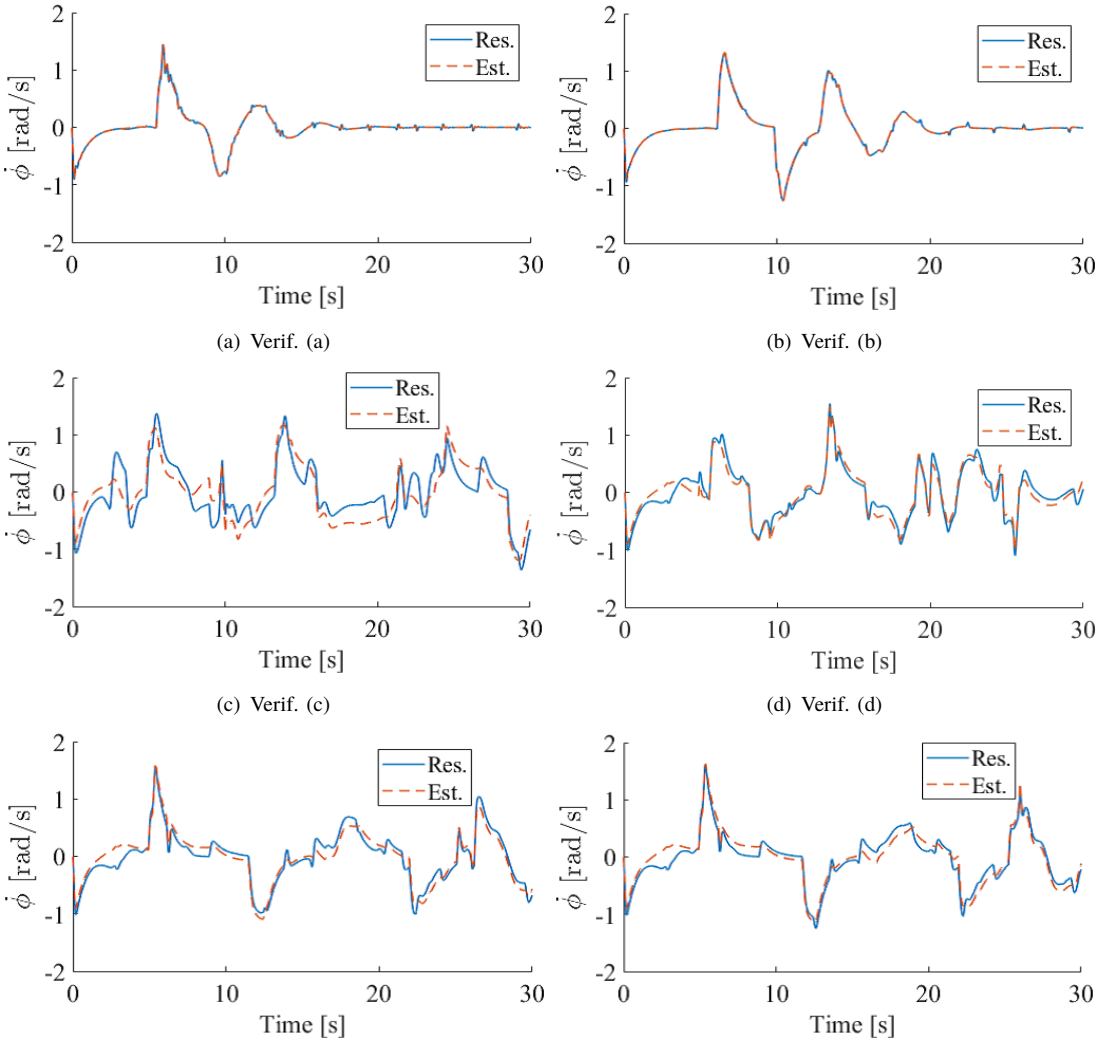

(a) Verif. (a)

(b) Verif. (b)

(c) Verif. (c)

(d) Verif. (d)

(e) Verif. (e)

(f) Verif. (f)

FIGURE 3.38: Simulation results : velocity estimation $\dot{\phi}$

3.5 Chapter summary

In this chapter, the KFD systems were explained. Some verification results show the effectiveness of the KFD with respect to observation noise reduction. However, the results indicated the drawback of the KFD that is sluggish and insufficient performance in disturbance estimation.

Moreover, the nonlinear KFD using UKF was explained and was applied to a quadrotor system. From the verification results, it is confirmed that the KFD method is effective in the nonlinear system. In addition to this, the effectiveness of the disturbance model, which is designed by the second-order model, is also shown in the case of the time-varying disturbance compensation. Therefore, the nonlinear KFD has the potential for control performance improvement for nonlinear control systems.

Chapter 4

Robust Disturbance Observer with Variable Gain for Observation Noise Reduction

4.1 Introduction

In the previous chapter, the MPC with disturbance suppression and KFD is presented. The main drawback of the KFD method is the sluggish speed in disturbance estimation.

In this section, two conclusive countermeasures for improving KFD are introduced. In Sec. 4.2, an adaptive Kalman filter with disturbance estimation (AKFD) is explained as the first method. The AKFD uses a forgetting factor for realizing the fast disturbance estimation and has a trade-off between noise sensitivity and estimation speed. Therefore, an improved AKFD, which uses a variable forgetting factor, is introduced in Sec. 4.3.

The variable forgetting factor-based adaptive Kalman filter (VFAKFD) realizes noise-free simultaneous estimation of state and disturbance. Additionally, the VFAKFD has the ability of nominal response realization of observers in various noisy environments.

The main objective of this section is to radically solve the problem of reduction of influences of observation noise including quantization noise in DOB techniques.

4.1.1 Background and related works

As previously stated, DOB is an estimation method for unknown disturbances and improves the robustness of control systems. However, in the case of implementation with low-resolution sensors, the disturbance estimates by DOB are affected by the observation noise. Therefore, in this chapter, a novel design method of the KFD for simultaneously estimating the system state and unknown disturbance considering the observation noise reduction is discussed. The proposed estimation method can be divided by two parts.

As the first part, to improve the estimation performance by KFD, a forgetting factor-based adaptive KF (FAKF) is used in this chapter. Moreover, the second part is an online adjustment method of the forgetting factor on the FAKF. The online adjustment method is utilized for making the balance of the estimation speed and reduction of observation noise. In this chapter, simulation validation results are provided including various types of noise environments for demonstrating the usefulness of the proposed estimation method.

DOBs[8, 12–14, 117], which can estimate and suppress the effects of unknown disturbances and model error, is a robust control methodology in motion control systems. Moreover, DOBs can be easily designed for many systems utilizing the inverse model, control input, and measured variables of the plant. Furthermore, some types of DOBs have been developed[99, 118–123].

Generally, DOB designs can be defined as a servo problem on disturbance estimation. Thus, the control and estimation performances can be improved by increasing the observer gain. However, using the high observer gain is challenging owing to the mechanical limitation, in actual systems. Unfortunately, general DOBs bring a trade-off between noise sensitivity and disturbance cancellation performance[14]. Furthermore, the control performance of DOB-based control systems depends on the disturbance estimation performance; therefore, an improved DOB used in noisy environments is a must.

Additionally, MDOBs designed to joint space to compensate for the robustness of motors use the velocity estimated from pseudo-differential[124]. General MDOBs, which use the fixed cutoff frequencies, do not provide a nominal response under an environment of quantization noise by optical encoders; therefore, the problems on the robustness and stability compensations by MDOB-based control systems to low-resolution sensors remain. Thus, applying DOBs to the system having large quantization errors is challenging. A temporary improvement method is to utilize the cutoff frequency of the DOB close to 0 (stability limit). However, this method makes a decrease in the estimation performance on the system state and disturbance. Thus, it is confirmed that the design methods of conventional DOBs are insufficient countermeasures against the quantization noise. Therefore, this chapter addresses the improvement of the trade-off and attempts on the accurate simultaneous estimation of the system state and unknown disturbance under noisy environments including quantization noise.

To address the trade-off, Kalman filtered DOB (KF-DOB)[125, 126], which is an MDOB filtered by Kalman filter(KF), and disturbance KF (DKF)[127], which is designed by an extended internal model with disturbance model, have been developed. The KF with disturbance estimation can reduce the influence of observation noise compared to general DOBs; however, it is necessary to increase the system noise for considering the uncertainty of the disturbance. Thus, the influences of increased system noise appear as estimation noise in the system state and disturbance estimates. Therefore, there is a similar trade-off between noise sensitivity and disturbance cancellation performance even with the KFs.

By contrast, the KF with disturbance estimation (KFD)[104], which handles the system noise as the uncertainty for the control input, cannot provide sufficient performance of disturbance suppression. Moreover, the KFD does not handle the estimation of unknown parameters and cannot provide fast estimation in unknown parameters because the internal parameters of the KFD denote the estimation error as fixed noise matrices. To solve the problem of the disturbance estimation speed, the adaptive design of noise matrices is a must.

This chapter proposes a design method of a KFD, and the proposed method can provide the simultaneous estimation for the system state and unknown disturbance considering the observation noise reduction. In the proposed method, the adaptive Kalman filter (AKF)[128–132], which includes a forgetting factor[133], is used in order to solve the trade-off. Moreover, AKF is an estimation method for dynamic unknown system state and parameter [134–136] and has the ability to correspond to the variation of the system by the forgetting factor. Additionally, AKF does not use for designing IDOB, since there is the same trade-off. Thus, this chapter provides a design method of a variable forgetting factor (VFF) using an online adjustment method, which considers solving the trade-off. In designing recursive least squares (RLS) methods, which aims to estimate unknown parameters, the VFF[137–139] has been utilized[140–143]. Using the VFF, the AKFD can adeptly treat observation noise reduction and provide the simultaneous estimation for the system state and unknown disturbance. In this chapter, to validate the usefulness and effectiveness of the proposed estimation method, some numerical verifications considering various noise environments are conducted.

4.2 Forgetting-factor based adaptive Kalman filter with disturbance estimation[115]

Nominal KFD can realize follows;

- Simultaneous estimation of the state and disturbance rejecting noise influences
- Only low-frequency disturbances can be estimated
- To realize highly accurate state estimation considering the influences of noise and disturbance

However, the KFD has a problem that the disturbance estimation is sluggish, and its application to the motion control system cannot be expected. The delayed disturbance estimates make the tracking errors in the control variable. Therefore, to apply KFD to the motion control system, elucidating the improved method of disturbance estimation is a must.

In this section, a method for the fast disturbance estimation of KFD is explained. Two improvement methods presented in this section are as follows: one is to augment disturbance models; the other is the utilization of an AKF that uses the forgetting factor. The improved KFDs can derive the estimates considering the influence of noise and disturbance.

The effectiveness of both design methods was shown in verification results via position control simulation. The plant model and conventional KFDs are explained in the previous section.

4.2.1 Proposed method

4.2.1.1 Disturbance estimation performance of KFDs

In order to show the advantages and disadvantages of the conventional KFD, the simulation comparison result of disturbance estimation with DOB is shown in Fig. 4.1. The plant is affected by (system noise: 1×10^{-3}, observation noise: 2×10^{-4}, input disturbance 0.5 N). From the result, it is confirmed that KFD is able to perform more accurate disturbance estimation in a noisy environment than DOB. The advantage of KFD is that it is possible to estimate the state with disturbance considering the influence of noise. However, even with a simple mechanism, it takes 250s to estimate the disturbance. The essential drawback of KFD is sluggish disturbance estimation.

4.2.2 Augmentation of disturbance model

KFD has a sluggish disturbance estimation speed, and it is difficult to deal with time-varying disturbances. Therefore, in order to consider the time-varying disturbance, the dimension of the internal model of KFD is extended.

Firstly, first-order (ramp) disturbance represented by "$d(k+1) = d(k) + \dot{d}(k)$" is assumed. Add the disturbance estimate (d) and the variation in the disturbance estimate ($\dot{d}$) to the state variable

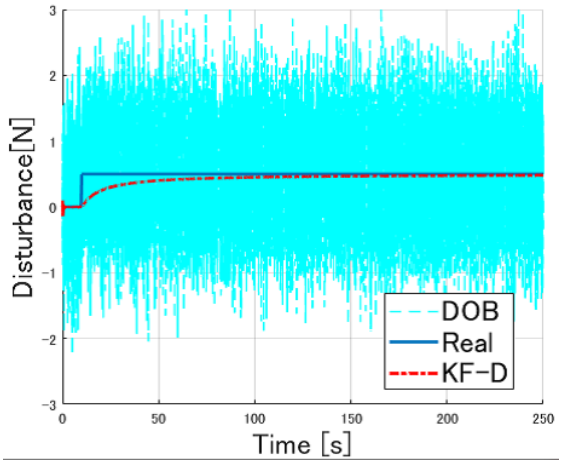

FIGURE 4.1: Simulation result: disturbance estimates by IDOB and KFD

($\boldsymbol{x}$), and then the state space model for ($\bar{\boldsymbol{x}} = \begin{bmatrix} \boldsymbol{x}^{\mathrm{T}} & d & \dot{d} \end{bmatrix}^{\mathrm{T}}$) is given by

$$\begin{bmatrix} \boldsymbol{x}(k+1) \\ d(k+1) \\ \dot{d}(k+1) \end{bmatrix} = \bar{\boldsymbol{A}}_d \begin{bmatrix} \boldsymbol{x}(k) \\ d(k) \\ \dot{d}(k) \end{bmatrix} + \bar{\boldsymbol{B}}_d u(k) \tag{4.1}$$

$$y(k) = \bar{\boldsymbol{C}}_d \begin{bmatrix} \boldsymbol{x}(k) \\ d(k) \\ \dot{d}(k) \end{bmatrix} \tag{4.2}$$

where, $\bar{\boldsymbol{A}}_d = \begin{bmatrix} \boldsymbol{A}_d & -\boldsymbol{B}_d & 0 \\ 0 & 1 & T_s \\ 0 & 0 & 1 \end{bmatrix}$, $\bar{\boldsymbol{B}}_d = \begin{bmatrix} \boldsymbol{B}_d \\ 0 \\ 0 \end{bmatrix}$, $\bar{\boldsymbol{C}}_d = \begin{bmatrix} \boldsymbol{C}_d & 0 & 0 \end{bmatrix}$.

Secondly, the second-order model of disturbance is explained based on"$d(k+1) = d(k) + \dot{d}(k)$, with $\dot{d}(k+1) = \dot{d}(k) + \ddot{d}(k)$". The augmented state vector can be discrebed as $\bar{\boldsymbol{x}} = \begin{bmatrix} \boldsymbol{x}^{\mathrm{T}} & d & \dot{d} & \ddot{d} \end{bmatrix}^{\mathrm{T}}$, and new state space mode is given by

$$\begin{bmatrix} x(k+1) \\ d(k+1) \\ \dot{d}(k+1) \\ \ddot{d}(k+1) \end{bmatrix} = \bar{\boldsymbol{A}}_d \begin{bmatrix} x(k) \\ d(k) \\ \dot{d}(k) \\ \ddot{d}(k) \end{bmatrix} + \bar{\boldsymbol{B}}_d u(k) \tag{4.3}$$

$$y(k) = \bar{\boldsymbol{C}}_d \begin{bmatrix} x(k) \\ d(k) \\ \dot{d}(k) \\ \ddot{d}(k) \end{bmatrix} \tag{4.4}$$

where, $\bar{\boldsymbol{A}}_d = \begin{bmatrix} \boldsymbol{A}_d & -\boldsymbol{B}_d & 0 & 0 \\ 0 & 1 & T_s & 0 \\ 0 & 0 & 1 & T_s \\ 0 & 0 & 0 & 1 \end{bmatrix}$, $\bar{\boldsymbol{B}}_d = \begin{bmatrix} \boldsymbol{B}_d \\ 0 \\ 0 \\ 0 \end{bmatrix}$, $\bar{\boldsymbol{C}}_d = \begin{bmatrix} \boldsymbol{C}_d & 0 & 0 & 0 \end{bmatrix}$. These high-order disturbance models are effective for time-varying disturbance estimation.

4.2.3 Design of adaptive Kalman filter

4.2.3.1 Adaptive Kalman filter with disturbance estimation

The FAKFD can be designed by the AKF used the forgetting factor. Moreover, to estimate the system state and disturbance simultaneously, an extended system model augmented by the disturbance estimates is utilized in the internal system model of the AKF. Furthermore, the

FAKFD can be easily designed by adding the forgetting factor to the design of the KFD. Additionally, the modified covariance matrix is given by

$$\boldsymbol{P}(k|k) = \{\lambda^{-1} \cdot \boldsymbol{I} - \boldsymbol{K}(k)\bar{\boldsymbol{C}}_d\}\boldsymbol{P}(k|k-1), \tag{4.5}$$

where λ $(0 < \lambda \leq 1)$ denotes the forgetting factor. In the fixed forgetting factor, in the case of $\lambda \approx 0$, the current state estimates independents of the previous state estimates and provide the fast state estimation. In this case, the observation noise effects in the state estimates are increased with the responsiveness of the estimate. By contrast, in the case of $\lambda \approx 1$, the state estimates considerably depend on the previous state estimates. Thus, the responsiveness of the state estimation is considerably reduced; however, the noise effect is simultaneously reduced.

In theory, the forgetting factor increases the error covariance matrix, then, the Kalman gain increases along with the increased error matrix. Therefore, the decrease of Kalman gain is prevented, and the updating of the estimation makes quickly.

In this section, replace λ^{-1} with γ, then new factor $\gamma = \lambda^{-1}$ is used for designing the FAKFD. In designing the γ, two design methods are assumed.
(a) Design as a scalar value to affect all state estimation of the extended system.

$$\gamma = const. \in \mathbb{R}^{1\times 1} \tag{4.6}$$

(b) Design as a diagonal matrix so that it affects only disturbance estimation.

$$\boldsymbol{\gamma} = \begin{bmatrix} \boldsymbol{I}_{n\times n} & \boldsymbol{0}_{n\times 1} \\ \boldsymbol{0}_{1\times n} & \gamma_d \end{bmatrix} \in \mathbb{R}^{n+1\,\times\, n+1} \quad where \quad \boldsymbol{x} \in \mathbb{R}^n \tag{4.7}$$

Note that the forgetting factor makes fast disturbance estimation; however, the low-noise sensitivity is lost.

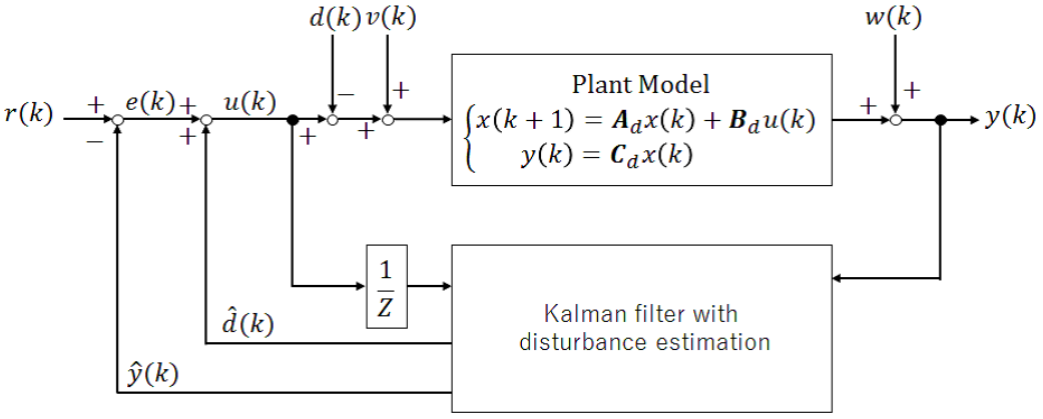

FIGURE 4.2: System diagram of control system

TABLE 4.1: Verification conditions

Run time	50 s
Sampling time	$T_s = 0.1\ s$
Initial state	$x_0 = 0$
Reference position	$r = 1 \quad (in \quad 10\ s)$
Distribution of system noise	$Q_n = 1 \times 10^{-3}$
Distribution of observation noise	$R_n = 2 \times 10^{-4}$

TABLE 4.2: Parameter of KFD

Covariance of system noise	$Q_{kl} = Q_n$
Covariance of observation noise	$R_{kl} = R_n$
Initial value of covariance matrix	$\boldsymbol{P}_0 = \boldsymbol{I}$
Initial state with disturbance	$\bar{\boldsymbol{x}}_0 = [0\ 0\ 0]^{\mathrm{T}}$

TABLE 4.3: Parameter of input disturbances

(a)	Stationary disturbance	$d = 5 \quad (\text{in} \quad 25\ s)$
(b)	Ramp type disturbance	$d(k+1) = d(k) + 0.1$
(c)	Low-frequency disturbance	$d = \sin(0.05 * t)$
(d)	High-frequency disturbance	$d = \sin(10 * t)$

4.2.4 Numerical verification

The proposed designed method is verified by the simulation in position control with disturbance and noise. Fig. 4.2 shows the block diagram of the verified control system. In this verification, the state and disturbance from the response value including noise are estimated. Tables 4.1 and 4.2 show verification conditions and tuning parameters of KFD. The applied disturbances are changed in each verification.

The comparison and verification results and explanations are separated from the following three points.

(i) Augmented disturbance models

(ii) Forgetting factor design

(iii) Integration of (i) + (ii)

In the comparison, the estimation performance is also focused, but also the control performance.

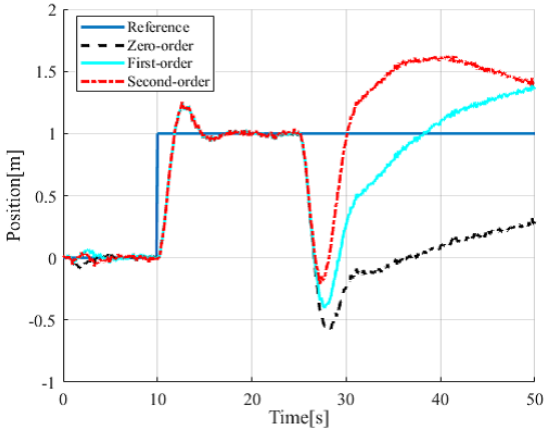

FIGURE 4.3: Simulation results(a): position response

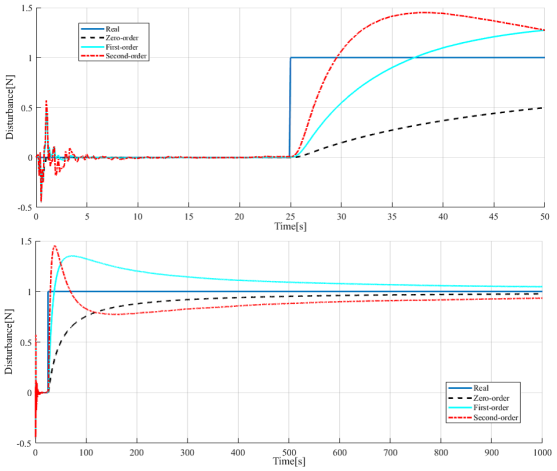

FIGURE 4.4: Simulation results(a): disturbance estimates

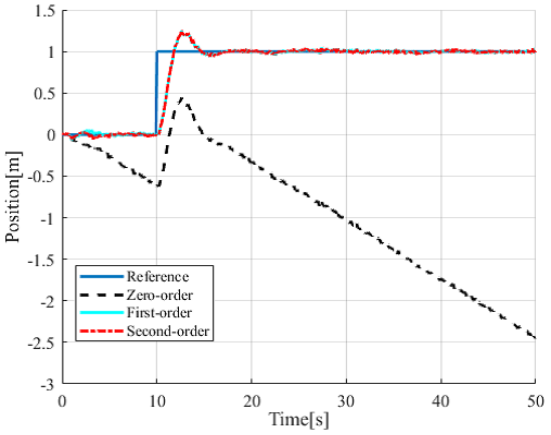

FIGURE 4.5: Simulation results(b): position response

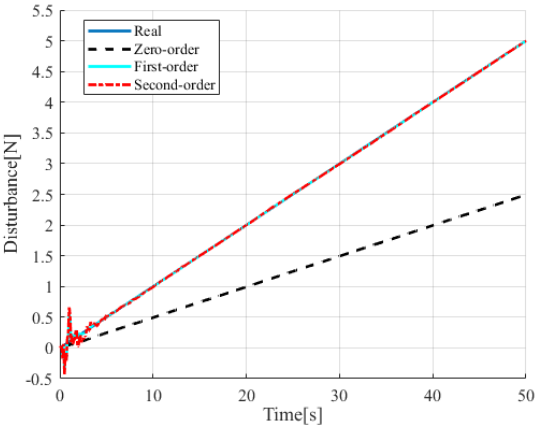

FIGURE 4.6: Simulation results(b): disturbance estimates

4.2.4.1 Verification of augmented disturbance model

In this verification, the zero, first, and second-order disturbance models are compared, and the dimension of the internal model for KFDs is different. Table 4.3 shows the applied disturbance condition. Therefore, it is possible to quantitatively evaluate the effect of extending the dimension of the disturbance estimation.

Figs. 4.3 and 4.4 show the results of position and disturbance responses with respect to step-type disturbance. It is confirmed that the augmented models make the overestimation of disturbance. Additionally, the drawback of KFD appears in Fig. 4.4. Moreover, the control performance for tracking is inadequate. In other words, it can be seen that the step-type disturbance estimation cannot be speeded up by the augmented models. Therefore, it is indicated that the drawback cannot be improved by the models.

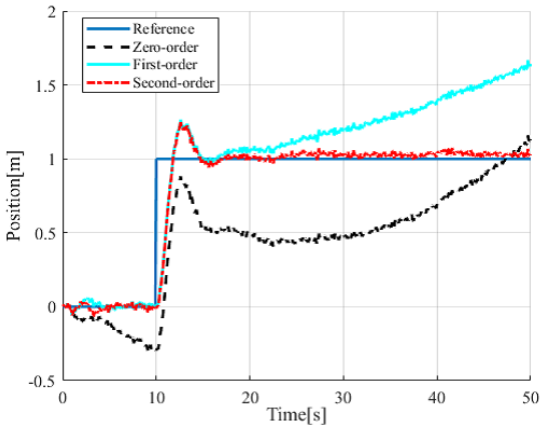

FIGURE 4.7: Simulation results(c): position

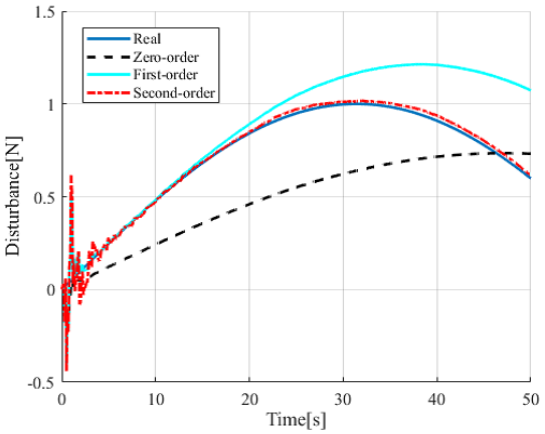

FIGURE 4.8: Simulation results(c): disturbance

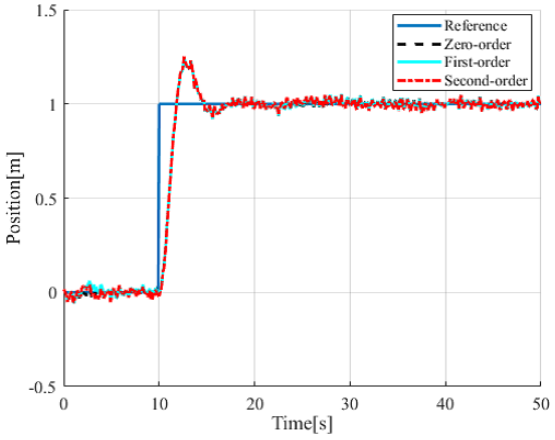

FIGURE 4.9: Simulation results(d): position

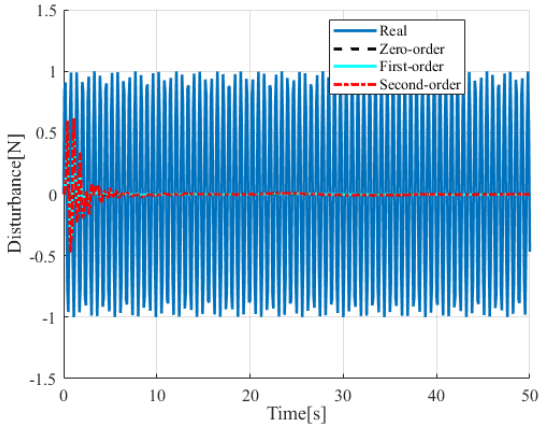

FIGURE 4.10: Simulation results(d): disturbance

Figs. 4.5 - 4.8 show the position and disturbance results of ramp-type and sine-wave disturbances. These results show that the zero-order model-based KFD tends to delay the disturbance estimation and cannot cope with the ramp-type disturbance. By contrast, the augmented model-based KF-D can handle ramp-type disturbances without the drawback. Therefore, these results indicated that the augmented models are useful for the time-varying disturbance. Additionally, in the case of low-frequency disturbances, the proposed method of the second-order model of disturbance is more effective and useful than the other methods. Therefore, it is evident that KFD is possible to deal with time-varying disturbances by extending the disturbance model. Moreover, it becomes possible to handle complicated disturbances that could not be handled by the conventional KFD.

Figs. 4.9 and 4.10 show the position and disturbance results under high-frequency sine-wave disturbance. The results show that the KFD handles high-frequency disturbance as noise. Additionally, the KFDs do not estimate disturbances, and the conventional method and the proposed method have equivalent performance. Table 4.4 shows all results in this verification.

TABLE 4.4: Simulation results

	zero-order	first-order	second-order
(a):step	N	N	N
(b):ramp	N	P	P
(c):sine	N	N	P
(d):noise	P	P	P

where N and P indicate Negative and Positive.

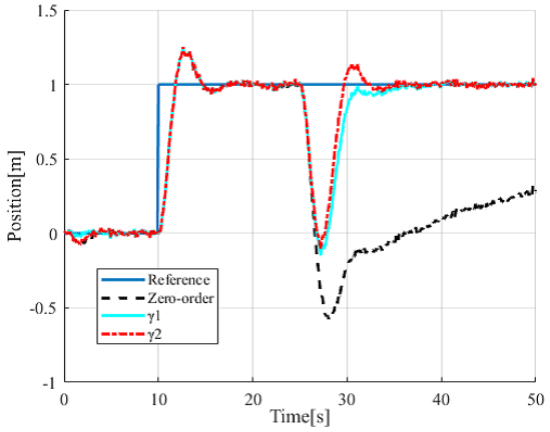

FIGURE 4.11: Simulation results: position response

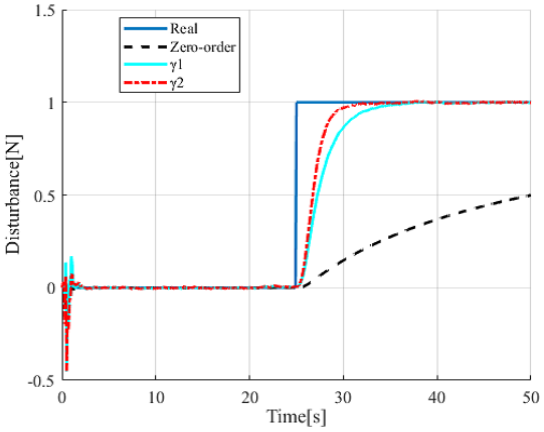

FIGURE 4.12: Simulation results: disturbance estimates

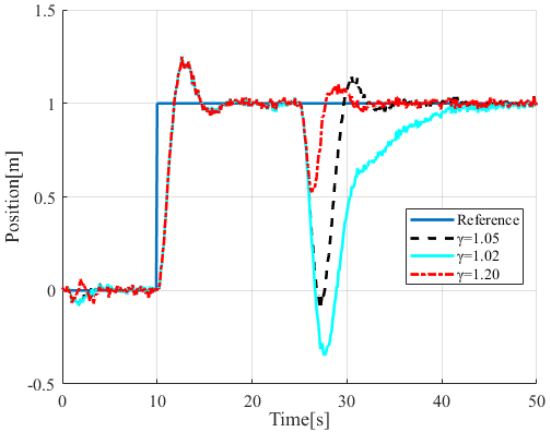

FIGURE 4.13: Simulation results (γ_d): position response

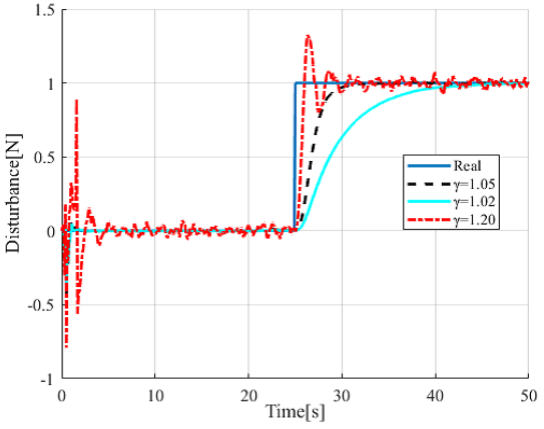

FIGURE 4.14: Simulation results(γ_d): disturbance estimates

From this table, except for the step-type disturbance, it is confirmed that the disturbance estimation speed of KFD can be improved by the augmented models. Furthermore, the proposed models can easily use in conventional DOBs.

TABLE 4.5: Estimation performance of the proposed γ_d in steady-state

γ_d	Estimation response	Noise infulence
(a):1.00	More than 1000 s	$\pm 0.01 \times 10^{-1}$
(b):1.02	25s	$\pm 0.03 \times 10^{-1}$
(c):1.05	5 s	$\pm 0.15 \times 10^{-1}$
(d):1.20	1 s	± 0.06

4.2.4.2 Forgetting factor design

In the previous verification, the results with the augmented models indicated that the KFD does not handle the step-type disturbance (see Fig. 4.4). Therefore, this verification aims to attempt the improvement for step-type disturbance estimation by using the forgetting factor-based AKFD. Moreover, in order to show the effectiveness of the forgetting factor, the internal model of KFDs uses the zero-order model.

In designing the AKFD, the two design methods of forgetting factors were introduced. The parameters are set to

$$\gamma_1 = 1.05 \tag{4.8}$$

, and,

$$\boldsymbol{\gamma}_2 = \begin{bmatrix} \boldsymbol{I}_{n\times n} & \boldsymbol{0}_{n\times 1} \\ \boldsymbol{0}_{1\times n} & \gamma_d \end{bmatrix} \quad \text{where} \quad \gamma_d = 1.05. \tag{4.9}$$

Figs. 4.11 and 4.12 show the compare results of position and disturbance concerning both design methods. Compared to the conventional KFD, the forgetting factor-based AKFD makes fast disturbance estimation. In both methods, the disturbance estimation performance is significantly improved. Additionally, the disturbance estimation of γ_2 is faster than γ_1. It is evident that the forgetting factor significantly assists to speed up the disturbance estimation performance of KFDs. The results indicate the effectiveness of the proposed method.

Moreover, the drawback of the AKFD is an increased noise sensitivity. The results in focusing on γ_2 of the tuning of the forgetting factor are shown in Figs. 4.13 and 4.14. The γ_d is set to 1.02, 1.05, and 1.20. Table 4.5 shows the compare results in γ_d. From the position result shown in Fig. 4.13, the large values of γ_d make high-tracking performance. By contrast, from the result of disturbance estimation, it is confirmed that the KFD with a large value of γ is significantly affected by noise influences. Moreover, the KFD with a small value of γ is seldom affected by noise influences. These results indicate that the factor γ_d decides the noise sensitivity of the KFDs. Additionally, the result indicates that the scalar factor γ_1 frequently generates noisy estimates. The proposed method enables the tune-up only focused on disturbance estimation performance in KFDs.

TABLE 4.6: Simulated conditions

No.	Extended order	Posterior covariance matrice	Type of disturbance
1*	zero-order	conventional	step
2	zero-order	prop. ($\boldsymbol{\gamma} = diag(\boldsymbol{I}, 1.05)$)	step
3	second-order	prop. ($\gamma = 1.05$)	step
4	second-order	prop. ($\boldsymbol{\gamma} = diag(\boldsymbol{I}, 1.05, 1.05, 1.05)$)	step
5*	zero-order	conventional	ramp
6	zero-order	prop. ($\boldsymbol{\gamma} = diag(\boldsymbol{I}, 1.05)$)	ramp
7	second-order	prop. ($\gamma = 1.05$)	ramp
8	second-order	prop. ($\boldsymbol{\gamma} = diag(\boldsymbol{I}, 1.05, 1.05, 1.05)$)	ramp
9*	zero-order	conventional	low frequency
10	zero-order	prop. ($\boldsymbol{\gamma} = diag(\boldsymbol{I}, 1.05)$)	low frequency
11	second-order	prop. ($\gamma = 1.05$)	low frequency
12	second-order	prop. ($\boldsymbol{\gamma} = diag(\boldsymbol{I}, 1.05, 1.05, 1.05)$)	low frequency

where, $*$ denotes the conventional mathod.

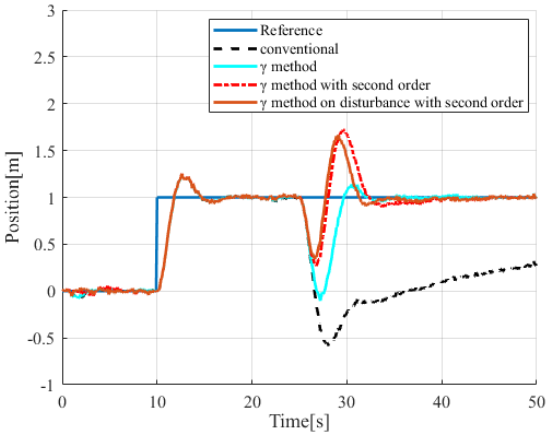

FIGURE 4.15: Comparative results: position response with respect to step-type disturbance

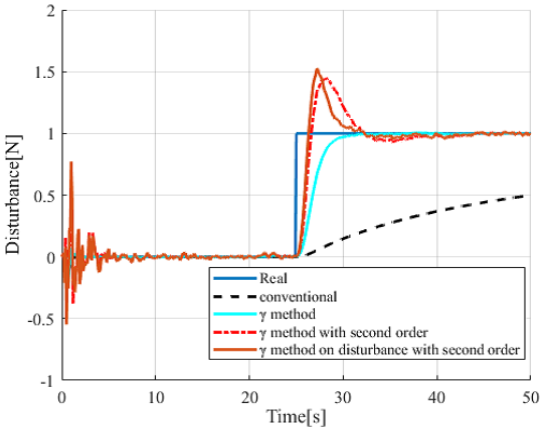

FIGURE 4.16: Comparative results: step-type disturbance

4.2.4.3 AKFD with augmented disturbance models

In this section, the results of integrating the above two methods are shown. Table 4.6 shows the verification conditions. The compare results include: γ_2, γ_1 with the augmented second-order model of disturbance, and γ_2 with the augmented second-order model of disturbance. The disturbances used in the verification are shown in Table 4.3. Figs. 4.15-4.20 show the compare results of position response, step-type disturbance, ramp-type disturbance, and sine-wave disturbance.

Figs. 4.15 and 4.16 show the result of position and disturbance on step-type disturbance (Table 4.6 -1,2,3,4).

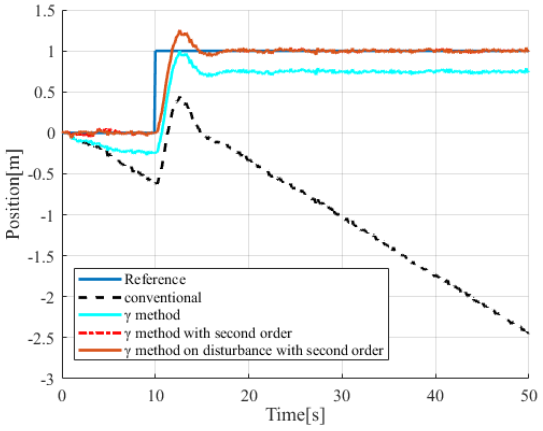

FIGURE 4.17: Comparative results: position response with respect to ramp-type disturbance

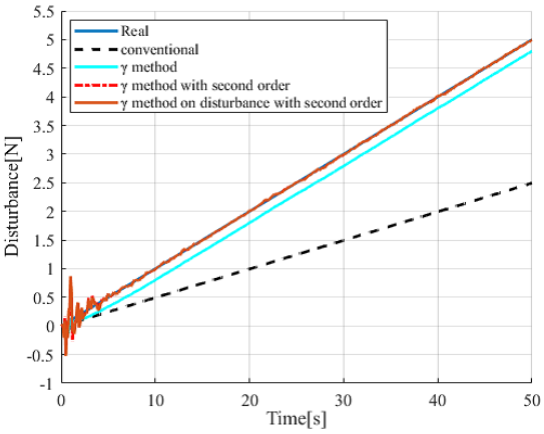

FIGURE 4.18: Comparative results: ramp-type disturbance

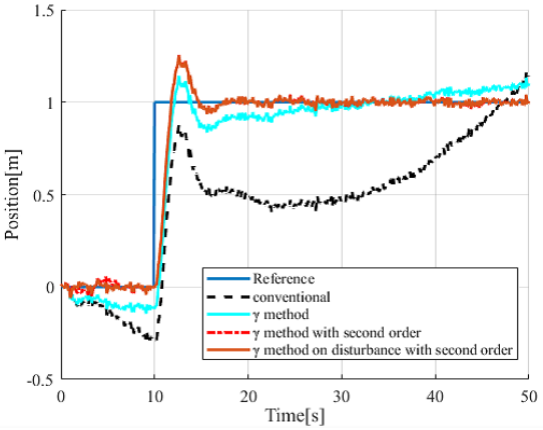

FIGURE 4.19: Comparative results: position response with respect to sine-wave disturbance

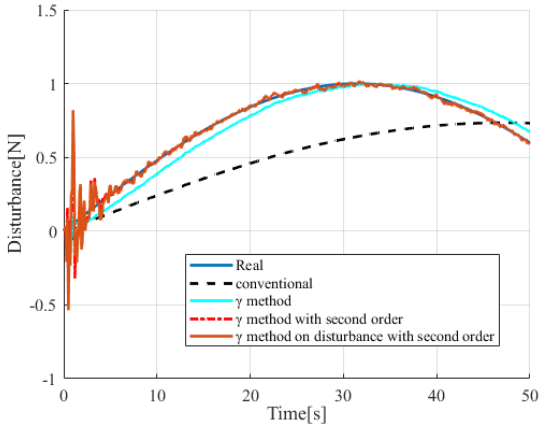

FIGURE 4.20: Comparative results: sine-wave disturbance

From the result of position response in step-type disturbance, it is evident that the tracking control performances of the proposed methods are higher than the conventional methods. The result of the disturbance estimation indicates that the proposed method without the augmented models is the most effective. Moreover, the augmented model-based KFDs generate the overestimated disturbance estimates. However, the convergence speed is fast from the overestimation. In light of this information, it is evident that the proposed method significantly improves the performance of KFDs.

Moreover, the results of the ramp-type and sine-wave disturbances show that the proposed method with the augmented models can handle the time-varying disturbance. These control and estimation performances cannot be achieved by the conventional methods, and the proposed method without augmented models.

TABLE 4.7: List of results of disturbance estimation by KF-D

disturbance	(i): Conventional	(ii):2-order models	(iii): γ	(ix): (ii) w/ (iii)
Step	large delay	large delay	positive	overshoot
Ramp	large delay	positive	small delay	positive
low frequency sine wave	large estimation error	small delay	small delay	positive

Table 4.7 shows all results. From the results, the KFD has the drawbacks of disturbance estimation and its speed. By contrast, the proposed factor is useful for improving the performance of step-type disturbance estimation. Additionally, it is confirmed that the proposed augmented designs improve the performance of the KFD. Overall, it is evident that the proposed method is useful for improving the KFDs.

4.2.5 Experiments

In order to verify the estimation performance of KFDs (Sec. 3.2 and Sec. 4.2), experiments of position control of the cart system were conducted. In the experimental system, the actual disturbances are generated by linear and nonlinear friction forces, sensor noise, and resolution of control input PWM (pulse width modulation).

In the experiments, the compared systems are as follows:

(i) MDOB,

(ii) IDOB,

(iii) KFD,

(iv) KFD w/ $\gamma = \mathrm{diag}(1, 1, 1.05)$,

(v) KFD w/ $\gamma = \mathrm{diag}(1, 1, 1.10)$,

(vi) KFD w/ $\gamma = \mathrm{diag}(1, 1, 1.10)$,

(vii) KFD based on first-order model,

(viii) KFD w/ $\gamma = \mathrm{diag}(1, 1, 1.05, 1.05)$ based on first-order model,

(ix) KFD based on second-order model,

(x) KFD w/ $\gamma = \mathrm{diag}(1, 1, 1.05, 1.05, 1.05)$ based on second-order model.

Moreover, the position control is described as

$$u(k) = K_p(y_{\mathrm{ref}} - \hat{y}(k)) - K_d\hat{v}(k) + \hat{d}(k), \tag{4.10}$$

where, $y_{\mathrm{ref}} = 0.1$[m] is the position reference, $K_p = 10$ and $K_d = K_p/\sqrt{2}$ denote the proportional and differential gain, and $\hat{v}$ is the velocity estimate.

To evaluate the noise reduction performance of each control system, the results of highpass filtered disturbance estimates are shown. Additionally, in the highpass filter, the passband frequency of the filter set to 150 [Hz].

Considering the noise reduction, the cutoff frequencies of the MDOB set to g_w= 0.6 [Hz] and g_d = 2[Hz]. Moreover, the pole of IDOB set to -8, -9, and -10 in a continuous system. Furthermore, in the KFD systems, the system and observation covariance matrices are set to 10^{-2} and 10^{-4}, and the initial error covariance matrix is set to $\mathrm{diag}(10^{-2}, 10^{-4}, 10^{-2}, \{10^{-2}, 10^{-2}\})$.

4.2.6 Results

The compared results involving the position response, control input, and disturbance estimator are shown in Figs. 4.21-4.30.

From each position result, it is confirmed that the KFD with adaptive factor is useful for offset-free tracking control. In particular, using $\gamma = 1.05$, the tracking performance is improved.

From the results on the highpass filtered disturbance estimates, in the actual system, the KFD has better noise reduction ability than the MDOB system. By contrast, the disturbance estimation speed by the KFD is slower than MDOB. However, it is even that the adaptive factor-based KFD (see Figs. 4.21 and 4.24) has better noise reduction performance and similar position response than MDOB.

Moreover, from the results of the compared magnitude of the adaptive factor, it is confirmed that the adaptive factor decides the response speed and noise sensitivity on disturbance estimates in actual systems (see Figs. 4.24-4.26).

Additionally, the results for augmented models are indicated that the disturbance estimates significantly affected by disturbance variation estimates in the actual system. Moreover, the undesired behaviors are confirmed by the results. Therefore, an improved estimation performance for the augmented models is a must. The effective countermeasure is tune-up considering the disturbance rate estimates (i.e., $\hat{\dot{d}}$ and $\hat{\ddot{d}}$).

However, it is confirmed the adaptive factor is also effective against augmented systems.

4.2.7 Summary

This section introduced how to improve the KFD method. The two improvement methods were shown. Moreover, the verification results show the effectiveness of the proposed methods.

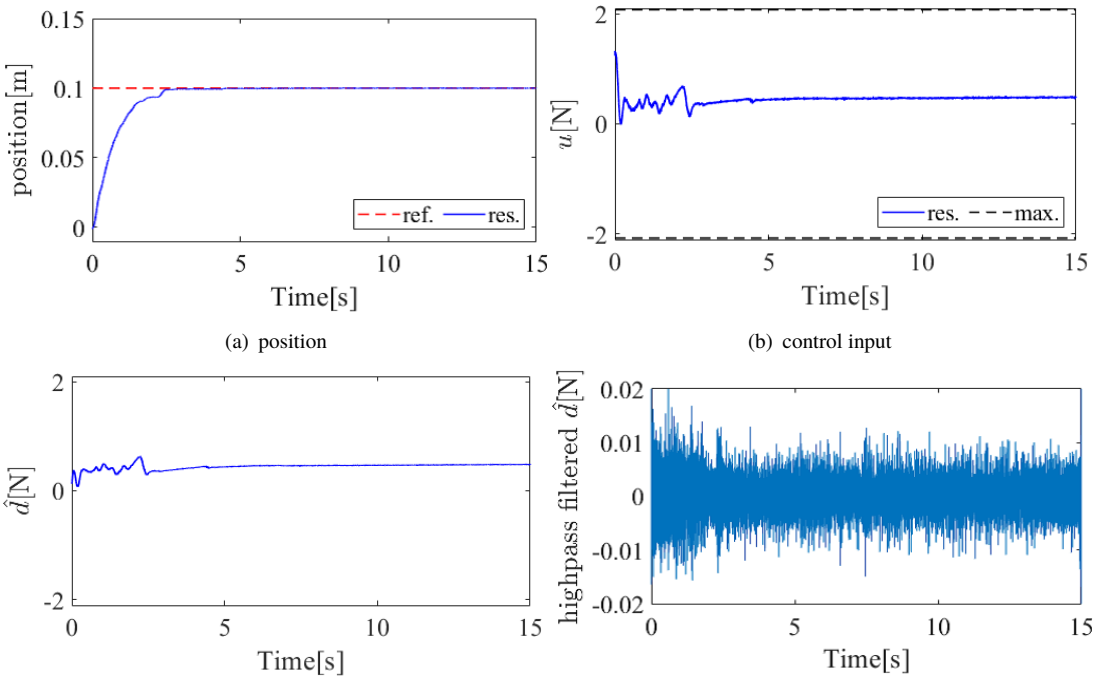

(a) position (b) control input

(c) disturbance estimates (d) Highpass-filter $\hat{d}$

FIGURE 4.21: Experimental result: MDOB.

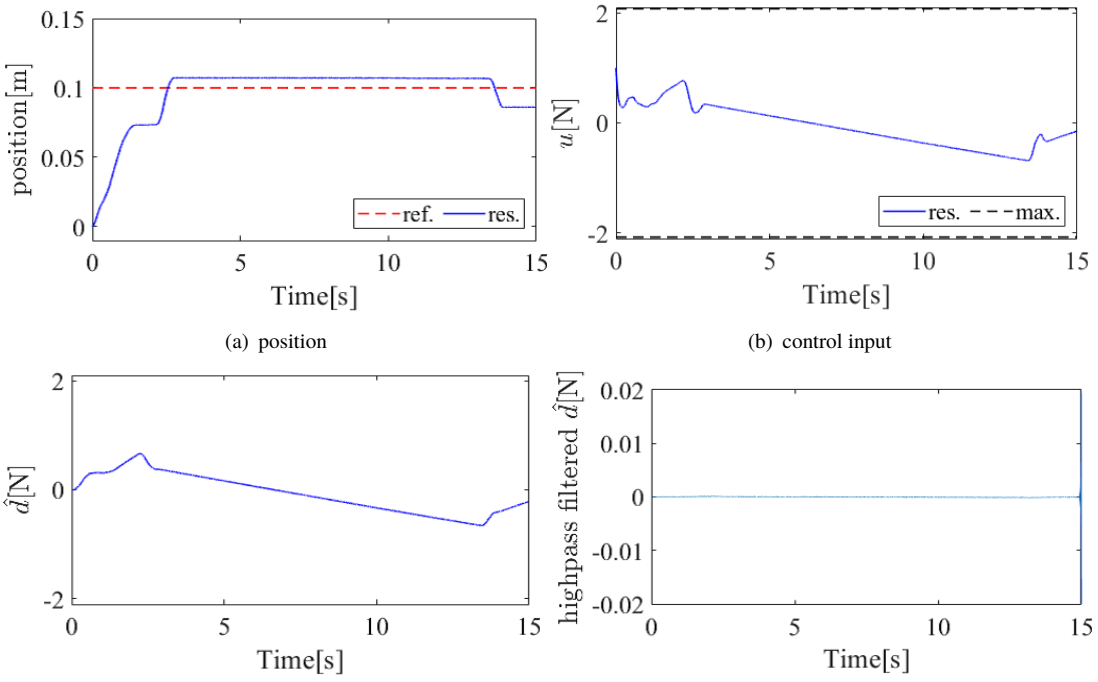

(a) position (b) control input

(c) disturbance estimates (d) Highpass-filter $\hat{d}$

FIGURE 4.22: Experimental result: IDOB.

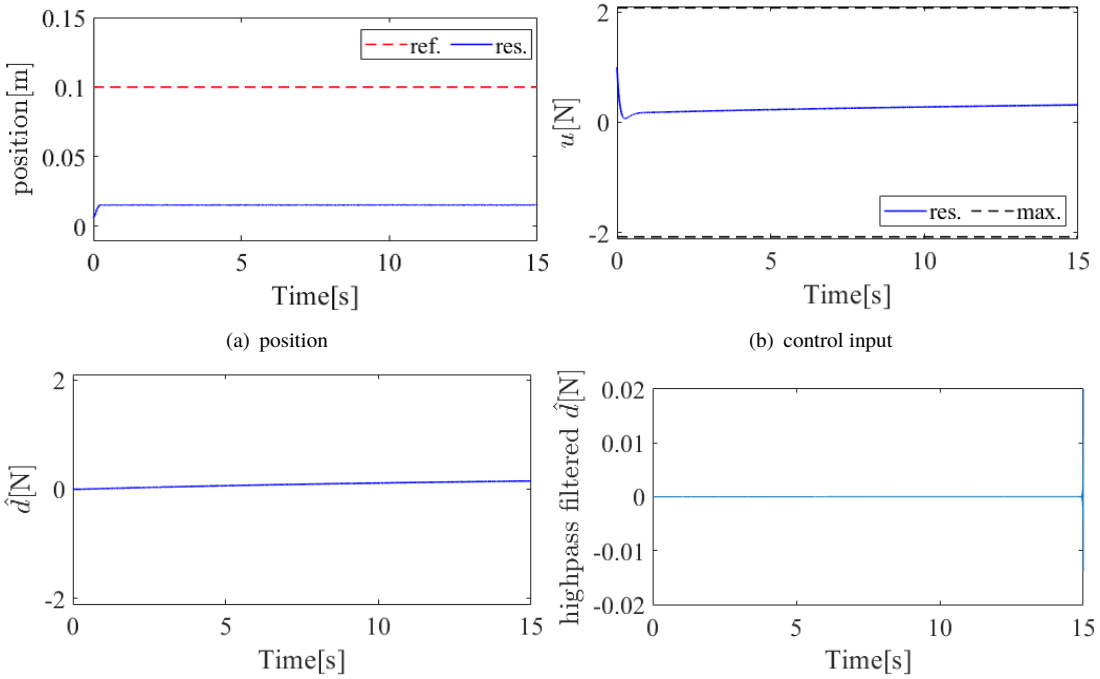

(a) position (b) control input

(c) disturbance estimates (d) Highpass-filter $\hat{d}$

FIGURE 4.23: Experimental result: KFD.

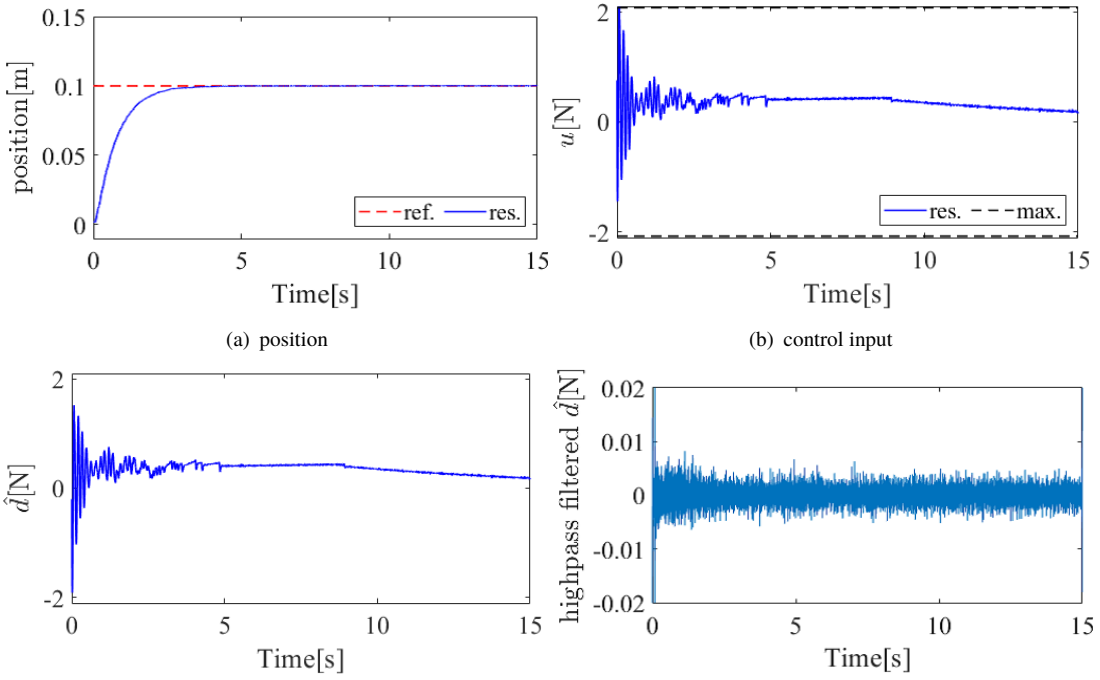

(a) position (b) control input

(c) disturbance estimates (d) Highpass-filter $\hat{d}$

FIGURE 4.24: Experimental result: KFD w/ $\gamma = 1.05$.

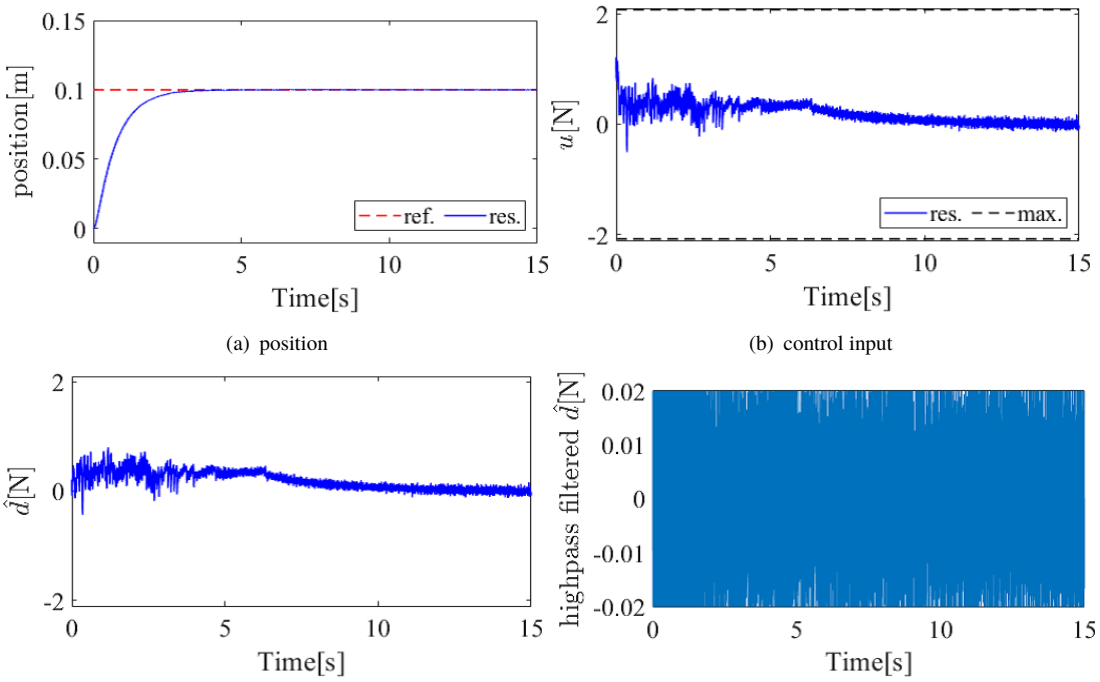

(a) position (b) control input

(c) disturbance estimates (d) Highpass-filter $\hat{d}$

FIGURE 4.25: Experimental result: KFD w/ $\gamma = 1.10$.

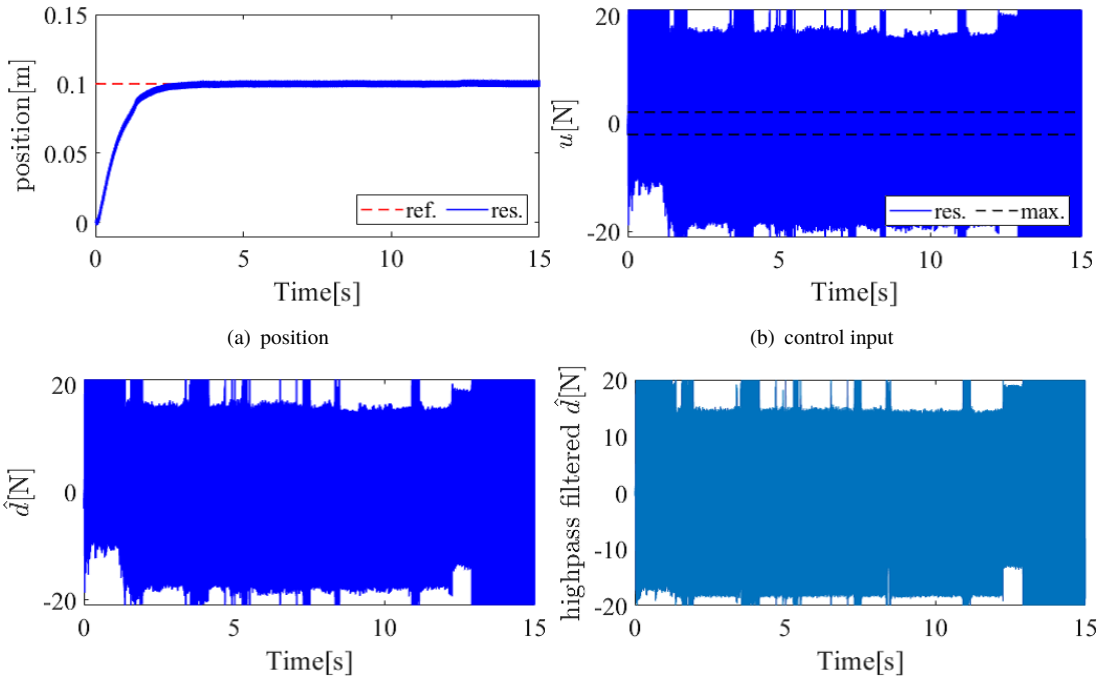

(a) position (b) control input

(c) disturbance estimates (d) Highpass-filter $\hat{d}$

FIGURE 4.26: Experimental result: KFD w/ $\gamma = 1.20$.

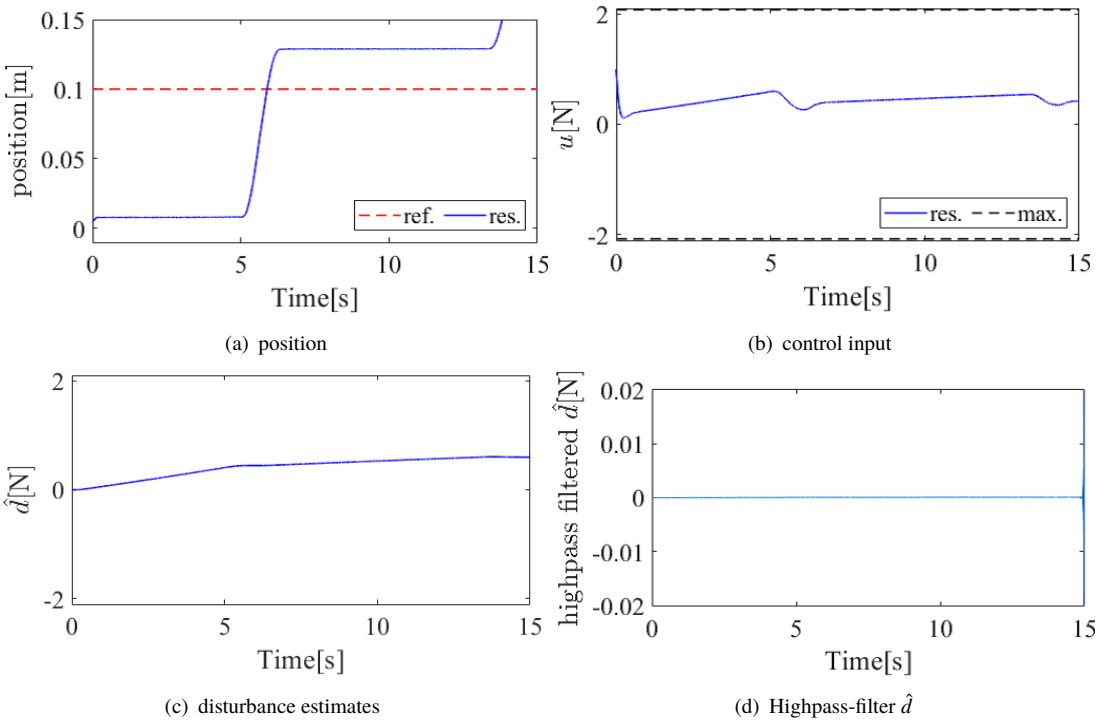

(a) position (b) control input

(c) disturbance estimates (d) Highpass-filter $\hat{d}$

FIGURE 4.27: Experimental result: KFD based on first-order disturbance model.

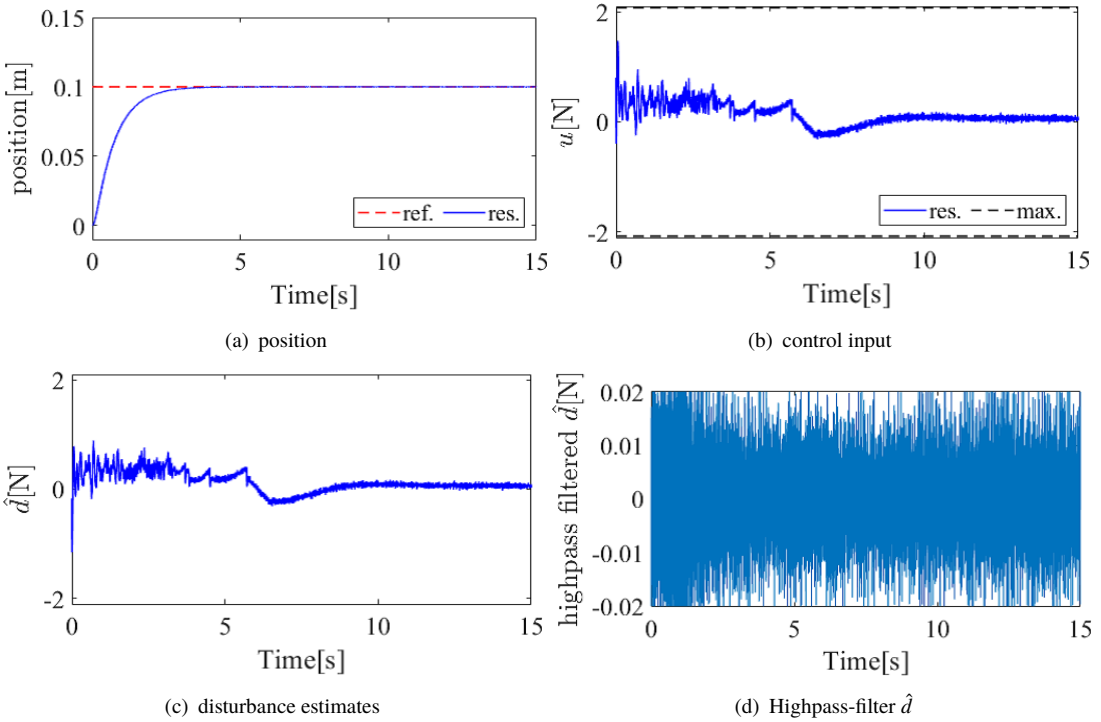

(a) position (b) control input

(c) disturbance estimates (d) Highpass-filter $\hat{d}$

FIGURE 4.28: Experimental result: KFD based on first-order disturbance model w/ $\gamma = 1.05$.

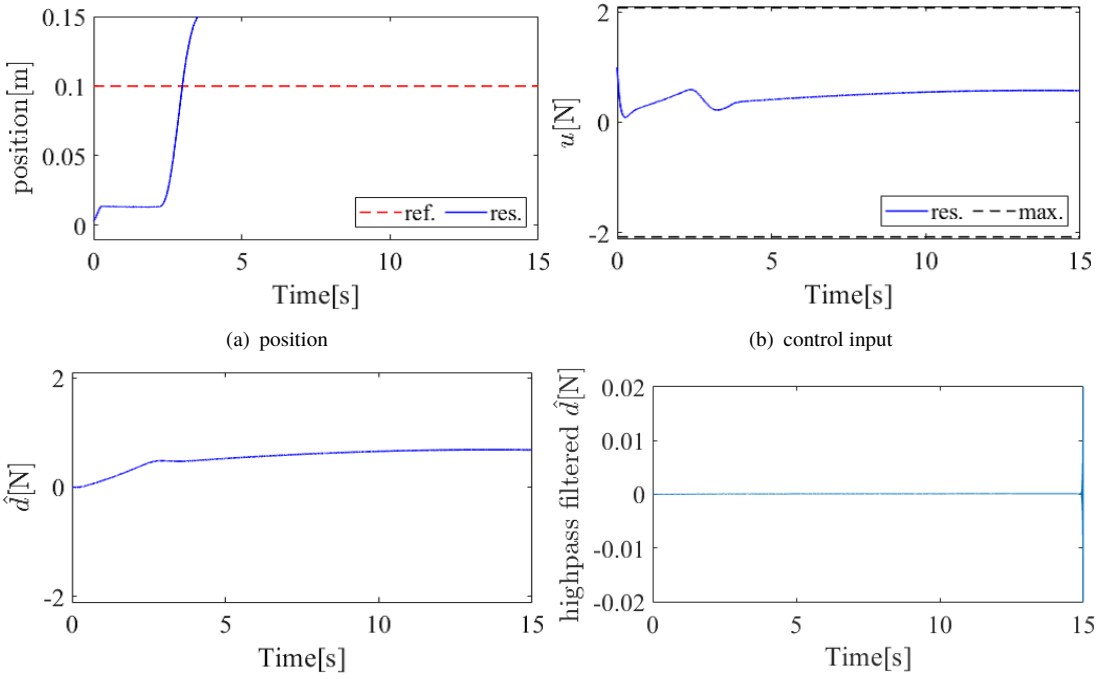

(a) position (b) control input

(c) disturbance estimates (d) Highpass-filter $\hat{d}$

FIGURE 4.29: Experimental result: KFD based on second-order disturbance model.

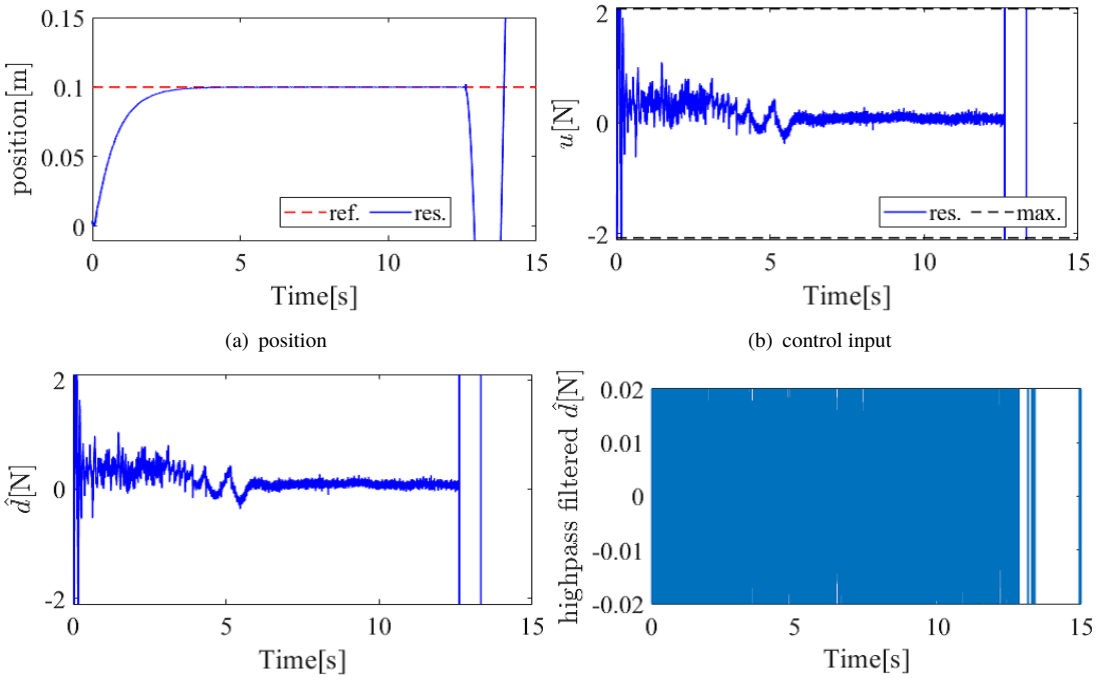

(a) position (b) control input

(c) disturbance estimates (d) Highpass-filter $\hat{d}$

FIGURE 4.30: Experimental result: KFD based on second-order disturbance model w/ $\gamma = 1.05$.

4.3 Variable forgetting factor-based adaptive Kalman filter with disturbance estimation

This section explains the proposed method of simultaneous estimation for the system state and disturbance. In the FAKFD, the trade-off cannot be solved. To address the trade-off, FAKFD and an online adjustment method of the forgetting factor are proposed in this section. The proposed estimation method consists of a FAKFD and an updating law of the VFF. As shown in the previous section, the FAKFD using a fixed forgetting factor and the extended system model can provide the fast simultaneous estimation of the state and disturbance. In the proposed method, to reduce the noise effects, a design method of VFF is introduced for the FAKFD. Additionally, the VFF is utilized for online adjustment of the noise sensitivity and estimation speed. Moreover, the proposed estimation method, which uses variable forgetting factor-based adaptive Kalman filter with disturbance estimation (VFAKFD), can simultaneously estimate the system state and unknown disturbance while considering the estimation speed and observation noise reduction.

4.3.1 Proposed method

4.3.1.1 Adaptive Kalman filter with disturbance estimation

In this section, the KFD law is defined by

$$\bar{\boldsymbol{x}}(k|k-1) = \bar{\boldsymbol{A}}_d\bar{\boldsymbol{x}}(k-1) + \bar{\boldsymbol{B}}_d\tau(k-1), \tag{4.11}$$

$$\boldsymbol{P}(k|k-1) = \bar{\boldsymbol{A}}_d\boldsymbol{P}(k-1)\bar{\boldsymbol{A}}_d^{\mathrm{T}} + \bar{\boldsymbol{B}}_d Q\bar{\boldsymbol{B}}_d^{\mathrm{T}}, \tag{4.12}$$

$$\boldsymbol{D}(k) = \bar{\boldsymbol{C}}_d\boldsymbol{P}(k|k-1)\bar{\boldsymbol{C}}_d^{\mathrm{T}} + R, \tag{4.13}$$

$$\boldsymbol{K}(k) = \boldsymbol{P}(k|k-1)\bar{\boldsymbol{C}}_d^{\mathrm{T}}\boldsymbol{D}^{-1}, \tag{4.14}$$

$$\hat{e}(k) = y - \bar{\boldsymbol{C}}_d\bar{\boldsymbol{x}}(k|k-1), \tag{4.15}$$

$$\bar{\boldsymbol{x}}(k|k) = \bar{\boldsymbol{x}}(k|k-1) + \boldsymbol{K}(k)\hat{e}(k), \tag{4.16}$$

$$\boldsymbol{P}(k|k) = \{\boldsymbol{I} - \boldsymbol{K}(k)\bar{\boldsymbol{C}}_d\}\boldsymbol{P}(k|k-1). \tag{4.17}$$

In contrast to the previous section, the forgetting factor affects all elements of the covariance matrix. Consider the accuracy of estimation of KFD, the variable adaptive factor is designed to affect all state estimations, because the variable parameters always correct estimation errors for all state variables. Note that the VFAKFD converges to general KF systems, and the convergence conditions of the VFAKFD are provided in this chapter.

The FAKFD is designed by adding the forgetting factor to the AKF. In the previous section, the forgetting factor designs to affect the disturbance estimation. In this section, the forgetting factor

is used for all state variables because the noise effects can be reduced by the VFF. For designing the VFF, the FAKFD can be described as

$$\boldsymbol{P}(k|k) = \lambda^{-1}(k)\{\boldsymbol{I} - \boldsymbol{K}(k)\bar{\boldsymbol{C}}_d\}\boldsymbol{P}(k|k-1), \tag{4.18}$$

4.3.1.2 Design of variable forgetting factor

To realize the improved estimation performance including noise reduction and fast responsiveness, the VFF using the online adjustment method is integrated into the FAKFD. In the related work to parameter estimation by an RLS using variable forgetting factor [140], a VFF design using the estimation error has been developed. Therefore, this section proposes an online adjustment method for the VFF based on the estimation error ($\hat{e}(k)$). In the VFF design, in addition to Eq. (4.18), Eq. (4.13) is given by

$$\boldsymbol{D}(k) = \bar{\boldsymbol{C}}_d\boldsymbol{P}(k|k-1)\bar{\boldsymbol{C}}_d^{\mathrm{T}} + \lambda(k). \tag{4.19}$$

Using the VFF as the covariance of the observation noise, the effects of the observation noise are directly considered.

Additionally, using the estimation error, the VFF ($\lambda(k)$) is defined as

$$\lambda(k) = \lambda_{max} - \frac{1}{1 + \bar{\boldsymbol{C}}_d\boldsymbol{P}(k|k-1)\bar{\boldsymbol{C}}_d^{\mathrm{T}}} \cdot \frac{\hat{e}^2(k)}{\alpha}, \tag{4.20}$$

where $\alpha > 0$ is the parameter of this adjustment law and reflects the observation noise. Moreover, λ_{max} denotes the maximum of $\lambda(k)$, and it decides the noise sensitivity of all estimates in the steady-state. Using this law, when $\hat{e}^2(k) >> 0$, $\lambda(k)$ close to 0. Thereby, the response speed is improved. On the other hand, when $\hat{e}^2(k) \approx 0$ (steady-state), λ close to λ_{max}; therefore, the influence of the noise in the estimates is significantly suppressed.

Additionally, to converge the estimation of the VFAKFD, the constraints on the VFF is set to

$$0 < \lambda_{min} \leq \lambda(k) \leq \lambda_{max} \leq 1. \tag{4.21}$$

The lower bound (λ_{min}) denotes the condition to ensure the positive $\lambda(k)$ to the large estimation errors. Furthermore, the lower limit λ_{min} decides the responsivity of the VFAKFD; however, a small λ_{min} creates noisy estimates. Thus, the design of λ_{min} considers the noise covariance in observation, and the design of λ_{max} considers to prevent the noise effects in the estimates. Additionally, the online adjustment method Eq. (4.20) is converged to λ_{max} when the estimation error is converged to 0. In the case of $\lambda_{max} = 1$, the proposed estimation method converges to the standard Kalman filter without the online adjustment method.

4.3.2 Numerical Verification: Quantization noise reduction

To validate the effectiveness and usefulness of the proposed estimation method, two numerical simulations of a position control with an external torque disturbance are conducted in noisy environments. In the simulations, the proposed method was compared with the conventional methods (MDOB[8], IDOB[99], KFD[104], and DKF[127]) and two FAKFDs using high and low forgetting factors. Considering the balance between the response speed of the estimates and the observation noise rejection, the parameters were set to $\lambda_{min} = 0.8$ and $\lambda_{max} = 1$ in the proposed VFAKFD system. Moreover, the verifications were properly performed using MATLAB/Simulink. In the position control, a PD control is used and can be described as

$$\tau(k) = K_p\{q_{\mathrm{ref}}(k) - \hat{q}(k)\} - K_d\hat{\dot{q}}(k) + \hat{\tau}_d(k), \tag{4.22}$$

where $q_{\mathrm{ref}} = 0$ [rad], K_p, K_d, and $\hat{\tau}_d$ denote a position reference, proportional gain, differential gain, and the disturbance estimates. Additionally, in the compared MDOB system, $\hat{q}(k)$ cannot be estimated; therefore, the measured variable $y(k)$ is directly used for position control.

Furthermore, the observation noise effects with respect to quantization noise were designed by quantization error generated by encoder models. Moreover, the quantization noise effects are decided using a number (n) with respect to the encoder bits, multiply, and gear ratio, and system sampling time (T_s). To design the effects, a pulse per revolution (PPR) including all parameters was defined by b_{reso}. The maximum quantization error (Q_{max})[124] using the PPR is given by

$$Q_{max} = \frac{2\pi}{b_{\mathrm{reso}}}, \tag{4.23}$$

and the maximum estimation error of the velocity can be described as

$$Q_v = \frac{Q_{max}}{T_s}. \tag{4.24}$$

Fig. 4.31 shows the response of the encoder model in case of ($n = 8$ and $T_s = 10^{-2}$s, $Q_{max} = 2\pi/2^8 = 0.0245$).

In all verifications, a step-type input disturbance τ_{dis} [Nm] is assumed, and it is given by

$$\tau_{\mathrm{dis}} = \begin{cases} 10 & (1 \le k) \\ 0 & (k < 1) \end{cases}. \tag{4.25}$$

Moreover, the state-space expressed DOBs can handle high-order disturbances using the high-order disturbance model to the internal model. Thus, to validate the simultaneous estimation

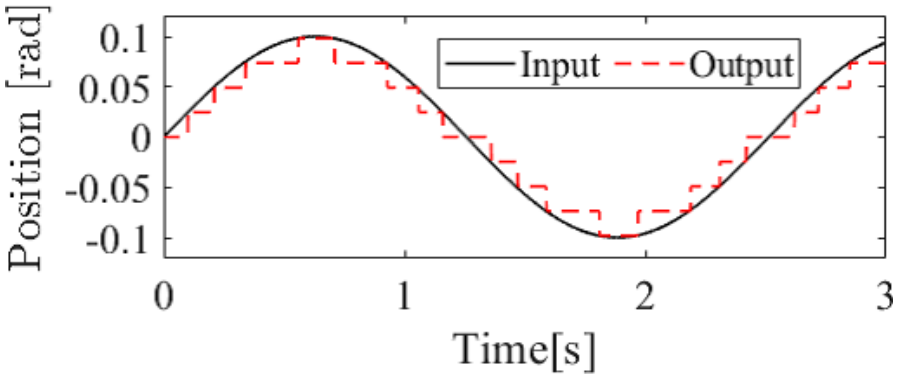

(a) Input and output angles

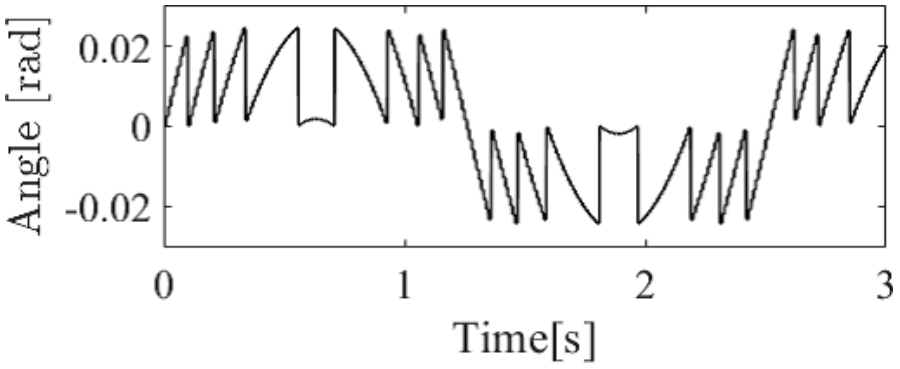

(b) Quantization error

FIGURE 4.31: Encoder model

performance by the proposed estimation system, this section only assumes the step-type disturbance. Additionally, the physical parameters were set to $j = 1$, and $c = 0$. The MDOB using $c = 0$ can handle the direct estimation of the external force, similar to other estimation methods.

Furthermore, all estimation methods were adjusted considering the reduction of noise effects. In the MDOB, it can provide fast disturbance estimation. However, the noise effect of the disturbance estimate is increased by fast estimation. Thus, the low cutoff frequencies were used in the compared MDOB.

4.3.2.1 VFF design of quantization noise reduction

The quantization noise effects can be described using n and T_s. Thus, the parameter α in the VFF can also be designed using n and T_s. Consider the noise effects, α is given by

$$\alpha = (b_{\text{reso}} \cdot T_s)^{-1}, \tag{4.26}$$

Using this equation, the VFF can easily adjust to various resolutions. However, the automatic tune law is a temporary way; therefore, an improved estimation performance is obtained by trial and error turn up.

4.3.2.2 Results

In this verification, $n = \{4, 8, 12, 48\}$ and $T_s = \{10^{-2}, 10^{-3}\}$ [s] are utilized to compare the reduction performance of quantization noise.

Figs. 4.32-4.35 shows the verification results on disturbance estimates and the VFF. In the results with the high-resolution and 10^{-3}[s], it is confirmed that the VFAKFD generates the disturbance estimation response similar to existing DOBs. On the other hand, in the results of the low-resolution, it can be confirmed that the VFAKFD significantly reduces the noise influences and can provide the proper disturbance estimates. By contrast, the estimations of disturbance by the conventional DOBs are significantly affected by the quantization noise. Therefore, it is evident that the VFAKFD brings smooth convergence of the disturbance estimates while rejecting the noise effects, and it can effectively perform the disturbance estimation to large quantization errors.

Furthermore, the VFAKFD has a better response more than the FAKFD without the online adjustment method. Therefore, it is confirmed that the design method of the VFF is effective for improving the disturbance estimation and the observation noise reduction. However, using high-resolution and large sampling time, the VFF makes slow response speed. This is attributed to the small α by the design of the online adjustment method Eq. (4.26). Therefore, this response speed can improve by the design of α. From the verification results, it is confirmed that the proposed method is effective for solving the trade-off. Moreover, the VFAKFD brings robust estimation considering the model error and observation noise since state estimation clearly includes the unknown disturbance effects as the disturbance estimates.

Moreover, the root mean square error (RMSE) on $\dot{q}$ in 5-10s is shown in Table 4.8. From Table 4.8, it is evident that the VFAKFD brings the highest performance on the unmeasured variable estimation. Furthermore, the result indicates that the VFAKFD can also provide noise-free and accurate estimations to the state variable, and it can better handle the low-resolution encoder while estimating disturbance compared with conventional methods. Indeed, the proposed method can treat simultaneous estimation and quantization noise reduction at the same time. Additionally, under the quantization noise, it is confirmed that it has an improved estimation performance with small estimation errors in the estimation on the unmeasured variables. Therefore, the proposed method is effective for realizing robust motion control under the quantization noise.

In conclusion, the VFAKFD simultaneously treats the quantization noise reduction and accurate disturbance estimation, and it has a proper estimation performance using low-resolution sensors than conventional DOBs.

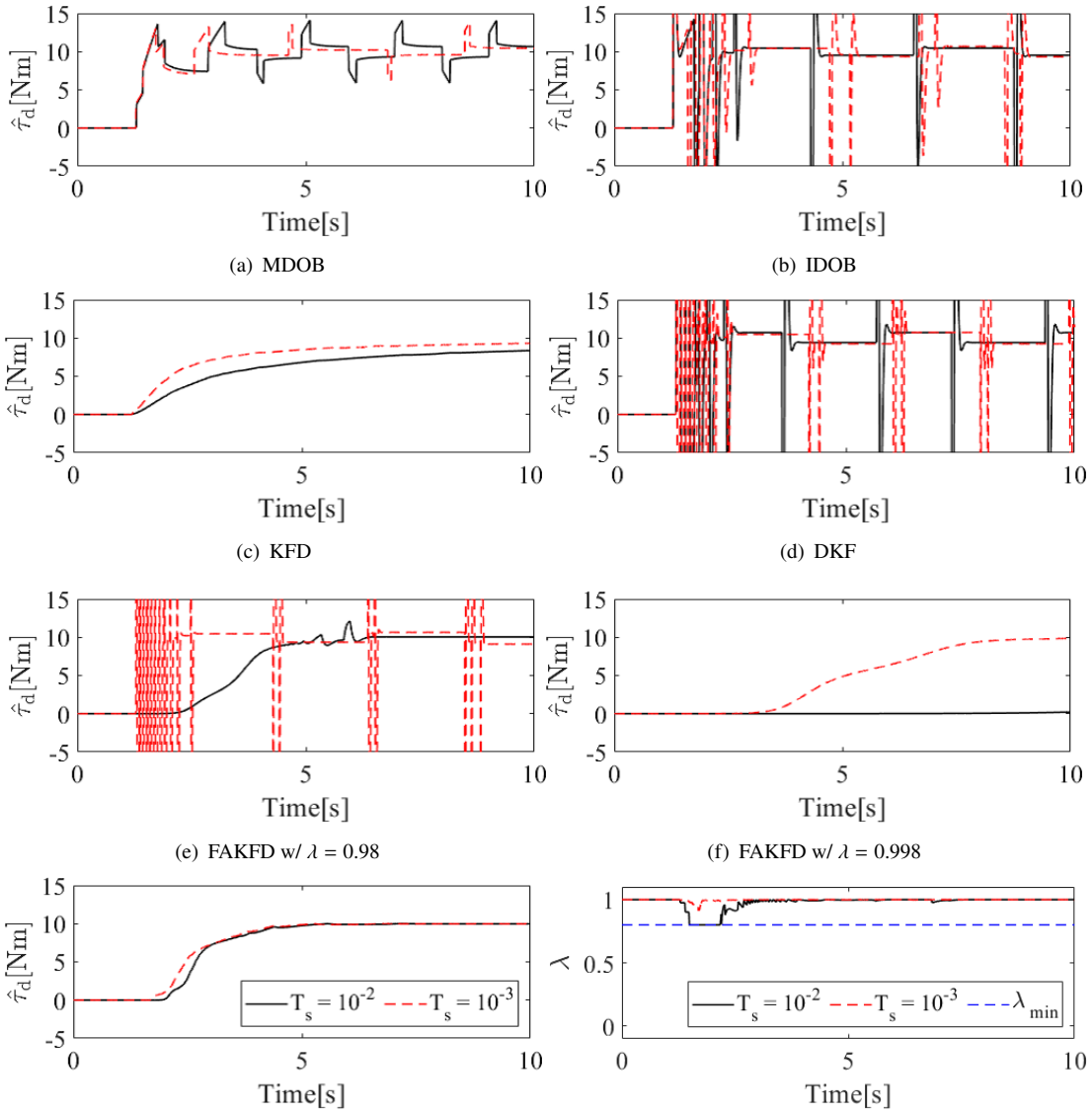

(a) MDOB (b) IDOB

(c) KFD (d) DKF

(e) FAKFD w/ $\lambda = 0.98$ (f) FAKFD w/ $\lambda = 0.998$

(g) VFAKFD (prop.) (h) λ in VFAKFD(g)

FIGURE 4.32: Simulation results: $n = 4$, 16 PPR.

TABLE 4.8: Simulation results 4.3.2: RMSE of $\dot{q}$.

T_s	n	Q_v	MDOB	IDOB	KFD	DKF	FAKFD ($\lambda = 0.98$)	FAKFD ($\lambda = 0.998$)	VFAKFD
10^{-2}	4	39.2	5.19	0.88	1.02	0.97	0.25	66.0	0.10
	8	2.45	0.65	0.06	1.01	0.06	0.06	66.0	0.01
	12	0.15	0.07	3.62×10^{-3}	1.01	3.12×10^{-3}	0.05	66.0	1.12×10^{-3}
	48	2.45	2.23×10^{-12}	9.46×10^{-14}	1.01	1.00×10^{-13}	0.05	66.0	6.12×10^{-11}
10^{-3}	4	392.7	11.10	1.02	0.49	1.53	1.37	6.95	0.09
	8	24.54	1.20	0.07	0.46	0.11	0.12	6.92	0.01
	12	1.53	0.32	3.92×10^{-3}	0.46	0.01	0.01	6.92	0.47×10^{-3}
	48	2.23×10^{-11}	141.93	6.49×10^{-14}	0.46	1.48×10^{-13}	1.51×10^{-13}	6.92	5.63×10^{-13}

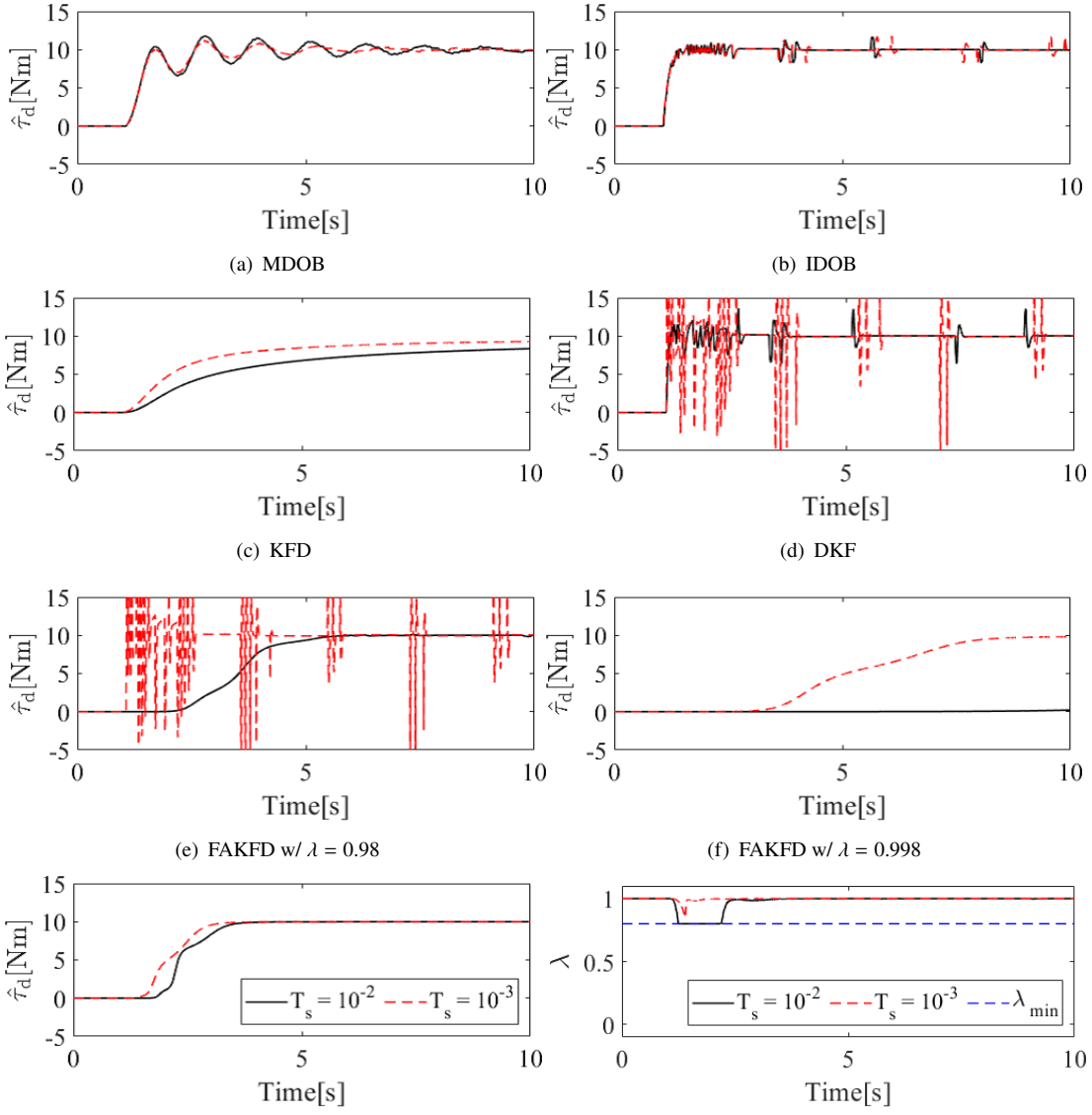

(a) MDOB (b) IDOB

(c) KFD (d) DKF

(e) FAKFD w/ $\lambda = 0.98$ (f) FAKFD w/ $\lambda = 0.998$

(g) VFAKFD (prop.) (h) λ in VFAKFD(g)

FIGURE 4.33: Simulation results: $n = 8$, 256 PPR.

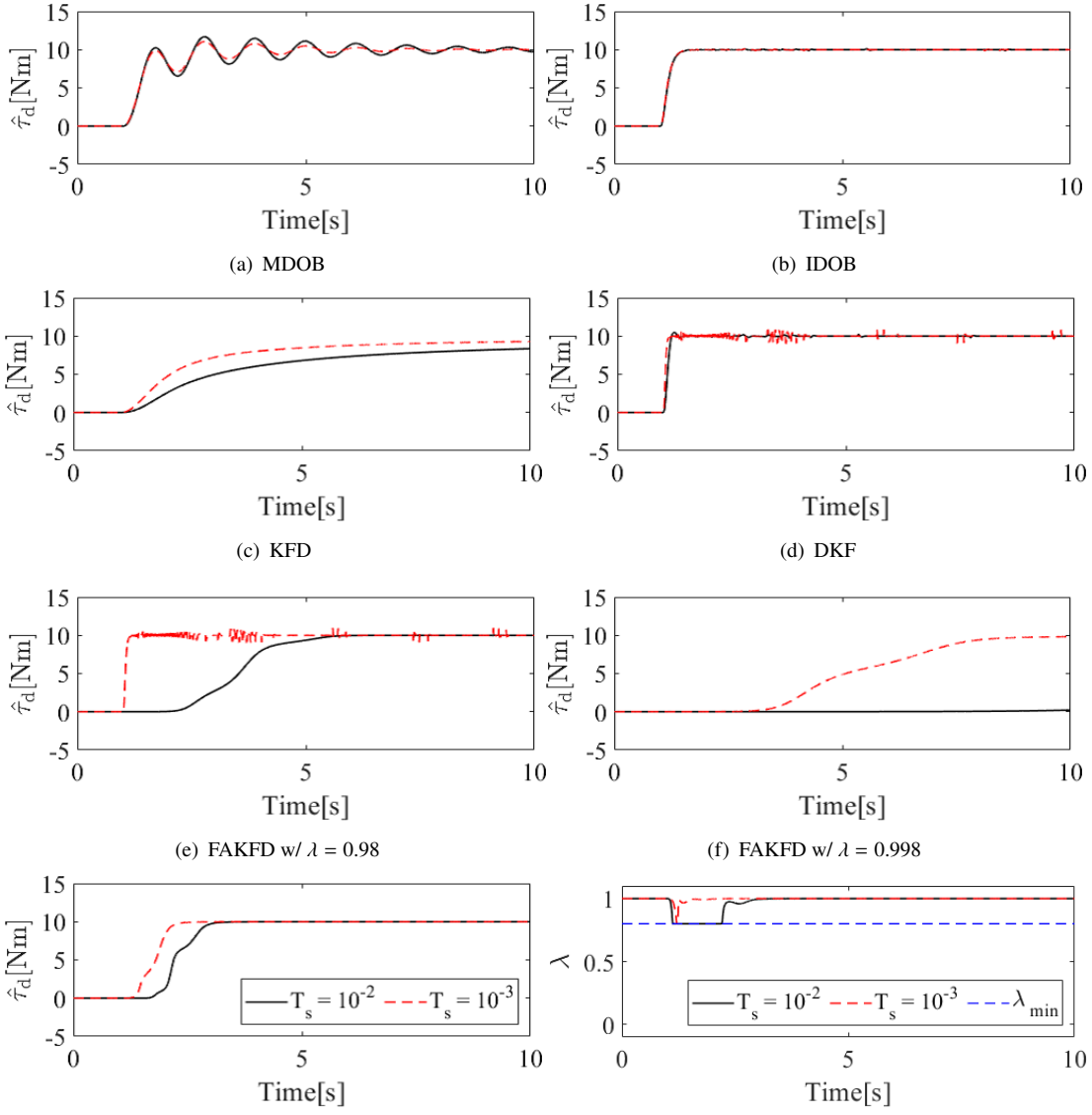

(a) MDOB (b) IDOB

(c) KFD (d) DKF

(e) FAKFD w/ $\lambda = 0.98$ (f) FAKFD w/ $\lambda = 0.998$

(g) VFAKFD (prop.) (h) λ in VFAKFD(g)

FIGURE 4.34: Simulation results: $n = 12$, 65536 PPR.

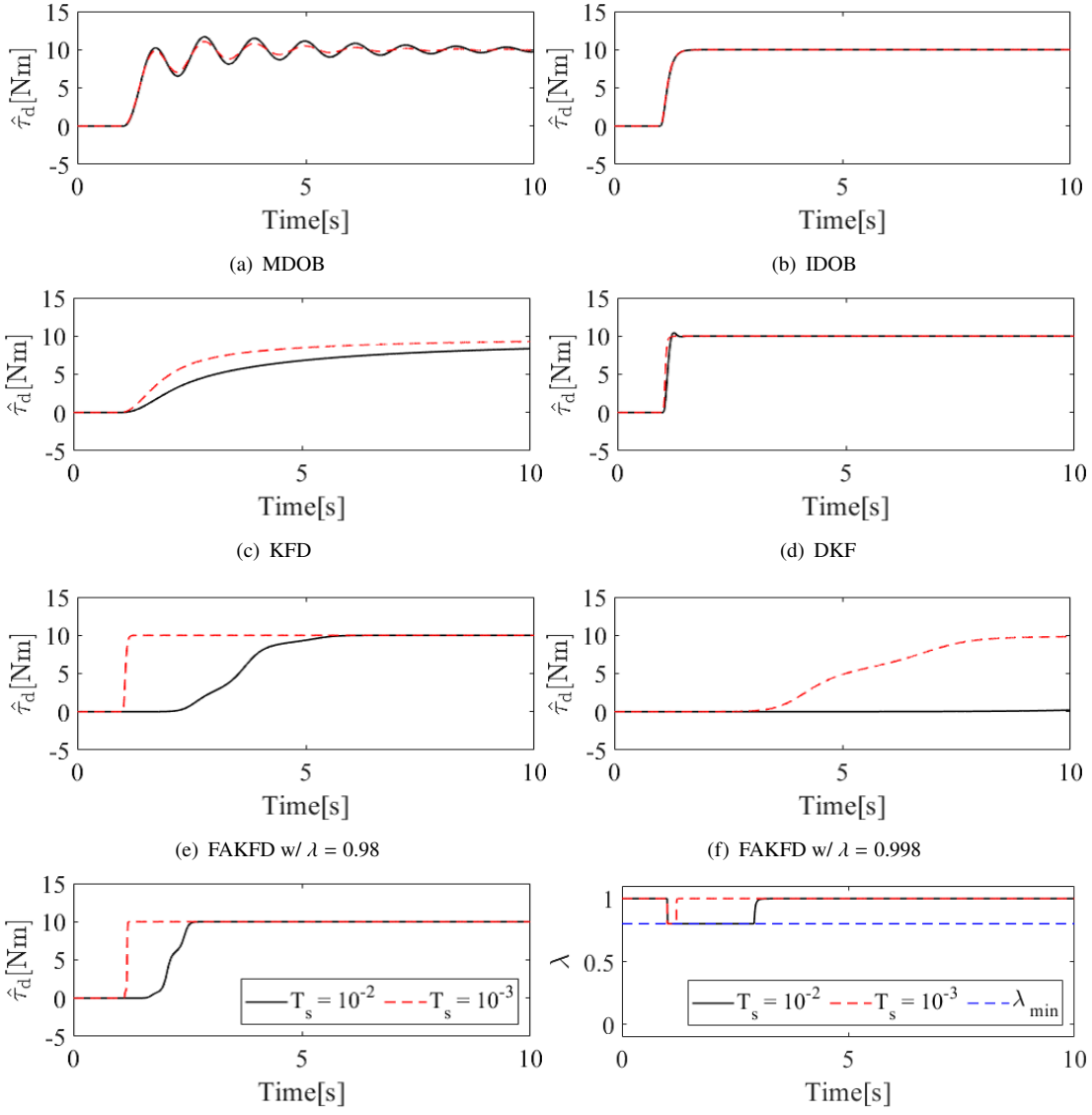

(a) MDOB (b) IDOB

(c) KFD (d) DKF

(e) FAKFD w/ $\lambda = 0.98$ (f) FAKFD w/ $\lambda = 0.998$

(g) VFAKFD (prop.) (h) λ in VFAKFD(g)

FIGURE 4.35: Simulation results: $n = 48$, 2.8147×10^{14} PPR.

TABLE 4.9: Simulation results 2.4.4: RMSE in unmeasured variable $\dot{q}$.

Noise	MDOB	IDOB	KFD	DKF	FAKFD ($\lambda = 0.98$)	FAKFD ($\lambda = 0.998$)	VFAKFD
white (variance 10^{-1})	141.93	0.33	0.14	1.36	1.54	0.01	0.58×10^{-3}
white (variance 10^{-4})	14.19	0.03	0.14	0.14	0.15	1.20×10^{-3}	0.81×10^{-3}

4.3.3 Numerical Verification: observation noise reductions

The proposed system has the ability to cope with white observation noise. This verification shows the simultaneous estimation under white noise environments. Moreover, the verification used the $n = 48$, $T_s = 10^{-3}$, and white noise as observation noise with variance 10^{-1} and 10^{-4}. The observation values are significantly influenced by the observation noises in comparison to quantization noise.

In order to cancel the influences of the noises, the α is designed as

$$\alpha = (0.1^2)^{-1} \tag{4.27}$$

Other conditions are the same as the previous verifications ($Q_v = 2.23 \times 10^{-11}$).

4.3.3.1 Results

Figs. 4.36-4.37 shows the results of disturbance estimates under both white noise environments. The results are indicated that the VFAKFD brings the highest estimation performance of the disturbance, and it can consider the balance between the response speed and noise reduction. Thus, the VFAKFD can provide similar performance for the disturbance estimates under the various noisy environments. The ability is effective for robust design in motion control systems used in tough environments.

Additionally, the VFAKFD makes a better noise reduction performance and estimates compared to the FAKFD; therefore, it is indicated that the online adjustment method and the VFF are useful for reducing the observation noise effects.

The RMSE results on $\dot{q}$ in 15-30s are shown in Table 4.9. From Table 4.9, it is evident that the VFAKFD brings the noise-free estimation compared to the conventional methods.

In conclusion, it is confirmed that the VFAKFD is useful and effective for handling simultaneous estimation, quantization noise reduction, and sensor noise reduction.

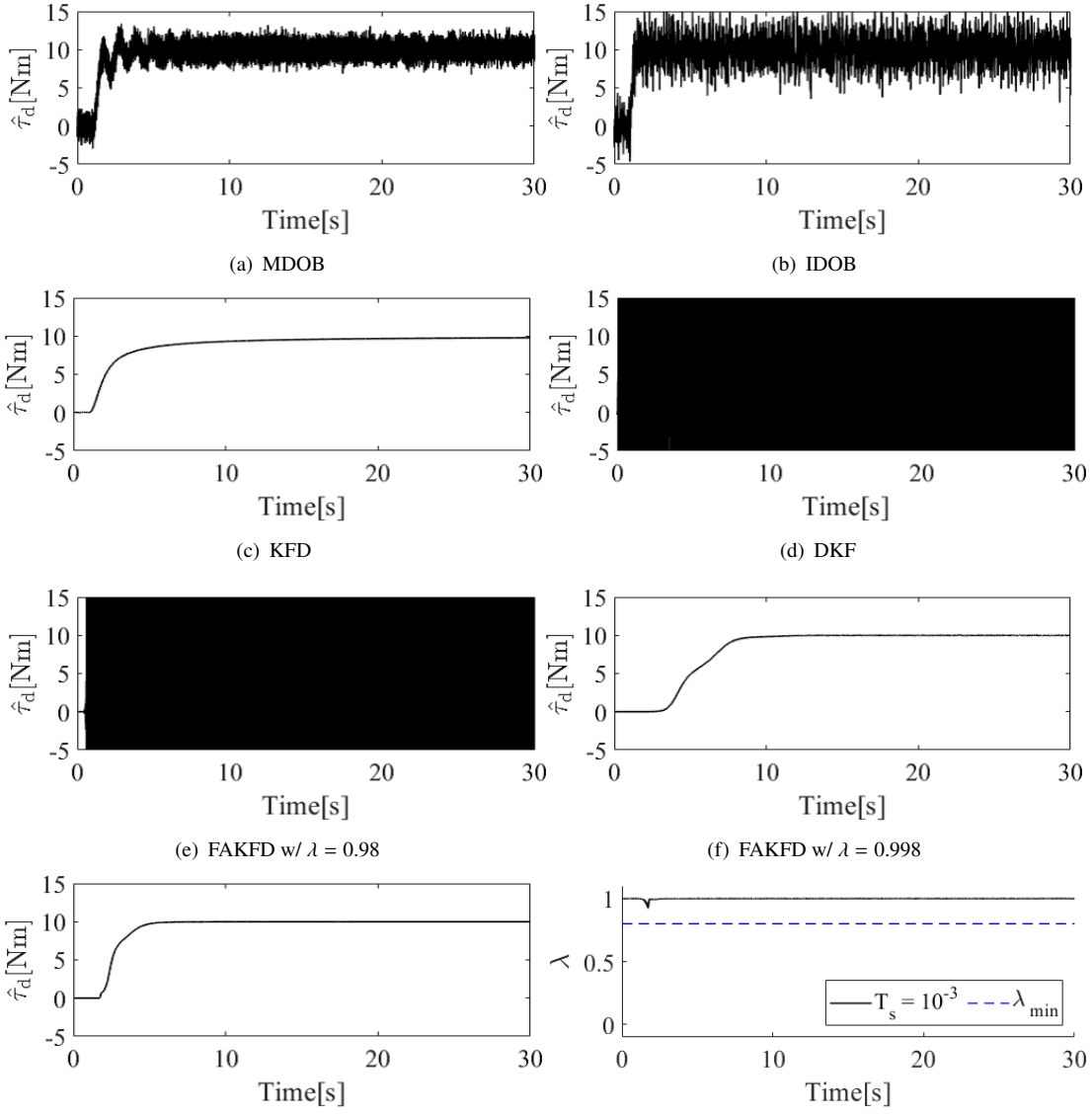

(a) MDOB (b) IDOB

(c) KFD (d) DKF

(e) FAKFD w/ $\lambda = 0.98$ (f) FAKFD w/ $\lambda = 0.998$

(g) VFAKFD (prop.) (h) λ in VFAKF(g)

FIGURE 4.36: Simulation results: $n = 48$, $T_s = 10^{-3}$[s], white noise (variance 10^{-1}).

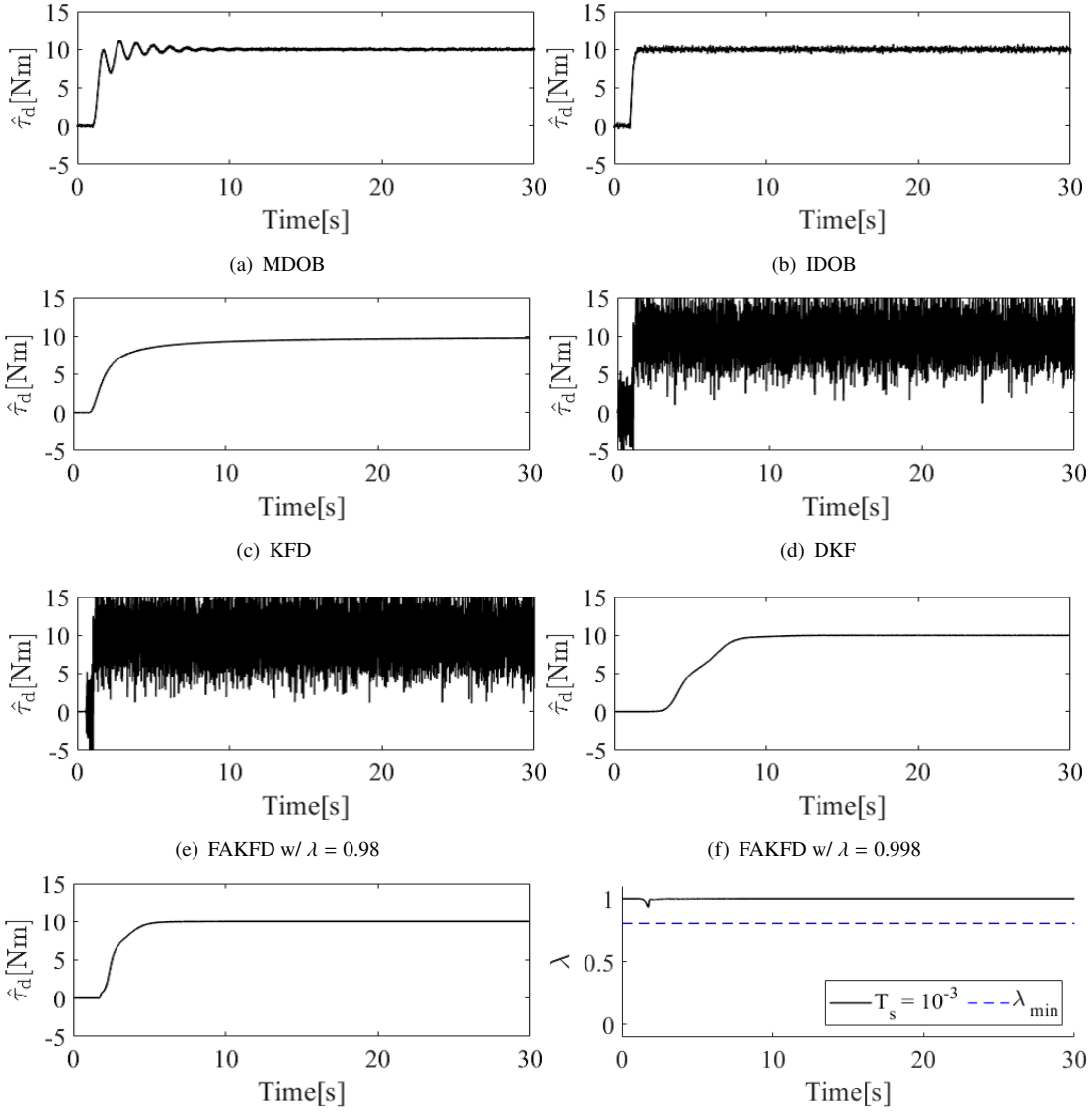

(a) MDOB (b) IDOB

(c) KFD (d) DKF

(e) FAKFD w/ $\lambda = 0.98$ (f) FAKFD w/ $\lambda = 0.998$

(g) VFAKFD (prop.) (h) λ in VFAKF(g)

FIGURE 4.37: Simulation results: $n = 48$, $T_s = 10^{-3}$[s], white noise (variance 10^{-4}).

4.3.4 Discussion

In this section, the validity of the design of the VFF is discussed.

To show the effectiveness of the VFF, the validated results on the forgetting factor and observer gain are illustrated. In this verification, the simulation conditions are the same as the previous section (observation noise reduction). The forgetting factors are designed within the VFF range (0.8-1) and set to [1, 0.998, 0.98, 0.95, 0.90, 0.80].

Figs. 4.38 and 4.38 show the compare results. From the results, it is confirmed that the proposed VFF method makes balanced performance in the estimation. Moreover, the low forgetting factor (0.8–0.9) generates noisy estimates. By contrast, the high forgetting factor (0.98–1) creates noise-free estimates; however, the estimates have a large response delay. In light of this information, the VFF can simultaneously make noise-free and fast estimations. Therefore, it is evident that the design method of the VFF is valid.

Additionally, in these simulations, the observer pole information in continuous and discrete-time systems is as shown in Figs. 4.40-4.43. The results compare with the constant forgetting factor 0.98. The approximate pole assignments of each observer were calculated by extended systems and Kalman gain (i.e., the eigenvalues of the system "$\bar{\boldsymbol{A}}_d - \boldsymbol{K}(k)\bar{\boldsymbol{C}}_d$"). Additionally, the digital pole (p_d) and continuous pole (p_c) are converted by $p_d = e^{T_s \cdot p_c}$.

The results show that the constant forgetting factors make to keep low eigenvalues of the observer. Therefore, the constant forgetting factors make noisy estimates by a high gain observer. By contrast, the VFF method can avoid keeping low eigenvalues of the observer in the steady state. In other words, the VFF makes noise-free estimates and fast estimation by variation of the pole placement of the observer.

4.3.5 Summary

In this section, a novel design method of DOB is shown. Under the various noisy environments, the proposed method can provide the observation noise reduction and accurate systems state and disturbance estimations.

The proposed estimation system significantly reduces the influence of observation noise in the state variable estimates. Moreover, the verification results indicate that the proposed estimation system has higher performance than conventional DOBs in some cases. Therefore, the proposed method is effective and useful for disturbance cancellation in motion control systems in noisy environments.

Furthermore, the proposed method using KF is easy to directly extend to a nonlinear system via nonlinear Kalman filters.

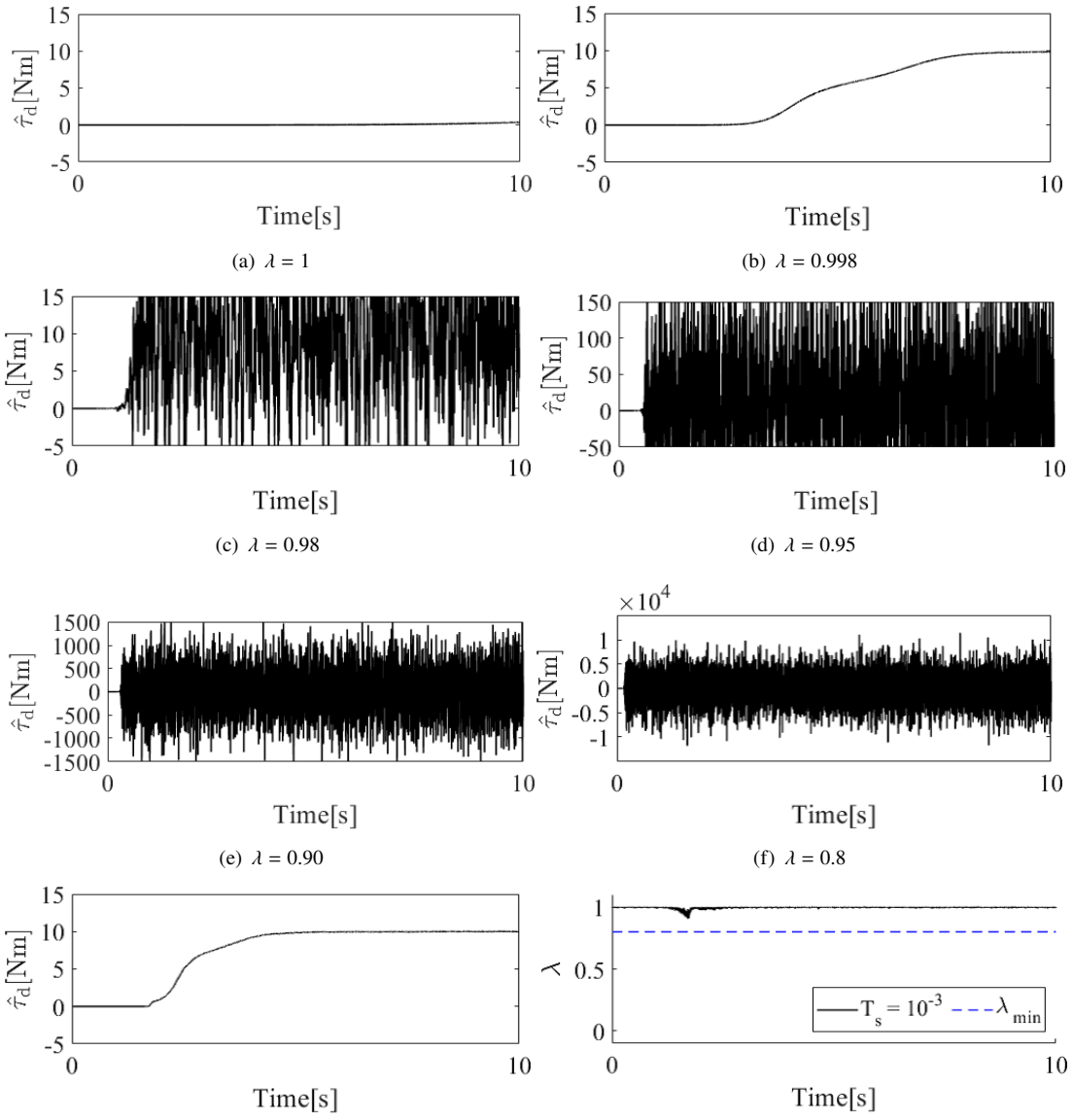

(a) $\lambda = 1$ (b) $\lambda = 0.998$

(c) $\lambda = 0.98$ (d) $\lambda = 0.95$

(e) $\lambda = 0.90$ (f) $\lambda = 0.8$

(g) VFF (h) λ in (g)

FIGURE 4.38: Verification results: forgetting factor, white noise (variance 10^{-1})

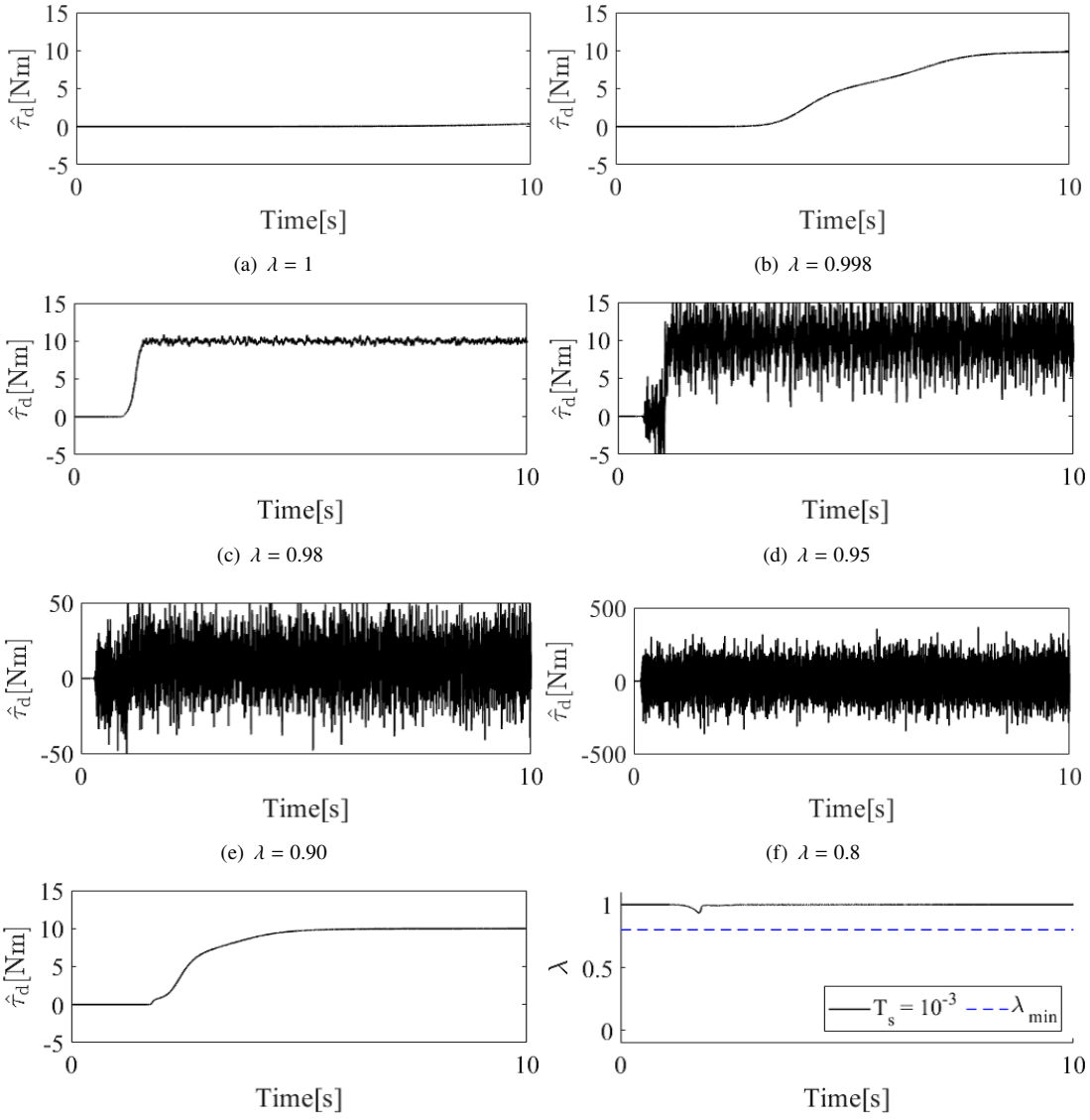

(a) $\lambda = 1$ (b) $\lambda = 0.998$

(c) $\lambda = 0.98$ (d) $\lambda = 0.95$

(e) $\lambda = 0.90$ (f) $\lambda = 0.8$

(g) VFF (h) λ in (g)

FIGURE 4.39: Verification results: forgetting factor, white noise (variance 10^{-4})

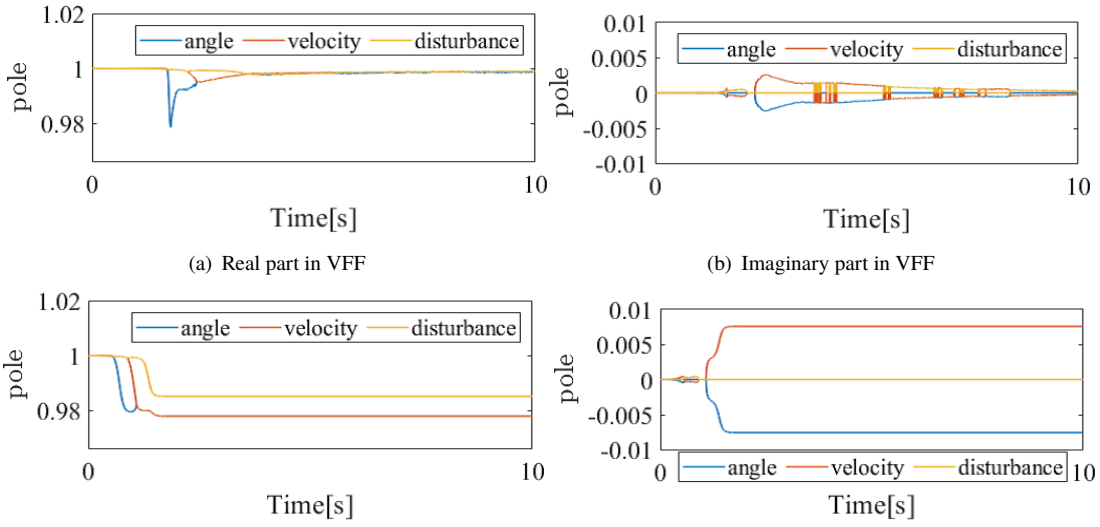

(a) Real part in VFF

(b) Imaginary part in VFF

(c) Real part in $\lambda = 0.98$

(d) Imaginary part in $\lambda = 0.98$

FIGURE 4.40: Discrete-time pole assignment of the observers, white noise (variance 10^{-1})

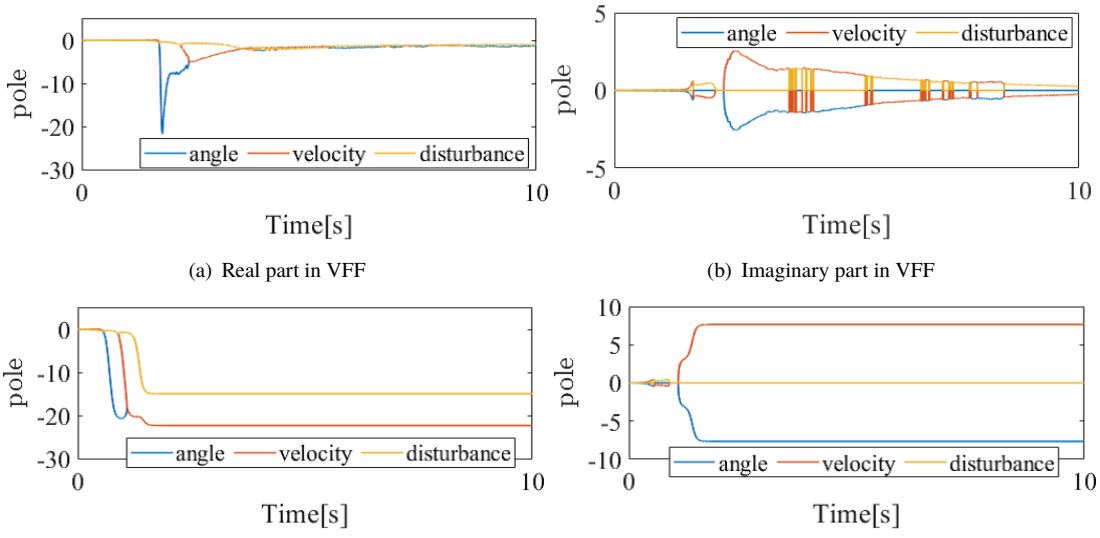

(a) Real part in VFF

(b) Imaginary part in VFF

(c) Real part in $\lambda = 0.98$

(d) Imaginary part in $\lambda = 0.98$

FIGURE 4.41: Continuous-time pole assignment of the observers, white noise (variance 10^{-1})

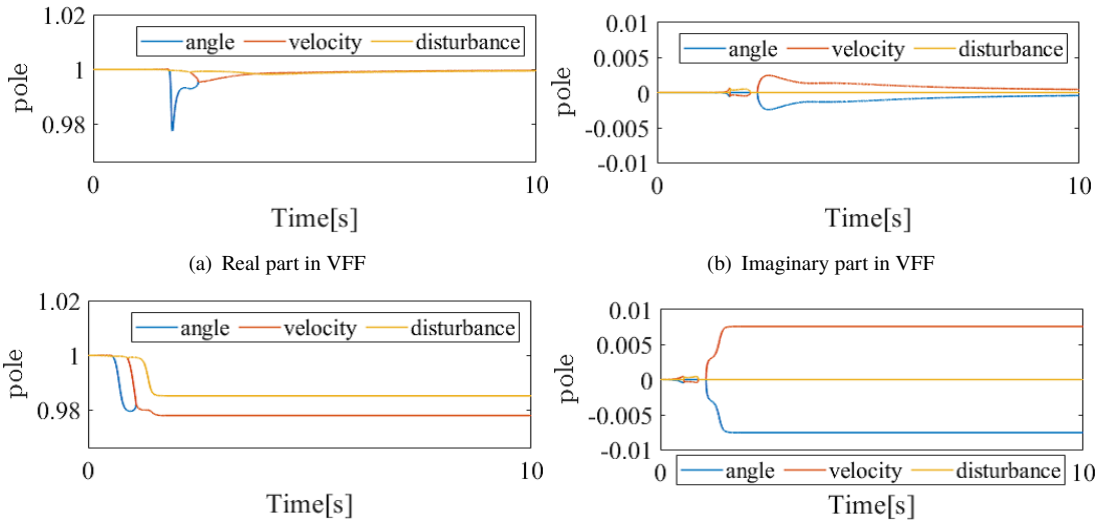

(a) Real part in VFF

(b) Imaginary part in VFF

(c) Real part in $\lambda = 0.98$

(d) Imaginary part in $\lambda = 0.98$

FIGURE 4.42: Discrete-time pole assignment of the observers, white noise (variance 10^{-4})

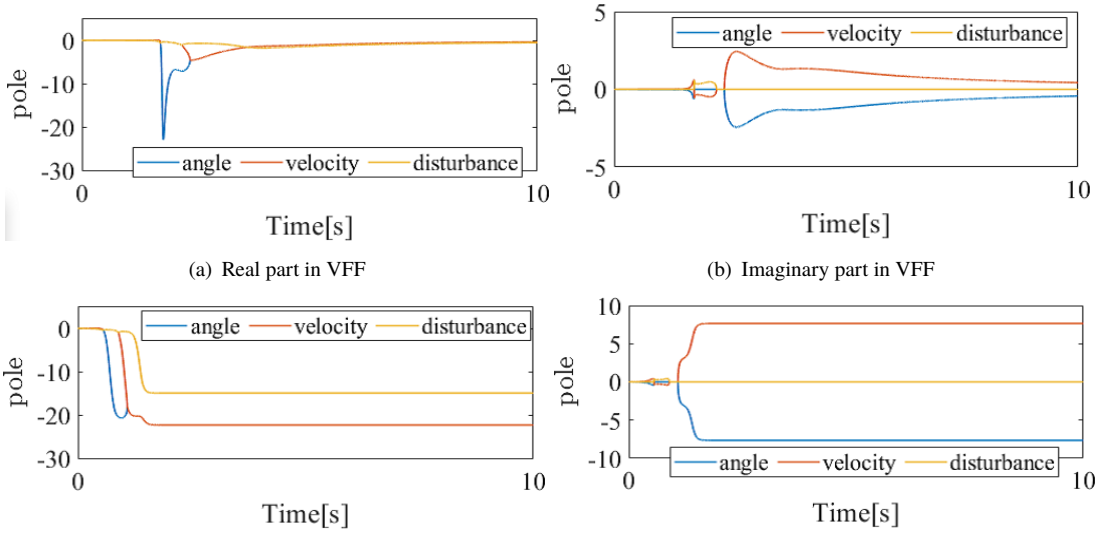

(a) Real part in VFF

(b) Imaginary part in VFF

(c) Real part in $\lambda = 0.98$

(d) Imaginary part in $\lambda = 0.98$

FIGURE 4.43: Continuous-time pole assignment of the observers, white noise (variance 10^{-4})

4.4 Chapter summary

In this chapter, the improved KFD methods were explained.

The proposed method can achieve a noise-free simultaneous estimation of state and disturbance. By using the proposed method, DOB can widely apply to many systems without any limitation.

In this chapter, the design of the VFF was introduced. The VFF is constrained by the lower and upper bounds limit. However, the variation range of the VFF is not considered. Therefore, the suppression of sudden change on the VFF is challenging. In order to generate stable and smooth responses of the VFF, an introduction of the variation range constraints on VFF has to be considered.

In addition to this, the design method of the VFF is not compensated in theory. Therefore, an improved design method considering stability and convergence is a must. In particular, the variation of VFF can resemble the variation of the pole of the observer. Therefore, to improve the estimation performance of the VFAKFD, reflecting the pole of the observer to the VFF has to be considered.

Chapter 5

Conclusion

In this dissertation: Robust Model-based Control in Motion Control Systems, the components for robust design on the constrained control systems and disturbance observer were presented. Under the title, robust design methods of constrained model-based control method and noise-free disturbance estimation method have been proposed. The main component of this dissertation is robust design methods for MPC systems using disturbance estimation techniques.

This dissertation consists of five chapters. In chapter 1, motivation, background, and objective for this research were described.

In chapter 2, the disturbance observer-based motion control, and its application to robust constrained motion control by model predictive control were presented. The two integration methods for disturbance observer and model predictive control in motion control and acceleration control are also presented. The integration systems show to improve the robustness to the disturbance in MPC systems using the disturbance estimates. Fortunately, the robustness simultaneously brings the offset-free tracking control performance. However, the robustness performance depends on the accuracy of the disturbance estimates. Moreover, the accuracy of the disturbance estimates is decided by the magnitude of the gains of the disturbance observers. Unfortunately, the fast and accurate disturbance observer is considerably affected by the observation noise effect. Therefore, the problems of the constrained motion control and disturbance observer-based control are clearly shown, that the main drawback is the increase of noise influences.

In chapter 3, in order to address the noise problem of constrained motion control, the Kalman filter-based disturbance observation and constrained motion control considering the noise influences were presented. The verification results indicate the drawback of the Kalman filter-based disturbance observer which is sluggish and insufficient performances in disturbance estimation. However, the effective ability of the Kalman filter-based disturbance observer was confirmed;

therefore, the verification results illustrate that the solution of the drawback is a must. Additionally, the ability of the Kalman filter with disturbance estimation to easily extend to the nonlinear systems using nonlinear Kalman filter techniques was also presented. In this chapter, as the application example, an underwater quadrotor control using nonlinear Kalman filters with disturbance estimation was shown, and the validated results indicated the usefulness and effectiveness of the Kalman filter with disturbance observer in nonlinear systems. An integration nonlinear control system with nonlinear model predictive control and nonlinear Kalman filter with disturbance estimation is expected as future works because it has the potential to realize robust constrained motion control in nonlinear systems.

In chapter 4, an improved disturbance estimation method including state estimation, which simultaneously solves the problem of the disturbance observer and Kalman filter with disturbance estimation, was presented. In order to improve the estimation and noise reduction performances, a variable forgetting factor was introduced to the Kalman filter with disturbance estimation. The proposed method can accurately and quickly estimate measured variables, unmeasured variables, and unmeasured disturbances. Moreover, the variable forgetting factor brings improved performance on estimation speed and noise reduction to all estimates. Additionally, from the verification results, it is evident that the proposed method can explicitly handle the observation noise reduction including white and quantization noises, unlike existing disturbance estimation methods. In particular, the proposed method can better treat low-resolution sensors; therefore, there are benefits for cost reduction by using the proposed method. In light of this information, it is concluded that this method is succeeded in expanding the application targets of the disturbance observers. As future works in this chapter, theoretical design and guarantee of stability and convergence are required. Additionally, to extend to usefulness, application to nonlinear Kalman filter systems is also required.

Experimental and numerical verifications for the proposed methods provide their effectiveness and validity. In the main contributions for this thesis, it is concluded that the developments for novel constrained control method considering disturbance and noise and novel noise-free simultaneous estimation method of state and disturbance.

Through this dissertation, a general problem in model predictive control, which relates to the online computation load, is not addressed. In theory, the robust performance by disturbance observers requires a shorter sampling time than model predictive control systems. Therefore, to improve the robust design methods proposed in this dissertation, the integration or application to fast model predictive control design methods have to consider as future works.

Bibliography

[1] A. Shimada, “EE text Motion Control,” Ohmsha, Ltd., 2004 (in Japanese).

[2] A. Shimada, “Disturbance Observer,” CORONA PUBLISHING CO., LTD., 2021 (in Japanese).

[3] K. J. Astrom, and L. Rundqwist, “Integrator windup and how to avoid it,” *Proc. 1989 American Control Conference*, pp. 1693-1698, 1989.

[4] G. A. Kiener, D. Lehmann, and K. H. Johansson, “Actuator saturation and anti-windup compensation in event-triggered control,” *Discrete Event Dyn. Syst.*, vol. 24, pp. 173-197, 2014.

[5] F. Blanchini, “Set invariance in control”, Automatica, vol. 35, no. 11, pp. 1747–1889, 1995.

[6] K. Hirata and K. Kogiso, “An Off-line Reference Management Technique for Constraint Fulfillment”, Transactions of the Institute of Systems, Control and Information Engineers, vol. 14, no. 11, pp. 554-559, 2001 (in Japanese).

[7] K. Hirata and Y. Ohta, “An Approximation of the State Reachable Set with Guaranteed Accuracy for Discrete–time Systems”, Transactions of the Institute of Systems, Control and Information Engineers, vol. 39, no. 6, pp. 585-589, 2003 (in Japanese).

[8] K. Ohishi, M. Nakao, K. Ohnishi and K. Miyachi, “Microprocessor-controlled DC motor for load-insensitive position servo system,” *IEEE Trans. Ind. Ele.*, vol. IE-34, no.1, pp. 44-49, Feb. 1987.

[9] E. Sariyildiz, H. Sekiguchi, T. Nozaki, B. Ugurlu, and K. Ohnishi, “A stability analysis for the acceleration-based robust position control of robot manipulators via disturbance observer,” *IEEE/ASME Trans. Mech.*, vol. 23, no.5, pp. 2369-2378, 2018.

[10] E. Sariyildiz, R. Oboe, and K. Ohnishi, “Disturbance observer-based robust control and its applications: 35th anniversary overview,” *IEEE Trans. Ind. Ele.*, vol. 67, no.3, pp. 2042-2053, 2020.

[11] W. Chen, J. Yang, L. Guo, and S. Li, "Disturbance-observer-based control and related methods—an overview," *IEEE Trans. Ind. Ele.*, vol. 63, no.2, pp. 1083-1095, 2015.

[12] S. Katsura, Y. Matsumoto, and K. Ohnishi, "Modeling of Force Sensing and Validation of Disturbance Observer for Force Control," IEEE Transactions on Industrial Electronics, vol.54, no.1, pp530–538, 2007.

[13] S. Komada, M. Ishida, K. Ohnishi, and T. Hori, "Disturbance observer-based motion control of direct drive motors," IEEE Transactions on Energy Conversion, vol.6, no.3, pp.553–559, 1991.

[14] H. An, J. Liu, C. Wang, and L. Wu, "Disturbance observer-based antiwindup control for air-breathing hypersonic vehicles," IEEE Transactions on Industrial Electronics, vol.63, no.5, pp.3038–3049, 2016.

[15] J. Smith, J. Su, C. Liu, and W. Chen, "Disturbance observer based control with anti-windup applied to a small fixed wing UAV for disturbance rejection," Journal of Intelligent & Robotic Systems, pp.1–18, 2017.

[16] S. Adachi, and I. Maruta, "Fundamentals of Kalman Filter," Tokyo Denki University Press, 2012 (in Japanese).

[17] J. Maciejowski, "Predictive Control with Constraints", Prentice Hall, 2002.

[18] R. E. Kalman, "A new approach to linear filtering and prediction problems," Transactions of ASME, Journal of Basic Engineering, vol.82, pp.35-45, 1960.

[19] S. Adachi, "Introduction to Model Predictive Control," JRSJ, vol.32, no.6, pp.499-502, 2014 (in Japanese).

[20] D. Q. Mayne, J. B. Rawlings, C. V. Rao, and P. O. M. Scokaert, "Constrained model predictive control: Stability and optimality," Automatica, vol. 36, no. 6, pp.789-814, 2000.

[21] T. Ohtsuka, "Introduction to Nonlinear Optimal Control," CORONA PUBLISHING CO.,LTD., 2011 (in Japanese).

[22] T. Ohtsuka, "Practical Applications of Control by Real-time Optimization," CORONA PUBLISHING CO.,LTD., 2015 (in Japanese).

[23] W. Liuping, "Model Predictive Control System Design and Implementation Using MATLAB®," Springer, 2009.

[24] N. Hirose, R. Tajima, K. Sukigara, N. Koyama, M. Tanaka, and S. Ito, "Posture Stabilization Control of Personal Robot based on Model Predictive Control," IEEJ Trans. on Industry Applications, vol.135, no.3, pp.172-181, 2015 (in Japanese).

[25] M. Ohshima, and M. Ogawa, 'Model Predictive Control-I," Systems, Control and Infromation, vol.46, no.5, pp.286-293, 2002 (in Japanese).

[26] G. Chowdhary, M. M*ü*hlegg, J. P. How, and F. Holzapfel, "Concurrent Learning Adaptive Model Predictive. Control," 52nd, IEEE Conference on Decision and Control, 2013.

[27] K. Suzuki, and K. Taji, "Fast Model Predictive Control with Simple Bounds Using Semismooth Newton Method," Trans. on SICE, vol. 50, no. 4 pp. 348-355, 2014 (in Japanese).

[28] B. Lindqvist, S. S. Mansouri, A. Agha-mohammadi, and G. Nikolakopoulos, "Nonlinear MPC for Collision Avoidance and Control of UAVs With Dynamic Obstacles," in IEEE Robotics and Automation Letters, vol. 5, no. 4, pp. 6001-6008, 2020.

[29] Y. Tadokoro, Y. Taya, T. Ibuki and M. Sampei, "Real-Time Model Predictive Control of Rigid Body Motion via Discretization Using the Cayley Map," in IEEE Access, vol. 8, pp. 17149-17159, 2020.

[30] J. -F. Mennemann, L. Marko, J. Schmidt, W. Kemmetmüller and A. Kugi, "Nonlinear Model Predictive Control of a Variable-Speed Pumped-Storage Power Plant," in IEEE Transactions on Control Systems Technology, vol. 29, no. 2, pp. 645-660, 2021.

[31] H. Fukushima, "Robust Model Predictive Control for Constrained Systems," Systems, control and information, vol.48, no.8, pp.321-326, 2004 (in Japanese).

[32] S. Yu, Y. Guo, Y. Zhou and H. Chen, "Robust model predictive control of linear systems with constraints," 2017 11th Asian Control Conference (ASCC), pp. 928-933, 2017.

[33] H. Yang, F. Deng, Y. He, D. Jiao, and Z. Han, "Robust nonlinear model predictive control for reference tracking of dynamic positioning ships based on nonlinear disturbance observer," Ocean Engineering, vol.215, no.1, 2020.

[34] J. A. Paulson and A. Mesbah, "Approximate Closed-Loop Robust Model Predictive Control With Guaranteed Stability and Constraint Satisfaction," in IEEE Control Systems Letters, vol. 4, no. 3, pp. 719-724, 2020.

[35] X. Xing, J. Lin, N. Brandon, A. Banerjee and Y. Song, "Time-Varying Model Predictive Control of a Reversible-SOC Energy-Storage Plant Based on the Linear Parameter-Varying Method," in IEEE Transactions on Sustainable Energy, vol. 11, no. 3, pp. 1589-1600, 2020.

[36] M. T. Watson, D. T. Gladwin, T. J. Prescott and S. O. Conran, "Dual-Mode Model Predictive Control of an Omnidirectional Wheeled Inverted Pendulum," in IEEE/ASME Transactions on Mechatronics, vol. 24, no. 6, pp. 2964-2975, 2019.

[37] U. Maeder, and M. Morari, "Offset-free reference tracking with model predictive control," Automatica, vol.46, no9, pp.1469-1476, 2010.

[38] U. Maeder, F. Borrelli, M. Morari, "Linear offset-free Model Predictive Control," Automatica, vol.45, no.10, pp.2214–2222, 2009.

[39] G. Pannocchia, J. B. Rawlings, "Disturbance models for offset-free model-predictive control," AIChE Journal, vol.49, no.2, pp.426–437, 2003.

[40] G. Pannocchia and A. Bemporad, "Combined Design of Disturbance Model and Observer for Offset-Free Model Predictive Control," in IEEE Transactions on Automatic Control, vol. 52, no. 6, pp. 1048-1053, 2007.

[41] T. Satoh, R. Abe, N. Saito, J. Nagase, and N. Saga, "Control of a two-link manipulator using disturbance observer-based model predictive control," Trans. on JSME, vol.81, no.827, 2015 (in Japanese).

[42] J. Yang, S. Li,, X. Chen, Q. Li, "Disturbance rejection of ball mill grinding circuits using DOB and MPC," Powder Technology, vol.198, no.2, pp.219–228, 2010.

[43] J. Yang, W., X, Zheng, S. Li, B. Wu, and M. Cheng, "Design of a prediction-accuracy-enhanced continuous-time MPC for disturbed systems via a disturbance observer," IEEE Transactions on Industrial Electronics, vol.62, no.9, pp.5807–5816, 2015.

[44] K. R. Muskea, T. A. Badgwell, "Disturbance modeling for offset-free linear model predictive control," Journal of Process Control, vol.12, no.5, pp.617–632, 2002.

[45] C. Jia, X. Wang, Y. Liang and K. Zhou, "Robust Current Controller for IPMSM Drives Based on Explicit Model Predictive Control With Online Disturbance Observer," in IEEE Access, vol. 7, pp. 45898-45910, 2019.

[46] Y. Tange, and C. Nakazawa, "Optimal Tuning for Disturbance Suppression Mechanism for Model Predictive Control," Transactions of the Institute of Systems, Control and Information Engineers, vol.47, no.9, pp.380-387, 2011 (in Japanese).

[47] Y. Tange, T. Matsui, K. Matsumoto, and H. Nishida, "A Disturbance Rejection for Model Predictive Control Using a Multivariable Disturbance Observer," Transactions of the Institute of Systems, Control and Information Engineers, vol.46, no.8, pp.448-455, 2010 (in Japanese).

[48] Y. Ma and Y. Cai, "A Fuzzy Model Predictive Control Based Upon Adaptive Neural Network Disturbance Observer for a Constrained Hypersonic Vehicle," in IEEE Access, vol. 6, pp. 5927-5938, 2018.

[49] J. Zhu and S. K. Nguang, "Fuzzy Model Predictive Control With Enhanced Robustness for Nonlinear System via a Discrete Disturbance Observer," in IEEE Access, vol. 8, pp. 220631-220645, 2020.

[50] A. Liu, W. -A. Zhang, L. Yu, H. Yan and R. Zhang, "Formation Control of Multiple Mobile Robots Incorporating an Extended State Observer and Distributed Model Predictive Approach," in IEEE Transactions on Systems, Man, and Cybernetics: Systems, vol. 50, no. 11, pp. 4587-4597, 2020.

[51] O. Wallscheid and E. F. B. Ngoumtsa, "Investigation of Disturbance Observers for Model Predictive Current Control in Electric Drives," in IEEE Transactions on Power Electronics, vol. 35, no. 12, pp. 13563-13572, 2020.

[52] L. Yan, F. Wang, M. Dou, Z. Zhang, R. Kennel and J. Rodríguez, "Active Disturbance-Rejection-Based Speed Control in Model Predictive Control for Induction Machines," in IEEE Transactions on Industrial Electronics, vol. 67, no. 4, pp. 2574-2584, 2020.

[53] F. Wang and L. He, "FPGA-Based Predictive Speed Control for PMSM System Using Integral Sliding-Mode Disturbance Observer," in IEEE Transactions on Industrial Electronics, vol. 68, no. 2, pp. 972-981, 2021.

[54] X. Zhang, B. Hou and Y. Mei, "Deadbeat Predictive Current Control of Permanent-Magnet Synchronous Motors with Stator Current and Disturbance Observer," in IEEE Transactions on Power Electronics, vol. 32, no. 5, pp. 3818-3834, 2017.

[55] J. Yang, W. X. Zheng, S. Li, B. Wu and M. Cheng, "Design of a Prediction-Accuracy-Enhanced Continuous-Time MPC for Disturbed Systems via a Disturbance Observer," in IEEE Transactions on Industrial Electronics, vol. 62, no. 9, pp. 5807-5816, 2015.

[56] H. T. Nguyen and J. Jung, "Disturbance-Rejection-Based Model Predictive Control: Flexible-Mode Design With a Modulator for Three-Phase Inverters," in IEEE Transactions on Industrial Electronics, vol. 65, no. 4, pp. 2893-2903, 2018.

[57] R. P. Aguilera, P. Lezana and D. E. Quevedo, "Switched Model Predictive Control for Improved Transient and Steady-State Performance," in IEEE Transactions on Industrial Informatics, vol. 11, no. 4, pp. 968-977, 2015.

[58] Y. Wang and S. Boyd, "Fast Model Predictive Control Using Online Optimization," in IEEE Transactions on Control Systems Technology, vol. 18, no. 2, pp. 267-278, 2010.

[59] H. Fujimoto, Y. Hori, A. Kawamura, "Perfect Tracking Control Method Based on Multirate Feedforward Control," Trans. on SICE, vol.36, no.9, pp.766-772, 2000 (in Japanese).

[60] D. L. Kleinman, "An Easy Way to Stabilieze a Linear Constant System," IEEE Trans. on Automatic Control, vol. 15, pp. 692, 1970.

[61] Y. A. Thomas, "Linear Quadratic Optimal Estimation and Control with Receding Horizon Control," Electronic Letters, vol. 11, pp. 19-21, 1975

[62] T. Ohhira, and A. Shimada, "Offset-free tracking movement control based on model predictive control with disturbance suppression using disturbance observer", Trans. on JSME, vol.83, no.856, 2017 (in Japanese).

[63] H. Fujimoto, "Application of Multirate Sampling Control to Robot Manipulator," JRSJ, vol.27, no.4, pp.410-413, 2009 (in Japanese).

[64] H. Fujimoto, "Motion Control Based on Multirate Sampling Control," Journal of the IEICE, vol.86, no.4, pp.270-276, 2003 (in Japanese).

[65] B. J. Rawlings, and D. Q. Mayne, "Model Predictive Control: Theory and Design," Nob Hill Publishing, 2010.

[66] MathWorks, "Provide LQR Performance Using Terminal Penalty Weights," `https://jp.mathworks.com/help/mpc/ug/using-terminal-penalty-to-provide-lqr-performance.html` (2021-6-25 accessed)

[67] T. Ohhira, K. Yokota, S. Tatsumi, and T. Murakami, "A Robust Hybrid Position/Force Control Considering Motor Torque Saturation," in IEEE Access, Vol. 9, pp.34515-34528, 2021.

[68] M. H. Raibert, and J. J. Craig, "Hybrid position/force control of manipulators," *J. Dyna. Syst., Meas., and Cont.*, vol.103, no.2, pp. 123-133, 1981.

[69] T. Yoshikawa, "Dynamic hybrid position/force control of robot manipulators–description of hand constraints and calculation of joint driving force," *IEEE J. Rob. and Aut.*, vol.3, no.5, pp. 386-392, 1987.

[70] S. Sakaino, T. Sato, and K. Ohnishi, "Precise position/force hybrid control with modal mass decoupling and bilateral communication between different structures," *IEEE Trans. Ind. Inf.*, vol. 7, no.2, pp. 266-276, 2011.

[71] Y. Hasegawa, T. Kitamura, S. Sakaino, and T. Tsuji, "Bilateral control of elbow and shoulder joints using functional electrical stimulation between humans and robots," *IEEE Access*, vol. 8, pp. 15792-15799, 2020.

[72] S. Xu, B. He, Y. Zhou, Z. Wang, and C. Zhang, "A hybrid position/force control method for a continuum robot with robotic and environmental compliance," *IEEE Access*, vol. 7, pp. 100467-100479, 2019.

[73] H. Cao, X. Chen, Y. He, and X. Zhao, "Dynamic adaptive hybrid impedance control for dynamic contact force tracking in uncertain environments," *IEEE Access*, vol. 7, pp. 83162-83174, 2019.

[74] Q. Xu, "Design and smooth position/force switching control of a miniature gripper for automated microhandling," *IEEE Trans. Ind. Inf.*, vol. 10, no.2, pp. 1023-1032, 2014.

[75] Z. Li, S. S. Ge, and S. Liu, "Contact-force distribution optimization and control for quadruped robots using both gradient and adaptive neural networks," *IEEE Trans. Neu. Net. Lea. Syst.*, vol. 25, no.8, pp. 1460-1473, 2014.

[76] Q. Yang, C. Xie, R. Tang, H. Liu, and R. Song, "Hybrid active control with human intention detection of an upper-limb cable-driven rehabilitation robot," *IEEE Access*, vol. 7, pp. 83162-83174, 2019.

[77] H. Park, J. Park, D. Lee, J. Park, M. Baeg and J. Bae, "Compliance-based robotic peg-in-hole assembly strategy without force feedback," *IEEE Trans. Ind.l Ele.*, vol. 64, no.8, pp. 6299-6309, 2017.

[78] A. García, V. Girbés-Juan, J. E. Solanes, L. Gracia, C. Perez-Vidal, and J. Tornero, "Human-robot cooperation for surface repair combining automatic and manual modes," *IEEE Access*, vol. 8, pp. 154024-154035, 2020.

[79] N. Hogan, "Impedance control: an approach to manipulation: part I—theory," *J. Dyna. Syst., Meas. Cont.*, vol.107, no.2, pp 1-7, 1985.

[80] R. Kikuuwe, "Torque-bounded admittance control realized by a set-valued algebraic feedback," *IEEE Trans. Rob.*, vol. 35, no.5, pp. 1136-1149, 2019.

[81] Q. Xu, and X, Sun, "Adaptive impedance control of robots with reference trajectory learning," *IEEE Access*, vol. 8, pp. 104967-104976, 2020.

[82] M. Bogdanovic, M. Khadiv, and L. Righetti, "Learning variable impedance control for contact sensitive tasks," *IEEE Roboti. and Auto. Lett.*, vol. 5, no. 4, pp. 6129- 6136, 2020.

[83] R. Ikeura, and H. Inooka, "Variable impedance control of a robot for cooperation with a human," *Proc. 1995 IEEE Inter. Conf. on Roboti.and Auto.*, pp. 3097-3102, 1995.

[84] L. Roveda, N. Castaman, P. Franceschi, S. Ghidoni and N. Pedrocchi, "A control framework definition to overcome position/interaction dynamics uncertainties in force-controlled tasks," *Proc. 2020 IEEE Inter. Conf. on Roboti.and Auto.*, pp. 6819-6825, 2020.

[85] G. Ferretti, G. Magnani, and P. Rocco, "Toward the implementation of hybrid position/force control in industrial robots," *IEEE Trans. Rob. Aut.*, vol. 13, no. 6, pp.38-845,1997.

[86] J. Roy, and L. L. Whitcomb, "Adaptive force control of position/velocity controlled robots: theory and experiment," *IEEE Trans. Rob. Aut.*, vol. 18, no. 2, pp. 121-137, 2002.

[87] G. Duelen, H. Munch, D. Surdilovic, and J. Timm, "Automated force control schemes for robotic deburring: development and experimental evaluation," *Proc. Int. Conf. on Ind. Ele., Con., Inst. Aut.*, pp.912-917. 1992.

[88] M. P. Polverini, D. Nicolis, A. M. Zanchettin, and P. Rocco, "Implicit robot force control based on set invariance," *IEEE Rob. Aut. Lett.*, vol. 2, no. 3, pp. 1288-1295, 2017.

[89] K. Ohishi, N. H. Wa, and S. Ohtaki, "Robust motion control with consideration algorithm of joint torque saturation for redundant manipulator," *Proc. IEEE Int. Conf. Ind. Ele.*, pp. 2255-2260 2002.

[90] T. Sugihara, "Solvability-unconcerned inverse kinematics by the Levenberg-Marquardt method," *IEEE Trans. Rob.*, vol. 27, no.5, pp. 954-991, 2011.

[91] J. Richalet, and D. O ' Donovan, "Predictive functional control principles and industrial applications," *Springer*, 2009.

[92] J. Richalet, S. Abu El Ata-Doss, C. Arber, H. B. Kuntze, A. Jacubasch, and W. Schill, "Predictive functional control - application to fast and accurate robots," *IFAC Proc. Vol.*, vol.20, no. 5 pp. 251-258, 1987.

[93] H. Liu, and S. Li, "Speed control for PMSM servo system using predictive functional control and extended state observer," *IEEE Trans. Ind. Ele.*, vol. 59, no. 2, pp. 1171-1183, 2012.

[94] T. Satoh, K. Kaneko, and Naoki Saito, "Performance improvement of predictive functional control: a disturbance observer approach," *Proc. Annu. Conf. the IEEE Ind. Ele.*, pp.617-622, 2011.

[95] S. Katsura, K. Irie, and K. Ohnishi, "Wideband force control by position-acceleration integrated disturbance observer," *IEEE Trans. Ind. Ele.*, vol. 55, no.4, pp. 1699-1706, 2008.

[96] N. Nakao, K. Ohnishi, and K. Miyachi, "A robust decentralized joint control based on interference estimation," *Proc. IEEE Inter. Conf. Rob. Aut.*, pp. 326-331, 1987.

[97] S. Komada, N. Machii, and T. Hori, "Control of redundant manipulators considering order of disturbance observer," *IEEE Trans. Ind. Ele.*, vol. 47, no.2, pp. 413-420, 2000.

[98] T. Umeno, T. Kaneko, and Y. Hori, "Robust servosystem design with two degrees of freedom and its application to novel motion control of robot manipulators," *IEEE Trans. Ind. Ele.*, vol. 40, no.5 1993.

[99] A. Shimada, and N. Hatakeyama, "Movement control of two-wheeled inverted pendulum robots considering robustness," *Proc. SICE Annu. Conf.*, pp. 3361-3366, 2008.

[100] J. Luh, M. Walker, and R. Paul, "Resolved-acceleration control of mechanical manipulators," *IEEE Trans. Auto. Cont.*, vol. 25, no.3, pp. 468-474, 1980.

[101] X. Liu, F. Zhao, Shuzhi S. Ge, Y. Wu, and X. Mei, "End-effector force estimation for flexible-joint robots with global friction approximation using neural networks," *IEEE Trans. Ind. Inf.*, vol. 15, no. 3, pp. 1730-1741, 2018.

[102] A. C. Smith, F. Mobasser, and Keyvan Hashtrudi-Zaad, "Neural-network-based contact force observers for haptic applications," *IEEE Trans. Rob.*, vol. 22, no. 6, pp. 1163-1175, 2006.

[103] T. Murakami, F. Yu, and K. Ohnishi, "Torque sensorless control in multidegree-of-freedom manipulator," *IEEE Trans. Ind. Ele.*, vol. 40, No. 2, pp. 259-265, 1993.

[104] T. Ohhira, and A. Shimada, "Movement Control Based on Model Predictive Control with Disturbance Suppression using Kalman Filter including Disturbance Estimation," *IEEJ Journal of IA*, vol.7, no.5, pp. 387-395, 2018.

[105] T. Ohhira, A. Kawamura, A. Shimada, and T. Murakami, "An underwater quadrotor control with wave-disturbance compensation by a UKF," The 21th World Congress of the International Federation of Automatic Control (IFAC2020), IFAC PapersOnLine, vol. 53, no.2, pp.9017-9022, 2020.

[106] S. Bouabdallah, P. Murrieri, and R. Siegwart, "Design and control of an indoor micro quadrotor," *Proc. of IEEE International Conference on Robotics and Automation*, pp. 4393–4398, 2004.

[107] J. Goslinski, W. Giernacki, and S. Gardecki, "Unscented Kalman Filter for an orientation module of a quadrotor mathematical model," *Proc. of 9th Asian Control Conference (ASCC)*, 2018.

[108] K. Hasselmann, P. T. Barnett, E. Bouws, et al.,"Measurements of wind-wave growth and swell decay during the Joint North Sea Wave Project (JONSWAP)," *Dtsch Hydrogr. Z. Suppl.*, vol.12, no.A8, pp. 1–95, 1973.

[109] S. Julier, J. Uhlmann, and F. H. Durrant-Whyte, "A new method for the nonlinear transformation of means and covariances in filters and estimators," *IEEE Transactions on Automatic Control*, vol.45, no.3, pp. 477–482, 2000.

[110] T. Madani, and A. Benallegue, "Backstepping control for a quadrotor helicopter," *Proc. of IEEE/RSJ International Conference on Intelligent Robots and Systems*, pp. 3255–3260, 2006.

[111] T. Maki, Y. Sato, T. Matsuda, R. Shiroku, and T. Sakamaki, "AUV Tri-TON 2: An intelligent platform for detailed survey of hydrothermal vent fields," *Proc. of 2014 IEEE/OES Autonomous Underwater Vehicles (AUV)*, pp. 4393–4398, 2014.

[112] L. Paull, S. Saccdi, M. Seo, and H. Li, "AUV Navigation and Localization: A Review," *IEEE J. Ocean. Eng.*, vol.39, no.1, pp.131–149, 2014.

[113] B, R. Wynn, et al., "Autonomous Underwater Vehicles (AUVs): Their past, present and future contributions to the advancement of marine geoscience," *Marine Geology*, no. 352, pp. 451–168, 2014.

[114] S. Wirtensohn, M. Schuster, J. Reuter, "Disturbance Estimation and Wave Filtering Using an Unscented Kalman Filter," *IFAC-PapersOnLine*, vol.49, no.23, pp. 518–523, 2016.

[115] T. Ohhira, and A. Shimada, "Proposal of high performance methods for linear Kalman filter with disturbance estimation and application to motion control systems," Trans. on JSME, vol.84, no.862, 2018 (in Japanese).

[116] E. Sariyildiz, "Acceleration Measurement Enhances the Bandwidth of Disturbance Observer in Motion Control Systems," *Proc. of 2021 IEEE International Conference on Mechatronics (ICM)*, 2021.

[117] Y. Nakajima, T. Nozaki, and K. Ohnishi, "Heartbeat Synchronization With Haptic Feedback for Telesurgical Robot," *IEEE Trans. Ind. Ele.*, vol. 61, no. 7, pp. 3753-3764, 2014.

[118] H. Liu, and S. Li, "Speed Control for PMSM Servo System Using Predictive Functional Control and Extended State Observer," *IEEE Trans. Ind. Electron.*, vol. 59, No.2, pp. 1171-1183, 2012.

[119] T. He, and Z. Wu, "Extended Disturbance Observer With Measurement Noise Reduction for Spacecraft Attitude Stabilization," *IEEE Access*, vol. 7, pp. 66137-66147, 2019.

[120] S. Lu, C. Tian, and P. Yan, "Adaptive Extended State Observer-Based Synergetic Control for a Long-Stroke Compliant Microstage With Stress Stiffening," *IEEE/ASME Trans. Mech.*, vol. 25, no. 1, pp. 259-270, 2020.

[121] G. Ichimasa, H. Okajima, K. Okumura, and N. Matsunaga, "Model Error Compensator with Parallel Feed-Forward Filter," *SICE Journal of Control, Measurement, and System Integration*, vol.10, no.5, pp. 468-475, 2017.

[122] K. Shao, J. Zheng, H. Wang, F. Xu, X. Wang, and B. Liang, "Recursive sliding mode control with adaptive disturbance observer for a linear motor positioner," *Mechanical Systems and Signal Processing*, vol.146, pp. 1-16, 2021.

[123] H. Pan, and W. Sun, "Nonlinear Output Feedback Finite-Time Control for Vehicle Active Suspension Systems," *IEEE Trans. Ind. infromat.*, vol. 15, no. 4, pp. 2073-2083, 2019.

[124] T. Tsuji, T. Hashimoto, H. Kobayashi, M. Mizuochi, and K. Ohnishi, "A Wide-Range Velocity Measurement Method for Motion Control," *IEEE Trans. Ind. Electron.*, vol. 56, no. 2, pp. 510-519, 2009

[125] T. T. Phuong, K. Ohishi, and Y. Yokokura, "Fine Sensorless Force Control Realization Based on Dither Periodic Component Elimination Kalman Filter and Wide Band Disturbance Observer," *IEEE Trans. Ind. Electorn.*, vol.67, no.1, pp. 757-767, 2020.

[126] Y. Nagatsu, and S. Katsura, "Kalman filter based equivalent elastic force feedback for time-delay compensation," *Proc. of IEEE 26th International Symposium on Industrial Electronics*, pp. 1714-1746, 2017.

[127] J. Hu, and R. Xiong, "Contact Force Estimation for Robot Manipulator Using Semiparametric Model and Disturbance Kalman Filter," *IEEE Trans. Ind. Electorn.* , vol.65, No.4, pp. 3365-3375, 2018.

[128] J. Dokoupil, and P. Václavek, "Forgetting Factor Kalman Filter with Dependent Noise Processes," *Proc. of IEEE 58th Conference on Decision and Control*, pp. 1809-1815, 2019.

[129] P. Shrivastava, T. Kok Soon, M. Y. I. Bin Idris, S. Mekhilef and S. B. R. S. Adnan, "Combined State of Charge and State of Energy Estimation of Lithium-Ion Battery Using Dual Forgetting Factor-Based Adaptive Extended Kalman Filter for Electric Vehicle Applications," *IEEE Trans. Vehic. Tech.*, vol. 70, no. 2, pp. 1200-1215, 2021.

[130] Y. Suzuki, A. Mita, "Estimation of Inter-story Drift Angle for Tall Buildings with Three Accelerometers Using Adaptive Extended Kalman Filter," J. Struct. Eng, vol.80, no.717, pp.1649-1656, 2015 (in Japanese).

[131] T. Sato, and K. Takei, "Development an Adaptive Kalman Filter and its Applications," Proceedings of JSCE, no.584, pp.163-173, 1998 (in Japanese).

[132] J. Sun, L. Tao, Z. Niu and B. Zhu, "An Improved Adaptive Unscented Kalman Filter With Application in the Deeply Integrated BDS/INS Navigation System," *IEEE Access*, vol. 8, pp. 95321-95332, 2020.

[133] K. A. Aguilar-Cruz, J. De Jesús Medel-Juárez, M. T. Zagaceta-Álvarez, R. Palma-Orozco and R. Urbieta-Parrazales, "Adaptive Filtering Approach With Forgetting Factor for Stochastic Signals Applied to EEG," *IEEE Access*, vol. 8, pp. 101274-101283, 2020.

[134] M. Takeno, and T. Katayama, "State and Parameter Estimation for Dynamical Systems by Using Unscented Kalman filter," Transactions of the Institute of Systems, Control and Information Engineers, vol.24, no.9, pp.231-239, 2011 (in Japanese).

[135] Y. Hattori, and S. Adachi, "Simultaneous Estimation of Nonlinear Systems Driven by Unknown Nonlinear Actuator Using Unscented Kalman Filter (UKF)," Trans. on SICE, vol.45, no.5, pp.286-288, 2009 (in Japanese).

[136] A. Baba, and S. Adachi, "Simultaneous State and Logarithmic Parameter Estimation of Lithium-Ion Batteries using UKF," IEEJ Trans. on Industry Applications, vol.133, no.12, pp.1139-1147, 2013 (in Japanese).

[137] Y. Xu, Z. Yang, Y. Liu and S. Jiang, "Accelerate Convergence of Polarized Random Fourier Feature-Based Kernel Adaptive Filtering With Variable Forgetting Factor and Step Size," *IEEE Access*, vol. 8, pp. 126887-126895, 2020.

[138] J. Dai, A. Xu, X. Liu, C. Yu, and Y. Wu, "Online Sequential Model for Multivariate Time Series Prediction With Adaptive Forgetting Factor," *IEEE Access*, vol.8, pp.175958-175971, 2020.

[139] J. Qu, F. Zhang, Y. Tang and Y. Fu, "Dynamic Visual Tracking for Robot Manipulator Using Adaptive Fading Kalman Filter," *IEEE Access*, vol. 8, pp. 35113-35126, 2020.

[140] M. Hu, W. Gao, Y. Zeng, H. Li, and Z. Yu, "Vehicle Mass and Road Grade Estimation Based on Adaptive Forgetting Factor RLS and EKF Algorithm," *Proc. of 5th Int. Conf. on Power and Renewable Energy*, pp342-346, 2020.

[141] Z. He, Z. Yang, X. Cui, and E. Li, "A Method of State-of-Charge Estimation for EV Power Lithium-Ion Battery Using a Novel Adaptive Extended Kalman Filter," *IEEE Trans. Vehic. Tech.*, vol.69, no.12, pp.14618-14630, 2020.

[142] S. Liu, J. Wang, Q. Liu, J. Tang, H. Liu, and Z. Fang, "Deep-Discharging Li-Ion Battery State of Charge Estimation Using a Partial Adaptive Forgetting Factors Least Square Method," *IEEE Access*, vol. 7, pp. 47339-47352, 2019.

[143] S. Yu, Q. Song, and S. Liu, "Motion artifact cancellation from a single channel SCG using adaptive forgetting factor recursive least square filter," *IEEE Access*, doi: 10.1109/ACCESS.2020.3013380., 2020.

Acknowledgments

This dissertation is a summary of my research from October 2014 to August 2021 as a member of the Motion Control Laboratory, College of Engineering and Design, Shibaura Institute of Technology, and a member of the Murakami Laboratory, Graduate School of Science and Technology, Keio University.

First of all, I would like to express my sincere gratitude to Professor Dr. Toshiyuki Murakami and Professor Dr. Akira Shimada for their support to conduct my research. They gave me incredible opportunities to start and conduct various studies. Also, I deeply appreciate the support from their laboratory members.

I appreciate the members of my Ph.D. dissertation committee, Professor Dr. Hiromitsu Ohmori, Professor Dr. Toru Namerikawa, and Professor Dr. Masaki Takahashi for their helpful comments and advice to improve this thesis.

Finally, I want to appreciate all the people who helped me to complete my research though I could not mention them here.

Takashi Ohhira
August, 2021